uOttawa

L'Université canadienne
Canada's university

FACULTÉ DES ÉTUDES SUPÉRIEURES ET POSTOCTORALES

uOttawa

L'Université canadienne
Canada's university

FACULTY OF GRADUATE AND POSDOCTORAL STUDIES

Mathieu Frenette
AUTEUR DE LA THÈSE / AUTHOR OF THESIS

Ph.D. (Chemistry)
GRADE / DEGREE

Department of Chemistry
FACULTÉ, ÉCOLE, DÉPARTEMENT / FACULTY, SCHOOL, DEPARTMENT

Advances in Free Radical Oxidation:
Mechanistic Studies, Fluorescent Probe Design and Radically Different Antioxidants

TITRE DE LA THÈSE / TITLE OF THESIS

Juan C. Scaiano
DIRECTEUR (DIRECTRICE) DE LA THÈSE / THESIS SUPERVISOR

CO-DIRECTEUR (CO-DIRECTRICE) DE LA THÈSE / THESIS CO-SUPERVISOR

EXAMINATEURS (EXAMINATRICES) DE LA THÈSE / THESIS EXAMINERS

Maria De Rosa

John Pezacki

Gino Di Labio

Alain St-Amant

Gary W. Slater
Le Doyen de la Faculté des études supérieures et postdoctorales / Dean of the Faculty of Graduate and Postdoctoral Studies

Advances in Free Radical Oxidation: Mechanistic Studies, Fluorescent Probe Design and Radically Different Antioxidants

Mathieu Frenette

Thesis submitted to the
Faculty of Graduate and Postdoctoral Studies
in partial fulfillment of the requirements for the degree of
Doctor of Philosophy
in the Ottawa-Carleton Chemistry Institute
Department of Chemistry, University of Ottawa

Université d'Ottawa · University of Ottawa

Candidate	Supervisor
Mathieu Frenette	Professor J. C. Scaiano

Your file Votre référence
ISBN: 978-0-494-51812-0
Our file Notre référence
ISBN: 978-0-494-51812-0

To my wife,

Marie-Claude Robert,

for being an ever increasing source of love and inspiration,

&

To my mentors,

Tito Scaiano, Keith Ingold, and Ross Barclay,

who helped me learn free radical chemistry at diffusion-controlled rates.

Abstract

Organic matter may contain predominantly paired electrons, but much of it was, at some point, shaped by reactions involving unpaired electrons, i.e., radicals. Free radicals are involved in many reactions including combustion, petroleum reforming, polymer and industrial synthesis, and oxidation reactions. This last class of radical reactions is the central theme of this thesis.

Oxidation of organic matter, including our own bodies and plastic, is accelerated by the presence of radicals and oxygen. This often undesired reaction can be limited by antioxidants that trap radicals and effectively stop oxidation.

Here, we report a new class of antioxidants based on dimers of persistent carbon-centered radicals. The dimers reversibly dissociate to form radicals, which we studied using Variable-Temperature UV-Visible and Electron Paramagnetic Resonance spectroscopies. Unlike most, these carbon-centered radicals do not react with oxygen ($k<5x10^3M^{-1}s^{-1}$). They do, however, efficiently trap peroxyl radicals ($k>10^8M^{-1}s^{-1}$). Using oxygen uptake kinetics, we measured rate constants between the reaction of dimers and peroxyl radicals (k_{inh}) that were higher than many commercial antioxidants such as butylated hydroxytoluene (BHT) and CIBA's Irganox HP-136. The antioxidant activity of dimers remarkably increases with temperature as more dimers dissociate to the active antioxidant form.

In the absence of antioxidants, radical-induced oxidation of polyunsaturated lipids and cholesterol generates electrophilic oxidation products. Of these, the formation of ketones has eluded a satisfactory explanation for many decades. We propose that αC-H abstraction from hydroperoxides, the major primary oxidation products, generates ketones and hydroxyl radicals (HO•) in a long overlooked path to these intermediates. The HO• was trapped by benzene to yield phenol and the mechanism was further investigated using computational chemistry.

The final sections describe the development and application of 7-mercapto-4-methylcoumarin (C-SH) as a prefluorescent probe to detect electrophilic lipid

oxidation products. For this, we performed the first photophysical study of C-SH and related coumarin-derivatives. It was found that alkylation of C-SH generally increases the fluorescence quantum yield while substitution by an electron withdrawing group renders C-SH non-fluorescent. We successfully employed the increase in fluorescence upon alkylation of C-SH to quantify lipid oxidation electrophiles such as 4-hydroxynonenal.

Acknowledgements

I was extremely lucky to have Tito Scaiano as a PhD supervisor. His support, guidance and well-equipped lab gave me the opportunity to become the best chemist possible. His kindness and composure are also exemplary; he will forever be a role model. I thank you and Elda for welcoming me so generously in the group.

In our field of research, Keith U. Ingold is legendary. His knowledge and understanding of free radical chemistry is unparalleled and his love of life (and skiing) is contagious. Ross Barclay taught me enough about antioxidants to stand on my own and his gift of an oxygen uptake apparatus was a great advantage. I feel privileged to have studied under Tito, Keith and Ross; the best free radical chemists in Canada. I also want to thank the examiners that (rapidly) read this thesis: Gino DiLabio, Maria DeRosa, John Pezacki and Alain St-Amant. Your questions were very insightful and I actually enjoyed defending my thesis with you.

The Scaiano group is a very stimulating place to conduct research—and this research is quite varied: photochemistry and free radicals, photolithography and nanotechnology, cell and material studies, DNA, proteins and lipids, fundamental and applied... Tito has a finger in every pie! Of course, the people that make his group are the key to this success.

Carolina Aliaga, Alexis Aspée, Enrique Font-Sanchis, Michelle Chrétien, Marie Lafferière, Kathy-Sarah Focsaneanu and Chris Coenjarts were the first to help me in the group. The knowledge they shared is the basis of my understanding in basic research. In what could be called version 2.0 of my stay in the group. A much more dynamic array of interactions developed. At this point, I knew enough to start my own projects, but not enough to be critical of them (I am still at this stage). So, I quickly amassed more projects than I could handle, which led to many interesting observations and collaborations. I'll start by thanking Jessie Blake and Paul Billone for the many discussions and the great friendship over the years. I hope we can end up in the same city again at some point. The group is a very social creature, and for

that I want to acknowledge the usual suspects (in approx. order of joining the group): Larisa Mikelson, Matthew Lukeman, Kathy McGilvray, Mark Perry, Eric Gagnon, Vincent Maurel, Claudio Carra, Carlos Sanrame, Colleen Sutton (and Chris), Belinda Heynes, Laetitia René-Boisneuf (and Nico), Eve Heafey, Robert Godin (representing North Tetagouche), Matthew Decan (and Natalie), Matthew Yorke, Vasilisa Fillipenko, María González Béjar, Liliana Jimenez, Natalia Pacioni and Kevin Stamplecoskie (and kittens). Rereading these names will certainly remind me of some of the best times of my life.

Thanks to Annette Campeau, Linda Baron, Gino Cuglietta, Eugenia Moreno, and particularly to Betty Yakimenko and Michel Grenier for the support over the years. Scientifically, I am indebted to Philip Campbell, and particularly Vasilisa Fillipenko and María González Béjar. It was a pleasure to learn and work with you.

I got involved in many "projects" outside of research and these have positively shaped me as a person. Apart from the "secret" drinking clubs and wine clubs, "Geeking Out", the band (that ended up playing at our wedding—thanks!), open mic nights at Nostalgica (with Pat Ang), and other random fun stuff, I was lucky to be involved with the Chemistry Graduate Student Association and Let's Talk Science. Together, CGSA and LTS consumed a lot of my time, but the outcome is not regrettable. I am certainly a better organizer and presenter because of my implication in these efforts. For this, I am indebted (in particular) to Patrick Crewson and Sue McKee for their leadership in the CGSA and LTS. I am happy to have crossed path with many fantastic people during my time in Ottawa: Ly Lo Cong, Joseph Moran, Mathieu Lemay, the Dr. David Bryce, the displaced New Orleans people, Roger Tam, Hasan Khan, Selena Sagan, Charles Russell, and many others. Good times indeed! À ma famille, je suis éternellement reconnaissant de m'avoir si bien dirigé et encadré. Jean-François et Émilie, je vous souhaite ce qu'il y a de mieux dans votre vie qui s'annonce déjà excitante.

Throughout this time, my pillar was Marie-Claude Robert—now my beloved wife. She is the reason I strive for excellence and her love makes me believe I can accomplish anything. Marie-Claude is the greatest gift my life could have.

Table of Contents

List of Figures

List of Schemes

List of Tables

List of Abbreviations

ΔG_{RX}	reaction free energy change
ΔG^{TS}	transition state free energy change (relative to reagents)
ΔH_{RX}	reaction enthalpy
ΔH^{TS}	transition state enthalpy (relative to reagents)
μM	micromolar
$^1O_2$	singlet molecular oxygen ($^1\Delta_2$)
4-HNE	4-hydroxynonenal
4-HPNE	4-hydroperoxynonenal
4-ONE	4-oxononenal
a.u.	arbitrary units
AChE	acetylcholine esterase
AIBN	2,2'-azo-bis-isobutyronitrile
A_{max}	absorbance maximum
BDE	bond dissociation energy
BHT	2,6-di-tert-butyl-4-hydroxytoluene
C_6H_6	benzene
Ch	cholesterol
Ch•	cholesterol radical (carbon-centered)
Ch=O	7-oxo-cholesterol (also, 7-ketocholesterol)
Ch-OH	7-hydroxycholesterol
ChOO•	cholesterylhydroperoxyl radical
Ch-OOH	7-hydroperoxycholesterol
CS-Adduct	7-mercapto-4-methylcoumarin covalently bound to electrophile
C-SH	7-mercapto-4-methylcoumarin
C-SMVK	methylvinylketone+C-SH product
C-SR	alkylated 7-mercapto-4-methylcoumarin
C-SS-C	7-mercapto-4-methylcoumarin disulfide
CYP-P450	cytochrome P450
DBHA	2,6-di-tert-butyl-4-hydroxyanisole
DFT	density functional theory
DMPO	dimethylpiperidine-N-oxide (spin trap)
DNA	deoxyribonucleic acid
DPPH	2,2-diphenyl-1-picrylhydrazyl radical
EDG	electron donating group
EI	electron impact
EPR	electron paramagnetic resonance
ε_{MAX}	molar absorption coefficient λ_{MAX}

EWG	electron withdrawing group
FRET	Förster (or fluorescence) resonance energy transfer
GC-MS	gas chromatography mass spectrometry
GS-Adduct	glutathione covalently bound to electrophile
GSH	reduced glutathione (free thiol)
HO•	hydroxyl radical
HOMO	highest occupied molecular orbital
HP-136	CIBA's Irganox HP-136®
HPLC	high-pressure liquid chromatography
HRMS	high resolution mass spectrometry
$h\nu$	light (photon)
IC	internal conversion
ISC	intersystem crossing
k_{isc}	rate constant for intersystem crossing
k_{obs}	observed rate constant
k_{rad}	radiative rate constant
k_{TT}	rate constant for triplet-triplet annhiliation
$k_{\alpha C\text{-}H}$	rate constant H-abstraction from secondary hydroperoxide
k_{inh}	rate constant for peroxyl radical trapping
k_{init}	rate constant for the decomposition of initiator
k_{O2}	rate constant for the addition of oxygen
k_{-O2}	rate constant for the dissociation of oxygen
k_p	propagation rate constant
kcal	kilocalorie = kilojoule/4.184
L•	lipid radical (carbon-centered)
L=O	lipid ketone (oxodiene)
λ_{EXC}	excitation wavelength
LFP	laser-flash photolysis
LH	polyunsaturated fatty acid
λmax	wavelength corresponding to maximum intensity
λmon	monitoring wavelength (fluorescence)
LOO•	lipid hydroperoxyl radical
LOOH	lipid hydroperoxide
LUMO	lowest unoccupied molecular orbital
m/z	molecular mass divided by charge
MDA	malondialdehyde
min	minimum
mM	millimolar
MVK	methylvinylketone
NIR	800nm-1400nm
nm	nanometers

PhH	benzene
PMHC	pentamethyl-4-hydroxychroman (vitamin E analog)
PTFE	polytetrafluoethylene
Φ_F	fluorescence quantum yield
$\Phi(^1O_2)$	singlet oxygen quantum quantum yield
Φ_{ISC}	intersystem crossing quantum yield
Φ_{VR}	quantum yield for vibrational relaxtion
R=O	generic dialkyl ketone
R-H	oxidizable substrate
R	rate of initiation
ROO•	alkylperoxyl radical
ROOH	alkylhydroperoxide
ROS	reactive oxygen species
s	seconds
S_Δ	fraction of triplet states that generate $^1O_2$
S_0	ground singlet state
S_1	lowest singlet excited state
S_n	upper singlet excited state
$\Sigma k_{non\text{-}rad}$	sum of non-radiative rate constants
T*	triplet excited state
T_1	lowest triplet excited state
$\tau_{triplet}$	triplet lifetime
τ_F	fluorescence lifetime
TBA	thiobarbituric assay
tBoc	tert-butoxycarbonate
TEMPO	2,2',6,6'-tetramethylpiperidine-N-oxide, free radical
UV	ultraviolet
v/v	volume/volume
V-601	2,2'-azobis(methyl-2-methylpropionate)
Visible	400nm-800nm
VR	vibrational relaxation
VT	variable temperature
VX	VX nerve agent, toxic organophosphate

1. Free Radical Oxidation: An Introduction

1.1 Persistent Carbon-Centered Radicals

When, in 1900, Moses Gomberg claimed to make trivalent triphenylmethyl radicals, most would not believe him.[1,2] The tetravalent carbon rule was in place and for many years, Gomberg's results were a matter of debate. Today, his discovery is recognized as the foundation of organic radical chemistry.

During these seminal experiments, Gomberg attempted the synthesis of hexaphenylethane—a compound that eludes isolation to this day—from triphenylmethylchloride and zinc powder in benzene. In the absence of oxygen, the reaction turned yellow due to triphenylmethyl radicals and the purified solution could be evaporated to afford the dimer as a reactive white powder. The correct structure of the dimer is not hexaphenylethane as originally believed, but rather a head-to-tail structure[3] determined in 1968 (Scheme 1-1). A stable peroxide is obtained under air.

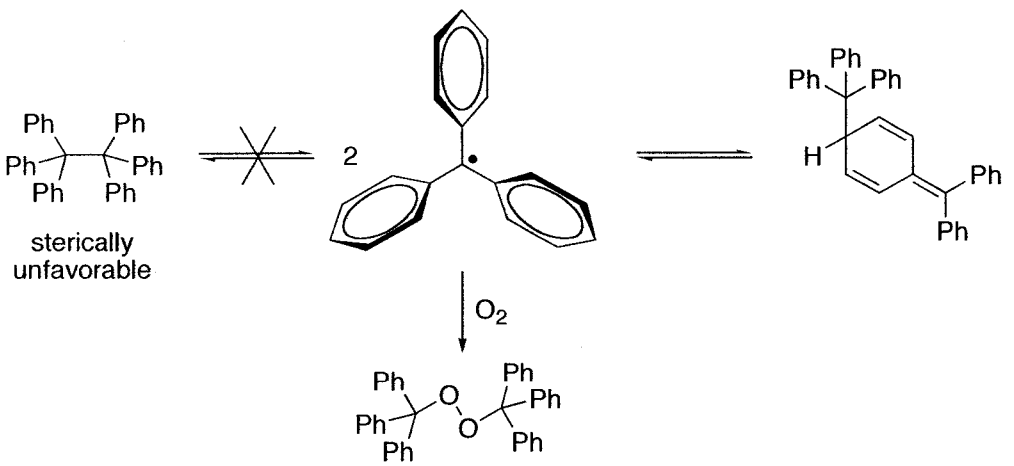

Scheme 1-1. Radical-dimer equilibrium of triphenylmethyl radicals. Under air, $Ph_3C\bullet$ reacts with oxygen to form a stable peroxide.

Since Gomberg's discovery, many persistent[4,5] carbon-centered radicals have been observed; some "famous" examples are shown in Scheme 1-2.

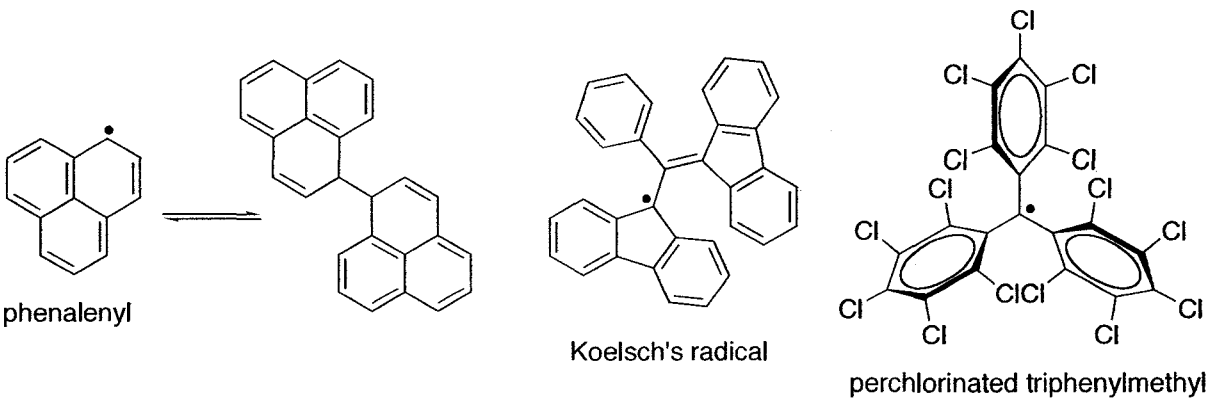

Scheme 1-2. Phenalenyl radicals form weakly bonded σ-dimers and react slowly with oxygen.[6] Koelsch's radical[7] and perchlorinated triphenylmethyl radicals[8] are remarkably stable, partly due to the steric hinderance at the radical center.

The radicals shown above are purposefully stabilized—these three radicals are amongst the most stable carbon-centered radicals reported. In the first portion of this thesis, some air stable carbon-centered radicals (Chapter 2) and their application as antioxidants (Chapter 3) will be presented. The stability of these radicals should not mask the fact that the great majority of free radicals are reactive intermediates.

Over the course of the previous century, radicals have grown from chemical curiosities to intermediates with a tremendous impact on everyday life. Free radicals are the intermediates that enable the petroleum refining that fuels our cars[9] (not to mention combustion itself[10]) and their reactions generate over 4×10^6 tons of

polymethylmethacrylate, polyvinylchloride, tetrafluoroethylene, and polystyrene every year.[11] The oxygen atom in acetone, for example, also spends a fraction of a second carrying an unpaired electron during the industrial synthetic process.[12]

A more complete understanding of radical reactivity and their reaction rate constants led the way for the rational design of many processes involving transient radicals. Amongst these, we find applications in organic synthesis[13] and "living" free-radical polymerization.[14-16] Even when radical chemistry is not desired, it often plays a role—in the next section we discuss autoxidation reactions that are responsible for the degradation of organic materials.

1.2 Free Radical Autoxidation

Oxygen is a reactive molecule—when given the opportunity. In many cases this "opportunity" is the presence of carbon-centered radicals. Indeed, thermodynamics highly favor the oxidation of organic matter, but this reaction is kinetically forbidden since oxygen is a ground state triplet (S=1), eq [1]. This is why molecular oxygen—one of the least energetically favorable arrangements of oxygen in molecules—can be present in such a high concentration.

[1] $R\text{-}H + {}^{t}O\text{-}O^{t} \dashrightarrow$ no reaction

Oxygen does, however, react very quickly with carbon-centered radicals (R•) to generate peroxyl radicals (ROO•), eq [2].[17] In turn, ROO• can react with surrounding molecules (R-H) to form another carbon-centered radical, eq [3]. This chain reaction, called autoxidation, means that a single radical can induce an amplified oxidation of R-H. Much of our kinetic understanding for these autoxidation reactions comes from the work of Howard and Ingold performed in the 1960s and 1970s.[18-23]

[2] $R\bullet + {}^{t}O\text{-}O^{t} \xrightarrow{fast} ROO\bullet$

[3] $ROO\bullet + R\text{-}H \xrightarrow{k_p} ROOH + R\bullet$

The autoxidation of R-H, a hydrocarbon (or aldehyde) in this example, generates hydroperoxides[20] (or peracids[22]) by H-atom abstraction reactions. Another common reaction for peroxyl radicals is addition to double bonds, which leads to an alternating co-polymer of oxygen and vinyl monomer.[18] The rate-determining step for this type of reaction is shown in eq [4]. Again, oxygen will quick react with the newly formed carbon-centered radical to form another peroxyl radical that will propagate the polymer growth.

[4] 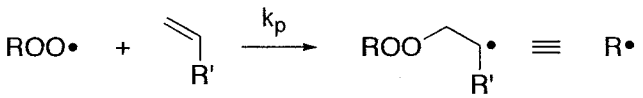

In most systems, the rate of radical initiation is slow and unpredictable. To give an idea of timescales, the rancidity of fish, milk and butter are examples of autoxidation reactions with unpleasant results.[24] For this reason, most experimental studies of autoxidation reactions are initiated at a slow, constant rate afforded by azo-initiators such as 2,2'-azo-bis-isobutyronitrile (AIBN) shown in eq [5].[25]

[5] 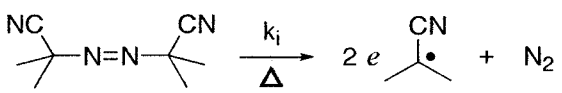

The autoxidation chain length, i.e., the number of oxygen molecules consumed per radical initiated, is limited by termination reactions. Since a radical has an unpaired electron and the surroundings have paired electrons, the only way to "kill" a radical is by reacting it with another radical. In the absence of antioxidants

(*vide infra*), the self-reaction of peroxyl radicals is the main termination pathway for free radical autoxidation, eq [6]. These termination reactions are very fast for primary or secondary peroxyl radicals ($2k_t=10^6$-$10^8 M^{-1}s^{-1}$),[19] but tertiary peroxyl radicals recombine much slower ($2k_t=10^3$-$10^5 M^{-1}s^{-1}$).[21]

[6] $\mathrm{ROO\bullet} + \mathrm{ROO\bullet} \xrightarrow{2k_t}$ non-radical products

For a chain reaction to occur, ROO• must react faster with the oxidizable substrate (propagation) than with another ROO• (termination). If the propagation reaction is H-atom abstraction, the C-H bond dissociation energy for R-H must be lower than the newly formed bond, ROO-H, which is ~88 kcal/mol for alkyl R-groups (~90-92 kcal/mol for electron withdrawing R-groups). Polyunsaturated lipids satisfy this criterion due to the low C-H BDE of 1,4-pentadiene (C-H BDE = 76.6 kcal/mol).[26] The kinetics of hydrocarbon autoxidations are treated in greater detail in chapter 3.

1.2.1 Lipid Peroxidation

Linoleate—the most abundant polyunsaturated fatty acid in animals—has been known to generate hydroperoxides upon exposure to air since the 1940s.[27] For a long time, it was believed that nature would not "allow" such radical chemistry to happen *in vivo.* Radical chemistry, to be fair, can be quite "messy". This is particularly true in complex organic systems (and it doesn't get more complex than biological systems). After some debate, it is now evident; this "mess" is taking place

in living systems. Consequently, the past 25 years have seen an explosion of interest in lipid oxidation (and other free radical reactions in vivo).[28]

The autoxidation of polyunsaturated lipids (LH) generates lipid hydroperoxides in a mechanism similar to the one described above.

[7] $L\bullet \overset{O_2}{\rightleftharpoons} LOO\bullet$

[8] $LOO\bullet + LH \xrightarrow{k_p} LOOH + L\bullet$

Ned Porter and co-workers were able to describe the formation of 4 major hydroperoxides according to the reversible addition of oxygen to the pentadienyl radical as seen below.[29] Typically, the products do not include the non-conjugated hydroperoxide at the central pentadienyl position; the addition of oxygen at this position is followed by an even faster dissociation. It is possible to trap this short-lived peroxyl radical with efficient hydrogen donors.[30,31]

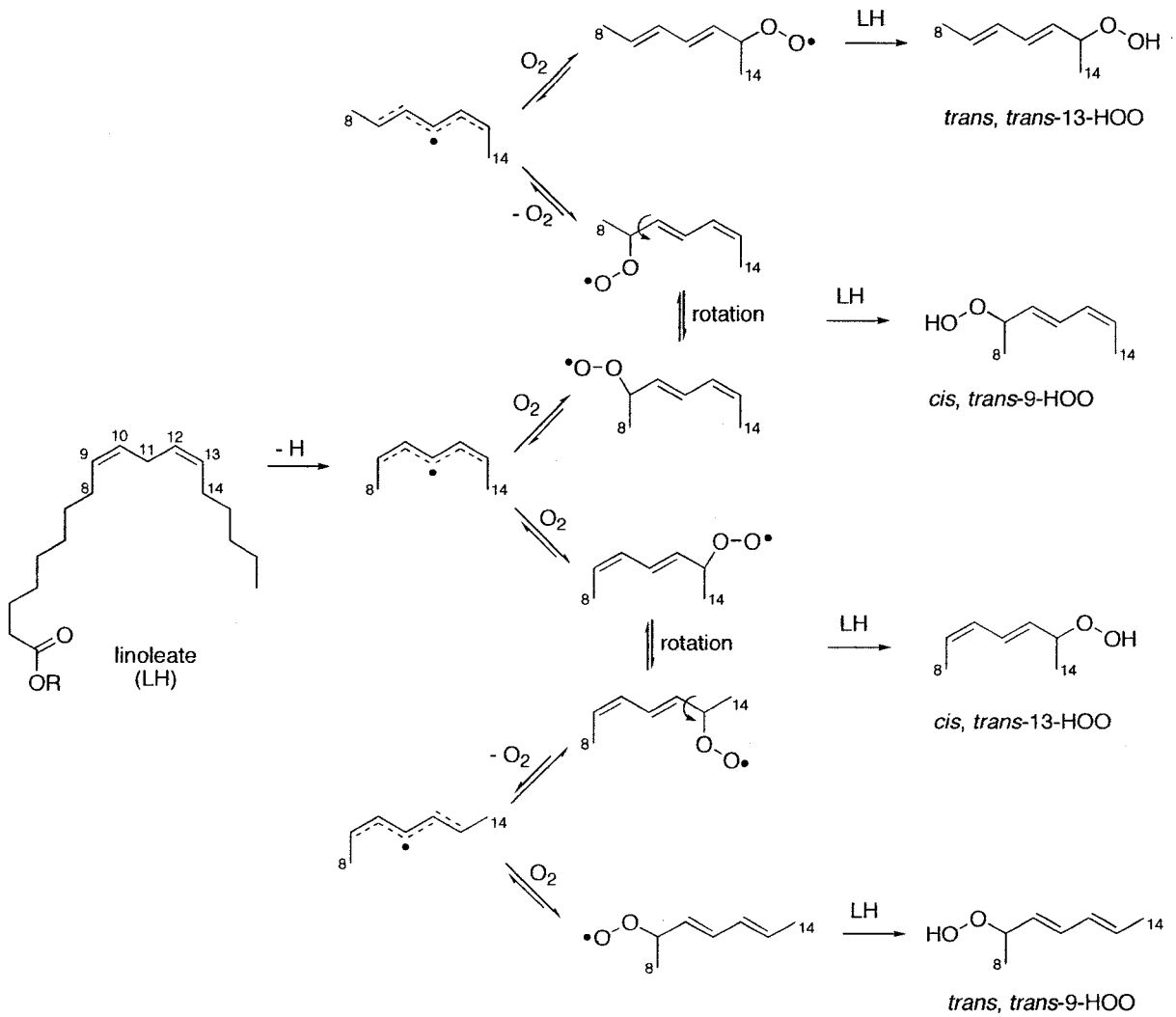

Scheme 1-3. The primary autoxidation products of linoleate include 4 major hydroperoxides with either a *cis,trans* or *trans,trans* diene geometry.

Further oxidation of lipid hydroperoxides generates an array of ketone and aldehyde products, many of which are electrophilic (Scheme 1-4).[32] These electrophiles can form covalent adducts with proteins and DNA—this appears to be a major reason for the nefarious effects of free radicals *in vivo*. Despite their perceived importance, the mechanisms involved in the formation of secondary lipid

oxidation products are not yet clear.[33] In chapter 4, we proposed that αC-H abstraction of lipid hydroperoxides by propagating peroxyl radicals are a path to lipid oxo-dienes and hydroxyl radicals.

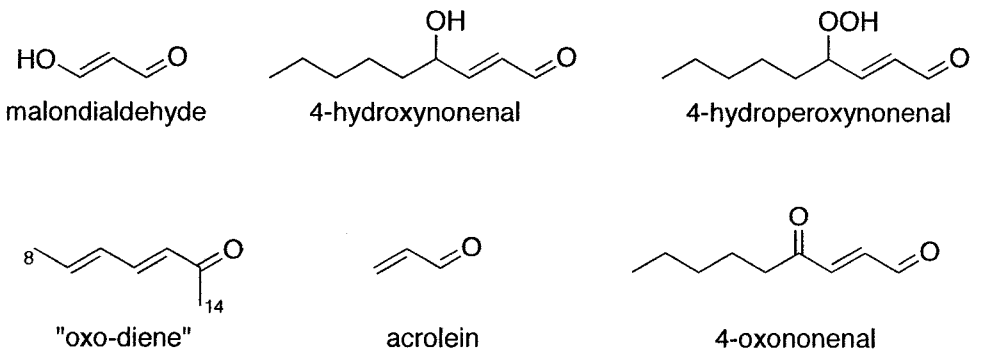

Scheme 1-4. Secondary lipid oxidation products.

As antioxidants prevent free radical autoxidations, glutathione prevents electrophilic damage induced by electrophilic oxidation products.[34,35] Reduced glutathione is a thiol-containing tripeptide that can react with lipid oxidation electrophiles (Scheme 1-5), thus acting as sacrificial reagent to prevent covalent modification of protein and DNA.

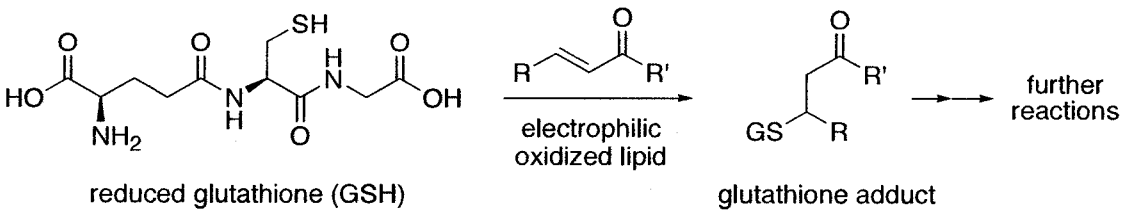

Scheme 1-5. Nucleophilic attack by glutathione with electrophilic lipid oxidation products.

In this brief introduction on lipid oxidation, the focus was placed on reactions that generate hydroperoxides, electrophiles and their covalent adducts. As it is observed in polymer decomposition, these reactions are mediated by autoxidation reactions involving peroxyl radicals. Molecules that prevent peroxyl radical reactions, therefore, have the potential to limit oxidative damage (broadly defined as the repercussions of uncontrolled oxidation reactions).

1.2.2 Chain-Breaking Antioxidants

If peroxyl radical recombination were the only termination step for free radical autoxidation, aerobic life could not exist. To deal with oxidative damage, all aerobic lifeforms have developed antioxidants defenses.[28] Amongst these, chain-breaking antioxidants directly react with reactive peroxyl radicals to stop autoxidation; vitamin E and vitamin C are examples of naturally occurring peroxyl radical scavengers (Scheme 1-6). Similarly, synthetic antioxidants such as butylatedhydroxytoluene (BHT) and CIBA's Irganox HP-136® were developed to prevent the autoxidation of plastics, lubricants, oils, and rubber. The food industry also recognized the deterioration of processed foods as a problem[36] and sought another solution. It was found that partial hydrogenation of lipids in processed foods limited autoxidation reactions; unfortunately, the trans-fatty acids generated during this process have negative impacts to human health.[37]

An efficient chain-breaking antioxidant (A-H) has to fit two criteria: (i) The antioxidant must react quickly with peroxyl radicals and (ii) the radical derived from the antioxidant must be inert to the surroundings. Of course, the antioxidant should also be non-toxic, stable under air and localize properly in the system of interest.

Good H-atom donors such as phenols meet the first criterion.[38] After donating a hydrogen to a propagating peroxyl radical, the resulting antioxidant radical should not react with the organic matter it is intended to protect. Furthermore, the antioxidant radical must be inert to oxygen since reacting with oxygen would generate another peroxyl radical. In most cases, the antioxidant radical will trap another peroxyl radical, i.e., each antioxidant breaks two autoxidation chains.

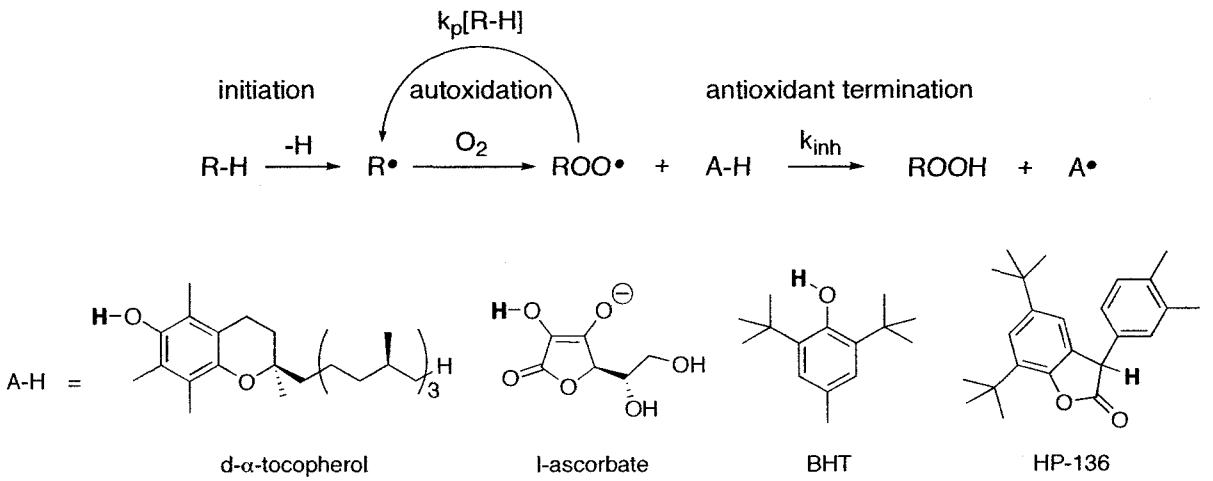

Scheme 1-6. Chain-breaking antioxidants (A-H) react with peroxyl radicals to stop autoxidation reactions. The radical resulting from the antioxidant termination, A•, can trap another peroxyl radical. The structures of some well-known antioxidants are also shown.

The case for antioxidants in polymers is clear-cut. They prevent degradation reactions and yellowing of the material that surrounds them. In humans, however, there is no clear evidence that antioxidant supplementation is beneficial (above a certain minimum to prevent scurvy or infertility). It is clear that more work needs to be done to understand the effect of free radicals in biology and medicine. For one, better tools are needed to monitor their effect. In the last portion of this thesis, I present some work towards a fluorescent probe to quantify the electrophiles presented in Scheme 1-4. The next section will demonstrate the potential of fluorescent probes to study free radical chemistry in complex systems.

1.3 Fluorescent Probes to Study Free Radical Oxidation

Fluorescence is the emission of light from an excited-state without change in multiplicity (e.g., singlet excited-state to singlet ground state). The great majority of molecules, however, are non-fluorescent. Instead, the excitation energy is dissipated via other pathways—thermal relaxation, intersystem crossing, energy transfer, and photochemistry.[39] To be appreciably fluorescent, a molecule must emit light as fast or faster than competing excited-state processes.

1.3.1 Excited-State Processes

The excited-state processes for organic compounds are well illustrated by the Jablonski diagram (Figure 1-1).[40] After absorbing a photon, an electronic excited state is formed and, through vibrational relaxation (VR) and internal conversion (IC), the lowest singlet excited state (S_1) is populated. In solution, this process is fast (picoseconds) and 100% efficient—this result, known as Kasha's Rule, means that photophysics and photochemistry of a molecule is independent of excitation wavelength. From S_1 many processes can occur: fluorescence, vibrational relaxation, inter-system crossing (ISC) to a triplet state, or chemistry. The chemistry that occurs from singlet excited-states, which is short lived (nanoseconds), includes electron transfer reactions, proton transfers, cis-trans isomerizations, homolytic cleavage of weak bonds or other reactions with low energetic barriers. Inter-system

crossing to the triplet is also common and photochemistry often occurs from this longer-lived excited state (micro- to milliseconds). The lifetime of the triplet is highly dependant on the environment, e.g., oxygen rapidly quenches triplet states.

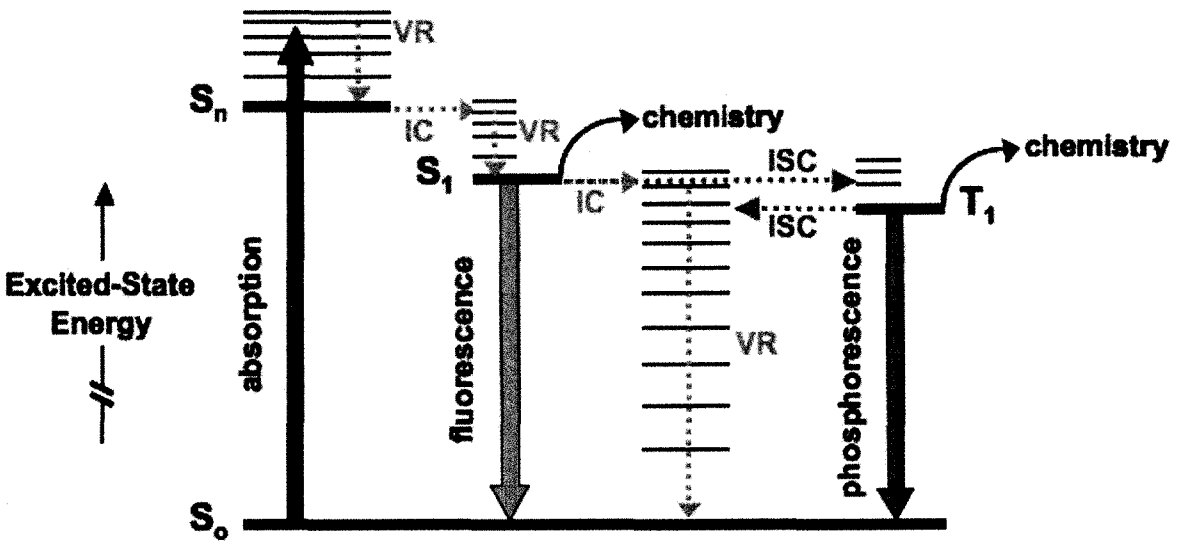

Figure 1-1. Jablonski Diagram showing absorption of light and possible excited-state processes. Notice how fluorescence emission occurs at lower energies (longer wavelengths) than absorption.

In kinetic arguments, the fraction of excited states that emit light (defined as the fluorescence quantum yield or Φ_F) is related to the rate of fluorescence (radiative rate) and competing rates (non-radiative). This is represented by eq [9], where k_{rad} is the rate constant for radiative decay (fluorescence) and $\Sigma k_{non\text{-}rad}$ is the sum all other (non-radiative) rate constants.

$$[9] \qquad \Phi_F = k_{rad} / (\sum k_{non-rad} + k_{rad}) = k_{rad} \tau_F$$

Since excited-state lifetimes are short ($\tau_F \sim$ nanoseconds), the processes that compete to dissipate the excited-state energy have small activation energies. Therefore, small changes in these energetic barriers can have important changes in excited state photochemistry. Fluorescent probes can be designed on this basis.

1.3.2 Examples of Fluorescent Probes

Fluorescent probes have become popular tools in biomedical sciences. As a testament to their importance, the 2008 Nobel Prize in chemistry was awarded for the discovery of green fluorescent protein and its modification to emit different colours.[41] In this example, the generation of the fluorescent chromophore is programmed by genetics and dictated by the protein composition. Interestingly, to generate the fluorophore, green fluorescent proteins undergo free radical oxidation that generates hydrogen peroxide as a byproduct.[41] Molecules that become fluorescent after a selective chemical modification are also gaining much interest; these are called fluorogenic probes or prefluorescent probes.

Two common designs for prefluorescent probes will be discussed:

(i) Modulation of excited-state quenching by chemical transformation.

(ii) Direct chemical modification of the chromophore.

1.3.2.1 Prefluorescent Probes Based on Excited-State Quenching

In the first approach, the chromophore remains unchanged after the desired event takes place; it is the covalently bound quencher that undergoes chemical transformation. This excited-state quencher could be an electron-donor (e.g., phosphine or an amine), an energy acceptor (lower excited state chromophore) or a stable free radical. Scaiano and co-workers employed the quenching of excited-states by stable nitroxyl radicals as prefluorescent probes on numerous occasions.[42-44] Scheme 1-7 demonstrates the use of a coumarin-TEMPO as a convenient way to measure of H-atom donating ability.

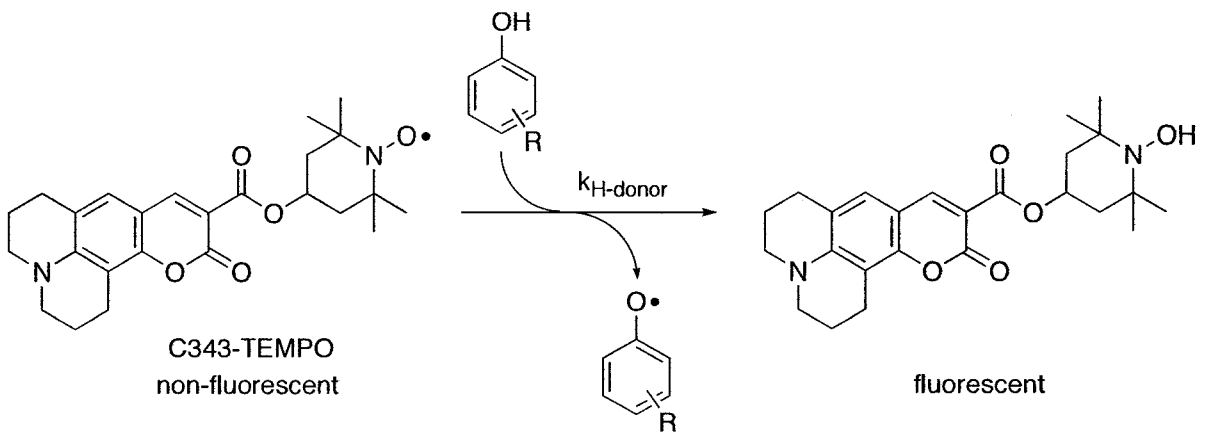

Scheme 1-7. Quinoline-TEMPO was used as a prefluorescent probe to monitor phenolic hydrogen donating ability.[44] The probe is non-fluorescent prior to reduction due to efficient excited-state quenching by the free radical.

Prefluorescent probes that detect hydrogen peroxide have been designed on a similar principle.[45] In the first case, the phosphine lone pair quenches the fluorescence, which is restored after oxidation to the phosphine oxide (Scheme 1-8).

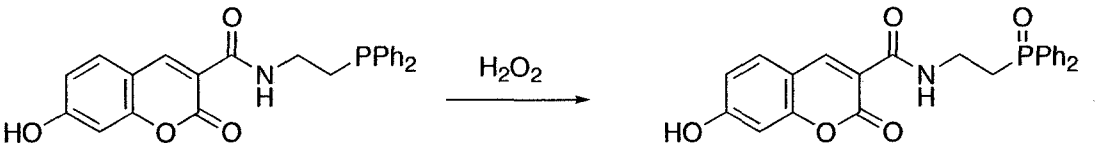

reduced fluorescence
(phosphine quenching)

high fluorescence

Scheme 1-8. Prefluorescent probe based on excited-state quenching of 7-hydroxycoumarin fluorophore by phosphine lone pair. Hydrogen peroxide oxidizes the phosphine, which is seen as a fluorescence increase.

1.3.2.2 Prefluorescent Probe by Chemical Modification of the Chromophore

Many fluorophores can be generated by specific chemical reactions from a non-fluorescent precursor. The simplest examples of chemically generated fluorophores are acid-base sensors. These molecules usually see their fluorescence emission shift in energy (colour) with pH, in addition to changes in fluorescence intensity. For example, the normally green fluorescence from coumarin-6 becomes red upon protonation. Marie Laferrière (PhD 2006) and Marius Gabriel Ivan (PhD 2007) used this phenomenon to monitor photogenerated acid in thin polymer films,[46] a key step in photolithography.

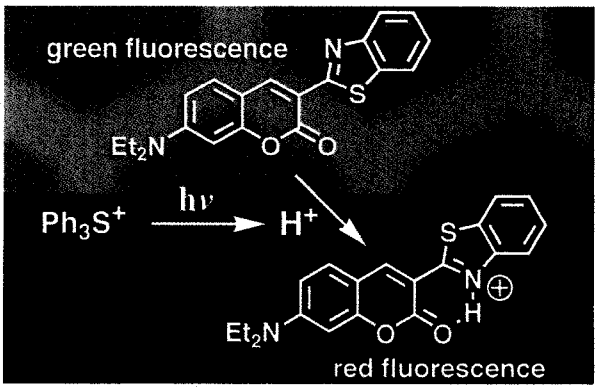

Figure 1-2. Irradiation of triphenylsulfonium salts by 157nm laser irradiation generates acid as can be seen by the change in fluorescence from coumarin 6 in this composite fluorescent image.[46]

There are many small molecule fluorophores described in the literature and endless ways of generating them via chemical reactions. This concept did not go unnoticed by the free radical community. Several probes were developed that become fluorescent after peroxyl radical attack, for example. One of the best known examples is 2,7'-dichlorofluorescin diacetate (Scheme 1-9).[47] This molecule can permeate cell walls, after which the acetate groups are cleaved and the fluorescent chromophore is regenerated by free radical oxidation. This approach is not selective, as any oxidant will oxidize fluorescin (after hydrolysis) to generate the more stable conjugated fluorophore.

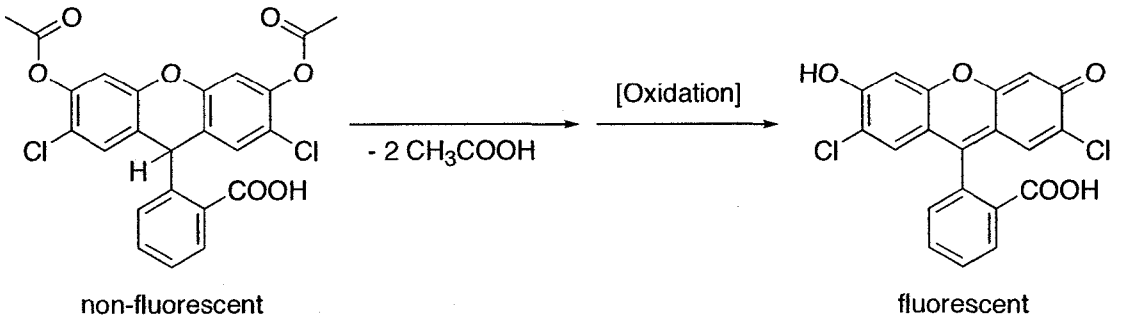

non-fluorescent fluorescent

Scheme 1-9. The non-fluorescent fluoresc*in* becomes fluorescent in cells after hydrolysis and oxidation to generate the fluorescent fluoresc*ein*.

Chang and Dickinson[48] recently developed a very promising prefluorescent probe that can detect hydrogen peroxide in normal living cells. Their design takes advantage of the selective cleavage of an aryl-boronate bond by hydrogen peroxide to generate the fluorescent reporter. They also tethered a triphenylalkyl phosphonium to help localize the prefluorescent probes in the mitochondria.

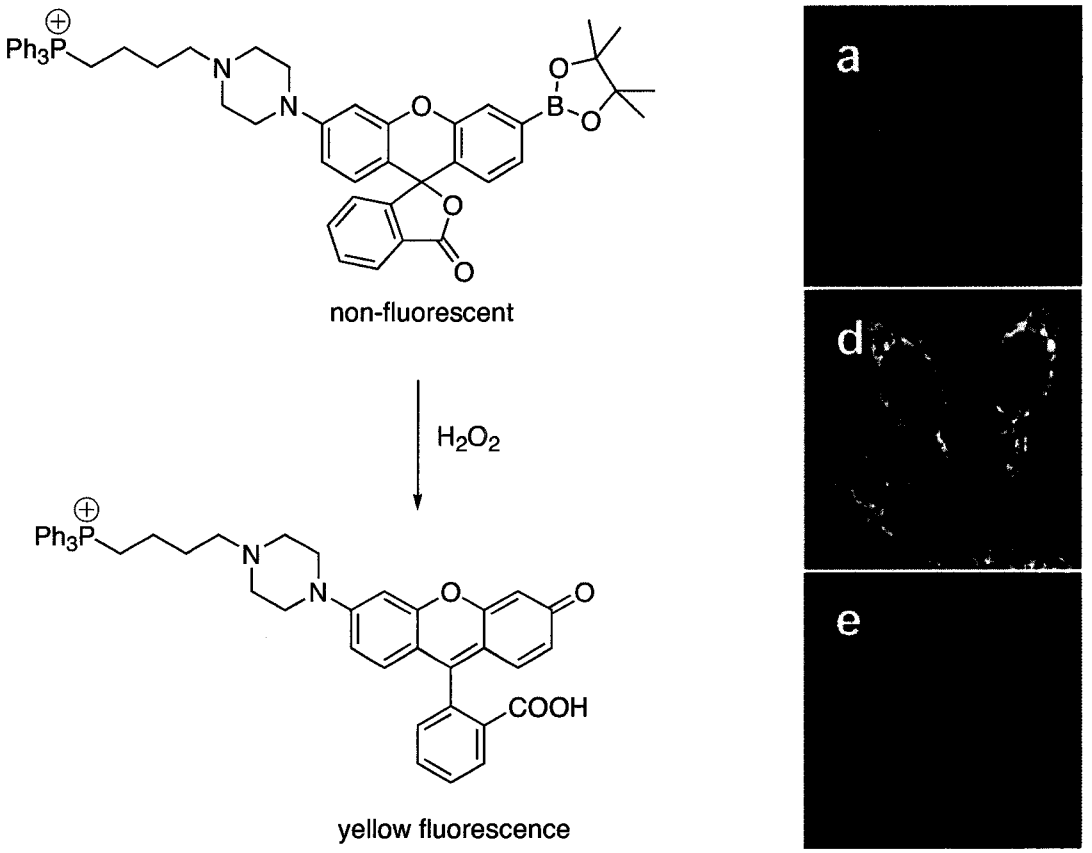

Figure 1-3. Prefluorescent probe based on the detection of hydrogen peroxide via the selective cleavage of an arylboronate-protected fluorophore. Remarkably, the probe can detect hydrogen peroxide at normal cell concentrations as seen in (a). Addition of hydrogen peroxide increases the fluorescence intensity (d) and (e) the use of a mitochondrial tracker confirms the prefluorescent probe's location. The nuclei are stained in blue.

Fluorescence can be detected in real time from fluorophores at low concentrations (single molecules can be detected). These advantages combined with well-designed prefluorescent probes has the potential to monitor events otherwise unseen.

1.4 Summary

Free radical reactions play an important role in the oxidative degradation of organic material such as plastics, lipids, processed foods, etc. The primary autoxidation for these diverse systems have similar mechanisms; peroxyl radical attacks on the surroundings to generate a carbon-centered radical, which then reacts with oxygen to regenerate a peroxyl radical. Efficient hydrogen atom donors, called antioxidants, can prevent this chain reaction.

In the absence of antioxidants, secondary oxidation reactions take place to generate electrophilic products that can covalently modify protein and DNA. These electrophiles can be sacrificially trapped by glutathione.

Yet, in 2008, there is still much to be discovered about oxidative damage *in vivo*. The complexity of the chemistry involved multiplied by the complexity of living organisms that succumbs to free radical oxidation will make this a problem worthy of scientific pursuit for decades to come. Free radical oxidation *in vivo* has been linked to Alzheimer's disease, cancer, atherosclerosis, and the process of aging itself;[28] therefore, understanding this complex chemistry should inspire a committed effort.

1.5 References

(1) Gomberg, M. "An Instance of Trivalent Carbon: Triphenylmethyl" *Journal of the American Chemical Society* **1900**, 22, 757-771.

(2) McBride, J. M. "The Hexaphenylethane Riddle" *Tetrahedron* **1974**, 30, 2009-2022.

(3) Lankamp, H.; Nauta, W. T.; Maclean, C. "A New Interpretation of Monomer-Dimer Equilibrium of Triphenylmethyl- and Alkylsubstituted-Diphenyl Methyl-Radicals in Solution" *Tetrahedron Letters* **1968**, 9, 249-254.

(4) Griller, D.; Ingold, K. U. "Persistent carbon-centered radicals" *Accounts of Chemical Research* **1976**, 9, 13-19.

(5) Hicks, R. "What's new in stable radical chemistry?" *Organic and Biomolecular Chemistry* **2007**, 5, 1321-1338.

(6) Zheng, S.; Lan, J.; Khan, S. I.; Rubin, Y. "Synthesis, Characterization, and Coordination Chemistry of the 2-Azaphenalenyl Radical" *Journal of the American Chemical Society* **2003**, 125, 5786-5791.

(7) Koelsch, C. F. "Syntheses with Triarylvinylmagnesium Bromides. α, γ-Bisdiphenylene-β-phenylallyl, a Stable Free Radical" *Journal of the American Chemical Society* **1957**, 4439-4441.

(8) Ballester, M.; Riera-Figueras, J.; Castaner, J.; Badfa, C.; Monso, J. M. "Inert carbon free radicals. I. Perchlorodiphenylmethyl and perchlorotriphenylmethyl radical series" *Journal of the American Chemical Society* **1971**, 93, 2215-2225.

(9) Alfke, G.; Irion, W. W.; Neuwirth, O. S. "Oil Refining" *Ullmann's Encyclopedia of Industrial Chemistry*; Wiley-VCH Verlag GmbH & Co., **2007**.

(10) Senkan, S.; Castaldi, M. "Combustion" *Ullmann's Encyclopedia of Industrial Chemistry*; Wiley-VCH Verlag GmbH & Co., **2007**.

(11) "Ullmann's Encyclopedia of Industrial Chemistry"; Wiley-VCH Verlag GmbH & Co., **2007**.

(12) Sifniades, S.; Levy, A. B. "Acetone" *Ullmann's Encyclopedia of Industrial Chemistry*; Wiley-VCH Verlag GmbH & Co., **2007**.

(13) Rowlands, G. "Synthetic methods: Part (i) Free-radical reactions" *Annual Reports on the Progress of Chemistry Section B* **2008**, 104, 19-34. See also other publications in this series.

(14) Georges, M. K.; Veregin, R. P. N.; Kazmaier, P. M.; Hamer, G. K. "Narrow molecular weight resins by a free-radical polymerization process" *Macromolecules* **1993**, 26, 2987-2988.

(15) Wang, J. S.; Matyjaszewski, K. "Controlled Living Radical Polymerization - Atom-Transfer Radical Polymerization in the Presence of Transition-Metal Complexes" *Journal of the American Chemical Society* **1995**, 117, 5614-5615.

(16) Chiefari, J.; Chong, Y. K.; Ercole, F.; Krstina, J.; Jeffery, J.; Le, T. P. T.; Mayadunne, R. T. A.; Meijs, G. F.; Moad, C. L.; Moad, G.; Rizzardo, E.; Thang, S. H. "Living free-radical polymerization by reversible addition-fragmentation chain transfer: The RAFT process" *Macromolecules* **1998**, 31, 5559-5562.

(17) Maillard, B.; Ingold, K. U.; Scaiano, J. C. "Rate constants for the reactions of free radicals with oxygen in solution" *Journal of the American Chemical Society* **1983**, 105, 5059-5099.

(18) Howard, J. A.; Ingold, K. U. "Absolute Rate Constants for Hydrocarbon Autoxidation: I. Styrene" *Canadian Journal of Chemistry* **1965**, 43, 2729-2736.

(19) Howard, J. A.; Ingold, K. U. "Absolute rate constants for hydrocarbon autoxidation. VI. Alkyl aromatic and olefinic hydrocarbons" *Canadian Journal of Chemistry* **1967**, 45, 793-802.

(20) Howard, J. A.; Ingold, K. U.; Symonds, M. "Absolute rate constants for hydrocarbon oxidation. VIII. The reactions of cumylperoxy radicals" *Canadian Journal of Chemistry* **1968**, 46, 1017-1022.

(21) Howard, J. A.; Adamic, K.; Ingold, K. U. "Absolute rate constants for hydrocarbon autoxidation. XIV. Termination rate constants for tertiary peroxy radicals" *Canadian Journal of Chemistry* **1969**, 47, 3793-3795.

(22) Zaikov, G. E.; Howard, J. A.; Ingold, K. U. "Absolute rate constants for hydrocarbon autoxidation. XIII. Aldehydes: photo-oxidation, co-oxidation, and inhibition" *Canadian Journal of Chemistry* **1969**, 47, 3017-3029.

(23) Korcek, S.; Chenier, J. H. B.; Howard, J. A.; Ingold, K. U. "Absolute Rate Constants for Hydrocarbon Autoxidation. XXI. Activation Energies for Propagation and the Correlation of Propagation Rate Constants with Carbon-Hydrogen Bond Strengths" *Canadian Journal of Chemistry* **1972**, 50, 2285-2297.

(24) Botsoglou, N. A.; Fletouris, D. J.; Papageorgiou, G. E. "Rapid, Sensitive, and Specific Thiobarbituric Acid Method for Measuring Lipid Peroxidation

in Animal Tissue, Food, and Feedstuff Samples" *Journal of Agricultural and Food Chemistry* **1994**, 42, 1931-1937.

(25) Barclay, L. R. C. "Model biomembranes: quantitative studies of peroxidation, antioxidant action, partitioning, and oxidative stress" *Canadian Journal of Chemistry* **1993**, 71, 1-16.

(26) Luo, Y.-R. "Handbook of Bond Dissociation Energies in Organic Compounds"; *CRC Press*, **2003**.

(27) Bolland, J. L. "Kinetics of olefin oxidation" *Quarterly Reviews* **1949**, 3, 1-21.

(28) Halliwell, B.; Gutteridge, J. M. C. "Free Radicals in Biology and Medicine"; *Oxford University Press*: Oxford; New York, **2007**.

(29) Porter, N. A. "Mechanisms for the autoxidation of polyunsaturated lipids" *Accounts of Chemical Research* **1986**, 19, 262-268.

(30) Brash, A. R. "Autoxidation of Methyl Linoleate: Identification of the Bis-allylic 11-Hydroperoxide" *Lipids* **2000**, 35, 947-952.

(31) Tallman, K. A.; Pratt, D. A.; Porter, N. A. "Kinetic Products of Linoleate Peroxidation: Rapid Fragmentation of Nonconjugated Peroxyls" *Journal of the American Chemical Society* **2001**, 123, 11827-11828.

(32) Esterbauer, H.; Schaur, R. J.; Zollner, H. "Chemistry and biochemistry of 4-hydroxynonenal, malonaldehyde and related aldehydes." *Free Radical Biology & Medicine* **1991**, 11, 81-128.

(33) Schneider, C.; Tallman, K. A.; Porter, N. A.; Brash, A. R. "Two distinct pathways of formation of 4-hydroxynonenal - Mechanisms of nonenzymatic

transformation of the 9-and 13-hydroperoxides of linoleic acid to 4-hydroxyalkenals" *Journal of Biological Chemistry* **2001**, 276, 20831-20838.

(34) Blackburn, M. L.; Ketterer, B.; Meyer, D. J.; Juett, A. M.; Bull, A. W. *Chemical Research in Toxicology* **1997**, 10, 1364-1371.

(35) Jian, W.; Lee, S. H.; Mesaros, C.; Oe, T.; Elipe, M. V. S.; Blair, I. A. *Chemical Research in Toxicology* **2007**, 20, 1008-1018.

(36) Frankel, E. N. "Antioxidants in lipid foods and their impact on food quality" *Food Chemistry* **1996**, 57, 51-55.

(37) Oomen, C. M.; Ocké, M. C.; Feskens, E. J. M.; Erp-Baart, M. A. J. "Association between trans fatty acid intake and 10-year risk of coronary heart disease in the Zutphen Elderly Study: a prospective population-based study" *The Lancet* **2001**, 357, 746-751.

(38) Burton, G. W.; Ingold, K. U. "Autoxidation of biological molecules. 1. Antioxidant activity of vitamin E and related chain-Breaking Phenolic Antioxidants in Vitro" *Journal of the American Chemical Society* **1981**, 103, 6472-6477.

(39) Turro, N. J.; Ramamurthy, V.; Scaiano, J. C. "Principles of Molecular Photochemistry: An Introduction"; *University Science Publishers*: New York, N.Y., **2008**, pp 493.

(40) Lakowicz, J. R. "Principles of Fluorescence Spectroscopy"; *Kluwer Academic/Plenum*: New York, **1999**, pp. 698.

(41) Tsien, R. Y. "The Green Fluorescent Protein" *Annual Reviews in Biochemistry* **1998,** 67, 509-544.

(42) Aliaga, C.; Aspee, A.; Scaiano, J. C. "A New Method to Study Antioxidant Capability: Hydrogen Transfer from Phenols to a Prefluorescent Nitroxide" *Organic Letters* **2003**, 5, 4145-4148.

(43) Aliaga, C.; Stuart, D. R.; Aspée, A.; Scaiano, J. C. "Solvent effects on hydrogen abstraction reactions from lactones with antioxidant properties." *Organic Letters* **2005**, 7, 3665-3668.

(44) Aliaga, C.; Jua´rez-Ruiz, J. M.; Scaiano, J. C.; Aspee, A. "Hydrogen-Transfer Reactions from Phenols to TEMPO Prefluorescent Probes in Micellar Systems" *Organic Letters* **2008**, 10, 2147-2150.

(45) Soh, N.; Sakawaki, O.; Makihara, K.; Odo, Y.; Fukaminato ..., T. "Design and development of a fluorescent probe for monitoring hydrogen peroxide using photoinduced electron transfer" *Bioorganic & Medicinal Chemistry* **2005**, 13, 1131-1139.

(46) Scaiano, J. C.; Laferriere, M.; Ivan, M. G.; Taylor, G. N. "A Protocol for the Verification of Acid Generation in 157 nm Lithography" *Macromolecules* **2003**, 36, 6692-6694.

(47) Bonini, M.; Rota, C.; Tomasi, A.; Mason, R. "The oxidation of 2′,7′-dichlorofluorescin to reactive oxygen species: A self-fulfilling prophesy?" *Free Radical Biology and Medicine* **2006**, 40, 968-975.

(48) Dickinson, B. C.; Chang, C. J. "A Targetable Fluorescent Probe for Imaging Hydrogen Peroxide in the Mitochondria of Living Cells" *Journal of the American Chemical Society* **2008**, 130, 9638-9639.

2. Dimers of Persistent Carbon-Centered Radicals: Synthesis and Properties

2.2 Graphical Abstract

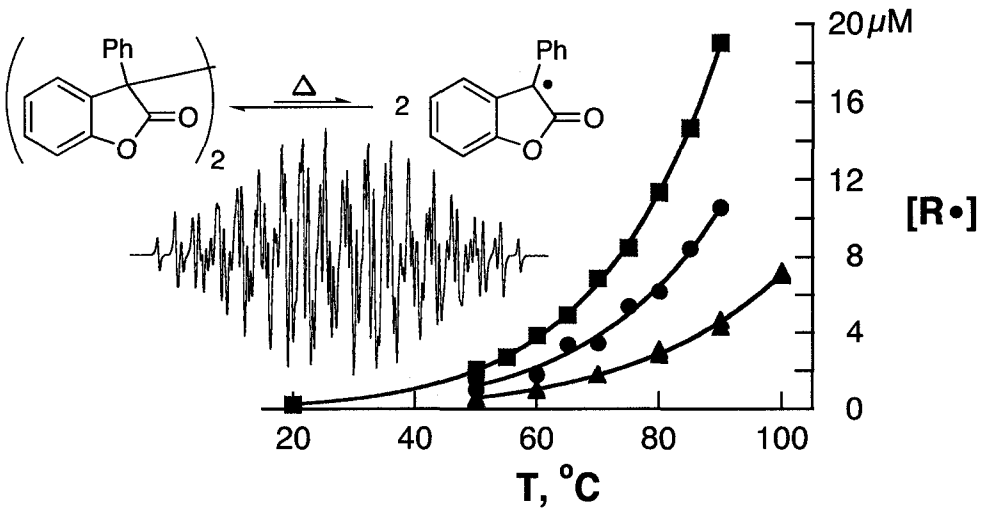

2.3 Persistent Carbon-Centered Radicals

The terms *transient*, *stabilized*, *persistent* and *stable* can describe a radical; in the order presented, they indicate a decrease in reactivity (or increase in lifetime). A *stable* radical is one you store in a bottle. The best-known examples are DDPH• and TEMPO•, but such stable radicals are the exception rather than the rule. On the other end of stability, CH_3• and HO• are *transient* because they have short lifetimes. Transient radicals undergo fast reactions with surrounding molecules and their self-reaction rates, if such reactions occur, are close to diffusion-controlled. Most radicals are short-lived (and transient) because radical reactions typically have low activation energies and fast reaction rates. With the exception of CH_3• and HO•, most radicals are also *stabilized* (or destabilized) by substituents—benzyl radicals are delocalized on phenyl groups and tert-butyl radicals are stabilized by hyperconjugation.

Ingold and Griller introduced the term *persistent* to describe a radical that does not undergo "fast" reactions with its surroundings.[1] Of course, the surroundings can be changed to make a radical more or less persistent. For example, Gomberg's triphenylmethyl radical is not persistent under aerated solution;[2] as most do carbon-centered radicals, it reacts with oxygen. In this chapter, I will describe air-stable, persistent carbon-centered radicals that can dissociate after self-reactions.

2.4 Carbon-Centered Radicals with Reduced Reactivity Towards Oxygen

Before I joined, several Scaiano group members investigated carbon-centered radicals with reduced reactivity towards oxygen using laser-flash photolysis. This work was inspired by an unusual antioxidant—CIBA's Irganox HP-136® (Scheme 2-1).[3] This antioxidant is unusual because the radical generated after H-atom donation is a carbon-centered radical. Scaiano was the first to accurately measure the rate constant between carbon-centered radicals and oxygen[4] and he found this number to be close to diffusion-controlled for all carbon-centered radicals investigated. This led to the questions: How can HP-136 be an antioxidant? Why doesn't the newly formed HP-136 radical react with oxygen to further propagate the autoxidation process?

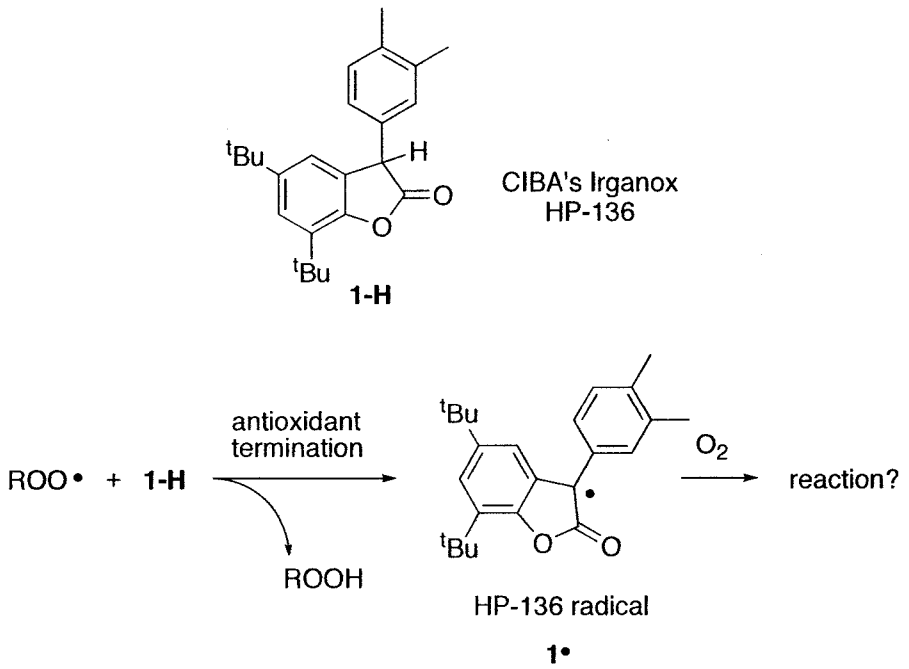

Scheme 2-1. CIBA's Irganox HP-136® (shown above) is the first commercial antioxidant that generates a carbon-centered radical (1•) after antioxidant termination. Our group wondered if this carbon-centered radical would react with oxygen to propagate the chain, as do most carbon-centered radicals.

Over the course of their work, my co-workers observed that HP-136 radical and other classes of carbon-centered radicals were unreactive towards oxygen.[5-9] I will briefly describe how the reactivity of carbon-centered radicals with oxygen was investigated using laser-flash photolysis. Di-*tert*-butylperoxide is photochemically cleaved using short (~10ns) pulsed laser irradiation to generate the highly reactive *tert*-butoxyl (^{t}BuO•) radicals in an inert solvent such as benzene, eq [1]. The ^{t}BuO• radicals then rapidly react ($k_{H\text{-}abs}$~10^6-10^7 $M^{-1}s^{-1}$) with the H-atom donors (R-H) to yield the carbon-centered radical of interest (R•). Since the carbon-centered radicals studied were delocalized, they exhibited strong absorbance in the ultraviolet and

visible region that could be monitored using time-resolved UV-Vis spectroscopy. The growth and decay of R• could then be monitored with and without the presence of oxygen. If R• reacts with O_2, the absorbance due to the carbon-centered radical would disappear faster (be quenched) by the presence of oxygen. If R• is inert to O_2, the transient absorbance should not change whether oxygen is present or not.

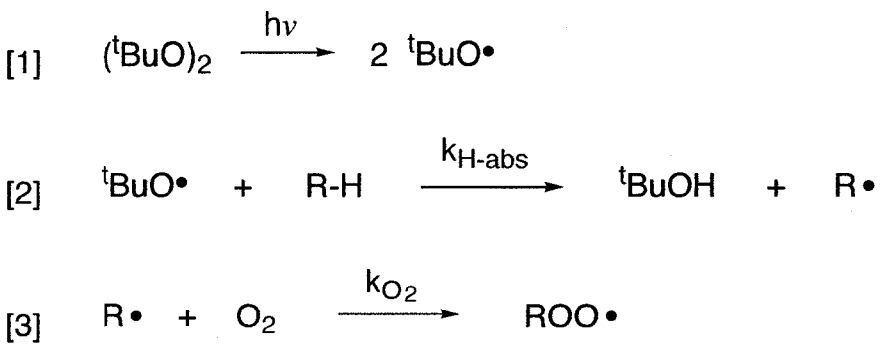

Carbon-centered radicals that do not react with oxygen (and some that do) are presented in Scheme 2-2. In this thesis, "no reaction" with oxygen implies that their transient absorbance was not affected by the presence of oxygen in the timescale of the laser experiment (~100μs). This effectively puts an upper limit for the reactivity of these carbon-centered radicals with oxygen (k_{O_2}) of about 5×10^3 $M^{-1}s^{-1}$; remarkably, this is over 10000 times slower than most carbon-centered radicals.[4]

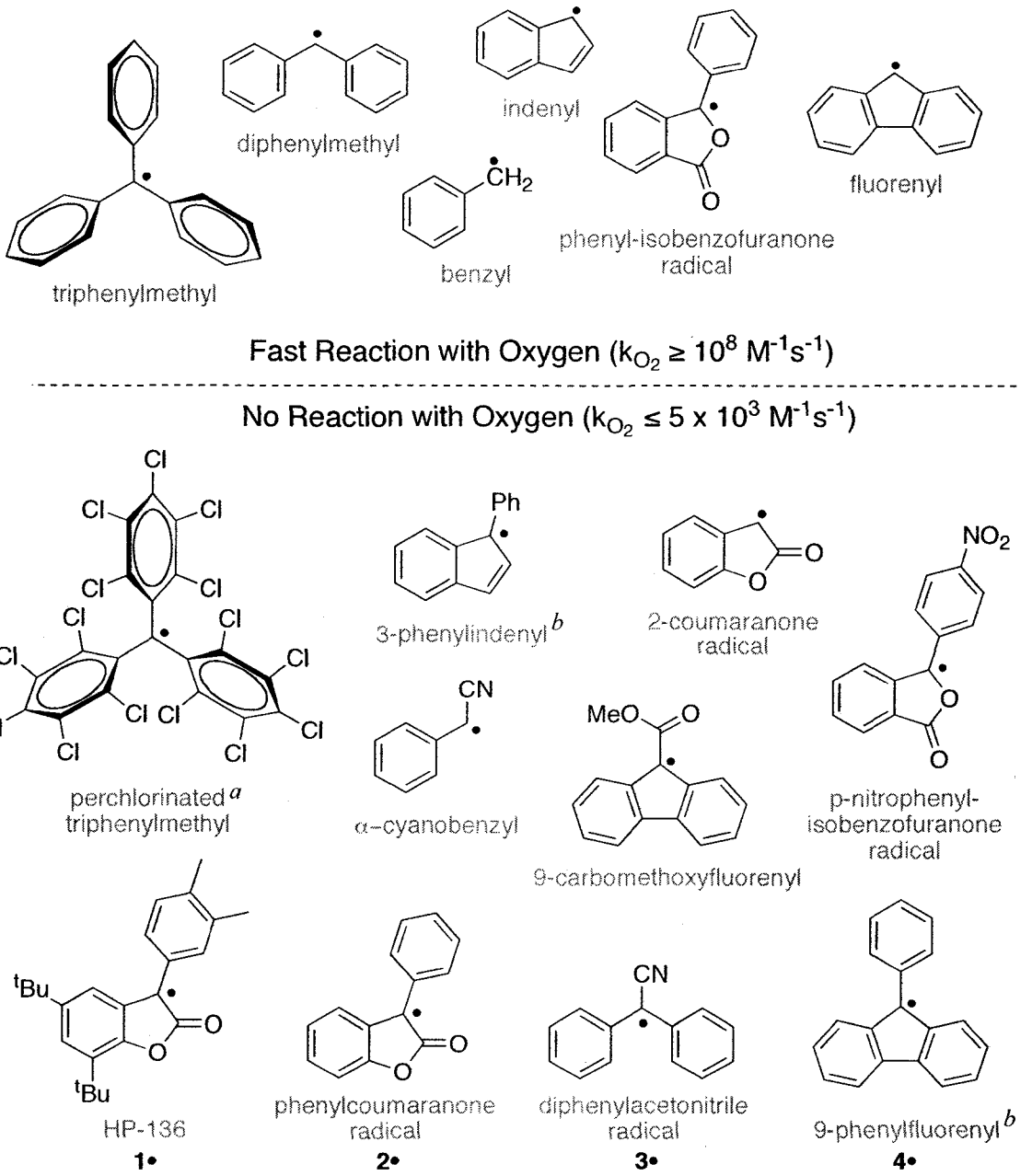

Scheme 2-2. Most carbon-centered radicals react with molecular oxygen at rates approaching diffusion-controlled ($k_{O_2}>10^8 M^{-1}s^{-1}$). Scaiano and co-workers observed that some carbon-centered radicals with rather simple structures do not react with molecular oxygen ($k_{O_2}\leq 5x10^3 M^{-1}s^{-1}$). [a]From Ballester's work[10] [b]3-phenyl-indenyl ($k_{O_2}=8.2x10^5 M^{-1}s^{-1}$) and 9-phenylfluorenyl ($k_{O_2}=7.6x10^5 M^{-1}s^{-1}$) react with O_2 at higher rates.

From the list of radicals shown above (and many others), Scaiano and co-workers put forward 5 parameters that contribute to the lack of reactivity of carbon-centered radicals towards oxygen.

(i) Steric effects

(ii) Benzylic resonance delocalization

(iii) Unpaired spin delocalization on heteroatoms

(iv) Favorable stereoelectronic effects

(v) Electron-withdrawing effects

In cases such as perchlorinated triphenylmethyl radicals, steric hindrance plays a major part in the lack of reactivity towards oxygen. In most radicals, however, sterics are not the deciding factor. For example, the propeller-shaped triphenylmethyl is certainly more sterically hindered than α-cyanobenzyl while this latter radical is more inert towards oxygen.[7]

Benzylic delocalization does stabilize a radical and, as expected, a stabilized radical is less reactive than an unstabilized radical (this includes reactions toward oxygen). This effect is demonstrated with the comparison of fluorenyl vs. 9-phenylfluorenyl; the former reacts with oxygen over 100 times faster than the latter.[8]

Most stable radicals are centered on heteroatoms such as 2,2,5,5-tetramethylpiperidine-N-oxyl (TEMPO•, nitrogen/oxygen centered) and N-diphenyl-N'-picric hydrazyl (DPPH•, nitrogen centered). Similarly, carbon-centered radicals that have significant spin-delocalization on heteroatoms display reduced reactivity towards oxygen. Additionally, the forced co-planarity of a radical allows for better delocalization of the unpaired electron. By this we mean that a propeller-shaped radical—such as triphenylmethyl radicals—can become more stabilized by changing the structure to allow a better delocalization—as in the case of 9-phenylfluorenyl radicals. Basically, the imparted stabilization reduces the reactivity of the radical.

The last parameter—electron-withdrawing effects—is particularly important. Since oxygen is electrophilic, a carbon-centered radical that is also electrophilic will reduce the reactivity between the two. This effect is demonstrated by the addition of a nitro-group to phenyl-isobenzofuranyl (which reacts with O_2) to give p-nitrophenyl-isobenzofuranyl radical (non-reactive). The structure of HP-136 radical, my personal favorite, scores on these five parameters and is particularly inert to oxygen.

2.5 Synthesis of Persistent Carbon-Centered Radical Dimers

My first assignment in the Scaiano group was to synthesize the dimers of these persistent, air-stable carbon-centered radicals. Over the next five years, I applied several successful synthetic strategies to make these weakly bound dimers; some are shown in Scheme 2-3. In this chapter, the focus will center on 4 dimers that were particularly well behaved; we introduce the nomenclature 1_2, 2_2, 3_2 and 4_2 for the dimers derived from radicals 1•, 2•, 3• and 4•. Notably, these four dimers appeared stable as crystalline solids and in solution; they could be heated and cooled without spectroscopic change. Other dimers including 9-carbomethoxy-fluorenyl dimer decomposed upon heating in solution and secondary radicals such as 2-coumaranone radicals generate unstable dimers that were not isolated from synthesis. These non-ideal examples will not be discussed further.

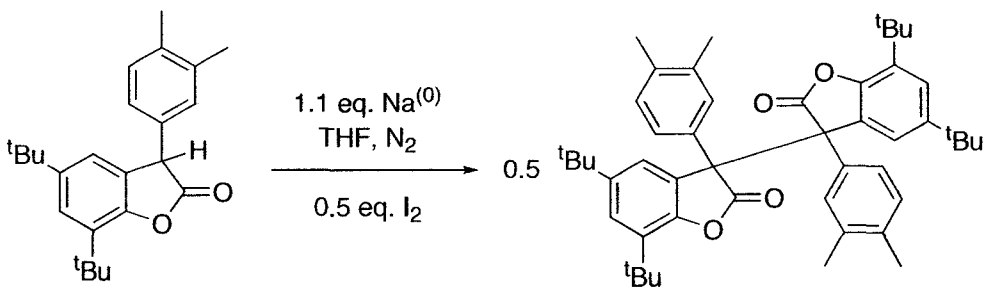

CIBA Irganox HP-136
1-H

HP-136 dimer
1_2

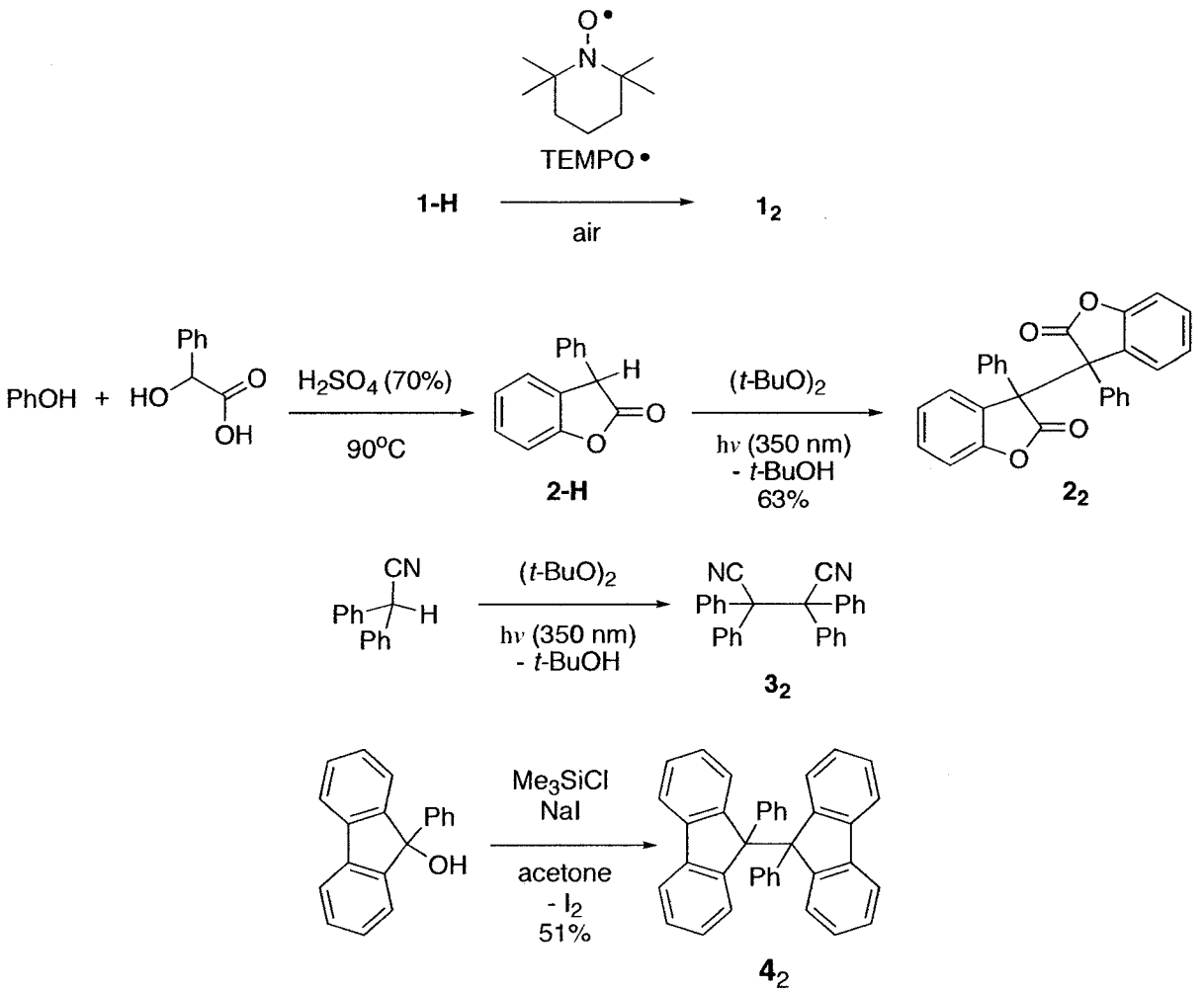

Scheme 2-3. Successful synthetic approaches used to make persistent carbon-centered radical dimers.

To synthesize the HP-136 dimer (1_2) from 1-H, we initially employed the same approach reported to make dimer 2_2—treatment with metallic sodium followed by oxidation with iodine.[11] This harsh treatment, however, led to low yields and complicated product mixtures. It is known that bases can lead to the opening of the lactone ring in similar compounds.[12] We recently employed a reaction with better yields and trivial purification for making 1_2 (and other dimers not discussed here).

Tetramethylpiperidine-N-oxide radical (TEMPO•) under air is used to oxidize 1-H to 1_2 in over 50% isolated yields. These reactions are performed under air, without stirring and the product crystallizes out of the reaction overnight; this synthesis couldn't be easier.

As photochemists, we also turned to light as a synthetic strategy to make these dimers. This approach is basically a large-scale version of the laser-flash photolysis experiments (eq [1] and [2]) using UV lamps instead of lasers for irradiation. I made over 100 grams of dimers 1_2, 2_2 and 3_2 using this reasonably clean photochemical synthesis. And finally, the conversion of 9-phenyl-9-fluorenol to dimer 4_2 was done by a tandem-reaction; Me_3Si-I is first generated in situ from NaI and Me_3SiCl (NaCl precipitates in acetone) and the alcohol is added to this solution. Immediately, the solution turned brown due to the release of I_2. Presumably, the iodine is the by-product of an impressive number of fast transformations occurring at the 9-fluorenyl position: alcohol to silyl protection to cation to iodide to radical to dimer. These last three synthetic approaches are original contributions to make symmetric quaternary carbon-carbon bonds.

We obtained crystals for dimer 1_2 suitable for structure determination, which we compare to the reported crystal structures of dimers 2_2 (from ref [13]) and 3_2 (from ref [14]) in Figure 2-1. The crystal structure of dimer 4_2 has not yet been reported. In all cases, the central C-C bonds are much longer than the typical 1.54 Å. Note that

more than one conformer is possible for dimer 1_2 and 2_2. In solution, it appears that more than one conformer exists as seen by the change in ^1H NMR in function of temperature (data not shown). Fellow graduate student Vasilisa Fillippenko is currently investigating this effect which was previously observed for 9-cyanofluorenyl dimers.[15]

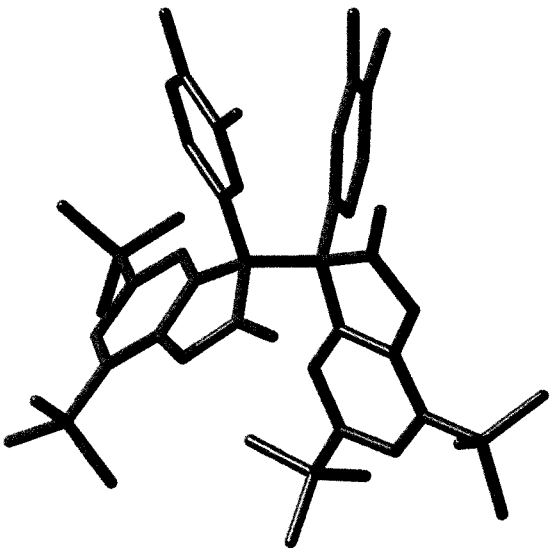

Dimer 1_2

Bond lengths (Å):
Central C-C **1.586**

Dihedral Angle:
Ph-C-C-Ph **59.0°**

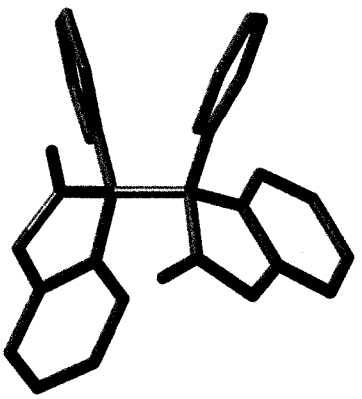

Dimer 2_2

Bond lengths (Å):
Central C-C **1.593**

Dihedral Angle:
Ph-C-C-Ph **60.8°**

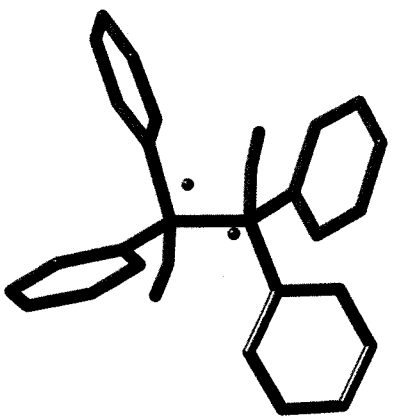

Dimer 3_2

Bond lengths (Å):
Central C-C **1.608**

Dihedral Angle:
CN-C-C-CN **171.4°**

Figure 2-1. Crystal structures for dimers 1_2 (this work), 2_2 (from ref [13]) and 3_2 (from ref [14]). The two dots in 3_2 are the result of disorder in the crystal.

2.6 Studying the Radical-Dimer Equilibrium in Solution

In solution, dimers 1_2 – 4_2 exist in thermal equilibrium with their radical form, e.g., Scheme 2-4. Increasing the temperature causes more dimers to dissociate to coloured radicals as can be seen by the naked eye. For example, a solution of HP-136 dimer turns blue upon heating (see Figure 2-2) and this colour disappears upon cooling. This effect has been observed previously for dimer 2_2.[11]

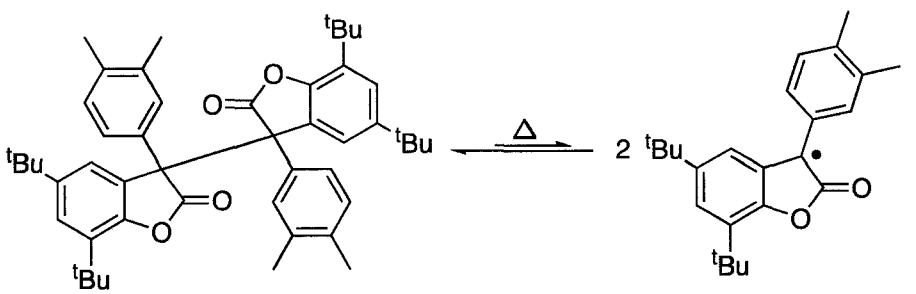

Scheme 2-4. Dimer-radical equilibrium for HP-136 dimer.

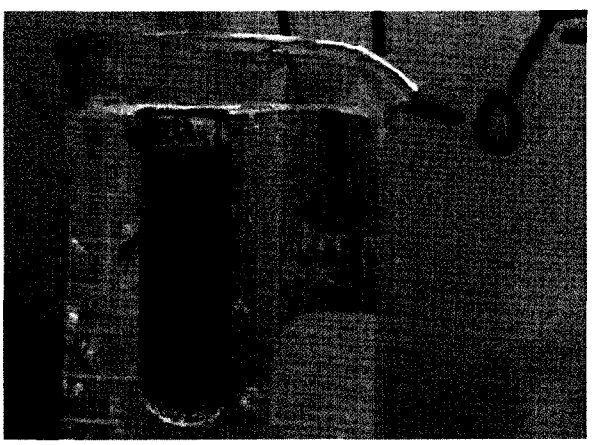

Figure 2-2. Heating HP-136 dimer in toluene (open to air) generates a persistent, blue-coloured radical (1•). This picture is extracted from a video that is available online as Supporting Information for ref [16].

2.6.1 *Variable-Temperature Absorbance of Dimer-Radical Systems*

Radicals 1• – 4• show strong absorbance in the ultraviolet and visible regions that could be used to monitor the dissociation of dimers. The absorbance spectra of dimers 1_2 – 4_2 taken at different temperatures are shown in Figure 2-3.

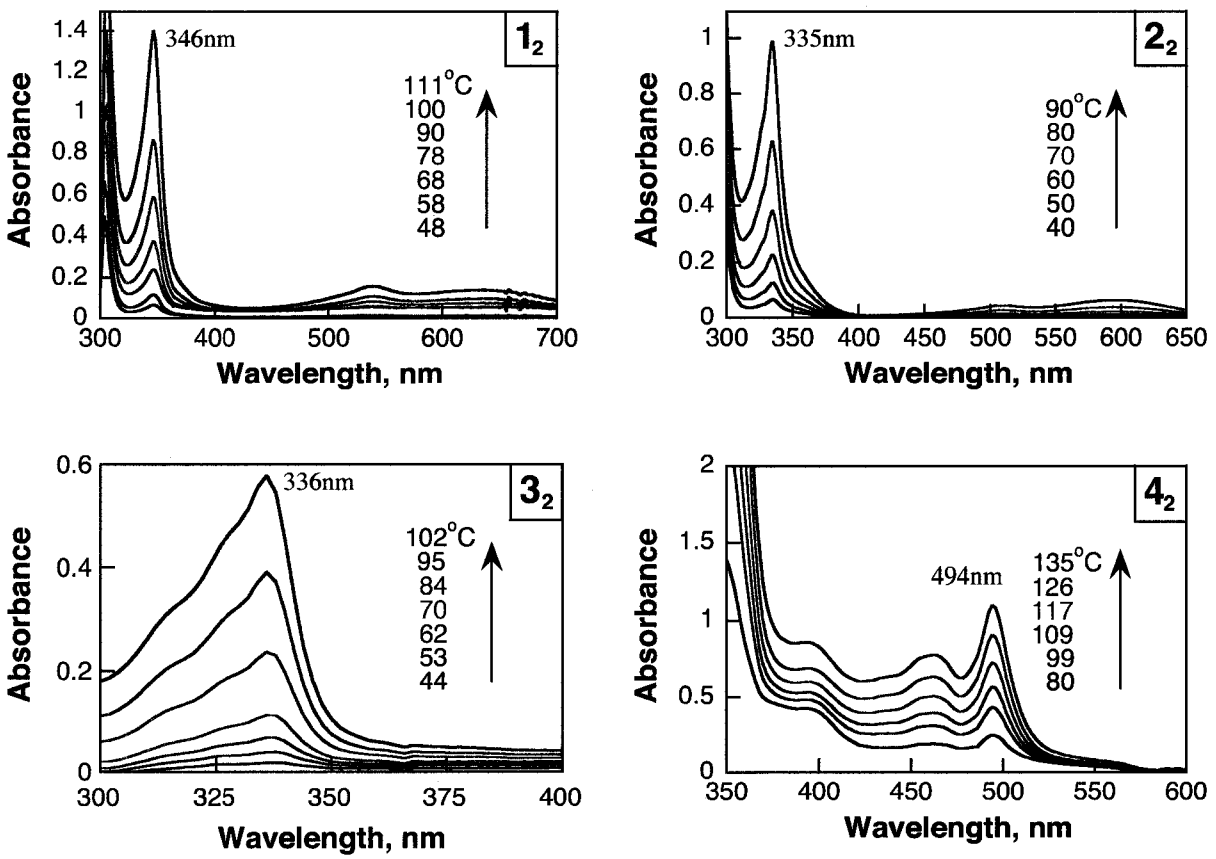

Figure 2-3. UV-visible absorbance spectra of dimers under nitrogen showing the increasing radical concentration with increasing temperature: 1_2 in toluene (10mM), 2_2 in toluene (20.8mM), 3_2 in toluene (17.4mM) and 4_2 in 1,3-dichlorobenzene (6.9mM). Acquisition temperatures and λ_{MAX} are indicated in each graph. The dimer solution at low temperature (<20°C) was taken as the "zero" therefore the absorbance seen here is due to the radical only.

As expected, the absorbance change from thermal dissociation of dimers matched the absorbance of radicals generated during laser flash photolysis experiments.[5-8]

Bond Dissociation Energies (BDE) can be estimated for these systems from the variable temperature UV-Visible absorbance using a modified van't Hoff equation. The original van't Hoff equation, eq [4], relates enthalpy and entropy with the equilibrium constant. The equilibrium constant for the dissociation of dimers is $K_{eq} = [R\bullet]^2/[R\text{-}R]$ where R• and R-R are the radical and dimer, respectively. In our case, ΔH represents the central carbon-carbon BDE. Assuming the dimer concentration, [R-R], to be constant (*vide infra*) and relating the absorbance (A) and concentration of radicals with Lambert-Beer's law, eq [5], the equation can be rearranged to eq [6].

[4] $$\ln K_{eq} = \ln\left(\frac{[R\bullet]^2}{[R-R]}\right) = \frac{-\Delta H}{RT} + \frac{\Delta S}{R}$$

[5] $$A = \varepsilon[R\bullet]l$$

[6] $$\ln A = \frac{-\Delta H}{2RT} + \frac{\Delta S}{2R} + \frac{\ln(\varepsilon^2 l^2 [R-R])}{2}$$

Equation [6] shows that a plot of ln *A* against the reciprocal temperature will yield -ΔH/2R from the slope. The last term of this equation includes the extinction

coefficient of the radical species (ε) and this number, if known, often carries significant error. Fortunately, the BDE can be estimated without the knowledge of the radical's extinction coefficient using this technique. Excellent linear correlation between ln *A* vs T^{-1} were obtained for dimers 1_2 – 4_2 (Figure 2-4) from which the corresponding carbon-carbon BDE were estimated; these are listed in Table 2-1.

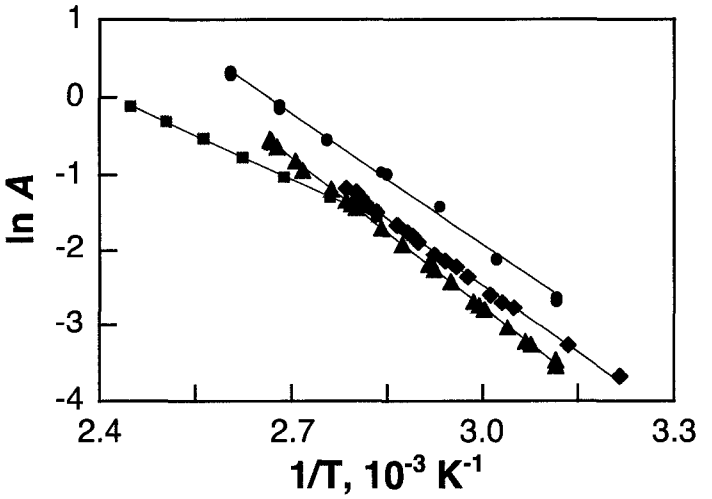

Figure 2-4. Van't Hoff plot according to eq [6] for dimer 1_2 (•), 2_2 (◆), 3_2 (▲) in toluene and 4_2 (■) in 1,3-dichlorobenzene under nitrogen. The slope of ln *A* vs 1/T gives a slope equal to -ΔH/2R according to eq [6]. The monitoring wavelengths for each radical are noted in the absorbance traces of Figure 2-3.

The assumption that the dimer concentration is constant is easily met by the systems under study. In the case of 1_2 for example, the absorbance at 111°C (the highest temperature used) is approximately 1.4 for an optical path of 1 cm and dimer concentration of 0.01 M. We used of a previously reported method[17] to estimate a radical molar absorption coefficient (ε) of 37 500 $M^{-1}cm^{-1}$ for 1• at 346 nm. From this

we evaluate a radical concentration of $3.7x10^{-5}$ M, or a dimer conversion of 0.19%, low enough to assume a constant dimer concentration.

Table 2-1. Monitoring wavelength, bond dissociation energies (BDE) and C-C bond length for dimers $1_2 - 4_2$ in toluene, under nitrogen.

Radical	Monitoring λ_{max} (nm)	Temperature range (°C)	C-C bond length (Å)	BDE (kcal mol^{-1})[e]
1•	346	48 – 111	1.586[a]	23.2
2•	336	37 – 100	1.596[b]	25.4
3•	336	48 – 102	1.608[c]	26.2
4•	494	80 – 135	1.653[d]	15.6

[a] From the crystal structure. [b] reference[13] [c] reference[14] [d] From density functional calculation using B3LYP/6-31g(d). [e] ± ~1 kcal/mol

The BDE values obtained for dimers $1_2 - 4_2$, ranging from 15 to 26 kcal/mol, are remarkably low for carbon-carbon bonds. Ethane for example has a BDE of 90 kcal/mol.[18] Some lower carbon-carbon BDEs have been reported in the literature, including the triphenylmethyl dimer (10.7 kcal/mol in benzene)[19] and the dimer derived from phenalenyl radicals (9.8 kcal/mol in toluene).[20] The triphenylmethyl and phenalenyl carbon-centered radicals, however, form "head-to-tail" dimers unlike the "head-to-head" dimers described in this chapter. As do most carbon-centered radicals, triphenylmethyl and phenalenyl radicals also react with oxygen (although the latter compound does so more slowly).[20]

2.6.2 *Variable-Temperature EPR Study of Dimer-Radical Systems*

From the variable-temperature UV-Vis experiments, we were able to estimate BDEs, but not ΔS or absolute radical concentrations. For this reason we decided to investigate the dissociation of dimers by Electron Paramagnetic Resonance (EPR) spectroscopy. Using EPR, we can quantify the concentration of radicals in solution using a stable radical as calibration. The nitroxide 4-oxo-TEMPO• was used in our case because of its simple, three-line EPR spectrum that could easily be integrated. The dimer 4_2 was not pursued in these investigations due to its poor solubility in non-polar solvents. Polar solvents necessary to dissolve dimer 4_2 complicate EPR spectroscopy due to their ability to absorb microwaves.

The radicals gave highly complex EPR signals resulting from hyperfine coupling with the aromatic hydrogen (and nitrogen in the case of diphenylacetonitrile radical). The EPR spectrum for radical 2• has been reported previously and we obtained a similar spectrum in this work. The EPR of radicals 1• and 3• are reported here for the first time; the full interpretation of EPR spectra shown in Figure 2-5 has yet to be resolved. Still, there is no doubt that the EPR signals are due to the radicals 1• – 3• formed by dissociated dimers $1_2 - 3_2$.

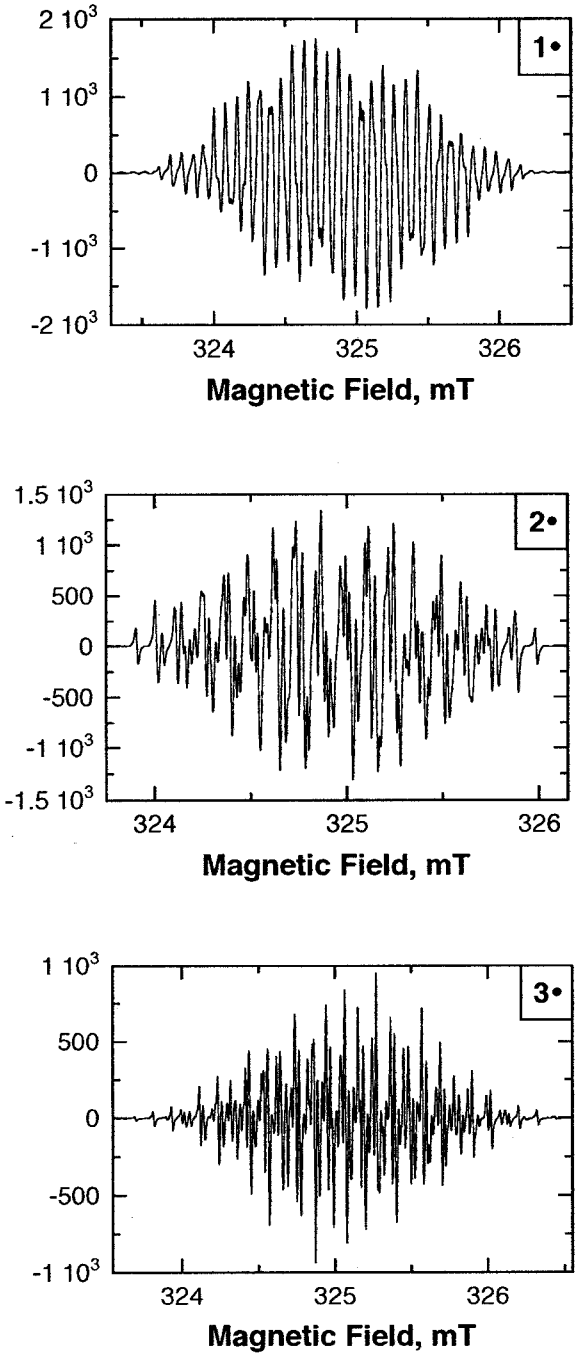

Figure 2-5. Steady-state EPR spectra of radicals 1•, 2• and 3• in toluene under nitrogen afforded by the thermal dissociation of dimers 1_2 (4.76mM, 90°C), 2_2 (20.7mM, 90°C), and 3_2 (20.1mM, 100°C).

The variable-temperature EPR spectra of dimers 1_2, 2_2 and 3_2 were twice-integrated at each temperature and calibrated using 4-oxo-TEMPO.[20] From these EPR integrations, we could estimate absolute radical concentrations for radicals 1• – 3•. Finally, from the absolute radical concentration, the van't Hoff equation, ln K_{eq} = ln([R]^2/[R-R]) = -ΔH/RT + ΔS/R, could be used directly. Excellent linear correlations (R^2>0.99) were obtained from the plot of ln K_{eq} vs. 1/T and the thermodynamic properties extracted from these plots are summarized in Table 2-2. Bond dissociation energies (BDE) and dissociation entropies (ΔS) were estimated from the slope and y-intercept of Figure 2-7, respectively. These thermodynamic parameters completely describe the equilibrium for dimers 1_2, 2_2 and 3_2.

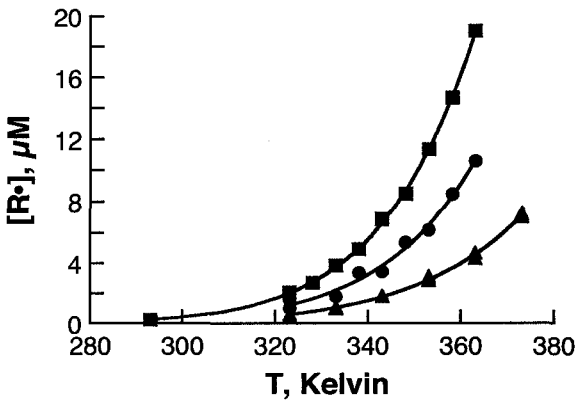

Figure 2-6. Absolute concentration of radicals 1_2 (•), 2_2 (♦), and 3_2 (▲) in toluene under nitrogen afforded by the thermal dissociation of dimer 1_2 (20.6mM), 2_2 (20.7mM), and 3_2 (20.1mM).

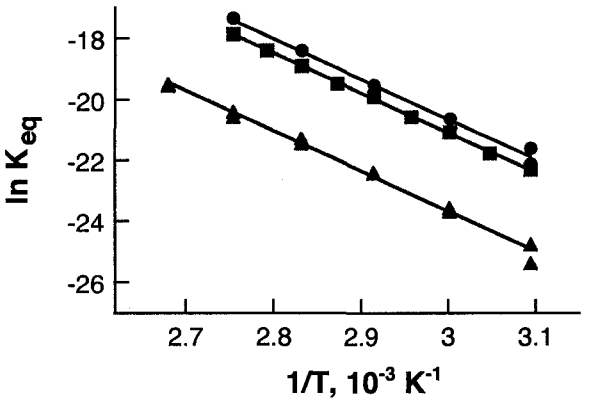

Figure 2-7. **The plot of ln K_{eq} vs 1/T according to the van't Hoff equation (eq [4]) for dimers 1_2 (•), 2_2 (♦), and 3_2 (▲) in toluene under nitrogen. The slope and intercept of these lines are equal -ΔH/2R and ΔS/2R, respectively.**

Table 2-2. **Bond dissociation energies (BDE) and entropy change (ΔS) for the dissociation of dimers 1_2, 2_2 and 3_2 in toluene, under nitrogen, as determined using variable-temperature EPR spectroscopy. Comparison with variable-temperature UV-visible data gave good estimates of molar absorption coefficient (ε) at the absorption maximum (λ_{MAX}) for the corresponding radicals 1•, 2• and 3•.**

Dimer	BDE [a] (kcal mol^{-1})	ΔS [b] (cal K^{-1} mol^{-1})	λ_{MAX} (nm)	ε ($M^{-1}cm^{-1}$)
1_2	25.2	31.3	346	80000
2_2	24.5	31.4	336	44000
3_2	26.3	31.8	336	65000

[a] ± ~1 kcal mol^{-1}. [b] ± ~ 2 cal K^{-1} mol^{-1}.

2.7 Some Reactivity of Carbon-Centered Radicals with Oxygen

Earlier we introduced carbon-centered radicals showing "no" reactivity to oxygen based on laser-flash photolysis data. The radicals, however, are not completely inert under air. In some variable temperature experiments where oxygen was introduced during variable-temperature heating of dimer 3_2, we observed the growth of a yellow compound indicating oxygen-induced decomposition. Lam and Liang were able to isolate the peroxide of dimer 3_2 from prolonged heating of diphenylacetonitrile (3-H) with di-tert-butylperoxide under air indicating some reaction of 3• with oxygen (Figure 2-8).[14]

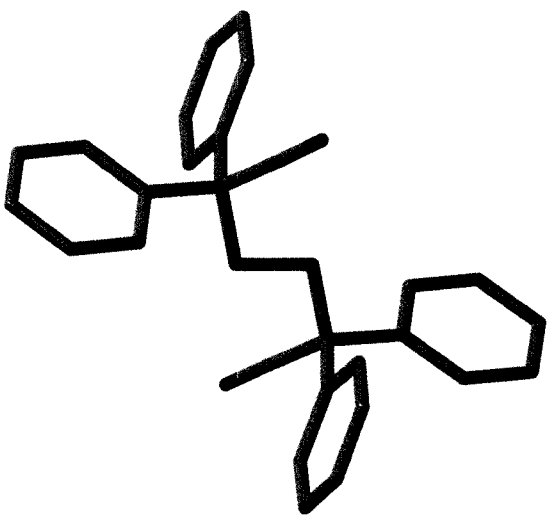

Figure 2-8. Crystal structure for bis-diphenylacetonitrile peroxide.[14] Bond lengths in Å: C-CN (1.493), C≡N (1.140), C-O (1.433), and O-O (1.4895). Dihedral angles: C-O-O-C (180°) and O-O-C-CN (60.8°). Atom colours: C are grey, O are red, and N are blue.

I also found that 4_2 under conditions of thermal dissociation under air eventually forms bis-9-phenylfluorene peroxide. This peroxide is probably the result of trapping of a small concentration of peroxyl radicals by a large excess of the carbon-centered radical in an excellent example of the operation of the Fischer-Ingold persistent free radical effect.[1,21] The structure of the bis-9-phenylfluorene peroxide, shown below, was confirmed by X-ray diffraction.

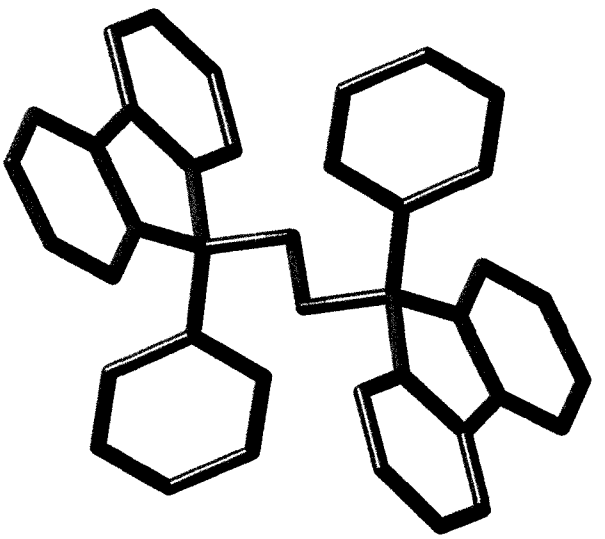

Figure 2-9. 9-Phenylfluorenyl dimer (4_2) was left in aerated solution at room temperature for over one week from which crystals of this symmetric peroxide were isolated. Bond lengths in Å: C-O (1.446) and O-O (1.498). Dihedral angles: C-O-O-C (180°) and Ph-C-O-O (65.7°). Atom colours: C are grey, O are red.

We could find no peroxides for dimers 1_2 and 2_2. Magnus and co-workers did find that heating a dimer similar to 2_2 under air generated a semiquinone in low yields (<5%)[22] (Scheme 2-5). The yield of semiquinone was higher if TEMPO• is added. Interestingly, alkyl substituents in the structure of HP-136 radical prevents

the formation of semiquinones and other non-ideal behavior. Indeed, CIBA's Irganox HP-136® was well designed to prevent reactions with oxygen.

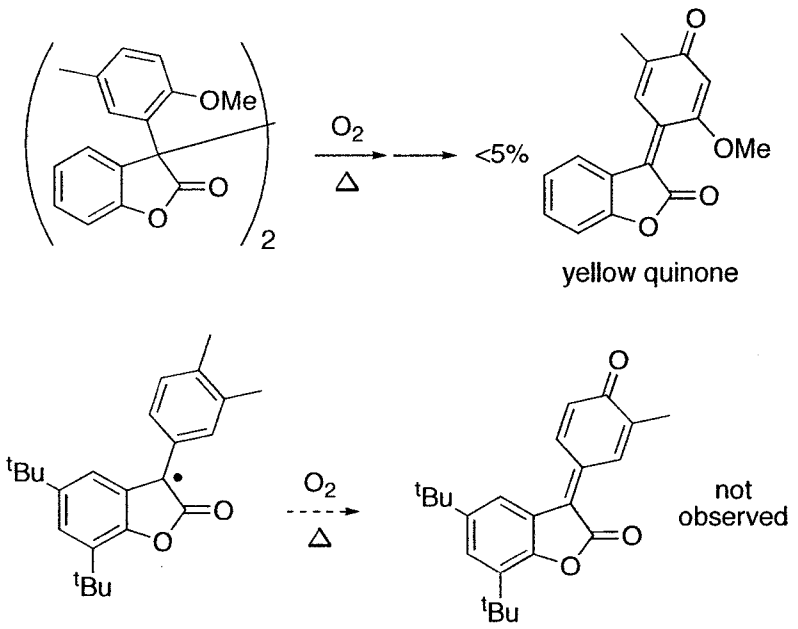

Scheme 2-5. Magnus and co-workers reported that heating dimer 2_2 under air for prolonged periods generated a small amount of semiquinone.[22] Alkyl substituents on the HP-136 radical prevent such reactions.

2.8 Discussion

Radicals are only reactive if given the opportunity. For this reason, the majority of persistent radicals are sterically hindered. Like putting a lion in a cage, even a phenyl radical can have an appreciable lifetime with strategically placed tert-butyl groups.[23] Starting with triphenylmethyl radicals introduced in 1900, persistent carbon-centered radicals have been the subject of curiosity for over a century[24] (with some hints at applications such as oxygen sensors[25]). The majority of persistent radicals are based on the triarylmethyl template. It has been suggested that the persistence of propeller-shaped triarylmethyl radicals can be attributed in large part to sterical hindrance.[1] In the case of perchlorinated triarylmethyl radicals, the radical center is particularly inert. In most other radicals, sterical hindrance may slow down reactions such as H-abstraction, but this effect alone rarely prevents reactions with the small oxygen molecule.

The radicals 1• – 4• discussed in this chapter are persistent, even under air. This lack of reactivity with oxygen cannot be attributed solely to steric hindrance. For example they dimerize via the central carbon, a far more sterically demanding process. An air-stable carbon-centered radical must therefore benefit from favorable electronic effects. While both electron-donating groups (EDG) and electron-withdrawing groups (EWG) can stabilize carbon-centered radicals, it was found that electron-withdrawing effects were particularly important to prevent their reactivity

with O_2. EDG-stabilized carbon-centered radicals, on the other hand, can form stronger bonds with oxygen due to hyperconjugation.[26] Simplistically, it can be said that electron-deficient carbon-centered radicals will react slower with electron-deficient oxygen.

$$R\bullet + O_2 \underset{k_\beta}{\overset{k_{O_2}}{\rightleftharpoons}} ROO\bullet$$

The low rates of reaction with oxygen for radicals 1•-4• can be understood as the dissociation reaction being faster than addition ($k_\beta > k_{O_2}$). Many radicals form reversible bonds with molecular oxygen—for example the reversible addition-dissociation of oxygen to lipid pentadienyl radicals dictates the ratio of *cis,trans* and *trans,trans* lipid hydroperoxide. Under this system, the addition of oxygen to the central carbon of the pentadienyl radical dissociates much faster than oxygen bound to the end positions (see Chapter 1). Under normal conditions, the oxygen will dissociate from the central carbon of pentadiene before ensuing reactions with the surroundings. Recently, it was observed that this peroxyl radical could be trapped in high concentrations of α-tocopherol, an excellent H-atom donor.[27]

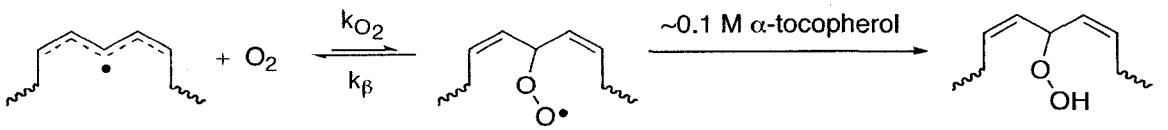

Carbon-centered radicals with low reactivity towards oxygen can therefore be understood as having faster dissociation (high k_β). The peroxyl radical formed, while presumably short lived, can react with surrounding molecules in certain conditions. We showed that 9-phenylfluorenyl radicals (4•) form symmetric peroxides after lengthy exposure to air, presumably by the reaction of the short-lived peroxyl radical with the surrounding carbon-centered radicals. The same was previously reported for diphenylacetonitrile radicals (3•). Benzofuranone radicals (1• and 2•) do not form peroxides, indicating a very fast k_β (and/or slow k_{O_2}). Interestingly, the rate of oxygen dissociation (k_β) will be faster at higher temperatures, so we can expect these radicals to display an even more reduced oxygen sensitivity at elevated temperatures.

Radicals 1• – 4• are remarkably well behaved for carbon-centered radicals. They form thermally labile dimers that could be heated and cooled without spectroscopic change. The concentration of radicals in toluene under nitrogen was constant for hours at elevated temperatures. And their lack of reactivity with oxygen made them particularly easy to handle. We used UV-Visible and EPR spectroscopy to measure thermodynamic properties of the dimer-radical equilibrium. In the case of dimer 3_2, the measured BDE was in perfect agreement between the two techniques (26.2 and 26.3 kcal/mol). There is some variation between BDEs measured by UV-vis absorbance and EPR spectroscopy for dimers 1_2 and 2_2. The main reason for

this discrepancy, we believe, is the limited temperature range used for these experiments.

Both techniques and the data analysis have their inherent limitations as quantitative tools for thermodynamic parameters. For UV-Vis measurements, a number of effects can change the absorbance (and as a result, the BDE):

(i) Baseline shifting with increasing temperature. In toluene, the baseline absorbance increases by ~0.03 from 25°C to 100°C. The sharp growth in absorbance near 300 nm is also due to toluene. We remedied this potential problem by subtracting the absorbance by the absorbance value at a non-absorbing region, e.g., above 700 nm.

(ii) Spectral "contamination" by coloured by-products. This was a problem in some experiments with dimers 3_2 and 4_2 (particularly when oxygen was inadvertently introduced in the solution). This effect is easily noticed after an experiment where new absorbance peaks remain at lower temperatures.

(iii) Changes in molar absorption coefficient (ε) with temperature and solvent expansion. We did not correct for these effects.

Since EPR is more selective to the species of interest we believe the EPR results are more accurate, although again, a larger temperature range would be required to reduce the error on these measurements. At lower temperatures,

however, the radical signals are very weak and small variations in signal intensity at low temperatures induce significant errors in the BDE determination. At higher temperatures, we are limited by solvent evaporation (and potentially, decomposition reactions). In any case, the dimers 1_2 – 4_2 have much weaker BDEs than typical carbon-carbon bonds.

The ΔS^{298K} values obtained for the dissociation of dimers 1_2, 2_2, and 3_2 are similar in value—all three have $\Delta S^{298K} \approx 31$ cal/mol·K. This value is higher than the ΔS measured for the triphenylmethyl radical-dimer equilibrium (ΔS~20cal/mol•K, in benzene)[19] and the phenalenyl radical-dimer equilibrium (ΔS~12cal/mol•K, in toluene).[20] The difference between the ΔS for dimers 1_2, 2_2 and 3_2 vs. triphenylmethyl radicals and phenalenyl radicals can be justified by the bonding arrangements of the dimers (Scheme 2-6).

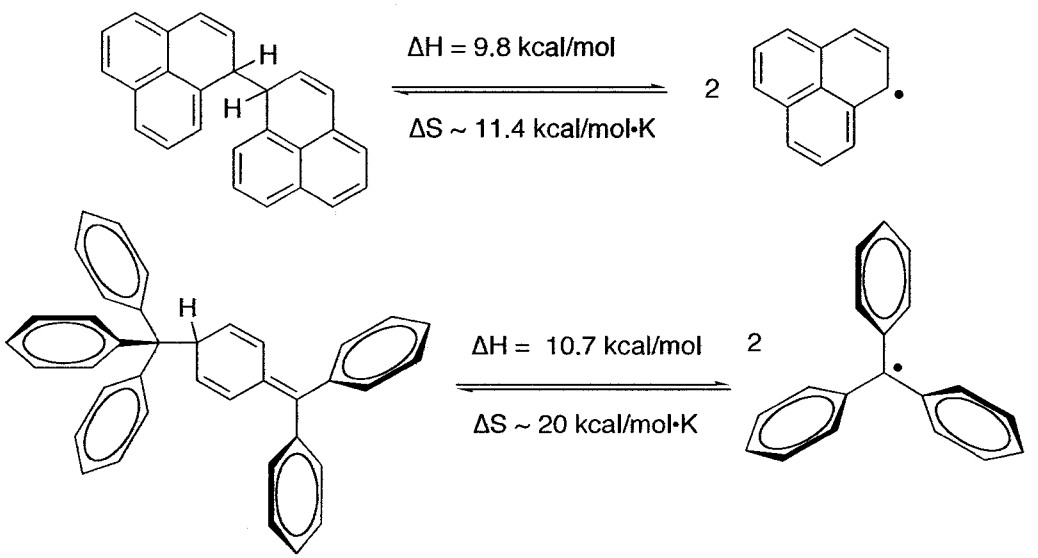

Scheme 2-6. Head-to-tail dimers from phenalenyl and triphenylmethyl radicals.

Since the dimers 1_2, 2_2 and 3_2 are bonded via the central carbon (head-to-head), the release in entropy upon dissociation is greater than dimers bonded in a "head-to-tail" arrangement. This latter geometry is less restrictive for the dimer and therefore, this arrangement is more free to move, i.e., greater entropy. The head-to-head dimers, on the other hand, are very restricted (lower entropy). We can then understand the greater entropic gain of separating dimers 1_2, 2_2 and 3_2 as a release of more restrictions than in the dimers from triphenylmethyl and phenalenyl.

2.9 Conclusions

We described the dimers of persistent carbon-centered radicals that have dramatically reduced reactivity with oxygen. In solution, the dimers exist in thermal equilibrium with the radical form which we studied using Variable-Temperature UV-Visible and EPR spectroscopy. Bond dissociation energies for these "head-to-head" dimers range from 15 to 26 kcal/mol. The thermodynamic properties estimated by EPR (shown below) can be used to estimate the radical concentrations [R•] at any given temperature or dimer concentration, [R-R];

$$[R\bullet] = [R-R]^{0.5} \exp(-\frac{\Delta H}{2RT} + \frac{\Delta S}{2R}).$$

Note: R = 8.314 J/(mol·K) = 0.001987 kcal/(mol·K)	ΔH kcal/mol	ΔS cal/mol.K	ε $M^{-1}cm^{-1}$
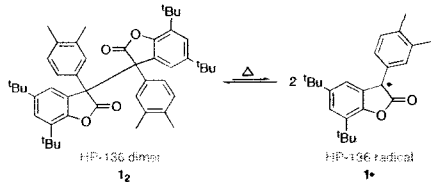	25.2	31.3	80000 (346nm)
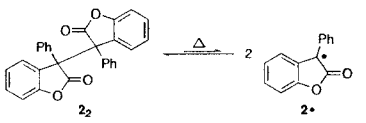	24.5	31.4	44000 (336nm)
	26.3	31.8	65000 (336nm)
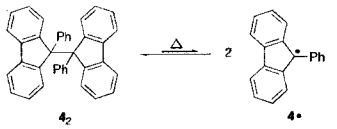	15.7	-	-

2.10 Experimental Details

Materials

All the chemicals were purchased from Aldrich unless specified otherwise. 3-phenyl-isocoumaranone was synthesized as previously described.[28] Irganox HP-136 was a generous gift from CIBA and was recrystallized before use to remove a minor isomer. ^{1}H and ^{13}C NMR spectra were recorded on a Bruker-Avance-300 spectrometer at 300 and 75.4 MHz, respectively. Mass spectrum (EI) was recorded on a Kratos-Concept-II instrument. Non-corrected melting point was determined on a Mel-Temp-II apparatus. The reactions were followed by TLC using precoated 0.25 mm thick silica gel 60 F254 on aluminium-backed plates using short wave UV light for compound detection. Before use, tert-butyl peroxide was filtered through a plug of neutral aluminium oxide to remove hydroperoxides.

Synthetic Procedures

HP-136 dimer (1_2)

Synthesis of $\mathbf{1_2}$ was carried out using the procedure reported for 3,3'-diphenyl-3H,3'H-[3,3']bibenzofuranyl-2,2'-dione (2_2).[11] mp 217-218°C (decomposition from white powder to dark yellow liquid) ^{1}H NMR ($CDCl_3$, 500 MHz) δ 1.15 (s, 6 H), 1.30 (s, 6 H), 2.16 (s, 18 H), 2.26 (s, 18 H), 6.34 (broad s, 2 H), 7.02 (broad s, 4 H), 7.08 (broad s, 2 H), 7.25 (d, 2 H). ^{13}C NMR δ 174.3 (s), 149.4 (s), 145.7 (s), 137.1

(s), 135.3 (s), 133.5 (s), 132.5 (d), 129.5 (s), 128.6 (d), 128.7 (d), 126.9 (s), 123.9 (d), 122.0 (s), 34.8 (s), 34.6 (s), 31.7 (q), 29.9 (q), 20.2 (q), 19.6 (q). MS m/z 349 (100), 334 (42), 307 (38), 291 (23). Crystal data: xyz coordinates are included in the Appendix at the end of this chapter.

HP-136 dimer (1_2) by TEMPO• Oxidation

HP-136 monomer 1-H (2.243g, 6.4mmol) was completely dissolved in an Erlenmeyer using the minimum amount of n-hexane (~150mL) at room temperature by using sonication to assist dissolution. To this almost saturated solution, one equivalent of tetramethylpiperidine-N-oxide radical (TEMPO•, 1g) was added and shaken to dissolve. The flask was left in the dark overnight exposed to air with a needle. We observed that the orange colour of TEMPO• cleared quite fast after the addition of TEMPO•. The next day, the orange colour reappeared and clear crystals had formed. The crystals were recovered by filtration and washed with cold n-hexane and isopentane. The solid was then dried under vacuum overnight (56% yield). The ^{1}H and ^{13}C NMR matched those obtained previously. Note: It was observed that a very small amount of TEMPO• remained in the product as was observed by EPR. Fellow graduate student Vasilisa Filippenko has optimized this procedure by using catalytic amounts of TEMPO and constantly purging of the reaction with oxygen. The TEMPO• impurity in this latter synthesis was removed by recrystallization from acetonitrile and dichloromethane.

meso-3,3'-Diphenyl-[3,3'-dibenzofuran]-2,2'-(3H,3'H)-dione (dimer 2_2)

A 500 mL, screw cap, Pyrex bottle was equipped with a magnetic stirring bar. In the flask were placed 3-phenyl-isocoumaranone (10 g, 47.5 mmol), tert-butyl peroxide (100 mL, 544.3 mmol) and benzene (150 mL). The stirred solution was bubbled with nitrogen for 20 min and irradiated at 350 nm for 62 h at 30°C. The resulting suspension was concentrated by rotary evaporation. The solid residue was washed with cold diethyl ether until a white solid was obtained. The filtrate was recrystallized from diethyl ether to furnish 6.2 g of the title compound as a white solid (63% yield). ^{1}H NMR data match those previously reported.[13] mp 161-168°C (decomposition from pink powder to dark red liquid), R_f = 0.34 (hexanes/ethyl acetate = 6:1), ^{1}H NMR ($CDCl_3$, 300 MHz): δ 7.38-7.18 (m, 12H), 7.09-7.01 (m, 4H), 6.46 (broad doublet, 2H, H4, H4', J = 6.4 Hz) ppm. 13C NMR ($CDCl_3$, 75.4 MHz): δ 173.9, 153.8, 131.3, 131.2, 131.0, 130.7, 130.2, 129.3, 129.1, 128.7, 128.0, 127.7, 127.6, 126.8, 124.3, 124.0, 111.8, 111.2 ppm. MS (EI) m/z = 209 $[M/2]^+$ (100%).

1,2-dicyano-1,1,2,2-tetraphenylethane (dimer 3_2)

To 100 mL of tert-butyl peroxide and 10 mL HMPA was added diphenylacetonitrile (10g, 50 mmol). The resulting solution (in a Pyrex bottle) was bubbled with nitrogen for 30 minutes. Irradiation was done with 350 nm lamps and followed by TLC for 8 days. (NOTE: reaction times will vary with intensity of light). The reaction mixture was then reduced in volume and the residue was recrystallized

in diethyl ether to afford 2.8 g of white crystals. (28% yield) mp 192-203°C (decomposition from yellow powder to dark orange liquid), ^{1}H NMR ($CDCl_3$, 300 MHz): δ 7.20-7.35 (broad m) ppm. ^{13}C NMR ($CDCl_3$, 75.4 MHz): δ 137.3, 130.5, 129.0, 128.5, 121.5, 59.5 ppm. MS (EI) m/z 192 $[M/2]^+$ (100%). This synthesis has been successfully scaled up to 30-gram batches using acetonitrile instead of HMPA as the solvent with similar yields after multiple recrystallizations.

9,9'-Diphenyl-(9,9')-bis-fluorenyl (dimer 4_2)

9-Phenyl-9-fluorenol (1.0 g, 3.87 mmol) was dissolved in dry, freshly distilled acetone (over CaH_2). This solution was added drop-wise to a solution of previously reacted trimethylsilyl chloride (0.51 mL, 1.2 eq.) and excess NaI (2.9 g, 5 eq.) in acetone, all under inert atmosphere (argon) at room temperature. The solution turned brown from the initial addition of 9-phenyl-9-fluorenol and darkened as the reaction was stirred overnight (12 hrs). After rotary evaporation under reduced pressure, the residue was washed with dichloromethane (100 mL) and 100mL of 10% $Na_2S_2O_3$(aq.) (the aqueous phase was clear and the dichloromethane layer was opaque with a white suspension). Simple filtration of this bilayer afforded the desired product (which was washed several times with ice cold acetone) to afford 480 mg of product as a white powder. (51% yield) mp 176-185°C (decomposition from pink powder to dark red liquid), ^{1}H NMR ($CDCl_3$, 200 MHz): δ 7.59–7.46 (6H), 7.30-7.09 (m, 16H), 6.93 (broad s, ~2H), 6.57 (broad s, ~2H) ppm. ^{13}C NMR: δ

147.5, 146.3, 141.5, 140.9, 131.5, 129.4, 129.2, 128.3, 127.7, 127.6, 127.6, 127.3, 127.2, 126.7, 126.4, 126.0, 119.8, 119.5, 93.5 ppm. MS (EI) m/z 241 $[M/2]^+$ (100%). HRMS calcd for $C19H13^+$ ($M/2^+$) 241.1012, found 241.1037.

Temperature Dependant UV-Vis Measurements

The UV-Vis absorption measurements were performed on a CARY-50 or Hewlett Packard 8452A spectrophotometer. A typical experiment was conducted as follows: A 1cm by 1cm rectangular quartz cell containing dimer in 3.0 mL of dry toluene (or in 1,3-dichlorobenzene in the case of dimer $\mathbf{4}_2$) was capped with a septum and a thermocouple probe was passed through the septum directly in the solution to measure the exact temperature of the solution at all times during the experiment. The sample was then purged with nitrogen and a nitrogen-filled balloon with needle was fixed through the septum to accommodate for gas expansion during heating. The heating was achieved with a custom designed, controllable block heater that fit in the spectrophotometer cavity. Room temperature absorbance spectra were set as the baseline. Absorbance measurements were taken every 3-5 degrees with at least 5 minutes in between measurements to allow the temperature and the solution to equilibrate.

Variable Temperature Electron Paramagnetic Resonance (VT-EPR)

EPR measurements were performed using a JEOL FA-100 X-Band EPR spectrometer (JEOL USA, Peabody, MA) equipped with a temperature-controlled

sample holder. The calibration with different concentrations of 4-oxo-TEMPO was done on the same day (with the same parameters) as the dimers sample. All samples were run in nitrogen-purged toluene. The acquisition parameters were the same for all analyzed samples: Power = 1mW, Modulation Frequency = 100KHz, Modulation Width = 0.01mT, and Time Constant = 0.03 sec. The EPR integrations were also corrected for temperature effects by multiplying the signal intensity by the temperature in Kelvin. The reference samples with 4-oxo-TEMPO were done at different temperatures (50-90°C). A calibration curve for 4-oxo-TEMPO is shown.

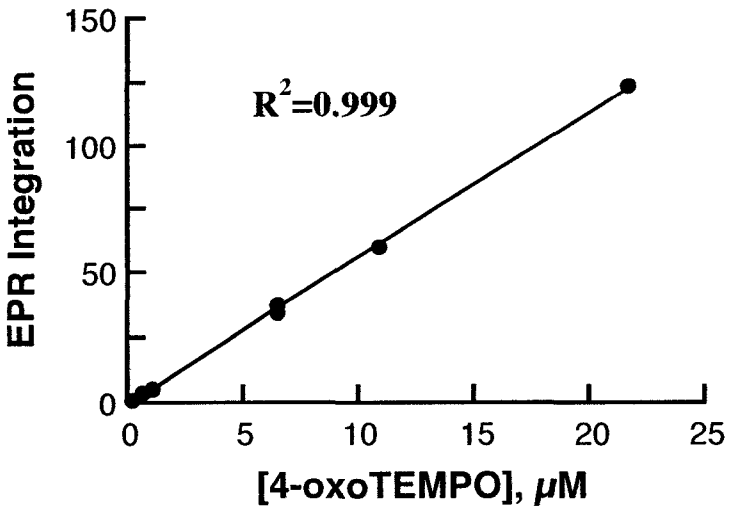

Figure 2-10. A typical calibration curve obtained from 4-oxo-TEMPO in toluene under nitrogen at different concentrations. This was used to quantify the concentration of persistent radicals.

2.11 References

(1) Griller, D.; Ingold, K. U. "Persistent carbon-centered radicals" *Accounts of Chemical Research* **1976**, 9, 13-19.

(2) Gomberg, M. "An Instance of Trivalent Carbon: Triphenylmethyl" *Journal of the American Chemical Society* **1900**, 22, 757-771.

(3) Nesvadba, P.; Evans, S.; Kroehnke, C.; Zingg, J. "Preparation of 3-aryl-2-benzofuranone stabilizers for polymers" 1995, DE 4432732.

(4) Maillard, B.; Ingold, K. U.; Scaiano, J. C. "Rate constants for the reactions of free radicals with oxygen in solution" *Journal of the American Chemical Society* **1983**, 105, 5059-5099.

(5) Scaiano, J. C.; Martin, A.; Yap, G. P. A.; Ingold, K. U. "A Carbon-Centered Radical Unreactive Toward Oxygen: Unusual Radical Stabilization by a Lactone Ring" *Organic Letters* **2000**, 2, 899-901.

(6) Bejan, E. V.; Font-Sanchis, E.; Scaiano, J. C. "Lactone-Derived Carbon-Centered Radicals: Formation and Reactivity with Oxygen" *Organic Letters* **2001**, 3, 4059-4062.

(7) Font-Sanchis, E.; Aliaga, C.; Focsaneanu, K. S.; Scaiano, J. C. "Greatly attenuated reactivity of nitrile-derived carbon-centered radicals toward oxygen" *Chemical Communications* **2002**, 1576-1577.

(8) Font-Sanchis, E.; Aliaga, C.; Bejan, E. V.; Cornejo, R.; Scaiano, J. C. "Generation and Reactivity toward Oxygen of Carbon-Centered Radicals Containing Indane, Indene, and Fluorenyl Moieties" *Journal of Organic Chemistry* **2003**, 68, 3199-3204.

(9) Font-Sanchis, E.; Aliaga, C.; Cornejo, R.; Scaiano, J. C. "Reactivity toward Oxygen of Isobenzofuranyl Radicals: Effect of Nitro Group Substitution" *Organic Letters* **2003**, 5, 1515-1518.

(10) Ballester, M.; Riera-Figueras, J.; Castaner, J.; Badfa, C.; Monso, J. M. "Inert carbon free radicals. I. Perchlorodiphenylmethyl and perchlorotriphenylmethyl radical series" *Journal of the American Chemical Society* **1971**, 93, 2215-2225.

(11) Karafiloglou, P.; Catteau, J. P.; Lablache-Combier, A. "Electron spin resonance study of a stable benzo [b] furanyl radical" *Journal of the Chemical Society* **1977**, 1545-1548.

(12) Suzuki, K.; Okawara, T.; Higashijima, T.; Yokomizo, K. "Inhibitory activities against topoisomerase I and II by isoaurostatin derivatives and their structure-activity relationship" *Bioorganic & Medicinal Chemistry Letters* **2005**, 15, 2065–2068.

(13) Mori, Y.; Niwa, A.; Maeda, K. "Structural study of chromotropic [dibenzofuran] diones by X-ray structure analysis and MO Calculation" *Acta Cryst. B.* **1995**, 51, 61-65.

(14) Lam, Y.; Lee, G. H.; Liang, E. "Conformations of 1, 2-Dicyano-1, 1, 2, 2-tetraphenylethane and Cyanodiphenylmethyl Peroxide" *Bulletin of the Chemical Society of Japan* **2001**, 74, 1033-1034.

(15) Lam, Y.; Koh, L. L.; Huang, H. H.; Wang, L. "Rotational isomerism and crystal structures of 9,9′-dicyano-9,9′-bifluorenyl and 9,9′-dinitro-9,9-bifluorenyl" *Journal of the Chemical Society, Perkin Trans. 2* **1999**, 1137-1142.

(16) Frenette, M.; MacLean, P. D.; Barclay, L. R.; Scaiano, J. C. "Radically Different Antioxidants: Thermally Generated Carbon-Centered Radicals

as Chain-Breaking Antioxidants" *Journal of the American Chemical Society* **2006**, 128, 16432-16433.

(17) Arends, I.; Mulder, P.; Clark, K. B.; Wayner, D. D. M. "Rate Constants for Termination and TEMPO Trapping of Some Resonance Stabilized Hydroaromatic Radicals in the Liquid Phase" *The Journal of Physical Chemistry* **1995**, 99, 8182-8189.

(18) Luo, Y.-R. "Handbook of Bond Dissociation Energies in Organic Compounds"; CRC Press, 2003.

(19) Neumann, W. P.; Uzick, W.; Zarkadis, A. K. "Sterically hindered free radicals. 14. Substituent-dependent stabilization of para-substitutedtriphenylmethyl radicals" *Journal of the American Chemical Society* **1986**, 108, 3762-3770.

(20) Zheng, S.; Lan, J.; Khan, S. I.; Rubin, Y. "Synthesis, Characterization, and Coordination Chemistry of the 2-Azaphenalenyl Radical" *Journal of the American Chemical Society* **2003**, 125, 5786-5791.

(21) Fischer, H. "Unusual selectivities of radical reactions by internal suppression of fast modes" *Journal of the American Chemical Society* **1986**, 108, 3925-3927.

(22) Magnus, P.; Venableneekreisberg, J.; Shen, L.; Lynch, V. "Some reactions of persistent benzofuranone radicals related to the 'old' diazonamide structure" *Tetrahedron Letters* **2005**, 46, 707-710.

(23) Barclay, L. R.; Griller, D.; Ingold, K. U. "2, 4, 6-Tri-tert-butylphenyl radical" *Journal of the American Chemical Society* **1974**, 96, 3011.

(24) Hicks, R. "What's new in stable radical chemistry?" *Organic and Biomolecular Chemistry* **2007**, 5, 1321-1338.

(25) Bratasz, A.; Kulkarni, A.; Kuppusamy, P. "A Highly Sensitive Biocompatible Spin Probe for Imaging of Oxygen Concentration in Tissues" *Biophysical Journal* **2007**, 92, 2918-2925.

(26) Pratt, D. A.; Porter, N. A. "Role of Hyperconjugation in Determining Carbon-Oxygen Bond Dissociation Enthalpies in Alkylperoxyl Radicals" *Organic Letters* **2003**, 5, 387-309.

(27) Tallman, K. A.; Pratt, D. A.; Porter, N. A. "Kinetic Products of Linoleate Peroxidation: Rapid Fragmentation of Nonconjugated Peroxyls" *Journal of the American Chemical Society* **2001**, 123, 11827-11828.

(28) Padwa, A.; Dehm, D.; Oine, T.; Lee, G. H. "Competitive keto-enolate photochemistry in the 3-phenylisocoumaranone system" *Journal of the American Chemical Society* **1975**, 97, 1837-1845.

2.12 Appendix. Coordinates for Crystal Structures.

2.12.1 XYZ coordinates for HP-136 dimer (1_2) crystal structure

R1 = 8.84, wR2 = 28.46

Atom	X	Y	Z
O	9.30256	7.44460	3.65698
O	9.54321	7.73026	5.85934
O	11.20017	10.02417	4.58970
O	10.55770	12.16530	4.67974
C	9.09282	8.13541	4.61146
C	9.16347	8.68858	6.79882
C	9.52555	8.62807	8.14800
C	9.04315	9.68470	8.90626
H	9.23412	9.67822	9.82623
C	8.29360	10.76510	8.41176
C	7.99775	10.75214	7.03331
H	7.50431	11.45656	6.65587
C	8.42386	9.71712	6.23416
C	10.37556	7.48501	8.71304
C	11.73887	7.41154	7.95853
H	12.26985	6.68335	8.31796
H	12.21686	8.24777	8.07409
H	11.57881	7.25813	7.01605
C	9.64809	6.14748	8.53707
H	8.79919	6.17557	9.00831
H	10.19452	5.43225	8.89951
H	9.48912	5.98758	7.59385
C	10.68906	7.69461	10.19654
H	9.86114	7.73134	10.70042
H	11.17368	8.52868	10.31022
H	11.23218	6.95994	10.52033
C	7.81119	11.88440	9.34223
C	8.94380	12.56721	10.03258
H	9.43834	11.92113	10.55785
H	8.59717	13.26299	10.61413
H	9.53218	12.96480	9.36849
C	6.74814	11.35068	10.26145
H	7.12015	10.63978	10.80547
H	6.01073	11.00279	9.73243
H	6.42911	12.06375	10.83549
C	7.05392	13.02098	8.53932
H	6.30768	12.63204	8.05533
H	7.66548	13.43369	7.90901
H	6.72496	13.69083	9.15839
C	5.72703	9.38003	5.12510
H	5.87385	9.77330	5.96552
C	4.42553	9.06240	4.74240
H	3.70358	9.26983	5.30894
C	4.19592	8.43360	3.51028
C	5.28437	8.17431	2.70212
H	5.14969	7.75511	1.87220
C	6.56379	8.51571	3.08594
H	7.28132	8.32556	2.51002
C	6.81658	9.12722	4.29105
C	3.31280	9.39084	5.61284
H	3.64618	9.81651	6.41575
H	2.83813	8.57838	5.84921
H	2.71007	9.99586	5.15136
C	5.04041	7.57360	1.38445
H	5.88710	7.43531	0.93047

H	4.48404	8.16782	0.85543
H	4.59002	6.72225	1.49701
C	2.77189	8.04250	3.09532
H	2.79507	7.62546	2.21737
H	2.21663	8.83767	3.05780
H	2.40540	7.42019	3.74064
C	8.26048	9.44270	4.74765
C	10.34354	10.85154	4.41824
C	9.31471	12.83947	4.59683
C	9.14581	14.17917	4.90561
C	7.80126	14.59404	4.85458
H	7.61470	15.49294	5.05756
C	6.72606	13.76862	4.52292
C	6.99431	12.44405	4.15673
H	6.29554	11.87576	3.89072
C	8.30022	11.97731	4.18900
C	10.31926	15.09751	5.25679
C	10.97276	14.60917	6.55007
H	11.71790	15.18826	6.77218
H	11.29400	13.70163	6.42700
H	10.32146	14.62861	7.26743
C	11.34919	15.08022	4.10645
H	12.09322	15.66148	4.32969
H	10.92861	15.39138	3.29042
H	11.67484	14.17485	3.97701
C	9.86555	16.53444	5.45414
H	10.63166	17.08761	5.67287
H	9.22198	16.57334	6.17938
H	9.45490	16.85856	4.63735
C	5.26450	14.27208	4.52329
C	4.96865	14.98299	3.22663
H	5.55814	15.75007	3.13659
H	4.04690	15.28334	3.22288
H	5.11216	14.37580	2.48376
C	5.04703	15.26173	5.69163
H	5.73255	15.94670	5.66912
H	5.09670	14.78419	6.53581
H	4.17274	15.67660	5.60909
C	4.25664	13.16143	4.67112
H	4.48625	12.61475	5.43650
H	4.25995	12.61259	3.87196
H	3.37352	13.54173	4.79868
C	4.93443	14.06681	2.81768
H	5.08235	13.15063	2.56255
H	5.52171	14.65238	2.30367
H	4.00936	14.31530	2.63759
C	5.27664	15.70902	4.65236
H	6.00963	16.06339	4.13084
H	5.39034	15.93806	5.58283
H	4.43768	16.05906	4.32594
C	4.49287	13.39696	5.12134
H	4.56683	12.54561	4.67112
H	3.57553	13.70812	5.08758
H	4.77216	13.30621	6.04431
C	10.01679	9.61556	1.78853
H	10.69458	9.26551	2.33743
C	10.05984	9.38435	0.42096
H	10.76634	8.88305	0.05628
C	9.06192	9.88566	-0.41383
C	8.04302	10.60737	0.14707
H	7.35197	10.92933	-0.40145
C	8.00548	10.87098	1.49813
H	7.31334	11.40038	1.84969
C	8.99789	10.35239	2.36332
C	11.09640	8.52868	-0.19510
H	10.95179	8.48762	-1.15559
H	11.04452	7.63627	0.18009
H	11.97290	8.90466	-0.01876

C	7.05723	10.84722	-0.66409
H	7.31113	10.59440	-1.56454
H	6.84418	11.79365	-0.64157
H	6.28119	10.33511	-0.39020
C	9.11711	9.58963	-1.91309
H	9.89977	9.04943	-2.10857
H	9.16789	10.42154	-2.40497
H	8.31899	9.10561	-2.17610
C	8.90958	10.61385	3.89747

2.12.2 XYZ coordinates for bis-9-phenyl-9-fluorenyl peroxide dimer crystal structure

R1 = 4.54, wR2 = 10.88

Atom	X	Y	Z
H	-3.08007	-3.80191	-3.30533
O	-0.52752	0.52928	-0.04919
C	0.16703	1.71656	-0.49511
C	0.14270	0.66225	-2.80688
H	-0.56677	0.11046	-2.53142
C	0.60929	0.58672	-4.11490
H	0.21577	-0.01785	-4.71675
C	1.64870	1.39555	-4.53387
H	1.95582	1.34819	-5.42127
C	2.23024	2.26979	-3.64759
H	2.94338	2.81493	-3.92680
C	1.76733	2.35034	-2.33851
H	2.16779	2.95472	-1.74011
C	0.71842	1.54714	-1.90571
C	1.15582	2.20393	0.56457
C	-0.63053	3.70763	0.58462
C	-1.50724	4.75892	0.84699
H	-1.32150	5.37826	1.52956
C	-2.65552	4.87358	0.08519
H	-3.25667	5.57523	0.25839
C	-2.93318	3.97405	-0.92462
H	-3.71639	4.07548	-1.43433
C	-2.06420	2.91338	-1.19877
H	-2.24751	2.30432	-1.89046
C	-0.92816	2.78892	-0.42344
C	-2.37761	-1.66844	-0.95037
H	-2.72380	-0.90793	-0.52005
C	-3.07955	-2.27420	-1.98202
H	-3.90044	-1.91063	-2.25969
C	-2.58914	-3.40421	-2.60918
C	-1.38267	-3.95374	-2.21907
H	-1.05537	-4.72827	-2.64075
C	-0.65697	-3.35164	-1.19803
C	1.50724	-4.75892	-0.84699
H	1.32150	-5.37826	-1.52956
C	2.65552	-4.87358	-0.08519
H	3.25667	-5.57523	-0.25839
H	3.71639	-4.07548	1.43433
C	2.37761	1.66844	0.95037
H	2.72380	0.90793	0.52005
C	3.07955	2.27420	1.98202
H	3.90044	1.91063	2.25969
C	2.58914	3.40421	2.60918
H	3.08007	3.80191	3.30533

C	1.38267	3.95374	2.21907
H	1.05537	4.72827	2.64075
C	0.65697	3.35164	1.19803
O	0.52752	-0.52928	0.04919
C	-0.16703	-1.71656	0.49511
C	-0.14270	-0.66225	2.80688
H	0.56677	-0.11046	2.53142
C	-0.60929	-0.58672	4.11490
H	-0.21577	0.01785	4.71675
C	-1.64870	-1.39555	4.53387
H	-1.95582	-1.34819	5.42127
C	-2.23024	-2.26979	3.64759
H	-2.94338	-2.81493	3.92680
C	-1.76733	-2.35034	2.33851
H	-2.16779	-2.95472	1.74011
C	-0.71842	-1.54714	1.90571
C	-1.15582	-2.20393	-0.56457
C	0.63053	-3.70763	-0.58462
C	2.93318	-3.97405	0.92462
C	2.06420	-2.91338	1.19877
H	2.24751	-2.30432	1.89046
C	0.92816	-2.78892	0.42344

3. Radically Different Antioxidants

3.1 Graphical Abstract

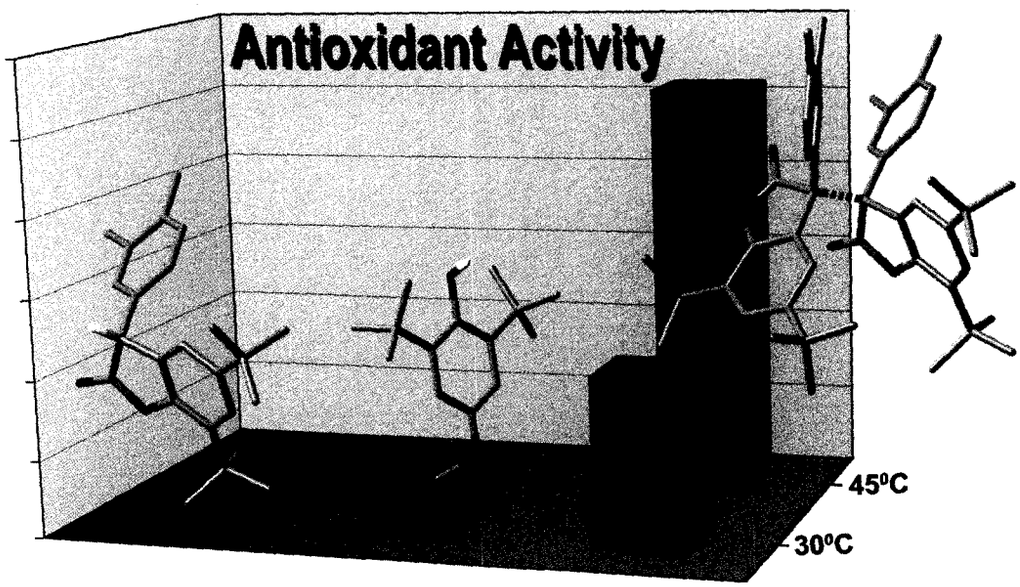

3.2 Idea: Dimers as Antioxidants.

The carbon-centered radicals (1• - 3•) described in the previous chapter are unusual regarding their reaction, or lack thereof, with oxygen.[1-5] For such sterically hindered radical centers, they are also unusual in their mode of dimerization; head-to-head rather than head-to-tail.[6] The dimers formed are in equilibrium with the nascent radicals due to very low BDEs of the central carbon-carbon bond. We introduced the term "dynamically stable" to describe their surprising stability in solution, under air.

These properties inspired the idea to use carbon-centered radicals as antioxidants. Before any experiments were performed, Prof. Scaiano applied for a patent on "Thermally Modulated Antioxidants".[7] Persistent carbon-centered radicals (A•) generated by the thermal dissociation of dimers (A-A), it was anticipated, would react with peroxyl radicals and act as chain-breaking antioxidants.

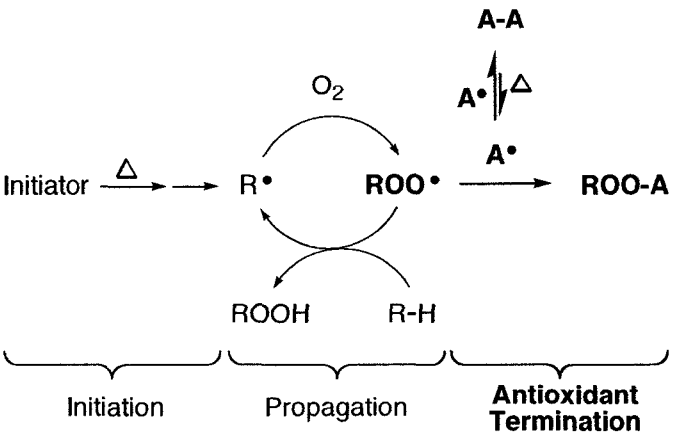

Scheme 3-1. Description of the concept presented in this chapter. The autoxidation of substrate R-H is inhibited by the presence of dimers (A-A). Thermal dissociation of dimers generates persistent carbon-centered radicals A• that trap propagating peroxyl radicals, ROO•, to stop the autoxidation.

Inspired by the radical-dimer equilibrium described in the previous chapter, graduate student Kathy-Sarah Focsaneanu and post-doctoral fellow Carolina Aliaga developed the use of persistent radicals to trap benzylic radicals as a synthetic tool to make quaternary carbon-carbon bonds.[8] This very nice work demonstrated dimers as "radical buffer solutions": persistent radicals effectively trap other radicals as they form. Reactions [1], [2] and [3] illustrate a successful application of this idea. As trapping occurs, the persistent radical concentration is replenished by dissociating dimers according to LeChâtelier's Principle. This process can continue until the dimers are consumed and the overall kinetics of this process are similar to the conditions leading to the Fisher-Ingold Persistent Free Radical Effect.[9,10]

[1] 

[2] 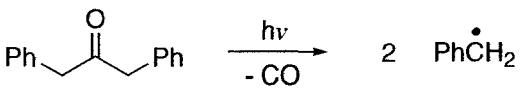

[3] 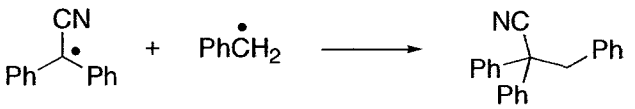

To establish the potential of the mechanism of Scheme 3-1, the antioxidant activity of the dimers had to be evaluated. Due to the growing interest in antioxidants and oxidative stress, many assays have been developed to quantify antioxidant activity. In reality the majority of recently developed assays for chain-breaking antioxidants use indirect methods to estimate antioxidant activity.[11] These indirect methods, including work from our laboratories,[12,13] are either based on the ability of antioxidants to act as H-atom donors to experimentally convenient radicals or on their reducing ability. Nonetheless, the assays developed are largely relevant and comparisons between similar classes of antioxidants do yield useful information.

The dimers 1_2, 2_2 and 3_2 presented here (Scheme 3-2) are a new class of antioxidants. Presumably, they would have scored very low with the use of these indirect tests since H-atom donation and reducing metal ions are certainly not abilities of carbon-centered radical dimers. This new class of antioxidants needed an "old" methodology to prove their worth.

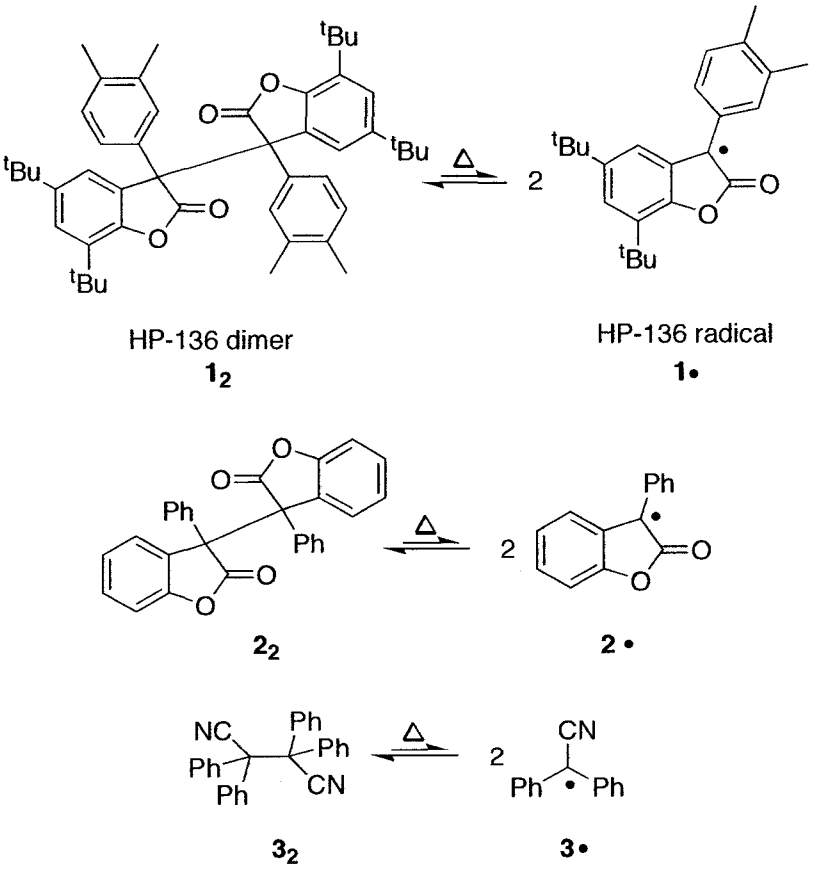

Scheme 3-2. Chemical structure of persistent carbon-centered radicals: HP-136 radical (1•), 3-phenyl-2-coumaranone radical (2•) and diphenylacetonitrile radical (3•) and their thermally labile dimers 1_2, 2_2 and 3_2.

3.3 Evaluating Antioxidant Ability: Oxygen Uptake Measurements.

The term antioxidant was derived, very simply, because antioxidants protect against free radical *oxidation*. Free radical oxidation consumes oxygen; therefore one of the first antioxidant assays was to measure oxygen consumption of fats with and without antioxidants. The molecules that reduced oxygen consumption the most were named the best antioxidants.[14] It was not until the 1960s that proper kinetic analysis could be extracted using oxygen uptake data.

While at the Sussex Drive NRC laboratories in Ottawa, Keith Ingold and J. A. Howard developed a competitive kinetics assay based on oxygen-uptake measurements.[15,16] The key to the method's success was to initiate free radical oxidation at a constant, known rate using azo-initiators and choosing a suitable substrate for autoxidation. To explain the technique, I will follow the experiments performed to estimate the dimers' antioxidant activity. Conceptually these experiments are very similar to the work of Ingold and Howard in the 1960s. The goal of the experiment is to measure the rate constant (k_{inh}) for the reaction between an antioxidant and a peroxyl radical as shown in [4]. The rate constant k_{inh} is taken as the measure of antioxidant activity; a higher k_{inh} will mean a better antioxidant. Other system-specific factors used to quantify antioxidant activity such as

preserving the color purity of a material or the flavor of foodstuff will not be discussed in this chapter.

[4] $ROO^{\bullet} + \text{antioxidant} \xrightarrow{k_{inh}} \text{non-radical products}$

The term "non-radical products" indicates the generation of a mixture of products that do not affect the measured oxygen uptake. Another measurement available from the measurement of oxygen-uptake is the "stoichiometric factor"; the number of peroxyl radicals trapped per antioxidant (*vide infra*). This number will be represented by "n" and most common phenolic antioxidants have n values of 2 because of reactions [5] and [6],

[5] 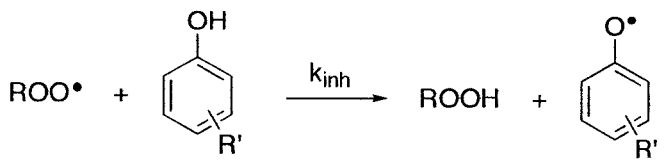

[6] 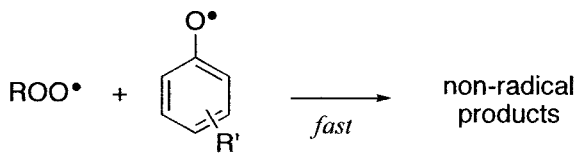

The rate of oxygen uptake during the *uninhibited* autoxidation of a substrate R-H (no antioxidants) can be represented by the elementary reactions [8] to [12]. Initiation occurs when thermal decomposition of an azo-initiator under air generates peroxyl radicals at a slow, steady rate; 2,2'-azo-bis-isobutyronitrile (AIBN), for

example, has a half-life of ~2000 hours at 30°C. The rate of inititiation (R_{init}) is given by eq [7].

[7] $$R_{init} = 2ek_{init}[Initiator] = 2eA\exp(-E_a/RT)[Initiator]$$

The initiator efficiency, e, represents the fraction of radicals R'• that escape the solvent-caged radical pair following nitrogen release. For example, e is ~0.66 for di-tert-butylhyponitrite in benzene but can drop below 0.1 in the more rigid environment of lipid membranes.[17] After escaping the solvent cage, the large majority of carbon-centered radicals will react with dissolved oxygen to become peroxyl radicals before ensuing reactions with their surroundings. The initiator-derived radical, R'OO•, will then react with the oxidizable substrate, R-H, to yield another carbon-centered radical, R•, as seen in reaction [9]. This reaction is illustrated as H-atom abstraction but a similar process can also involve addition to a double bond.

[8] $$R'N{=}NR' \xrightarrow[-N_2]{k_{init}} 2e\ R'\bullet \xrightarrow[fast]{O_2} 2e\ R'OO\bullet$$

[9] $$R'OO\bullet + R\text{-}H \longrightarrow R'OOH + R\bullet$$

These initiation and transfer steps, [8] and [9], lead to the autoxidation of R-H and the observed oxygen uptake; notice that each propagation cycle, steps [10] and [11], consumes one oxygen molecule. Under air-saturated solutions, the reaction of R• with O_2 is a fast reaction, therefore, the rate-determining step is reaction [11] with

rate constant k_p. This reaction is usually H-atom abstraction or addition to a double bond. We will discuss antioxidant assays with R-H = cumene, methyl linoleate and styrene later in this chapter.

[10] $$R\bullet \xrightarrow[fast]{O_2} ROO\bullet$$

[11] $$ROO\bullet + R\text{-}H \xrightarrow{k_p} ROOH + R\bullet$$

Since the reaction R• + O_2 is faster than ROO• + R-H, the majority of free radicals at any given time will be peroxyl radicals, not the shorter-lived carbon-centered radicals. For this reason, termination will take place predominantly between two peroxyl radicals. At 30°C, termination rate constants $2k_t$ have values between 10^6-10^8 $M^{-1}s^{-1}$ for secondary peroxyl radicals and 10^3-10^5 $M^{-1}s^{-1}$ for tertiary peroxyl radicals.[18]

[12] $$ROO\bullet + ROO\bullet \xrightarrow{2k_t} \text{non-radical products}$$

In this idealized but relevant example, proper kinetic treatment gives the rate expression for the observed oxygen uptake, eq. [13]. For minor variations on the autoxidation of organic substrates that are ignored here, the reader is referred to Denisov and Afanas'ev's excellent book entitled "Oxidation and Antioxidants in Organic Chemistry and Biology".[19]

$$[13] \quad -\frac{d[O_2]}{dt} = \frac{k_p}{(2k_t)^{0.5}}[R-H](R_{init})^{0.5}$$

The ratio $k_p/(2k_t)^{0.5}$ is called the oxidizability of a substrate; a higher value indicates a substrate that is more prone to autoxidation. For example, at 30°C styrene[20] has an oxidizability of $6.3\times10^{-3}M^{-1/2}s^{-1/2}$, cumene's[21] oxidizability is 1.5×10^{-3} $M^{-1/2}s^{-1/2}$ and tetrahydrofuran,[22] which all chemists should know not to distill to dryness, has an oxidizability of $0.8\times10^{-3}M^{-1/2}s^{-1/2}$.

The value for R_{init} can be estimated using equation [7] with the knowledge of e and k_{init} (or e, A and E_a); many of these values have been measured.[19,23] In most cases, however, we measured R_{init} by a process sometimes described as a "free radical titration". The addition of an effective phenolic antioxidant to an autoxidizing solution *inhibits* or reduces the rate of oxygen uptake until the antioxidant is completely consumed by peroxyl radicals. After antioxidant depletion, the rate of oxygen uptake returns to the *uninhibited* rate as predicted by equation [13] (see Figure 3-1 below for example). From the inhibition period, τ, the concentration of antioxidant, [ArOH], and the stoichiometric factor, n = 2 is assumed, we can estimate R_{init} using $R_{init} = n\,[ArOH] / \tau$. As expected, the experimentally determined results are very close to those calculated using Arrhenius parameters.

3.4 Inhibited Autoxidation of Cumene.

The ability of dimers to prevent the autoxidation of cumene (2-isopropylbenzene) was measured in chlorobenzene at 30°C, a common starting point for antioxidant investigations.[24] Cumene autoxidation is also a key reaction step for the industrial synthesis of phenol and acetone,[25] although in the latter case inhibition is not desired.

Initiation of the autoxidation reaction was afforded by thermal decomposition of AIBN and the rate of initiation was determined by the "free radical titration" technique described earlier. The propagation steps for the autoxidation of cumene are shown below (eq. [14] and [15]). At 30°C, the propagation rate constant (k_p) is 0.18 $M^{-1}s^{-1}$.[21]

[14] 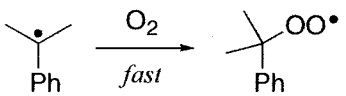

[15] 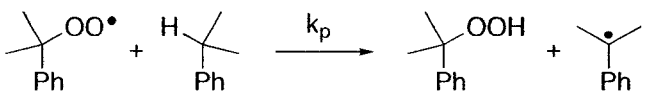

Finally, we inhibit the autoxidation of cumene with the addition of a small amount of antioxidant. In our case the antioxidant is a carbon-centered radical dimer; 2_2 is shown in the scheme below. The idea was to trap peroxyl radicals with persistent carbon-centered radicals.

[16] 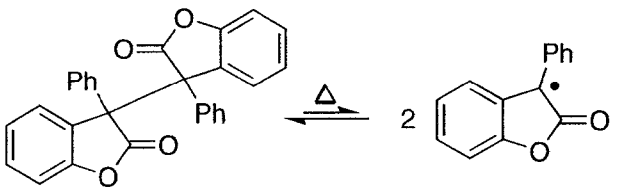

[17] 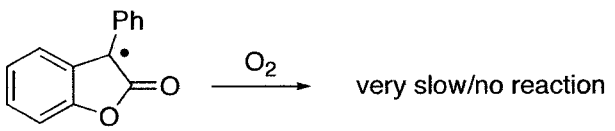

[18] 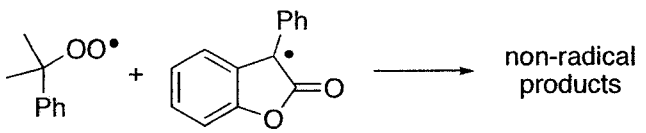

In this system, dimers 1_2, 2_2 and 3_2 all behave as ideal antioxidants (see Figure 3-1), completely stopping the autoxidation of cumene. Also, each dimer trapped two peroxyl radicals (n = 2.0±0.1) as expected since two persistent radicals are formed during dissociation. The result of n=2 for all dimers is important because it implies that peroxides formed during the termination steps do not decompose at a significant rate. It should be noted that hydroperoxides and mixed peroxides are also formed during phenolic antioxidant termination steps.

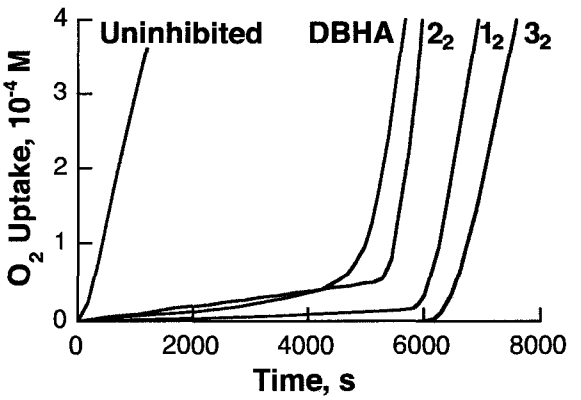

Figure 3-1. Profiles of oxygen-uptake during AIBN (~17 mM) initiated autoxidation of cumene (~5.4 M) in chlorobenzene at 30°C under air. Curve Uninhibited: Uninhibited oxygen-uptake. Curve DBHA: inhibited by 3,5-di-*tert*-butyl-4-hydroxyanisole (DBHA), 4.3 μM. Curve 2_2: Inhibited by 2_2, 5.34 μM. Curve 1_2: Inhibited by $(HP-136)_2$, 5.7 μM. Curve 3_2: Inhibited by 3_2, 5.7 μM.

We also evaluated the antioxidant activity for the commercial HP-136 (1-H, Scheme 3-3) in this system of cumene in chlorobenzene. Surprisingly, at micromolar concentrations, we observed no inhibition of oxygen uptake by HP-136. We were able to see retardation of oxygen uptake at higher concentrations of HP-136, but no clear inhibition period (see Figure 3-2). With these results and the approximation that all termination steps are performed by HP-136, we could estimate $k_{inh} \sim 100$ $M^{-1}s^{-1}$ (see experimental section for kinetic treatment). This k_{inh} compares unfavorably to "slow" antioxidants such as BHT, $k_{inh}=1.2x10^4M^{-1}s^{-1}$.[26] In hindsight, we can justify HP-136's low k_{inh} from the fact that the minor enol form, not the major keto form, is responsible for most antioxidant termination.[27]

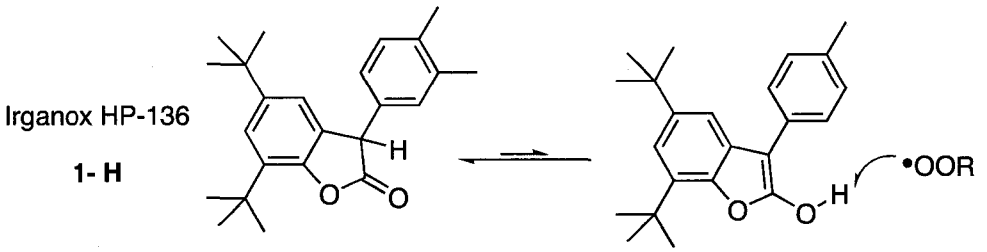

Scheme 3-3. Synthetic antioxidant Irganox HP-136 introduced by CIBA. Post-doctoral fellow Carolina Aliaga demonstrated that the minor enol form of HP-136 is the major hydrogen donor.[27]

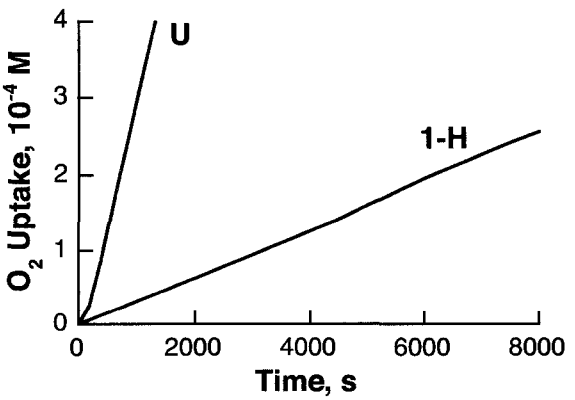

Figure 3-2. Profiles of oxygen-uptake during AIBN (~17 mM) initiated autoxidation of cumene (~5.4 M) in chlorobenzene at 30°C under air. Curve U: Uninhibited oxygen-uptake. Curve 1-H: inhibited by HP-136, 240 μM.

The antioxidant performance of dimers 1_2, 2_2 and 3_2 in cumene/chlorobenzene is promising. To evaluate k_{inh} by *competitive* kinetics, however, there needs to be a *competition* between propagation and antioxidant termination. An empirical rule of at least 5 propagation turnovers, $\nu=(-d[O_2]/dt)/R_{init}$, was decided to get reliable results. In the cumene experiments, the turnover numbers were closer to 0; therefore no k_{inh} could be measured. Since k_p is only 0.18

$M^{-1}s^{-1}$ for cumene, we decided to inhibit the autoxidation of styrene with $k_p = 41\ M^{-1}s^{-1}$ to allow for a kinetic competition between propagation and antioxidant termination.

3.5 Inhibited Autoxidation of Styrene.

Styrene autoxidation generates an alternating co-polymer of styrene and oxygen as the major reaction product.[28] After an initiating peroxyl radical adds to a styrene double bond, the benzilic radical reacts with oxygen and the resulting peroxyl radical adds to another styrene to allow the chain to grow. At partial pressure of O_2 in air, the rate-determining step is peroxyl radical addition; self-termination will therefore take place between the longer-lived peroxyl radicals. The propagation steps for the autoxidation of styrene are shown below, with ROO• and R'OO• representing the poly(peroxystyrene)peroxyl radical.

[19] 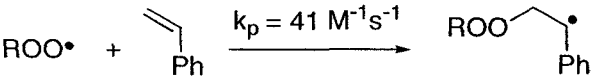

[20] 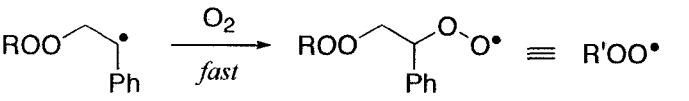

poly(peroxystyrene)peroxyl radical

Once again, the solvent is chlorobenzene due to its inertness to peroxyl radicals, good dissolving properties and its low vapour pressure. Typical traces for styrene autoxidation at 30°C inhibited by dimers 1_2, 2_2 and 3_2 are shown in Figure 3-3. In these, it is possible to distinguish an inhibited and uninhibited region that have slower and faster oxygen uptake, respectively. The point at which the extrapolated lines from both regions intercept corresponds to the inhibition period, τ.

During the inhibition period, proper kinetic treatment leads to the integrated form for the rate of oxygen uptake.[26]

$$[21] \quad \Delta[O_2]_t = -(k_p / k_{inh})[Styrene]\ln(1 - t/\tau)$$

From the slope of $\Delta[O_2]$ vs. $-\ln(1-t/\tau)$, shown in Figure 3-4, we can extrapolate k_{inh} for each dimer. These values, which are between 20-70 x 10^4 $M^{-1}s^{-1}$, are given in function of total dimer concentration (see Table 3-1). In other words, the rate constant k_{inh} is quoted for the nominal reaction.

$$[22] \quad ROO\bullet \xrightarrow{k_{inh}[A\text{-}A]} \text{non-radical products}$$

This allows the antioxidant activity of dimers 1_2, 2_2 and 3_2 to be compared to standard phenolic antioxidants. Mole per mole, HP-136 dimer (1_2) is ~4 times faster at trapping peroxyl radicals in styrene at 30°C than 2,6-di-*tert*-butyl-4-methoxyphenol[29] and more than 1000 times faster than the commercial Irganox HP-136® (1-H). This may explain why the HP-136 monomer (1-H) is more widely used as an antioxidant for high temperature processing and long-term protection.[30] In fact, radical trapping by HP-136 can generate the dimers that are the subject of this contribution.

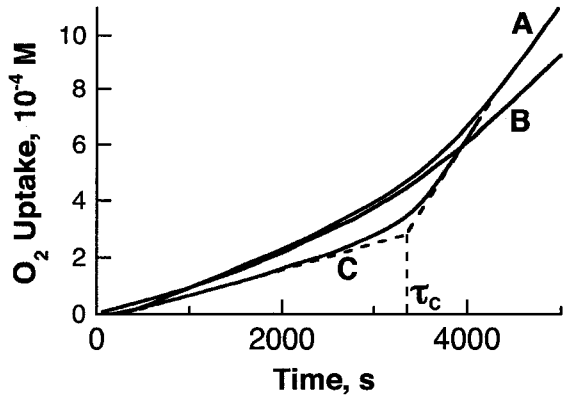

Figure 3-3. Profiles of oxygen-uptake during AIBN initiated (~17mM) autoxidation of styrene (~2.5 M) in chlorobenzene at 30°C under air. Curve A, blue: inhibited by $(HP\text{-}136)_2$, 13.0 μM. Curve B, red: inhibited by 3_2, 6.6 μM. Curve C, green: inhibited by 2_2, 14.8 μM.

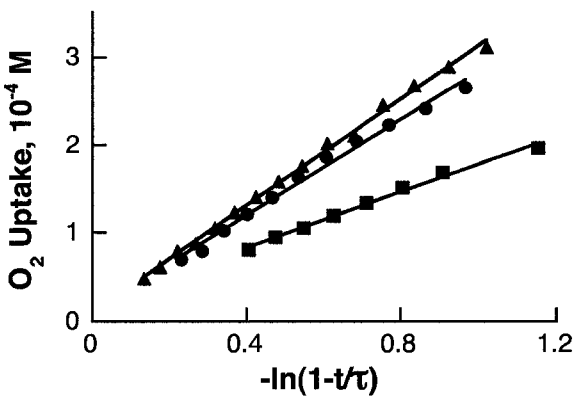

Figure 3-4. Plot of oxygen-uptake in function of –ln(1-t/τ) as described in eq. [21]. Inhibited by 13.0 μM $(HP\text{-}136)_2$ (blue circles), 14.8 μM 2_2 (green squares), 6.6 μM 3_2 (red triangles).

From Variable-Temperature EPR experiments described in the previous chapter, we can also estimate the reaction between the peroxyl radicals and the persistent carbon-centered radicals (eq [23]), under the assumption that the thermodynamic properties obtained in toluene are equal to those in chlorobenzene/styrene.

[23] $ROO\bullet + A\bullet \rightarrow ROO\text{-}A$

Since only dissociated dimers are "active" antioxidants, $k_{[23]}$ can be estimated using $k_{inh}[A\text{-}A] = k_{[23]}[A\bullet]$. As expected, the radical-radical reaction is almost diffusion controlled in all three cases. The bimolecular rate constant $k_{[23]}$ are calculated as ~$3x10^8$ $M^{-1}s^{-1}$, ~$4x10^8$ $M^{-1}s^{-1}$, and ~$8x10^8$ $M^{-1}s^{-1}$ for the reaction between poly(peroxystyrene)peroxyl radical and radical 1•, 2•, and 3•, respectively. In effect, these carbon-centered radicals are better peroxyl radical traps, i.e., antioxidants, than α-tocopherol[26] (k_{inh}=$3.2x10^6$ $M^{-1}s^{-1}$). Diphenylacetonitrile radicals (3•) react faster with peroxyl radicals than do radicals 1• and 2•, although the antioxidant activity for dimer 3_2 is the lowest amongst the three. This is because the bond dissociation energy for dimer 3_2 is higher; therefore, the concentration of 3• is comparatively lower.

3.5.1 Isolating the Termination Product of Dimer Antioxidants

To better understand the termination step, we reacted the HP-136 dimer with AIBN under air and isolated the main reaction product. As expected, we obtained the mixed peroxide according to eq [24]. This product appeared quite stable in solution (the NMRs showing its structure, see Experimental Section, were acquired after many hours in solution). This is important since thermal degradation could lead to further oxidation reactions.

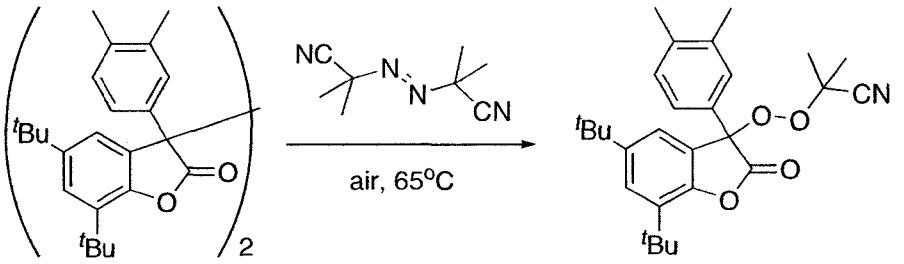

[24] 1_2 1-OO-C$(CH_2)_2$CN

3.5.2 Low Stoichiometric Factors for Dimers in Viscous Solvents

Collaborators Patricia D. Maclean and Ross Barclay at the University of Mount Alison in New-Brunswick have also studied the antioxidant activity of phenylcoumaranone dimers (2_2) using methyl linoleate as the oxidizable substrate.

In methyl linoleate/chlorobenzene, the dimer 2_2 behaves as an ideal antioxidant; it completely stops the autoxidation of methyl linoleate and does so with a stoichiometric factor of 2. Their results show very similar behavior for the inhibited autoxidation of methyl linoleate by dimer 2_2 and 2,2,5,7,8-pentamethyl-6-hydroxychroman (PMHC, a vitamin E analog).[31] Our collaborators also found surprising results for the antioxidant activity of 2_2 in viscous media. In pure methyl linoleate, a viscous liquid, the inhibition period was very short when dimer 2_2 was used as an antioxidant. In this system, the measured stoichiometric factors (n) for dimer 2_2 were as low as 0.01 (!) while PMHC's remained close to 2. I also measured very low stoichiometric factors for dimer 2_2 in Triton X-100 micelles. It appears that viscous solvents slow down the dimer's rate of dissociation to the point where

replenishing radical concentration becomes a rate-limiting step. This hypothesis agrees with the efficient, but short inhibition period observed in these experiments. Persistent radicals already present in the solution will efficiently trap peroxyl radicals, but dimers in viscous solvents fail to replenish the concentration of the persistent radicals. More work is needed to evaluate this hypothesis. During the acquisition of their results, I was in the progress of synthesizing lipid-soluble dimers (with long hydrophobic side-chains) to evaluate their antioxidant activity in biomimetic membranes. The unforeseen problem that dimers dissociate too slowly in rigid environments put a stop to this later project. I have since focused my efforts on the synthesis of water-soluble dimers, with some success, but without antioxidant evaluation at this point.

3.5.3 Effect of Temperature on the Antioxidant Activity of Dimers

As a proof of concept, we also investigated the effect of temperature on the antioxidant activity of HP-136 dimer (1_2) and diphenylacetonitrile dimer (3_2). These results are shown in Figure 3-5. At higher temperatures, more dimers will dissociate into the active radical form and this should result in a proportional increase of k_{inh}. To properly estimate k_{inh} at this temperature, however, we need to know k_p for the autoxidation of styrene at 45°C. Fortunately, Ingold and Howard have measured the Arrhenius parameters for k_p and the data obtained can be analyzed with the k_p calculated at this temperature.[20] At 45°C, k_{inh} for HP-136 dimer ($k_{inh}=1\times10^6 M^{-1}s^{-1}$) is

2.42 times higher than k_{inh} at 30°C. Likewise, the radical concentration is 2.46 times higher at 45°C than at 30°C. Heating affords a higher concentration of persistent radicals, thereby increasing the observed antioxidant activity. These results are very promising for the use of dimers as temperature-modulated antioxidants. In many cases such as polymer processing, antioxidants are needed at higher temperatures, i.e., when initiation reactions take place at higher rates.

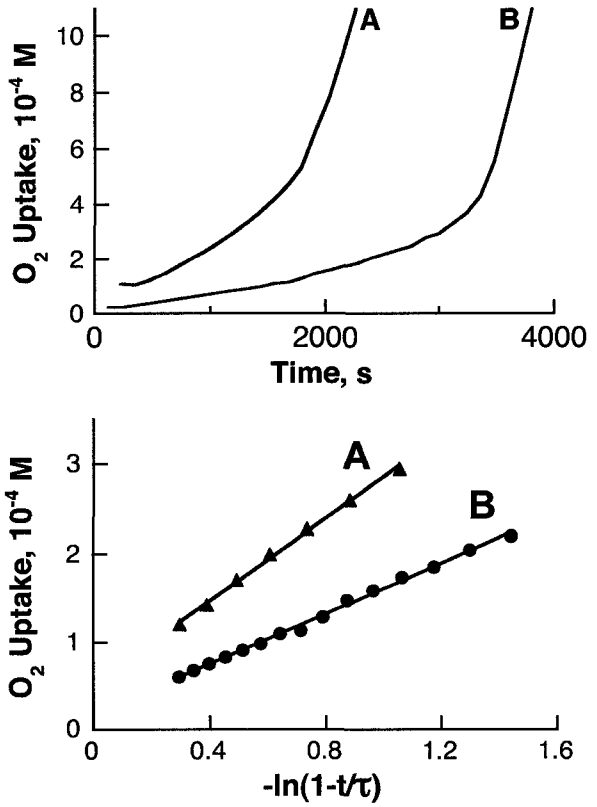

Figure 3-5. **(Top) Profiles of oxygen-uptake during AIBN initiated (7.1mM) autoxidation of styrene (2.0 M) in chlorobenzene at 30°C under air. Curve A, red: Inhibited by dimer 3_2, 23.9μM; Curve B, blue: Inhibited by $(HP\text{-}136)_2$, 108μM.**

(Bottom) Plot of oxygen-uptake in function of –ln(1-t/τ) as described in eq. [21] for data in Figure 3-5. Curve A, red: Inhibited by dimer 3_2, 23.9μM; Curve B, blue: Inhibited by $(HP\text{-}136)_2$, 108μM.

Table 3-1. Kinetic data for the trapping of peroxyl radicals by antioxidant dimers.

Inhibitor	Substrate	T (°C)	C-C BDE [a] (kcal/mol)	n [b]	k_{inh}, (10^4 $M^{-1}s^{-1}$)
Vitamin E[c]	Styrene	30		2	320
$(HP\text{-}136)_2$	Cumene	30	25.2	1.9	*No O_2 Uptake*
$(HP\text{-}136)_2$	Styrene	30	25.2	~0.8	43 ± 9
$(HP\text{-}136)_2$	Styrene	45	25.2	~0.4	104 ± 17
2_2	Cumene	30	24.5	2.1	*No O_2 Uptake*
2_2	Styrene	30	24.5	~0.6	67 ± 6
3_2	Cumene	30	26.3	2.0	*No O_2 Uptake*
3_2	Styrene	30	26.3	~1.4	22 ± 7
3_2	Styrene	45	26.3	~1.0	~61
DBHA[c]	Styrene	30		2	11

[a] Bond dissociation energies in toluene from VT-EPR, see Chapter 2. [b] $n = \tau R_i / [A_2]_{initial}$. Cumene gave more accurately measurable τ values (and therefore n values) than styrene because both k_p and k_t are significantly smaller in cumene than in styrene. Possible mechanisms for the lower n values measured in styrene are mentioned in the discussion. [c] k_{inh} for α-tocopherol and 2,6-di-*tert*-butyl-4-hydroxy-anisole are from reference[29].

3.6 Discussion

The concept presented in this chapter—using persistent radicals to trap peroxyl radicals—is rather simple. Radical-radical reactions are fast and fast reactions are what antioxidants should do with peroxyl radicals. It may seem surprising that designing antioxidants via this approach has not received more attention before this work.

Phenol-derived radicals, for example, trap peroxyl radicals at close to diffusion-controlled rates.[18] This is why the stoichiometric factor of most phenolic antioxidants is 2. However, phenolic radicals usually do not dissociate after dimerization; they irreversibly couple via the aromatic rings rather than through oxygen-to-oxygen bonding.[32] Therefore, the concept of an antioxidant based on the dimer of phenol-derived radicals, such as alpha-tocopheryl radicals, is not practical. TEMPO• and DPPH•, while both very stable as far as radicals go, are also ineffective antioxidants—in fact they are mostly used as *oxidants*, not antioxidants.[33]

Many stabilized carbon-centered radicals are known for their ability to form labile dimers. Gomberg's triphenylmethyl radical has this property and so does the triphenylene radical; unfortunately, they also have the property of reacting with oxygen and this limits their use as antioxidants. Therefore, to use the concept of fast radical-radical reactions to stop autoxidation, the antioxidant radicals have to be

inert to their environment and able to trap peroxyl radicals. These two requirements are met by the dimers 1_2, 2_2 and 3_2 and this explains their successful use as antioxidants.

The dimers' observed k_{inh} in chlorobenzene at 30°C (20-60x10^4 $M^{-1}s^{-1}$) are higher than hindered phenols such as DBHA (11x10^4 $M^{-1}s^{-1}$), but they are far from the efficiency of alpha-tocopherol (320x$10^4M^{-1}s^{-1}$).[26] Remarkably, k_{inh} for dimer 1_2 is over 1000 times faster than CIBA's Irganox HP-136® that inspired their design.

A significant advantage of this new class of antioxidants is that they are not affected by hydrogen bonding solvents. Phenolic antioxidants display large solvent effects due to the hydrogen bonding of the phenolic hydrogen, which reduces k_{inh}. For example, the antioxidant activity for alpha-tocopherol, the most active form of vitamin E, decreases by a factor of 100 when the solvent is changed from hexanes to ethyl acetate.[34] The mechanism of this effect, which is general for all phenolic antioxidants, is shown in Scheme 3-4.

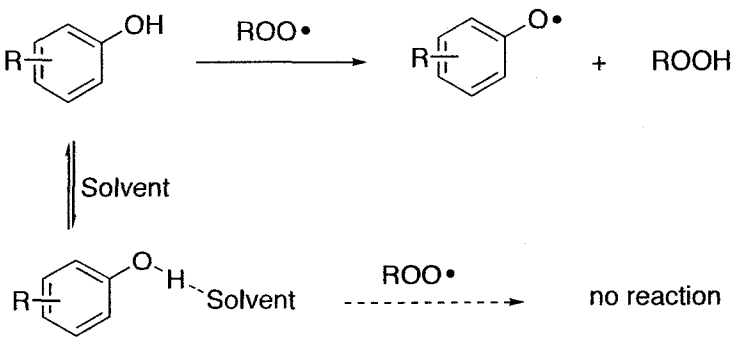

Scheme 3-4. Hydrogen bond accepting solvents can lower phenolic antioxidant activity by H-bonding the phenol hydrogen.

The dimers presented here are not expected to suffer from such deactivation. Fellow graduate student Vasilisa Filippenko currently investigates the solvent effect on dimers' antioxidant activity and her results, shown in Figure 3-6, are very promising. As we hoped, the antioxidant activity of HP-136 dimer was largely constant in solvents of varying H-bond accepting ability. Para-methoxyphenol, however, saw its antioxidant activity decrease by more than 20x when the solvent was changed from chlorobenzene to acetonitrile.

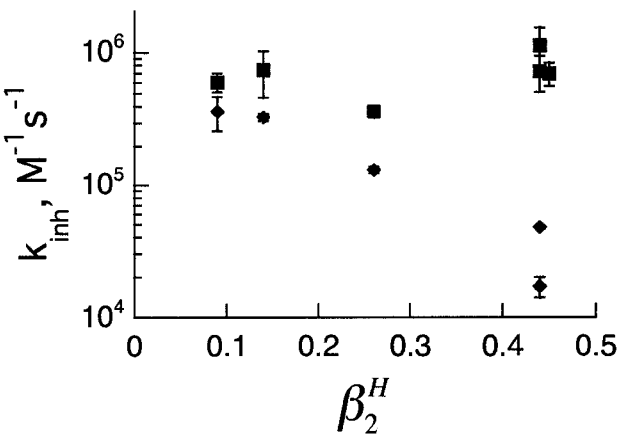

Figure 3-6. Antioxidant activity (k_{inh}) for HP-136 dimer (■) and para-methoxyphenol (◆) measured in ~0.6 mL styrene and ~1.4 mL of co-solvents with varying β_2^H values (from *J. Chem. Soc., Perkin Trans. 2*, 1989, 699-711; *ibid.*, 1990, 521-530). This parameter is a measure of the H-bond accepting properties of that solvent; a higher value indicates a better H-bond acceptor.

3.6.1 *Why are the Stoichiometric Factors in Styrene lower than in Cumene*

As observed for many efficient phenolic antioxidants,[35] we measured *lower* stoichiometric factors, n, for dimers in styrene than in cumene. In the inhibited autoxidation of cumene the stoichiometric factors were consistently 2.0 ± 0.2. This result is expected since a dimer will dissociate into two antioxidant radicals—each traps one propagating cumylperoxyl radical. Experiments run with styrene as the oxidizable substrate, however, gave lower stoichiometric factors for all dimers. The reason for the low "n" measured in styrene is less than clear at this point. Some possible explanations for lower stoichiometric factors are discussed below.

(i) Thermal cleavage of the mixed peroxides formed during the termination between A• and the propagating peroxyl radicals.

Since experiments that used cumene and (dilute) methyl linoleate as the oxidizable substrate consistently gave n=2, we have no reason to believe the peroxide bond would be so labile. Reaction [25] is unlikely to play a large role in the lower than ideal stoichiometric factors found in styrene. It should be noted that peroxides are also formed during antioxidant termination by phenolic antioxidants.

(ii) Direct addition to styrene by a persistent carbon-centered radical.

[26] 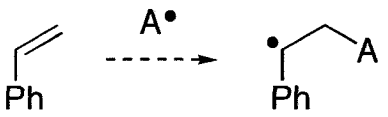

This reaction would be analogous to the reaction of TEMPO• to styrene discovered by Connolly and Scaiano.[36] We found no evidence of this reaction occurring between radical 2• and styrene by NMR. A $CDCl_3$ solution containing equimolar styrene and dimer 2_2 was held at 45°C under air for hours and no change was observed in the NMR spectrum (data not shown).

(iii) A reaction between A• and the poly(peroxystyrene)—at the peroxide bond (reaction [27]) or abstraction of a benzylic hydrogen (reaction [28])—would generate reactive alkoxyl radicals.

[27] 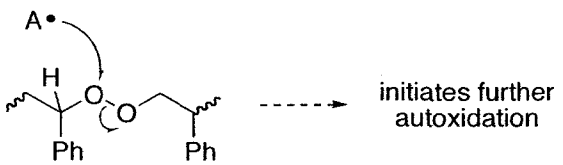

[28] 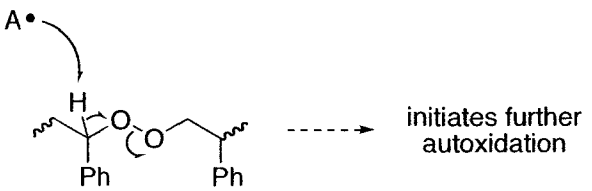

Reaction [28] is exothermic (as modeled by DFT calculations), but the reaction's relevance to the low "n" problem is far from certain.

Much thought (and computational chemistry and some experiments) have attempted to resolve the lower stoichiometric factor in styrene experiments,

however, we cannot yet point to the mechanism that is the underlying cause. The time I invested in thinking about this problem was not wasted since it inspired the work presented in the next chapter.

3.7 Conclusion

We have developed a new class of antioxidants based on fast radical-radical reactions. Dimers of persistent carbon-centered radicals were found to inhibit the autoxidation of cumene, methyl linoleate and styrene in chlorobenzene at 30°C. The measured antioxidant activities (k_{inh}) compare favorably with other antioxidants based on hindered phenolic antioxidants. We also showed that dimers of HP-136 (1_2) were much better antioxidants than the commercially sold Irganox HP-136 (1-H). There are notable advantages to this new class of antioxidants when compared to typical phenolic antioxidants:

(i) They are stable at room temperature in solid form. Very active antioxidants like vitamin E, for example, slowly degrade at room temperature.

(ii) Their antioxidant activity (k_{inh}) dramatically increases with increasing temperature as more dimers dissociate to the active radical form.

(iii) They do not suffer H-bonding deactivation by polar solvents and so, the k_{inh} are not reduced in polar solvents.

3.8 Experimental Details

Oxygen Uptake Apparatus

The oxygen uptake apparatus was designed and built at Mount Allison University in Sackville, New-Brunswick by Prof. Ross Barlcay and co-workers. A sketch of the instrument obtained from our Sackville collaborators (below) shows the important parts of the oxygen uptake apparatus including the reference and sample

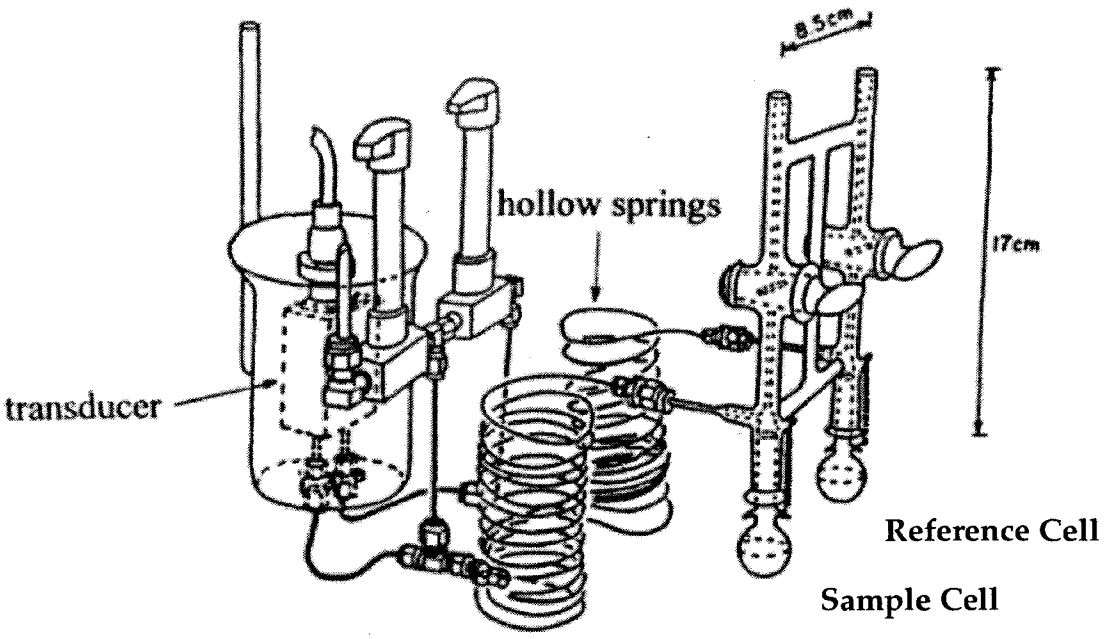

cells, the hollow springs and the pressure transducer that measures the pressure difference between the two cells. The gas filled portion of the apparatus is submerged in a temperature-controlled water bath to keep all the gases at the same temperature.

Materials.

All the chemicals were purchased from Aldrich unless specified otherwise. Chlorobenzene was HPLC grade and used as received. 2,2,5,7,8-Pentamethyl-6-chromanol (PMHC) was twice recrystallized from hexanes/dichloromethane before use. The purification of styrene was carefully done by a two-step procedure to remove inhibitor and polymerized products: the commercially obtained product (stored at -20°C) was distilled from bulb-to-bulb under reduced pressure and then filtered through a plug of silica gel or neutral aluminum oxide. The purified styrene was kept at 4°C and used within 2-3 weeks. Cumene (stored at 4°C) was filtered through silica gel before use. 2,2'-Azo-bis-isobutyronitrile (AIBN) was twice recrystallized from ethanol/dichloromethane and stored at 4°C. The dimers were synthesized as described in chapter 2.

Recrystallization Procedure.

A specially designed recrystallization procedure was used for most compounds used in this thesis to prevent further thermal degradation. Before the procedure, the compound's solubility is established in ethanol (b.p. 78°C), hexanes (b.p. ~70°C) and dichloromethane (b.p. 40°C) – the compounds were usually very soluble in dichloromethane and poorly soluble in either hexanes or ethanol. The product is added to the "worst" solvent (ethanol or hexanes) in an Erlenmeyer flask such that at least 2 cm high of solvent covers the bottom of the flask. Ethanol was

generally preferred over hexanes due to the enhanced solubility of oxidized products in the more polar solvent. The mixture is stirred with a magnetic stirrer over a heating plate. After the temperature reaches ~40°C, dichloromethane is added to the Erlenmeyer using a squirt bottle with care taken to remove undissolved solids from the flask walls. A minimum of dichloromethane is added to dissolve all the solids and the flask is then retired to a dark cupboard with a dustless tissue loosely covering the opening. Since the dichloromethane has a lower boiling point than either ethanol or hexanes, it evaporates faster to leave the product in a poorly dissolving environment where it recrystallizes. The crystals are recovered by filtration or simple decantation, washed with isopentane (b.p. 30°C) and air-dried. Fast recrystallization times and good quality crystals were consistently obtained using this technique.

Oxygen Uptake Apparatus: Preparations.

The day before an experiment, the oxygen-uptake apparatus has to be "conditioned" with the proper solvent mixture. The goal is to equilibrate the interior of the apparatus with the vapour pressure of the solvents to be used for the experiment. First, clean cells are placed at the sample and reference side and the system is pumped down under vacuum for a few hours (> 1 h) with care taken to avoid abrupt pressure variations inside the apparatus (to prevent membrane deformation). A flow of dry air through the apparatus was sometimes used to dry the

system instead of a vacuum. The temperature of the bath is held at ±5 m°C of the desired reaction temperature, reference and sample cells with appropriate solvents are shaken in the water bath overnight. A small opening to air allowed excess pressure release without significant solvent evaporation.

The next morning, a baseline was run for ~1 hour to verify proper equilibration of the system and then, "pressure checks" were performed by removing 10-100 uL of air from the sample and reference sides to verify the proper calibration of the instrument.

Oxygen Uptake Apparatus: Calibration.

The oxygen uptake apparatus measures change in resistance across a thin metallic membrane (part of the pressure transducer unit) as pressure varies across the membrane. A chart recorder or computer monitored changes in resistance reported as a voltage signal. Since the relationship between volts and pressure is linear in the region of interest, we can find the calibration factor between voltage and moles of oxygen using reactions that consume known rates of oxygen. For this, we used AIBN-initiated oxidation of pure styrene (13.3 mg AIBN in 2.0 mL styrene). Ingold and Burton have carefully measured the rate of oxygen uptake for this system and all the relevant rate constants are known.[20]

Oxygen Uptake Apparatus: Measuring R_{init}.

To start the oxidation, the initiator is injected in the sample side. After equilibration, the uninhibited rate of oxygen uptake should be constant. This rate is predicted by eq [29].

$$[29] \quad -\frac{d[O_2]}{dt} = \frac{k_p}{(2k_t)^{0.5}}[R-H](R_{init})^{0.5}$$

The rate of initiation, R_{init}, is measured independently by using R_{init} = n [PMHC] / τ as described earlier in the chapter. PMHC is injected in both the sample and the reference side. The reaction time is started exactly when the antioxidant is injected in the sample side and the inhibition period (τ) is the time is takes to consume the PMHC as seen by the inflection from inhibited to uninhibited rate of oxygen uptake.

Oxygen Uptake Apparatus: Measuring n.

The stoichiometric factor (n) can be determined for an antioxidant that gives a clear inhibition period (τ) and if R_{init} is known using n = τ *R_{init} / [Antioxidant].

Oxygen Uptake Apparatus: Measuring k_{inh}.

The antioxidant is injected in both the sample and the reference side. Again, the reaction time is started when the dimer is injected in the sample cell and the rate of oxygen uptake is measured until it returns to the uninhibited rate. From the rate of

oxygen uptake during the inhibition period, it is possible to measure the catalytic chain length using the formula: ν=-(d[O_2]/dt)/R_{init}. If this number is greater than 5, the experimental results can be used to calculate k_{inh}. The data between ~10% and ~70% of the inhibited region is plotted according to eq [21] as shown in Figure 3-4; from the slope, k_{inh} can be estimated.

Synthesis of mixed peroxide 1-OOC(CH_3)$_2$CN

In 10 mL of benzene, 0.5 g of dimer 1_2 (0.7 mmol) and 1.17 g AIBN (7 mmol) was stirred and heated at 65°C under air for 10 hours. A TLC of the reaction mixture showed that all the dimer was consumed and the solvent was removed under reduced pressure. To facilitate the seperation by column chromatography, most of the AIBN was first removed by recrystallization in hexanes/dichloromethane. Column chromatography on silica gel with 10:1 hexanes:ethyl acetate gave the main reaction product as a thick, pale yellow oil. The identity of the product was confirmed by ^{1}H NMR, ^{13}C NMR and COSY, see below.

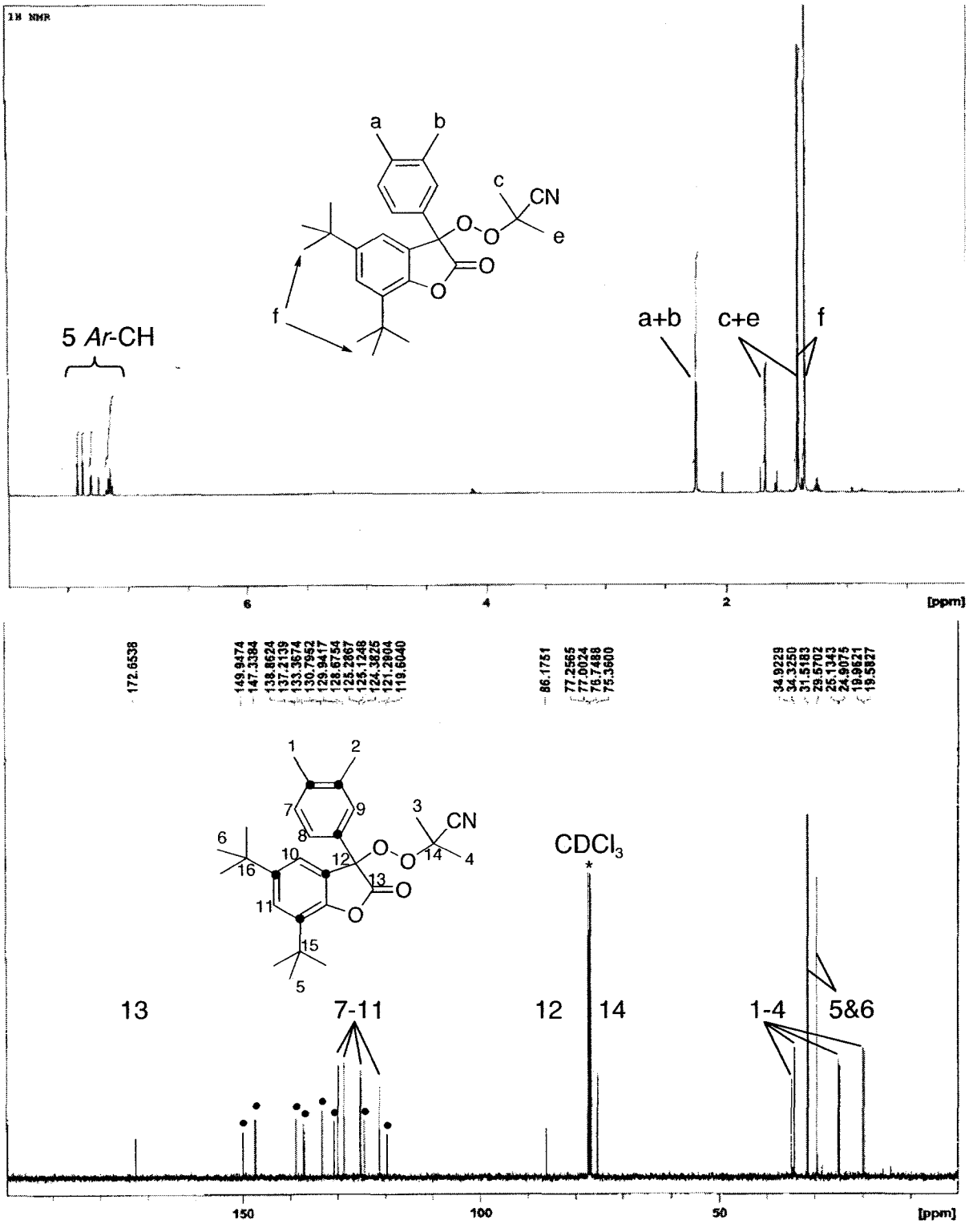

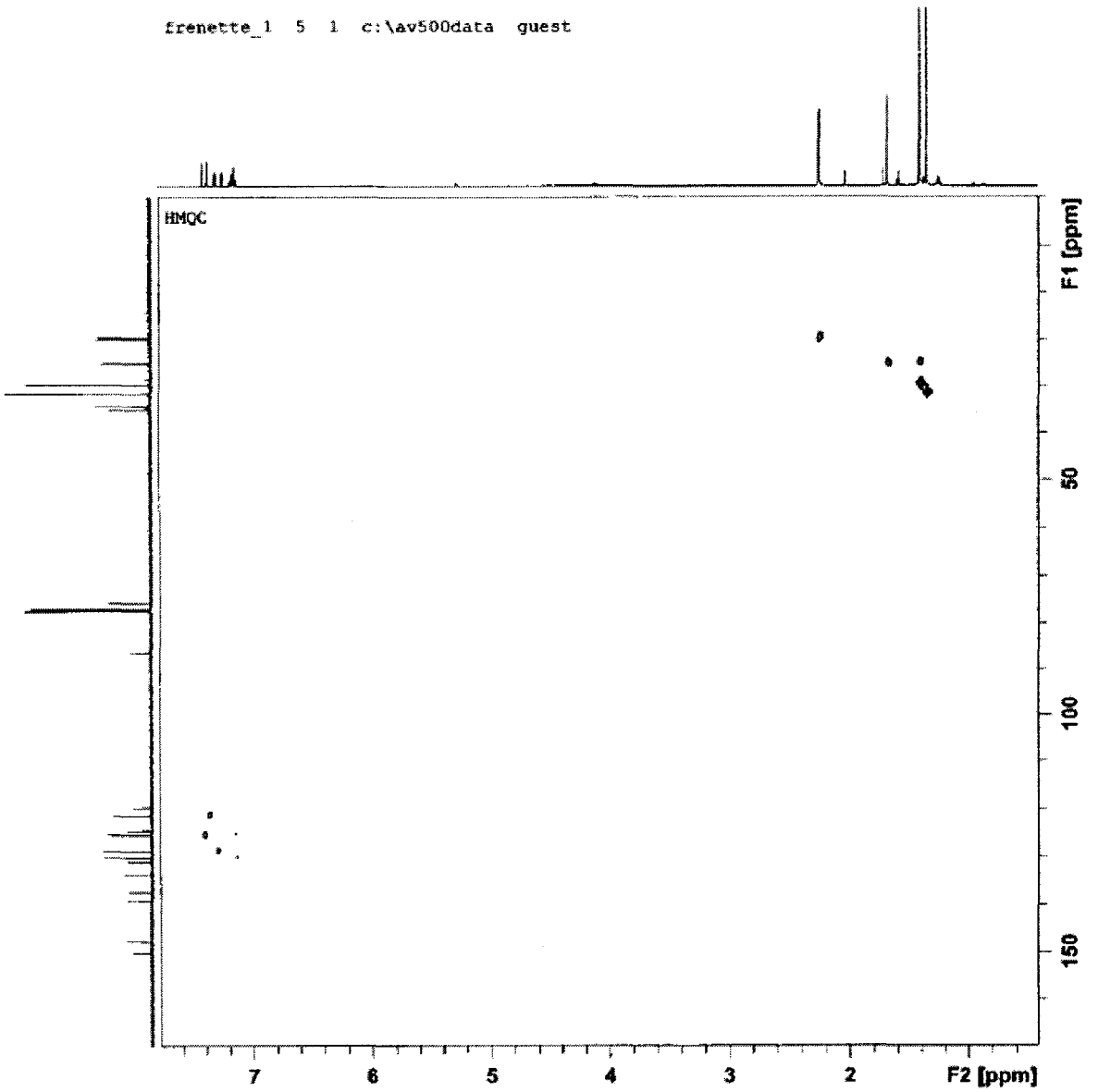

3.9 References

(1) Maillard, B.; Ingold, K. U.; Scaiano, J. C. "Rate constants for the reactions of free radicals with oxygen in solution" *Journal of the American Chemical Society* **1983**, 105, 5059-5099.

(2) Scaiano, J. C.; Martin, A.; Yap, G. P. A.; Ingold, K. U. "A Carbon-Centered Radical Unreactive Toward Oxygen: Unusual Radical Stabilization by a Lactone Ring" *Organic Letters* **2000**, 2, 899-901.

(3) Bejan, E. V.; Font-Sanchis, E.; Scaiano, J. C. "Lactone-Derived Carbon-Centered Radicals: Formation and Reactivity with Oxygen" *Organic Letters* **2001**, 3, 4059-4062.

(4) Font-Sanchis, E.; Aliaga, C.; Focsaneanu, K. S.; Scaiano, J. C. "Greatly attenuated reactivity of nitrile-derived carbon-centered radicals toward oxygen" *Chemical Communications* **2002**, 1576-1577.

(5) Font-Sanchis, E.; Aliaga, C.; Bejan, E. V.; Cornejo, R.; Scaiano, J. C. "Generation and Reactivity toward Oxygen of Carbon-Centered Radicals Containing Indane, Indene, and Fluorenyl Moieties" *Journal of Organic Chemistry* **2003**, 68, 3199-3204.

(6) Frenette, M.; Aliaga, C.; Font-Sanchis, E.; Scaiano, J. C. "Bond Dissociation Energies for Radical Dimers Derived from Highly Stabilized Carbon-Centered Radicals" *Organic Letters* **2004**, 6, 2579-2582.

(7) Scaiano, J. C. " Preparation of thermally modulated carbon-centered free radical antioxidants." 2005, Patent # WO/2005/070913.

(8) Focsaneanu, K. S.; Aliaga, C.; Scaiano, J. C. "Clean Photochemical Synthesis Mediated by Radical-Radical Reactions: Radical Buffer or the Persistent Free Radical Effect?" *Organic Letters* **2005**, 7, 4979-4982.

(9) Griller, D.; Ingold, K. U. "Persistent carbon-centered radicals" *Accounts of Chemical Research* **1976**, 9, 13-19.

(10) Fischer, H. "Unusual selectivities of radical reactions by internal suppression of fast modes" *Journal of the American Chemical Society* **1986**, 108, 3925-3927.

(11) Huang, D.; Ou, B.; Prior, R. L. "The chemistry behind antioxidant capacity assays" *Journal of Agricultural and Food Chemistry* **2005**, 53, 1841-1856.

(12) Aliaga, C.; Aspée, A.; Scaiano, J. C. "A New Method to Study Antioxidant Capability: Hydrogen Transfer from Phenols to a Prefluorescent Nitroxide" *Organic Letters* **2003**, 5, 4145-4148.

(13) Aliaga, C.; Jua´rez-Ruiz, J. M.; Scaiano, J. C.; Aspe´e, A. "Hydrogen-Transfer Reactions from Phenols to TEMPO Prefluorescent Probes in Micellar Systems" *Organic Letters* **2008**, 10, 2147-2150.

(14) Mattill, H. A. "Antioxidants and the Autoxidation of Fats" *Journal of Biological Chemistry* **1931**, 90, 141-151.

(15) Howard, J. A.; Ingold, K. U. "The Inhibited Autoxidation of Stryene. Part 1. The Deuterium Isotope Effect for Inhibition by 2,6-di-tert-butyl-4-methylphenol" *Canadian Journal of Chemistry* **1962**, 40, 1851-1864.

(16) Howard, J. A.; Ingold, K. U. "The Inhibited Autoxidation of Styrene. Part II. The Relative Efficiencies of Meta- and Para-substituted Phenols" *Canadian Journal of Chemistry* **1963**, 41, 1744-1751.

(17) Barclay, L. R. C.; Ingold, K. U. "Autoxidation of biological molecules. 2. Autoxidation of a model membrane. Comparison of the Autoxidation of Egg Lecithin Phosphatidylcholine in Water and in Chlorobenzene." *Journal of the American Chemical Society* **1981**, 103, 6478-6485.

(18) Ingold, K. U. "Peroxy radicals" *Accounts of Chemical Research* **1969**, 2, 1-9.

(19) Denisov, E. T.; Afanas'ev, I. B. "Oxidation and Antioxidants in Organic Chemistry and Biology"; Taylor & Francis: Boca Raton, FL, 2005, pp 981.

(20) Howard, J. A.; Ingold, K. U. "Absolute Rate Constants for Hydrocarbon Autoxidation: I. Styrene" *Canadian Journal of Chemistry* **1965**, 43, 2729-2736.

(21) Howard, J. A.; Ingold, K. U.; Symonds, M. "Absolute rate constants for hydrocarbon oxidation. VIII. The reactions of cumylperoxy radicals" *Canadian Journal of Chemistry* **1968**, 46, 1017-1022.

(22) Howard, J. A.; Ingold, K. U. "Absolute rate constants for hydrocarbon autoxidation. XVII. The oxidation of some cyclic ethers." *Canadian Journal of Chemistry* **1969**, 47, 3809-3815.

(23) Denisov, E. T.; Denisova, T. G.; Pokidova, T. S. "Handbook of free radical initiators"; Wiley-Interscience: Hoboken, N.J., 2003, pp 879.

(24) Mojumdar, S. C.; Becker, D. A.; DiLabio, G. A.; Ley, J. J.; Barclay, L. R. C.; Ingold, K. U. "Kinetic Studies on Stilbazulenyl-bis-nitrone (STAZN), a Nonphenolic Chain-Breaking Antioxidant in Solutions, Micelles, and Lipid Membranes" *Journal of Organic Chemistry* **2004**, 69, 2929-2936.

(25) Sifniades, S.; Levy, A. B. "Acetone"; Wiley-VCH Verlag GmbH & Co., 2007.

(26) Burton, G. W.; Ingold, K. U. "Autoxidation of biological molecules. 1. Antioxidant activity of vitamin E and related chain-Breaking Phenolic Antioxidants in Vitro" *Journal of the American Chemical Society* **1981**, 103, 6472-6477.

(27) Aliaga, C.; Stuart, D. R.; Aspée, A.; Scaiano, J. C. "Solvent effects on hydrogen abstraction reactions from lactones with antioxidant properties." *Organic Letters* **2005**, 7, 3665-3668.

(28) Mayo, F.; Miller, A.; Russell, G. "The Oxidation of Unsaturated Compounds: The Oxidation of Unsaturated Compounds. IX. The Effects of Structure on the Rates and Products of Oxidation of Unsaturated Compounds" *Journal of the American Chemical Society* **1958**, 80, 2500-2507.

(29) Burton, G. W.; Doba, T.; Gabe, E.; Hughes, L.; Lee, F. L.; Ingold, K. U. "Autoxidation of biological molecules. 4. Maximizing the antioxidant activity of phenols" *Journal of the American Chemical Society* **1985**, 107, 7053-7065.

(30) Nesvadba, P.; Evans, S.; Kroehnke, C.; Zingg, J. " Preparation of 3-aryl-2-benzofuranone stabilizers for polymers" 1995, Patent # DE 4432732.

(31) Unpublished results from Patricia D. MacLean and L. R. C. Barclay.

(32) Mahoney, L. R.; Weiner, S. A. "Mechanistic study of the dimerization of phenoxyl radicals" *Journal of the American Chemical Society* **1972**, 94, 585-590.

(33) Vogler, T.; Studer, A. "Applications of TEMPO in Synthesis" *Synthesis* **2008**, 1979-1993.

(34) Valgimigli, L.; Banks, J. T.; Lusztyk, J.; Ingold, K. U. "Solvent Effects on the Antioxidant Activity of Vitamin E" *Journal of Organic Chemistry* **1999**, 64, 3381-3383.

(35) Barclay, L. R. C.; Vinqvist, M. R.; Mukai, K.; Itoh, S. "Chain-breaking phenolic antioxidants: steric and electronic effects in polyalkylchromanols, Tocopherol Analogs, Hydroquinones, and Superior Antioxidants of the Polyalkylbenzochromanol and Naphthofuran Class" *Journal of Organic Chemistry* **1993**, 58, 7416-7420.

(36) Connolly, T. J.; Scaiano, J. C. "Reactions of the “stable” nitroxide radical TEMPO. Relevance to “living” free radical polymerizations and autopolymerization of styrene." *Tetrahedron Letters* **1997**, 38, 1133-1136.

4. Evidence for Hydroxyl Radical Formation during Lipid (Linoleate) and Cholesterol Autoxidation

4.1 Graphical Abstract

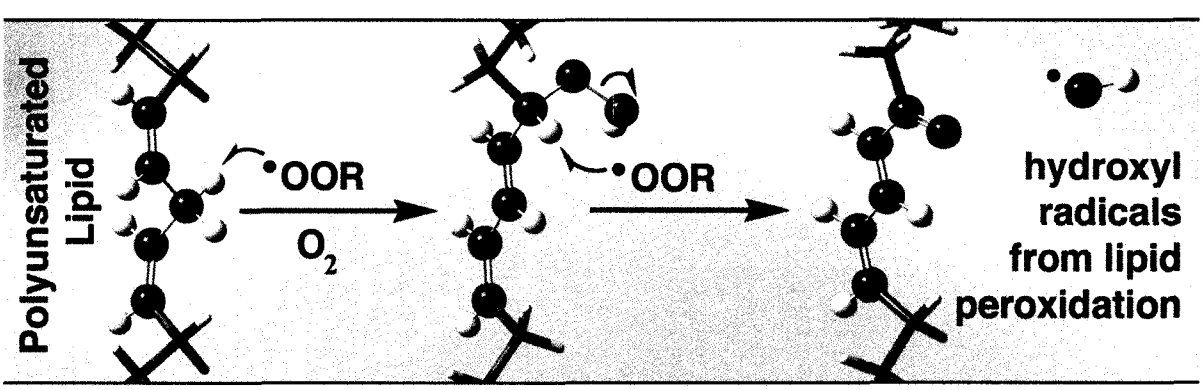

4.2 Proposed Mechanism for HO• Formation During Lipid (Linoleate) Autoxidation

Reactive oxygen species (ROS) are collectively responsible for most of the free radical oxidation occurring in living organisms and hydroxyl radicals (HO•) are the most reactive of all ROS. Some observed oxidation products appear to be derived from reactions involving HO• and so, mechanisms for the formation of hydroxyl radicals *in vivo* has been the subject of research interests for many decades.[1] Presumably, the most abundant source of HO• *in vivo* is the Fe- and Cu-catalyzed Fenton decomposition of hydrogen peroxide.[2] Other sources of hydroxyl radicals in biologically relevant systems include UV[3] or gamma irradiation[4] and the association-fragmentation of superoxide and nitric oxide.[5] In this chapter, we provide strong experimental evidence that free radical autoxidation of polyunsaturated lipids (LH) and cholesterol (Ch), both very common reactions resulting from oxidative stress, also generates hydroxyl radicals.

Polyunsaturated lipids (LH) are prime targets for free radical autoxidation. The major primary oxidation products are hydroperoxides (LOOH, Scheme 4-1) and the mechanisms involved in their formation are well established.[6-9]

If free radical oxidation of lipids is allowed to continue in the absence of chain-breaking antioxidants, ketones and aldehydes are formed and these molecules are known to be biologically active.[10,11] (In Chapter 6 we introduce a

prefluorescent probe to detect such products.) Despite significant interest in lipid autoxidation, the mechanism for the formation of lipid ketones (L=O, also called oxodienes) has eluded a satisfactory explanation for many years.[12] In this Chapter we provide evidence for a simple mechanism that forms ketones from the corresponding lipid hydroperoxides (Scheme 4-2) via αC-H abstraction. Notably, the proposed mechanism provides a pathway in which hydroxyl radicals are formed during metal-independent lipid autoxidation. Note that, in this chapter, we use the terms oxidation, autoxidation and peroxidation interchangeably.

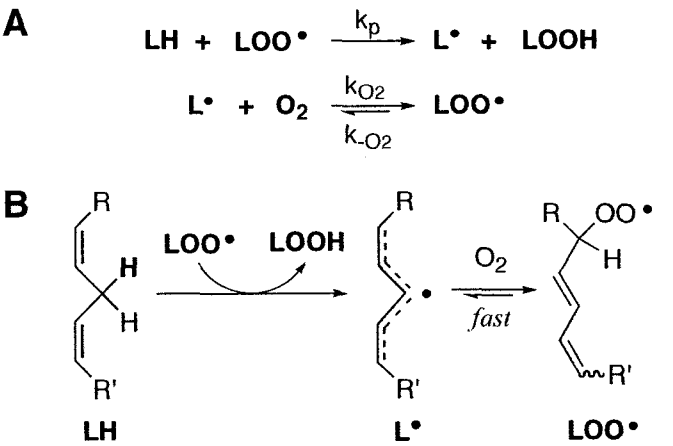

Scheme 4-1. (A) General lipid peroxidation mechanism, and (B) Mechanism as it applies to polyunsaturated fatty acids. Only propagation steps are shown. Methyl linoleate has R,R'= $-(CH_2)_4CH_3$ and $-(CH_2)_7C(O)OCH_3$.

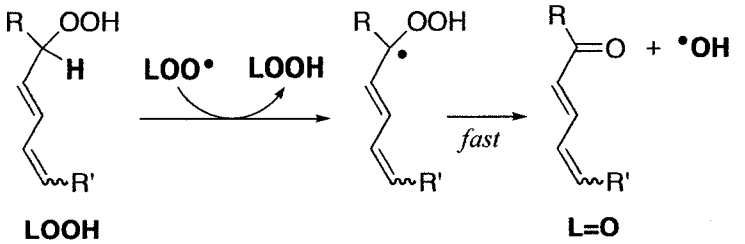

Scheme 4-2. Proposed mechanism: αC-H abstraction from LOOH by LOO• to form an oxodiene (L=O) and a hydroxyl radical.

We note that the most likely reaction of peroxyl radicals with hydroperoxides is in fact H-abstraction from the LOO-H bond; however, this is effectively an identity reaction, which at most exchanges one peroxyl radical for another.

At first glance the generation of an extremely reactive HO• from a comparatively selective lipid peroxyl radical (LOO•) may seem unlikely. However, the reaction shown in Scheme 4-2 is very exothermic—breaking the weak peroxide bond is energetically compensated by ketone formation (*vide infra*). Reactions of this type were proposed to explain the formation of ketones in the high temperature autoxidation of alkanes.[13] More recently, this mechanism was invoked to explain the formation of cyclohexanone and acetophenone during the autoxidation of cyclohexane[14,15] and ethylbenzene,[16] respectively. In theory, this mechanism could explain the formation of hydroxyl radicals from any secondary (or primary) hydroperoxide.

4.3 Monitoring HO• Formation using Benzene to Phenol Reaction

To explore the viability of the reaction proposed in Scheme 4-2, we studied the autoxidation of methyl linoleate (**LH**) initiated by the free radical initiator 2,2'-azo-bis-isobutyronitrile (AIBN). The reactions were carried out in the dark at 37°C under air in benzene. We chose benzene as a solvent because it is inert to most free radicals, including peroxyl radicals, but not to hydroxyl radicals. If hydroxyl radicals are formed, they will react quantitatively with benzene to form a benzene-HO• adduct that will produce phenol in approximately 50% yield (Scheme 4-3).[17]

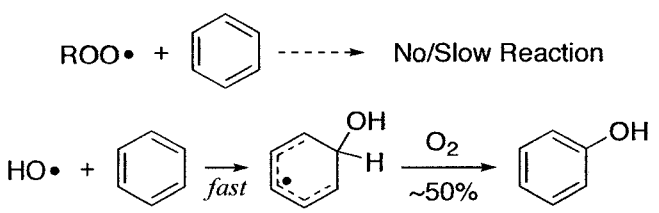

Scheme 4-3. We used benzene as a probe to detect hydroxyl radicals. The product of this selective reaction, phenol, can easily be quantified by GC-MS.

The generation of phenol from benzene is a selective test for HO• since the control experiment (with no oxidizable lipid, but with a peroxyl radical source) did not yield significant amounts of phenol (Figure 4-1, TOP graph, trace "CONTROL"). In Figure 4-1, we plot the measured phenol concentration (by GC-MS) as the oxidation of methyl linoleate in benzene progresses. While the yields of phenol are modest, these results are strong evidence that HO• is formed during lipid peroxidation. We propose that the source of HO• is from the reaction of LOO• with LOOH according to

Scheme 4-2. The upward curvature for the formation of phenol supports a secondary oxidation as its precursor.

We also monitored by GC-MS the formation of the major hydroperoxide peak (LOOH, m/z=310 after reduction to the alcohol with Ph_3P) and the major ketone peak (L=O, m/z=308). The growth of L=O and phenol both show a similar upward curvature, but LOOH shows a slight downward curvature (Figure 4-1, MIDDLE graph). This supports the mechanism proposed in Scheme 4-2. The difference between phenol and LOOH formation also appeases concerns that unreduced hydroperoxides could generate hydroxyl radicals in the GC-MS injector and would account for the phenol formed.

To estimate the extent of oxidation, we also measured the oxygen consumed during the autoxidation of LH (Figure 4-1, BOTTOM graph). The rate of oxygen uptake was surprisingly constant over 50 hours. During this period, over 30mol-% oxygen was consumed (relative to LH, the initial methyl linoleate concentration). From the rate of oxygen uptake and the calculated rate of initiation, $R_{init}=2ek_{init}[AIBN]$,[18] we can estimate the chain length for this particular system.

$$\nu = (-d[O_2]/dt)/R_{init} = (4.0\pm0.3)\times10^{-7}M.s^{-1}/(7.6\times10^{-9}M.s^{-1}) = 53.$$

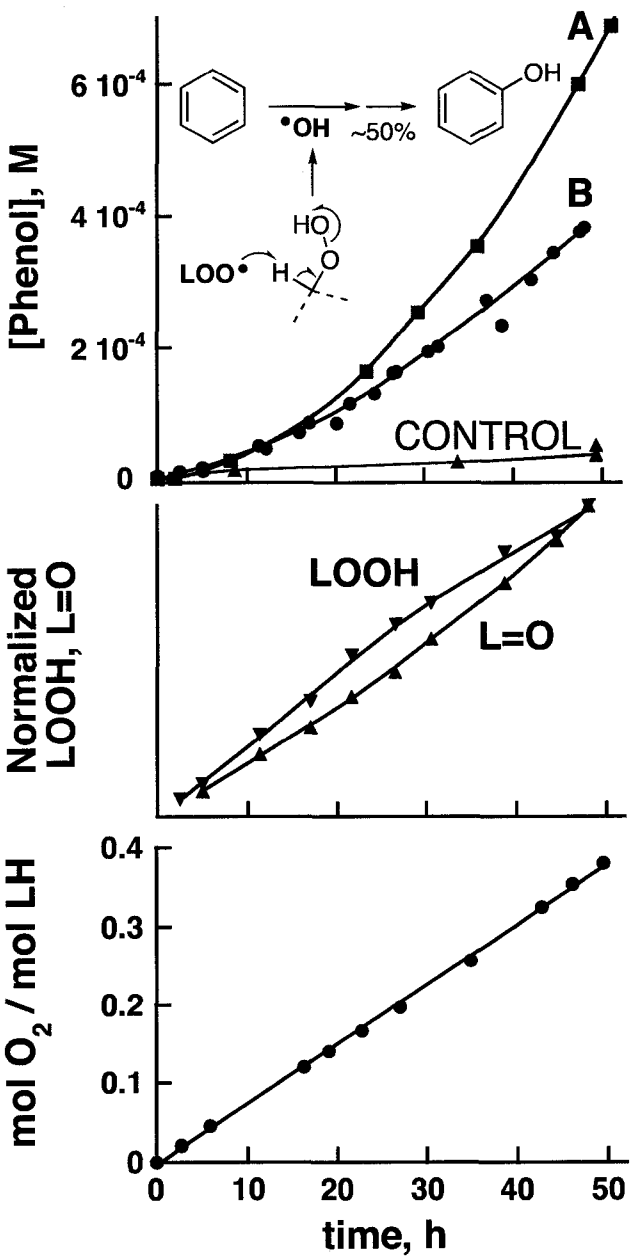

Figure 4-1. **The x-axis (time in hours) is shared for all graphs. All solutions were initiated by AIBN (0.0189M) at 37°C under air, in benzene. TOP Graph: Phenol content measured by GC-MS after Ph_3P reduction. Conditions: (A) 0.372M methyl linoleate (LH) and 0.0189M AIBN; (B) 0.189M LH and 0.0189M AIBN; (CONTROL) 0M LH and 0.0189M AIBN. MIDDLE Graph: Lipid hydroperoxide (LOOH, m/z=310 after Ph_3P reduction) and lipid oxodiene (L=O, m/z=308) measured during the autoxidation of 0.189M LH with 0.0189M AIBN. BOTTOM Graph: Oxygen consumed (plotted as ratio of lipid content) for conditions identical to those of trace (B) above.**

Under these conditions, the yield of phenol per oxygen molecule consumed is 0.56% after 48 hours. At this point, the oxygen consumed represented ~36 mol-% of the initial lipid LH. This corresponds to an effective yield of ~2% for HO• per oxygen consumed; the factor of "4" between phenol yield and hydroxyl radical yield is derived from two facts:

(i) The yield of phenol from the reaction between HO• and benzene is only ~50%.[17]

(ii) There is a stoichiometric need for two oxygen molecules to produce one HO•.[17] If this later point were not taken into account, the maximum yield of HO• would be 50%.

In our opinion, the yield of hydroxyl radicals is most likely higher than 2% since phenol is a known, albeit slow, H-atom donor to peroxyl radicals[19] (k_{inh} ~ 300 $M^{-1}s^{-1}$) and these reactions will lower the measured yield of phenol. Also, some hydroxyl radicals will react with methyl linoleate instead of the solvent, further lowering the yield of phenol. Still, the use of benzene as a probe for hydroxyl radicals was very useful in this context. GC-MS detection of phenol proved selective, sensitive and quantitative.

In a control experiment, cumene (2-propylbenzene) was oxidized in benzene (1:1 v/v) at 37°C under air using 0.0189M AIBN as the initiator. No growth in phenol was observed after 48 hours in this experiment. This important control experiment

showed that secondary hydroperoxides are required for hydroxyl radical generation, as expected from the proposed αC-H abstraction mechanism.

The level of oxidation reported here is well above those of naturally occurring lipids, however, we think the proposed reaction is more probable in membranes due to the geminate co-localization of both reagents; in other words, LOOH and L•/LOO• are "born" together in the lipid membrane.

4.4 Evidence and Proposed Mechanism for Hydroxyl Radical Formation during Cholesterol Autoxidation

"Oxysterols, and particularly 7-ketocholesterol, appear to be strongly involved in the physiopathology of atherosclerosis." –from reference[20]

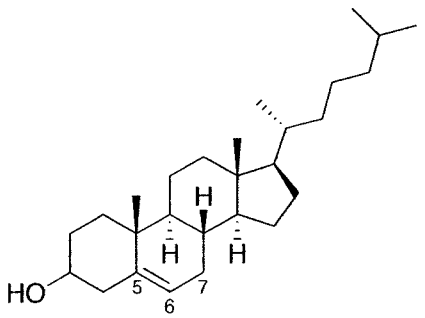

cholesterol
Ch

Cholesterol-derived free-radical oxidation products are commonly found in atherosclerosis plaques.[21] Of these, 7-ketocholesterol (Ch=O, also called 7-oxocholesterol) is generated in significant amounts and appears particularly relevant[20] but the mechanism for its formation has received limited attention. Two mechanisms are usually presented to explain the formation of Ch=O: (i) dehydrogenation from the corresponding alcohol (Ch-OH) and (ii) water loss from the corresponding hydroperoxide (Ch-OOH). Here, we introduce αC-H abstraction from Ch-OOH as another possible mechanism for the formation of 7-ketocholesterol (Scheme 4-4 (B)).

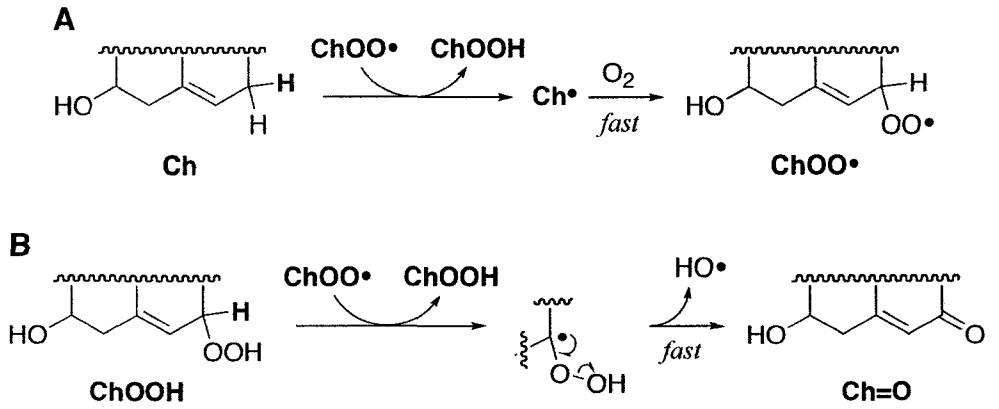

Scheme 4-4. (A) Propagation steps for the autoxidation of cholesterol and (B) proposed secondary oxidation to form 7-ketocholesterol and a hydroxyl radical.

Again, the proposed mechanism yields hydroxyl radicals and thus, we decided to monitor the formation of hydroxyl radicals with their reaction in benzene to yield phenol.[17] The phenol generated was quantified by GC-MS (after reducing the hydroperoxides with Ph_3P) and the results are shown below (Figure 4-2). Again, the yield of phenol curves upward indicating that hydroxyl radicals are generated during the secondary oxidation step.

With the azo-initiator used for these experiments, we found a non-negligible amount of phenol generated in the control experiment (no cholesterol). The yield of phenol was low and it did not curve upwards as in the case of cholesterol autoxidation, so we are confident that the majority of phenol generated in the cholesterol autoxidation is from hydroxyl radicals.

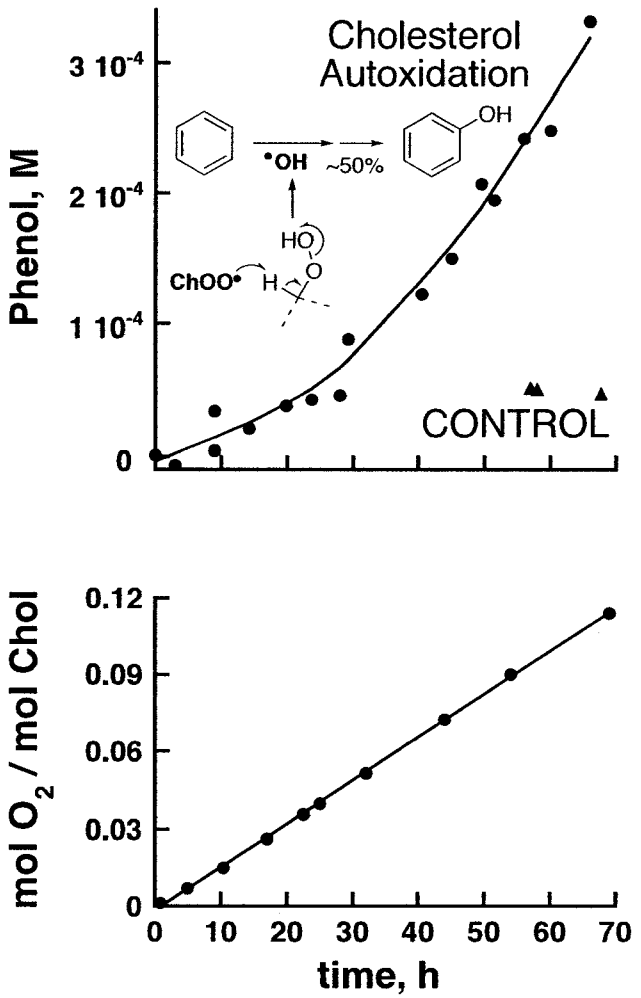

Figure 4-2. **The x-axis (time in hours) is shared for both graphs. The autoxidations were performed at 37°C under air, in benzene. TOP Graph: Phenol content measured by GC-MS. Conditions: (Cholesterol Autoxidation, circles) 0.2M cholesterol and 0.05M V-601 azo-initiator; (CONTROL, triangles) 0M cholesterol and 0.05M V-601 azo-Initiator. BOTTOM Graph: Oxygen consumed (plotted as ratio of cholesterol content) from the autoxidation of 0.2M cholesterol initiated by 0.05M V-601 azo-initiator (see structure).**

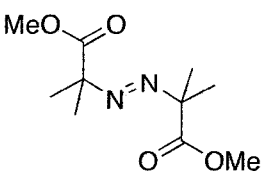

V-601 azo-initiator

Under these conditions, the yield of phenol per oxygen molecule consumed is 1.5% after 66 hours—this corresponds to an effective reaction yield of ~6% for HO• per oxygen consumed, given the ~50% yield of phenol from HO• + PhH and the stoichiometric need for two oxygen molecules to produce one HO• radical.

After 66 hours of reaction, the oxygen consumed relative to the initial cholesterol concentration is only 10.9 mol-%. At the same level of oxygen uptake (10.9 mol-%), *cholesterol autoxidation generated 4.2 times more hydroxyl radicals than methyl linoleate autoxidation.* (The initial concentration of methyl linoleate and cholesterol were similar—0.189M and 0.2M, respectively—and both autoxidations were performed in benzene at 37°C under air in the dark with an azo-initiator.) This comparison suggests that αC-H abstraction is more prevalent in the case of cholesterol hydroperoxides than for linoleate hydroperoxides (with respect to their reduced counterparts). This result is in agreement with the observation of a higher concentration of 7-ketocholesterol (Ch=O) than oxodienes (L=O) in biological lipid samples.[21] Analogously, αC-H abstraction is faster in cyclohexane hydroperoxides than in ethylbenzene hydroperoxides indicating that cyclic hydroperoxides are more prone to αC-H abstraction than non-cyclic analogs; Hermans *et al.* measured relative $k_{\alpha C\text{-}H}/k_p$ for cyclohexane and ethylbenzene to be ~55[14,15] and ~10,[16] respectively (Scheme 4-5).

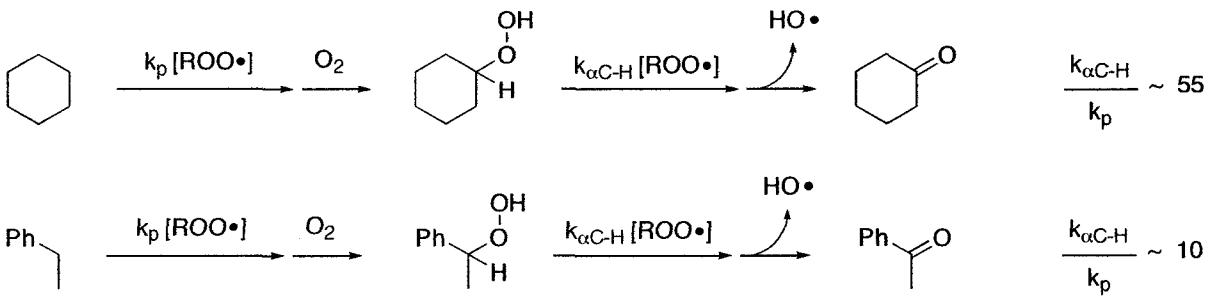

Scheme 4-5. Herman's *et al.* estimated the ratio for the primary (k_p) and secondary ($k_{\alpha C\text{-}H}$) rate constant for the autoxidation of cyclohexane and ethylbenzene. Both secondary oxidation reactions were faster than the primary oxidation, but the secondary oxidation of cyclohexane competed more favorably.

4.5 Relative Rate Constant Estimates for Primary vs. Secondary Oxidation Reaction

We have shown that free radical induced autoxidation of methyl linoleate (LH) and cholesterol (Ch) in benzene yield phenol that we interpret as hydroxyl radical generation. Importantly, autoxidation of cumene in benzene did not generate phenol, indicating that secondary hydroperoxides are required as implied by the proposed αC-H abstraction mechanism.

According to the proposed mechanism, hydroxyl radicals are generated by the sequential reactions [1] and [2], shown below using a generic "R-H" to represent methyl linoleate (LH) or cholesterol (Ch). These two reactions are competitive pathways for peroxyl radicals and we can estimate their relative rate constants by comparing the rate of oxygen uptake and the rate of phenol formation. (ROOH designates a hydroperoxide and R=O is the ketone product resulting from αC-H abstraction of ROOH.)

[1] $$\text{R-H} \xrightarrow{k_p[\text{ROO}\bullet]} \xrightarrow[\textit{fast}]{+\,O_2} \text{ROOH}$$

[2] $$\text{ROOH} \xrightarrow{k_{\alpha\text{C-H}}[\text{ROO}\bullet]} \text{R=O} + \text{HO}\bullet \xrightarrow[\textit{fast}]{} \xrightarrow[(\sim 50\%)]{+\,O_2}$$ 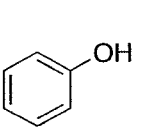

For αC-H abstraction from ROOH to occur—and hydroxyl radicals to be generated—this process needs to compete with H-abstraction from R-H. In other

words, HO• will be generated only if $k_{\alpha C\text{-}H}$[ROOH] is significant compared to k_p[R-H]. This condition is not met at low oxidation levels since [ROOH]<<[R-H]. As more R-H is oxidized to ROOH, however, $k_{\alpha C\text{-}H}$[ROOH] will increase and to a lesser extent, k_p[R-H] will decrease. This explains the upward curvature in the yield of HO• (measured as phenol) seen in Figure 4-1 and Figure 4-2.

The following analysis will give a rough estimate of the rate constants k_p and $k_{\alpha C\text{-}H}$ for methyl linoleate and cholesterol autoxidation. The ratio k_p[R-H]/$k_{\alpha C\text{-}H}$[ROOH] is equal to the rate of reaction [1] divided by the rate of reaction [2]. This ratio can be approximated as the measured rate of oxygen uptake divided by twice the rate of phenol generated as shown in eq [3]. The factor "2" before the rate of phenol is due to the ~50% yield of reaction benzene+HO•→phenol.[17]

[3] $$\frac{k_p[R-H]}{k_{\alpha C-H}[ROOH]} = \frac{d[ROOH]/dt}{d[HO\bullet]/dt} \approx \frac{-d[O_2]/dt}{2 \cdot d[Phenol]/dt}$$

4.5.1 *Estimating $k_{\alpha C\text{-}H}$ for the Secondary Oxidation of Methyl Linoleate*

For methyl linoleate, we perform the calculations after 20 h reaction at 37°C, thus ensuring a low conversion, yet enough accumulation of hydroperoxide to make reaction [2] a significant pathway. The rate of oxygen uptake can be determined from the bottom trace in Figure 4-1, where the slope of the plot is 7.7 x 10^{-3} h^{-1}. When one takes into account that the LH concentration is 0.189 M, then the rate of

oxygen uptake is 1.45 x 10^{-3} $M^{-1}h^{-1}$. For phenol we base our analysis on curve B in Figure 1, where the tangent to the curve after 20h gives a slope of ~0.7 x 10^{-5} $M^{-1}h^{-1}$. Further, oxygen uptake analysis yields a conversion of 15% after 20 h; that is the ratio LH:LOOH is ~85:15 after this time. With this information, we can estimate $k_p/k_{\alpha C\text{-}H}$ ~ 18. There is no doubt that this is a rough estimate, but it is accurate enough to state that $k_{\alpha C\text{-}H}$, while significant, is slower than k_p.

$$\frac{k_p}{k_{\alpha C-H}} \approx \frac{-d[O_2]/dt}{2 \cdot d[Phenol]/dt} \times \frac{[LOOH]}{[LH]}$$

$$\frac{k_p}{k_{\alpha C-H}} \approx \frac{1.45 \times 10^{-3}}{2 \cdot (0.7 \times 10^{-5})} \times \frac{15}{85}$$

$$\frac{k_p}{k_{\alpha C-H}} \approx 18$$

4.5.2 *Estimating $k_{\alpha C\text{-}H}$ for the Secondary Oxidation of Cholesterol*

For cholesterol, we perform the calculations after 66 h reaction at 37°C. The rate of oxygen uptake is 3.28 x 10^{-4} $M^{-1}h^{-1}$, which corresponds to a conversion of ~10.9% of Ch to ChOOH. The rate of phenol formation is ~0.77 x 10^{-5} $M^{-1}h^{-1}$. With this information, we can estimate $k_p/k_{\alpha C\text{-}H}$ ~ 2.6. Again, there is no doubt that this is a rough estimate, but it is accurate enough to state that $k_{\alpha C\text{-}H}$ is on the same order of reactivity as k_p.

$$\frac{k_p}{k_{\alpha C-H}} \approx \frac{-d[O_2]/dt}{2 \cdot d[Phenol]/dt} \times \frac{[ChOOH]}{[Ch]}$$

$$\frac{k_p}{k_{\alpha C-H}} \approx \frac{3.28 \times 10^{-4}}{2 \cdot (0.77 \times 10^{-5})} \times \frac{10.9}{89.1}$$

$$\frac{k_p}{k_{\alpha C-H}} \approx 2.6$$

4.6 Computational chemistry

We turned to computational chemistry to further understand the proposed mechanism that forms hydroxyl radicals and lipid ketones. First, we calculated the radical stabilization energy of the hydroperoxide substituent using the high level G3 method. The radical stabilization energy of a substituent Y, RSE(Y), is defined as the stabilization of methane's C-H BDE offered by Y-substitution. Mathematically,

$$RSE(Y) = BDE(YCH_2\text{-}H) - BDE(CH_3\text{-}H).$$

We calculated an RSE(–OOH) of -6.0 kcal/mol, which is significant but less important than RSE(–OH)= -7.9 kcal/mol or RSE(–OCH_3)= -7.8 kcal/mol. We associate this small difference to stereoelectronic effects illustrated in Scheme 4-6. The oxygen next to the carbon in H_2C•–OOH is less electron-rich than those in –OH and –OCH_3 substitued analogs, therefore, –OOH will not share its lone pair as efficiently with the unpaired electron on the carbon.

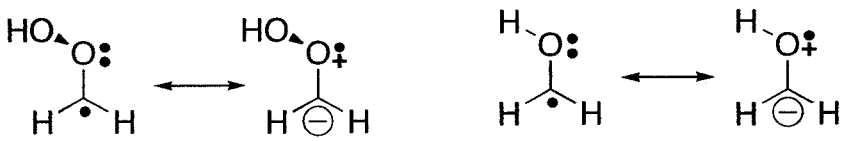

RSE_{G3}(–OOH)=-6.0 kcal/mol RSE_{G3}(–OH)=-7.9 kcal/mol

Scheme 4-6. Calculated radical stabilization energies (RSE) at the G3 level of theory for –OOH and –OH substituents. RSE_{G3}(–OH) is larger than RSE_{G3}(–OOH) because the contribution of the resonance structure on the right is more important in the former case. Note that once formed the H_2C•–OOH radical would collapse to formaldehyde and hydroxyl radical.

We then set out to compare the H-donating ability of the unsaturated lipids (LH) and the corresponding lipid hydroperoxide (LOOH). To this end, the reaction thermodynamics between a model peroxyl radical ($CH_3OO\bullet$) and representative LOOH and LH fragments were calculated (see Figure 4-3).

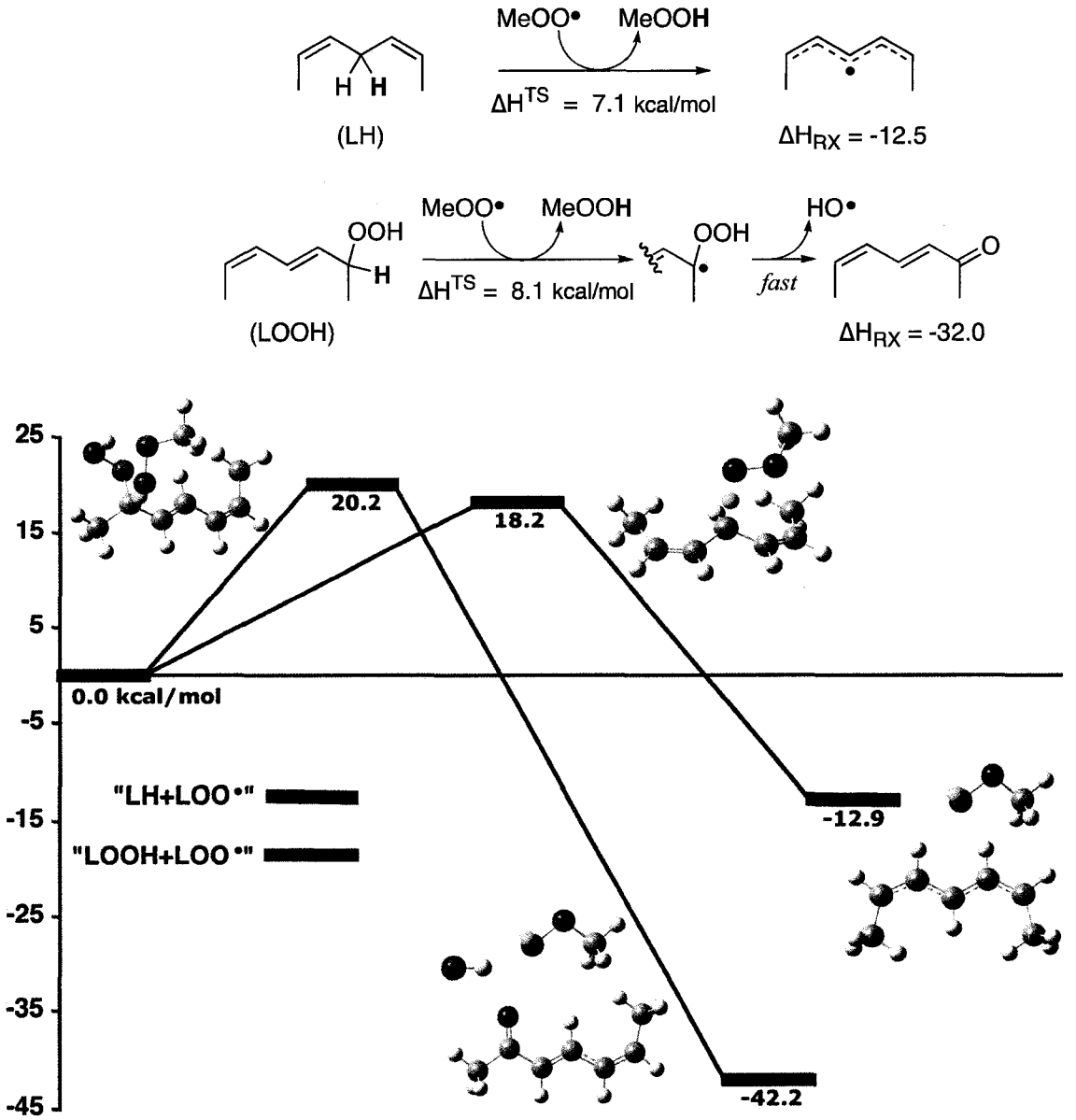

Figure 4-3. Calculated Enthalpy (top) and Free Energy (bottom) for the reaction of linoleate fragments, LH and LOOH, with a peroxyl radical, MeOO•, using the B3LYP/6-311+g(2d,2p) level of theory. (Bottom): "LH+LOO•" and "LOOH+LOO•" correspond to the H-atom abstraction in Schemes 4-1 and 4-2, respectively. The H-atom transferred is highlighted in green, other hydrogens are light grey, carbons are grey and oxygen atoms are red. The LOOH fragment shown in this figure has a *cis,trans* geometry; the *trans,trans* LOOH had similar thermodynamics (ΔG^{TS} = 20.3 kcal/mol and ΔG_{Rx} = -42.4 kcal/mol).

While the secondary reaction has a slightly higher transition state free energy, there is no doubt that the release of a hydroxyl radical is *very* thermodynamically favorable with an exergonicity (ΔG_{RX}) of -42.2 kcal/mol. In other words, the secondary reaction leading to HO• release is thermodynamically favored over primary oxidation, but kinetically it is not. This result agrees with the analysis presented in section 4.5.1 that shows k_p to be greater than $k_{\alpha C\text{-}H}$ for methyl linoleate autoxidation.

4.7 Discussion

We have proposed that αC-H abstraction of secondary hydroperoxides can generate hydroxyl radicals based on the following evidence:

(i) During the free radical autoxidation of methyl linoleate and cholesterol, hydroxyl radicals react with benzene, the solvent, to yield phenol, which was quantified by GC-MS.

(ii) The growth in phenol showed an upward curvature indicating that hydroxyl radicals are generated during a secondary oxidation mechanism.

(iii) In the case of methyl linoleate, the growth in lipid ketone (L=O) showed a similar upward curvature as phenol formation while lipid hydroperoxides (LOOH) had a slight downward curvature.

(iv) Oxygen uptake data allowed us to quantify the yield of phenol as a function of the oxygen consumed. We found that after 10.9% oxygen uptake with respect to the oxidizable substrate, cholesterol autoxidation generated 4.2 times more phenol than methyl linoleate autoxidation. This result agrees with the observation that ketones are formed more readily during cholesterol autoxidation than linoleate autoxidation.

(v) Calculated activation energies for the primary and secondary oxidation of linoleate fragments agree with the estimated rate constants for these reactions; in both cases, we find that $k_{\alpha C\text{-}H}$ is slower than k_p.

(vi) A control experiment shows that tertiary hydroperoxides do *not* generate hydroxyl radicals as shown during the autoxidation of cumene in benzene.

The use of benzene as a probe to detect hydroxyl radicals was very useful in this context. Other HO• probes such as dimethylsulfoxide yield complex products under air[22] and spin-traps such as 5,5'-dimethylpiperidine-N-oxide (DMPO) are not selective to hydroxyl radicals.[23] Another probe, terephthalate (benzene-1,4-dicarboxylic acid), becomes fluorescent after reacting with HO• and this approach could be used for aqueous samples.[24]

As we are often reminded in physical organic chemistry lectures, it is impossible to "prove" a mechanism. We can only disprove other possibilities. This proposed mechanism may be disproved in the future, but we do not have the evidence to do so here. Because the yield of hydroxyl radicals is so low and the level of oxidation required is so high, the relevance of this mechanism to biological lipid autoxidation is questionable. Perhaps the cholesterol example is more relevant. It is known that cholesterol oxidation leads to complex products. Could is be a result of hydroxyl radicals generated by the proposed mechanism?

We do *not* presume, however, that ketone formation is exclusively the result of αC-H abstraction from secondary hydroperoxides. For one, secondary peroxyl radicals are known to recombine and form a ketone and alcohol by the Russell mechanism.[25] Secondary alcohols will also yield ketones via αC-H abstraction, but hydroxyl radicals are not the product of such reactions.

Likewise, hydroxyl radicals could be generated by other reactions. Thermal decomposition of hydroperoxides, while thermodynamically unfavorable, could generate hydroxyl radicals. Another possibility is that peroxyl radicals will add to an adjacent double bond, and the resulting radical will attack the hydroperoxide to yield HO• as shown below.

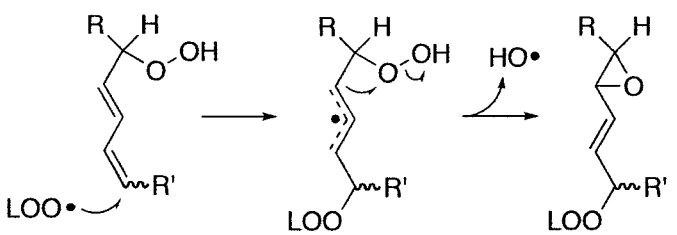

Scheme 4-7. The addition of a peroxyl radical to the diene of LOOH could generate hydroxyl radicals after the formation of an epoxide.

In any case, the αC-H abstraction mechanism could be a missing piece of the great puzzle of free radical oxidation and a source of hydroxyl radicals generated in lipid and cholesterol autoxidation.

Hydroxyl radicals are extremely reactive. In non-aqueous media, hydroxyl radicals will react where they are generated since the rate constant for

HO•+molecule is diffusion-controlled for almost any molecule.[4] For this reason, the reaction products derived from hydroxyl radicals will appear random in any complicated mixture of compounds (such as biological samples). It is therefore difficult to measure the true damage done by HO•-derived products in biological samples since no single reaction product will be generated in a significant yield. Additionally, the reaction of HO• with most organic matter will yield a non-characteristic water molecule. For these reasons and others, the relevance of hydroxyl radicals *in vivo* is poorly understood. Are products such as oxo-guanine a result of hydroxyl radical reactions or hydroxyl-radical-like reagents? How relevant are hydroxyl radicals in oxidative stress? Peroxyl radicals certainly play a major part in the chemistry of lipid peroxidation, but it cannot be ruled out that hydroxyl radicals generated during propagation steps are "hidden occurrences". In most cases the reactions of HO• will swiftly regenerate a peroxyl radical, thereby yielding no observable change in the overall kinetics (or the product distribution in complex systems). To be sure, if hydroxyl radicals are generated during lipid peroxidation as suggested in this chapter, we are talking about a few percent at most. The products they generate, however, will not be as predictable and remediable to living organisms as peroxyl radical generated products. A hydroxyl radical could, for example, initiate free radical reactions with any protein amino acid, and an unpaired electron inside a protein can yield significant chemical changes. If aging is caused by a buildup of "interfering junk" in the body, as the free radical theory of aging

implies, then hydroxyl radical damage may be a source. Hopefully, the results presented in this chapter will inspire more studies that will address these questions.

4.8 Conclusion

We have provided evidence that hydroxyl radicals are generated during linoleate and cholesterol autoxidation. The reactions were carried out in benzene, where hydroxyl radicals reacted with the solvent to generate phenol that was easily quantified by GC-MS. After 10.9% oxidation, the yield of hydroxyl radicals (per oxygen consumed) was ~6.1% for cholesterol autoxidation and ~1.4% for methyl linoleate autoxidation. We propose that αC-H abstraction from hydroperoxides, the main autoxidation products, generates ketones and hydroxyl radicals in a long overlooked path to these products. DFT calculations also confirmed the slightly higher barrier for the secondary oxidation of methyl linoleate and the very exothermic nature of the proposed reaction.

4.9 Experimental Details

Materials

Methyl linoleate (>99%) and cholesterol were obtained from Sigma. Phenol, triphenylphosphene, cholesterol and 2,2'-azo-bis-isobutyronitrile were from purchased from Aldrich. V-601 (2,2'-azobis(methyl-2-methylpropionate)) was obtained from Wako Chemicals (Japan). Benzene was HPLC-grade.

GC-MS Analysis

The gas chromatogram (model 6890N) and the mass selective detector (model 5973) were from Agilent Technologies. The column was a DB-5 (30m length, 0.32mm I.D.).

The autoxidation of methyl linoleate (freshly opened ampoules) and cholesterol was carried out in a Lab-line shaker held at 37°C in the dark. All autoxidations were initiated by 2,2'-azo-bis-isobutyronitrile (AIBN, twice recrystallized) and HPLC-grade benzene was the solvent. Efforts were made to keep the system under air without allowing benzene to evaporate during the long reaction times. For this reason, larger than necessary volumes were oxidized in a long-neck, narrow-opening, round-bottom flask. The opening was fixed with a rubber septum and a needle protruded the septum to replenish the system of air. Aliquots of 250μL were taken at different reaction times and were immediately added to

100μL of 0.25M Ph_3P in benzene (to reduce the hydroperoxides to alcohols). The pre-measured GC-MS vials containing the Ph_3P solution were frozen at -40°C until the reaction mixture was added; this prevented oxidation or evaporation of Ph_3P in benzene and once the oxidizing sample is added, the cooling limited further autoxidation reactions until analysis. To detect the phenol generated during the reaction, this mixture was injected directly in the GC-MS taking care to by-pass the mass detection during the lipid and Ph_3P/Ph_3PO regions, as the lipids are too concentrated and could damage the detector. To detect lipid oxidation products, the entire reduced sample was diluted to a total of 10mL with dichloromethane and analyzed by GC-MS.

The oxidation of cholesterol was performed the same as above, except that V-601 was used as the azo-initiator instead of AIBN.

The phenol was quantified by extracting m/z=94.2±0.5 from the Total Ion Chromatogram, integrating the corresponding peak, and comparing these results with a similarly analyzed calibration curve using an authentic standard (Figure 4-4).

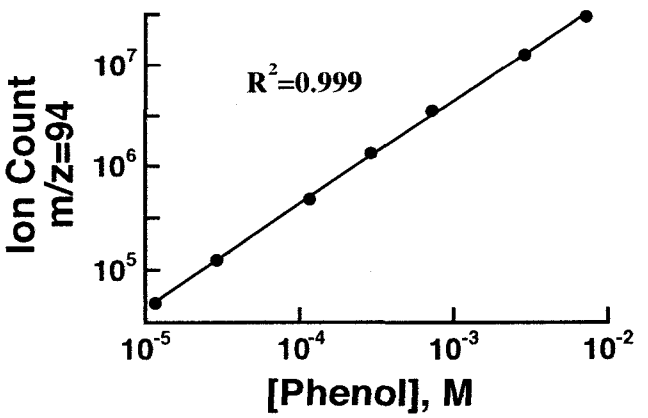

Figure 4-4. Calibration curve for phenol analyzed by GC-MS. We present the data as a double-log plot to show the linearity of our detector over almost three orders of magnitude in phenol concentration.

A typical mass selective chromatogram (m/z=94.2) shows the growth of phenol during the autoxidation of methyl linoleate in Figure 4-5. A Total Ion Chromatogram (TIC) from the lipid region from the diluted sample after 50h of reaction time is also shown (Figure 4-6).

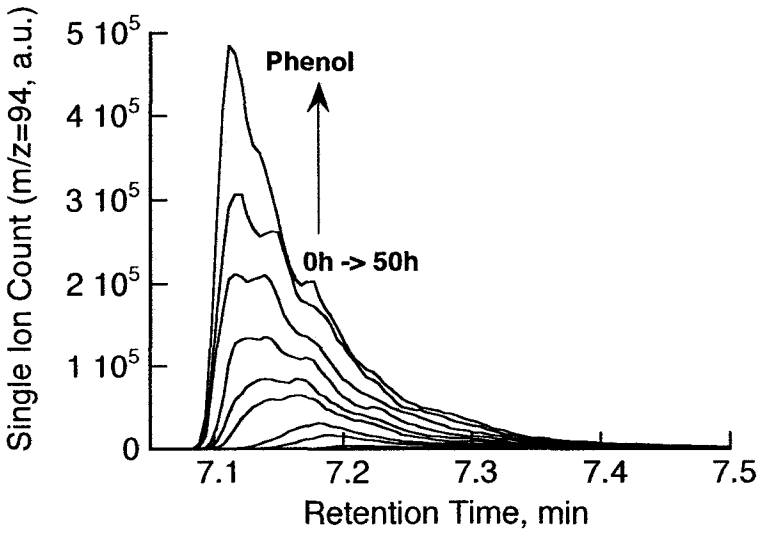

Figure 4-5. **Mass selective chromatogram showing the growth of the phenol peak during the autoxidation of methyl linoleate by AIBN in benzene at 37°C. The shift of the peak to shorter times was also observed during the calibration with the authentic sample.**

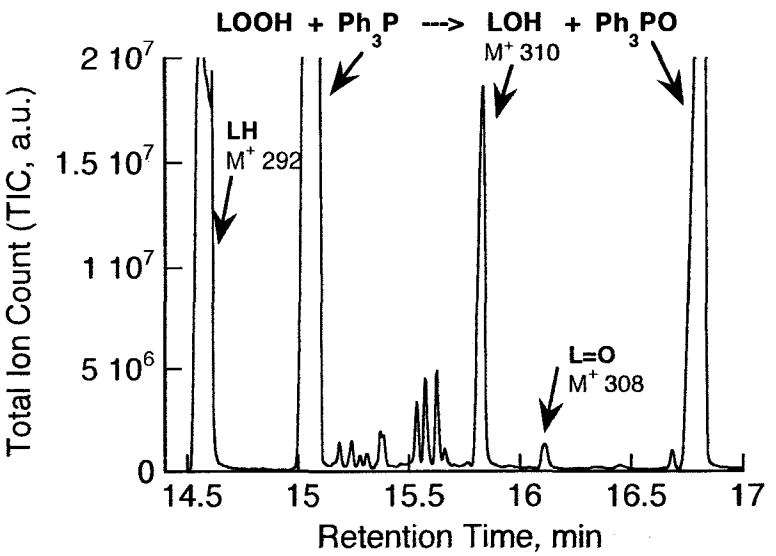

Figure 4-6. **Total Ion Chromatogram for a diluted sample (see experimental details) of 0.189M methyl linoleate and 0.0189M AIBN after 50 hours at 37°C under air. The peaks for LOH and L=O that were plotted in Figure 4-1 are indicated. Note: The peaks corresponding to LH, Ph_3P and Ph_3PO are saturated at this concentration.**

Control Experiment: Cumene Autoxidation

A solution of 1:1 v/v cumene:benzene was autoxidized at 37°C under air for 48h. A mass selective GC-MS was run for phenol (m/z=94.2±0.5) before and after the reaction and both samples showed negligible phenol (signals blended with baseline).

Oxygen Uptake Measurements

The oxygen uptake data was acquired on a home-built differential pressure sensor, which was a very generous gift from L. Ross C. Barclay of Mount Alison University in New Brunswick. This instrument is described in greater detail in "Howard, J. A. Advance In Free Radical Chem. (London) 1972:4, 49-173" and in the experimental section of Chapter 3.

The pressure difference between a sample containing the oxidizable substrate (methyl linoleate or cholesterol) and initiator (AIBN or V-601) in benzene is compared to a reference cell (same as sample but without oxidizable substrate) by means of a pressure transducer. This device measures pressure difference as a voltage signal that is analyzed by a computer. To quantify oxygen uptake data, the cells were calibrated against a reaction that has a well-known rate of oxygen uptake (AIBN-initiated autoxidation of pure styrene).[26]

Computational Chemistry

Density Functional Theory calculations were performed using B3LYP (Becke's 3-parameter exchange [Becke, A. D. J. Chem. Phys., 1993, 98, 5648] and Lee, Yang and Parr's correlation [C. Lee, W. Yang and R. G. Parr, Phys. Rev. B, 1988, 37, 785]) with a triple-ζ basis set (6-311+g(2d,2p)) as implemented in the Gaussian 03 software package.[27] This level of theory was found to be satisfactory to estimate bond dissociation energies for lipid peroxidation reactions by Pratt, Mills and Porter.[9] Transition states were confirmed by examining that only one imaginary vibrational frequency corresponding to the reaction coordinate existed. As reported before by Vereecken et al.[28] for other similar radicals, the $R_2C{\cdot}(OOH)$ intermediate drawn in Scheme 4-2 does not have a barrier for the decomposition to the ketone (L=O) and hydroxyl radical according to DFT calculations.

4.10 Appendix. Lowest Energy Conformer Geometry for Relevant Structures

All geometries were optimized using B3LYP/6-311+g(2d,2p))

"LH" fragment (*cis,cis*-2,5-heptadiene)

```
E(UB+HF-LYP) =  -274.024389826
Sum of electronic and zero-point Energies=          -273.854583
Sum of electronic and thermal Energies=             -273.845624
Sum of electronic and thermal Enthalpies=           -273.844680
Sum of electronic and thermal Free Energies=        -273.889128
```

Atomic Number	Coordinates (Angstroms) X	Y	Z
6	2.319501	0.538338	-0.399512
1	2.878959	1.177987	-1.074953
6	1.004641	0.742598	-0.321773
1	0.579533	1.522575	-0.945006
6	3.143702	-0.475915	0.337173
1	3.898764	0.015216	0.956259
1	2.550187	-1.119715	0.982794
6	-1.004660	-0.742625	-0.321788
1	-0.579611	-1.522612	-0.945046
6	-2.319505	-0.538300	-0.399511
6	-3.143682	0.475944	0.337198
1	-2.550387	1.118587	0.984177
1	-3.899922	-0.015142	0.954867
1	-2.878984	-1.177879	-1.075005
6	0.000004	-0.000053	0.524162
1	-0.507404	0.711196	1.178231
1	0.507443	-0.711359	1.178145
1	-3.683696	1.115833	-0.365069
1	3.685109	-1.114614	-0.365086

"LH+MeOO•" Transition State

```
Imaginary Frequency: -1496.9027 cm-1
E(UB+HF-LYP) =  -464.294211501 Hartree
Sum of electronic and zero-point Energies=          -464.086075
Sum of electronic and thermal Energies=             -464.072408
```

```
 Sum of electronic and thermal Enthalpies=            -464.071464
 Sum of electronic and thermal Free Energies=         -464.129004

---------------------------------------------
  Atomic          Coordinates (Angstroms)
  Number         X           Y           Z
---------------------------------------------
     6      -3.051764   -0.310605   -0.306930
     1      -3.883667   -0.554483   -0.958737
     6      -1.894498    0.028942   -0.895028
     1      -1.864339    0.017072   -1.979504
     6      -3.339154   -0.400979    1.159362
     1      -3.601724   -1.425861    1.434762
     1      -2.497119   -0.099387    1.778268
     6       0.300462    1.236931   -0.978883
     1       0.262413    1.134152   -2.058283
     6       1.203090    2.095534   -0.476231
     6       1.460957    2.409541    0.964463
     1       0.802207    1.872312    1.643267
     1       1.340647    3.479346    1.153776
     1       1.819309    2.636256   -1.186293
     6      -0.627671    0.377948   -0.232229
     1      -0.017777   -0.723760   -0.166732
     1      -0.730074    0.633683    0.818402
     1       2.492295    2.165125    1.234398
     1      -4.197355    0.221517    1.424746
     8       0.615386   -1.891918   -0.082868
     8       1.907992   -1.669551   -0.519676
     6       2.767167   -1.512031    0.609208
     1       3.767464   -1.393023    0.195963
     1       2.488770   -0.625909    1.180656
     1       2.720394   -2.396967    1.243279
---------------------------------------------
```

"L•" fragment (*cis,cis*-2,5-heptadienyl radical)

```
 E(UB+HF-LYP) =  -273.401605117 Hartree
 Sum of electronic and zero-point Energies=           -273.245450
 Sum of electronic and thermal Energies=              -273.236475
 Sum of electronic and thermal Enthalpies=            -273.235531
 Sum of electronic and thermal Free Energies=         -273.280389

---------------------------------------------
  Atomic          Coordinates (Angstroms)
  Number         X           Y           Z
---------------------------------------------
     6      -2.487760    0.362146    0.000003
     1      -3.330986    1.042995    0.000048
     6      -1.238853    0.914909    0.000018
     1      -1.187964    1.999528    0.000043
     6      -2.828702   -1.093549   -0.000020
```

1	-3.431991	-1.351872	-0.875113
1	-1.950771	-1.735786	-0.000705
6	1.238853	0.914909	-0.000018
1	1.187964	1.999528	-0.000043
6	2.487760	0.362146	-0.000003
6	2.828702	-1.093549	0.000020
1	1.950770	-1.735786	0.000689
1	3.431977	-1.351875	0.875121
1	3.330986	1.042995	-0.000048
6	0.000000	0.239124	0.000000
1	0.000000	-0.842205	0.000000
1	-3.430830	-1.352172	0.875795
1	3.430844	-1.352169	-0.875787

"**LOOH**" fragment (6-hydroperoxy-*cis,trans*-2,4 -heptadiene)

E(RB+HF-LYP) = -424.436292853 Hartree

Sum of electronic and zero-point Energies=	-424.258785
Sum of electronic and thermal Energies=	-424.247534
Sum of electronic and thermal Enthalpies=	-424.246590
Sum of electronic and thermal Free Energies=	-424.296127

Atomic Number	Coordinates (Angstroms) X	Y	Z
6	3.231810	-0.187028	-0.426642
1	4.014656	-0.423312	-1.139341
6	1.971781	-0.468076	-0.789366
1	1.816483	-0.912105	-1.766943
6	0.769077	-0.241621	-0.006664
1	0.879903	0.198559	0.977723
6	3.704395	0.420043	0.857924
1	2.895980	0.646753	1.548883
6	-0.465349	-0.549207	-0.424194
1	-0.608421	-0.985848	-1.409065
6	-1.710776	-0.321890	0.377001
1	-1.457254	0.026714	1.380134
6	-2.606776	-1.552814	0.450948
1	-2.071147	-2.368236	0.935379
1	-2.897750	-1.878731	-0.547826
8	-2.546869	0.686008	-0.238238
8	-1.915209	1.975044	-0.061406
1	-1.386414	2.049573	-0.867993
1	4.251301	1.346587	0.665577
1	4.402189	-0.251181	1.365089
1	-3.507870	-1.333624	1.021492

"LOOH+MeOO•" transition state

Imaginary Frequency: -1477.1609 cm-1
E(UB+HF-LYP) = -614.703999478 Hartree
Sum of electronic and zero-point Energies= -614.487320
Sum of electronic and thermal Energies= -614.471703
Sum of electronic and thermal Enthalpies= -614.470759
Sum of electronic and thermal Free Energies= -614.531861

Atomic Number	Coordinates (Angstroms) X	Y	Z
6	-1.545814	-0.414883	-0.196655
1	-1.455234	-0.043754	0.814844
6	-0.466068	-0.987399	-0.771709
1	-0.546666	-1.367314	-1.784195
6	0.858542	-1.135622	-0.172405
1	1.578778	-0.211794	-0.641789
6	1.620338	-2.407184	-0.511781
1	1.106782	-3.271737	-0.086316
1	2.629880	-2.366721	-0.114615
8	0.802730	-0.824143	1.202802
8	2.149006	-0.727106	1.730535
1	2.397736	0.170423	1.447044
1	1.673403	-2.528310	-1.592955
8	2.338224	0.765766	-1.137342
8	2.489582	1.650343	-0.064844
6	1.564491	2.731674	-0.213117
1	1.760677	3.393154	0.629361
1	1.749136	3.250767	-1.152513
1	0.538872	2.366492	-0.177487
6	-2.818873	-0.292154	-0.864910
1	-2.857324	-0.668175	-1.881860
6	-3.946417	0.235354	-0.353857
1	-4.818724	0.252028	-0.998109
6	-4.151551	0.806834	1.013091
1	-4.939185	0.262152	1.540273
1	-3.256158	0.778755	1.629115
1	-4.486201	1.845429	0.948056

"L=O" fragment (*cis,trans*-3,5-heptadien-2-one)

```
E(RB+HF-LYP) =  -348.077261114 Hartree
Sum of electronic and zero-point Energies=          -347.926384
Sum of electronic and thermal Energies=             -347.916879
Sum of electronic and thermal Enthalpies=           -347.915935
Sum of electronic and thermal Free Energies=        -347.961494
```

Atomic Number	Coordinates (Angstroms) X	Y	Z
6	2.864331	-0.516559	0.000036
1	3.652549	-1.262001	0.000078
6	1.598462	-0.968035	-0.000141
1	1.445221	-2.041654	-0.000219
6	0.405296	-0.154783	-0.000209
1	0.504406	0.923801	-0.000469
6	3.333543	0.902918	0.000132
1	3.959673	1.095459	-0.874805
1	2.521864	1.625535	0.000251
6	-0.846658	-0.645366	0.000075
1	-1.016991	-1.715925	0.000330
6	-2.033189	0.241681	0.000035
6	-3.384227	-0.443449	0.000093
1	-3.481762	-1.086393	-0.877570
1	-4.177069	0.298745	-0.000068
8	-1.938892	1.456861	-0.000071
1	-3.481853	-1.086200	0.877870
1	3.959763	1.095300	0.875038

4.11 References

(1) Halliwell, B.; Gutteridge, J. M. C. "Free Radicals in Biology and Medicine"; Oxford University Press: Oxford; New York, 2007.

(2) Halliwell, B.; Gutteridge, J. M. C. "Oxygen toxicity, oxygen radicals, transition metals and disease" *Biochemical Journal* **1984**, 219, 1-14.

(3) Taira, J.; Mimura, K.; Yoneya, T.; Hagi, A.; AkiraMurakami; Makino, K. "Hydroxyl Radical Formation by UV-Irradiated Epidermal Cells" *Journal of Biochemistry* **1992**, 111, 693-695.

(4) Buxton, G. V.; Greenstock, C. L.; Helman, W. P.; Ross, A. B. "Critical review of rate constants for reactions of hydrated electrons, hydrogen atoms and hydroxyl radicals (•OH/O•–) in aqueous solution" *Journal of Physical and Chemical Reference Data* **1988**, 17, 513-886.

(5) Coddington, J. W.; Hurst, J. K.; Lymar, S. V. "Hydroxyl Radical Formation during Peroxynitrous Acid Decomposition" *Journal of the American Chemical Society* **1999**, 121, 2438-2443.

(6) Ingold, K. U. "Peroxy Radicals" *Accounts of Chemical Research* **1969**, 2, 1-9.

(7) Porter, N. A. "Mechanisms for the Autoxidation of Polyunsaturated Lipids" *Accounts of Chemical Research* **1986**, 19, 262-268.

(8) Halliwell, B.; Gutteridge, J. M. C. "*Free Radicals in Biology and Medicine*, 3rd ed." Oxford University Press: New York, 1999.

(9) Pratt, D. A.; Mills, J. H.; Porter, N. A. "Theoretical Calculations of Carbon-Oxygen Bond Dissociation Enthalpies of Peroxyl Radicals Formed in the

Autoxidation of Lipids" *Journal of the American Chemical Society* **2003**, 125, 5801-5810.

(10) Esterbauer, H.; Schaur, R. J.; Zollner, H. "Chemistry and biochemistry of 4-hydroxynonenal, malonaldehyde and related aldehydes" *Free Radical Biology & Medicine* **1991**, 11, 81-128.

(11) Gardner, H. W. "Oxygen radical chemistry of polyunsaturated fatty acids" *Free Radical Biology & Medicine* **1989**, 7, 65-86.

(12) "... more definitive research is needed to understand the mechanistic origins of oxodiene[s]." -H. W. Gardner, 1989 (from reference (11) above).

(13) Jensen, R. K.; Korcek, S.; Mahoney, L. R.; Zinbo, M. "Liquid-Phase Autoxidation of Organic Compounds at Elevated Temperatures. 2. Kinetics and Mechanisms of the Formation of Cleavage Products in n-Hexadecane Autoxidation" *Journal of the American Chemical Society* **1981**, 103, 1742-1749.

(14) Hermans, I.; Nguyen, T.; Jacobs, P.; Peeters, J. "Autoxidation of Cyclohexane: Conventional Views Challenged by Theory and Experiment" *ChemPhysChem* **2005**, 6, 637-645.

(15) Hermans, I.; Jacobs, P.; Peeters, J. "The Formation of Byproducts in the Autoxidation of Cyclohexane" *Chemistry - A European Journal* **2007**, 13, 754-761.

(16) Hermans, I.; Peeters, J.; Jacobs, P. A. "Autoxidation of Ethylbenzene: The Mechanism Elucidated" *Journal of Organic Chemistry* **2007**, 72, 3057-3064.

(17) Pan, X. M.; Schuchmann, M. N.; Von Sonntag, C. "Oxidation of benzene by the OH radical. A product and pulse radiolysis study in oxygenated aqueous solution" *Perkin Transactions. 2* **1993**, 3, 289-297.

(18) Van Hook, J. P.; Tobolsky, A. V. "The Thermal Decomposition of 2,2'-Azo-bis-isobutyronitrile" *Journal of the American Chemical Society* **1957**, 80, 779-782.

(19) Howard, J. A.; Ingold, K. U. "Inhibited autoxidation of styrene. Part II. The relative inhibiting efficiencies of meta- and para-substituted phenols" *Canadian Journal of Chemistry* **1963**, 41, 1744-1751.

(20) Berthier, A.; Lemaire-Ewing, S.; Prunet, C.; Montange, T. "7-Ketocholesterol-induced apoptosis. Involvement of several pro-apoptotic but also anti-apoptotic calcium-dependent transduction pathways" *FEBS Journal* **2005**, 272, 3093-3104.

(21) Brown, A. J.; Jessup, W. "Oxysterols and atherosclerosis" *Atherosclerosis* **1999**, 142, 1-28.

(22) Popham, P. L.; Novacky, A. "Use of Dimethyl Sulfoxide to Detect Hydroxyl Radical during Bacteria-Induced Hypersensitive Reaction" *Plant Physiology* **1991**, 96, 1157-1160.

(23) Rosen, G. M.; Pou, S.; Britigan, B. E.; Cohen, M. S. "Spin trapping of hydroxyl radicals in biological systems" *Methods in Enzymology* **1994**, 233, 105-111.

(24) Gomes, A.; Fernandes, E.; Lima, J. "Fluorescence probes used for detection of reactive oxygen species" *Journal of Biochemical and Biophysical Methods* **2005**, 65, 45-80.

(25) Ingold, K. U. "Peroxy radicals" *Accounts of Chemical Research* **1969**, 2, 1-9.

(26) Howard, J. A.; Ingold, K. U. "Absolute Rate Constants for Hydrocarbon Autoxidation: I. Styrene" *Canadian Journal of Chemistry* **1965**, 43, 2729-2736.

(27) Frisch, M. J. T., G. W.; Schlegel, H. B.; Scuseria, G. E.; Robb, M. A.; Cheeseman, J. R.; Montgomery, Jr., J. A.; Vreven, T.; Kudin, K. N.; Burant, J. C.; Millam, J. M.; Iyengar, S. S.; Tomasi, J.; Barone, V.; Mennucci, B.; Cossi, M.; Scalmani, G.; Rega, N.; Petersson, G. A.; Nakatsuji, H.; Hada, M.; Ehara, M.; Toyota, K.; Fukuda, R.; Hasegawa, J.; Ishida, M.; Nakajima, T.; Honda, Y.; Kitao, O.; Nakai, H.; Klene, M.; Li, X.; Knox, J. E.; Hratchian, H. P.; Cross, J. B.; Bakken, V.; Adamo, C.; Jaramillo, J.; Gomperts, R.; Stratmann, R. E.; Yazyev, O.; Austin, A. J.; Cammi, R.; Pomelli, C.; Ochterski, J. W.; Ayala, P. Y.; Morokuma, K.; Voth, G. A.; Salvador, P.; Dannenberg, J. J.; Zakrzewski, V. G.; Dapprich, S.; Daniels, A. D.; Strain, M. C.; Farkas, O.; Malick, D. K.; Rabuck, A. D.; Raghavachari, K.; Foresman, J. B.; Ortiz, J. V.; Cui, Q.; Baboul, A. G.; Clifford, S.; Cioslowski, J.; Stefanov, B. B.; Liu, G.; Liashenko, A.; Piskorz, P.; Komaromi, I.; Martin, R. L.; Fox, D. J.; Keith, T.; Al-Laham, M. A.; Peng, C. Y.; Nanayakkara, A.; Challacombe, M.; Gill, P. M. W.; Johnson, B.; Chen, W.; Wong, M. W.; Gonzalez, C.; and Pople, J. A.; "Gaussian 03, revision D.01" Gaussian, Inc. 2003, Wallingford, CT.

(28) Vereecken, L.; Nguyen, T.; Hermans, I.; Peeters, J. "Computational study of the stability of alpha-hydroperoxyl- or alpha-alkylperoxyl substituted alkyl radicals" *Chemical Physics Letters* **2004**, 393, 432-436.

5. Photophysical Properties of 7-Mercapto-4-methylcoumarin (C-SH) and Derivatives

5.1 Graphical Abstract

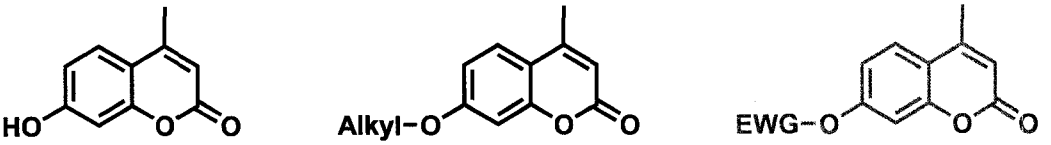

highly fluorescent **weakly fluorescent** **non-fluorescent**

Most fluorescent in polar, protic solvents

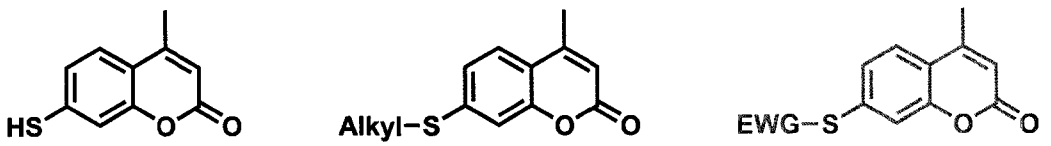

weakly fluorescent **highly fluorescent** **non-fluorescent**

Most fluorescent in non-polar, non-protic solvents

5.2 Coumarin-Based Fluorophores

The coumarin core is prevalent in photochemistry. Coumarin derivatives have been used as photorelease templates[1,2] amongst other applications, but their most used property is their fluorescence; for lasing,[3] as optical brighteners[4] and as fluorescent probes. Coumarin itself (Scheme 5-1), a naturally occurring compound that smells of fresh-cut grass, is not a very useful fluorophore. It has a low-lying n,π* excited state that is, like most n,π* states in organic molecules, non fluorescent.[5]

A common strategy to make coumarin fluorescent is to add an electron-donating substituent at the 7 position; alcohols and amines are the most abundant examples. Substitution at the 3 and/or 4 position is also common to prevent [2+2] dimerization reactions[6,7] and often create a bathochromic shift in the absorption and emission maximum.[8,9] There has been much less work devoted to 7-mercapto-substituted coumarins, the subject of this chapter.

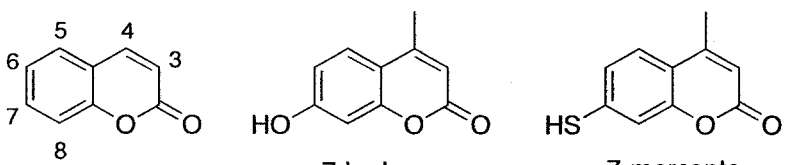

coumarin | 7-hydroxy-4-methylcoumarin C-OH | 7-mercapto-4-methylcoumarin C-SH

Scheme 5-1. Coumarin is non-fluorescent due to a low-lying n,π* excited state. Substitution at the 7-position with electron donating groups usually enhances the fluorescence as in the case of C-OH. In this chapter, we will describe the photophysical effects of a 7-mercapto group in C-SH.

5.2.1 Prefluorescent probes based on 7-hydroxycoumarin

The development and application of fluorescent probes based on 7-hydroxycoumarin (also called umbelliferone) are well represented in the literature (*vide infra*). One of the more used fluorophore in this context is 7-hydroxy-4-methylcoumarin (C-OH). As the free alcohol, C-OH is fluorescent (although highly solvent dependant), but when the alcohol is protected the fluorescence quantum yield is generally lower. This contrast in fluorescence between unprotected and protected, i.e., C-OH vs. C-OR, has been very useful in fluorescent probe applications. Since fluorescence is most sensitive against a dark background, successful fluorescent probes are designed to increase the fluorescence quantum yield when a desirable event occurs; the terms "prefluorescent" probe and fluorogenic probe have been used in this context. In the case of 7-hydroxycoumarin-based probes, the event monitored is usually deprotection of a non-fluorescent C-OR to generate the fluorescent C-OH. A popular example is 4-methylcoumarin-7-phosphate; this prefluorescent probe has been extensively used as an enzymatic dephosphorylation assay (Scheme 5-2).[10] Aryl-protected 7-hydroxycoumarins (e.g., C-OPhOH) have been used to detect reactive oxygen species.[11] In our group, post-doctoral fellow Carlos Sanrame developed C-OSi(Me)$_2$^{t}Bu to detect fluoride in thin polymer films.[12] I also show a probe for the enzyme lipase based on the same non-fluorescent C-OR to fluorescent C-OH deprotection,[13] but many more examples exist.[14]

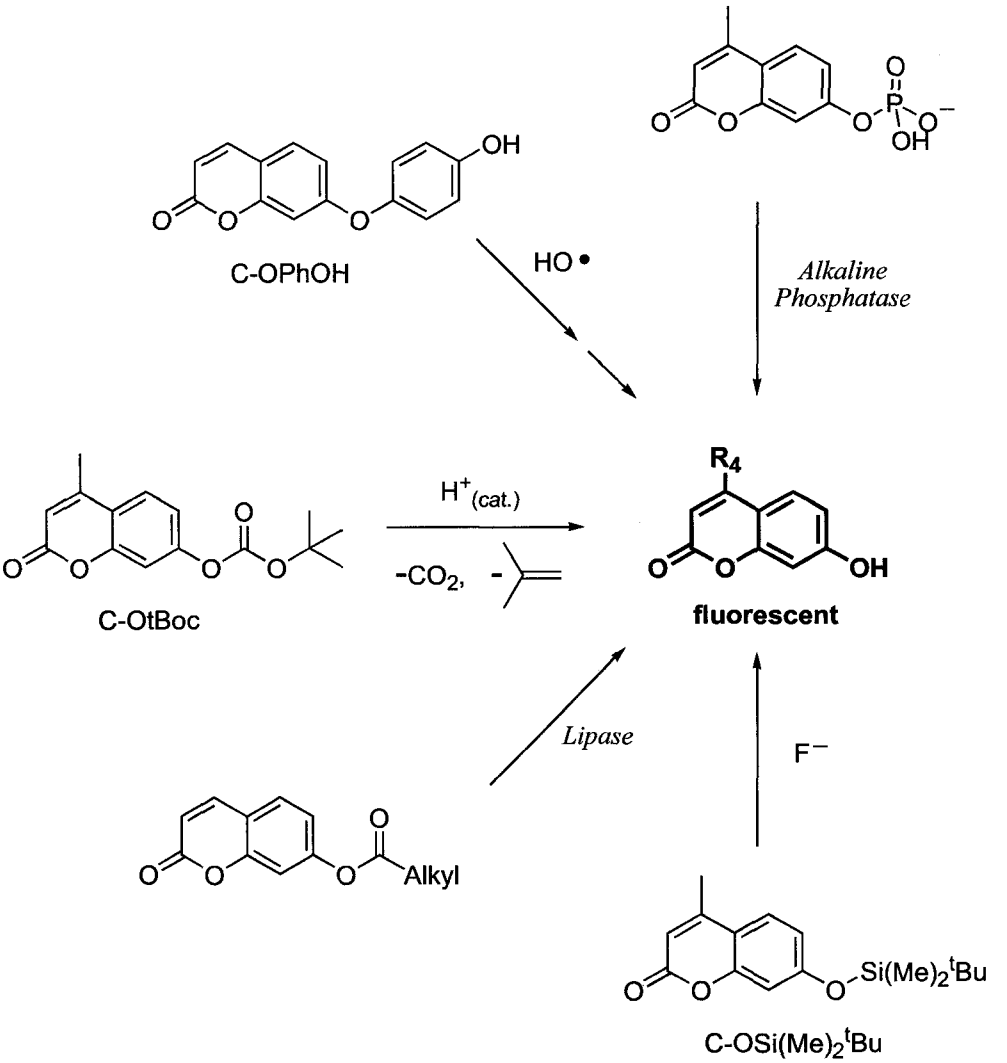

Scheme 5-2. Some examples of prefluorescent probes based on the non-fluorescent C-OR to fluorescent C-OH approach. Note: R_4=H or CH_3 depending on the prefluorescent probe structure. From the top, counter-clockwise: Alkaline phosphatase probe, 4-methylcoumarin-7-phosphate, becomes fluorescent after phosphate removal.[10] C-OPhOH becomes fluorescent after hydroxyl radical attack.[11] C-OtBoc monitors acid-catalyzed deprotection of tBoc groups (see below).[15,16] Lipase activity can be measured by the ester-hydrolysis of a lipid-protected coumarin.[13] And silyl-protected C-OSi(Me)$_2$^{t}Bu was used as a sensitive fluoride sensor in polymer films.[12]

I also employed this fluorescent probe strategy to monitor chemistry occurring in thin polymer films during my time in the group. Following the work of

graduate student Christopher Coenjarts, I used a non-fluorescent 7-tert-butoxycarbonate-4-methylcoumarin (C-OtBoc) probe that becomes fluorescent after acid-catalyzed deprotection to C-OH, shown in Figure 5-1.[15,16]

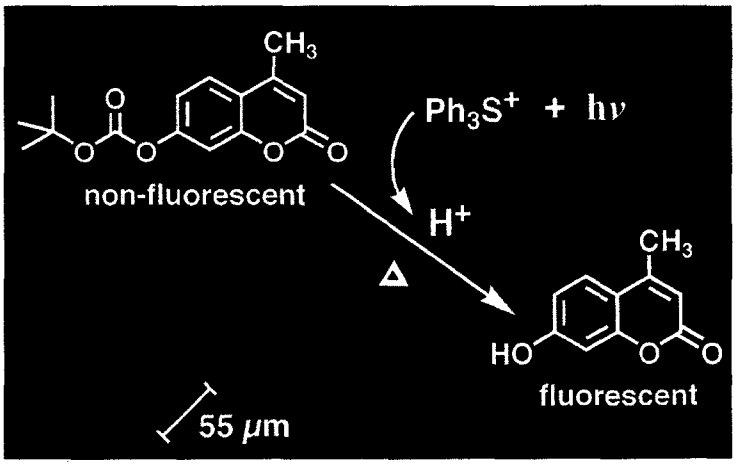

Figure 5-1. Fluorescence image of a patterned polymer film (~1μM thick) containing C-OtBoc and photoacid generator Ph_3S^+; the blue fluorescent regions show the areas where photogenerated acid deprotected tBoc groups and released the fluorescent C-OH.

Deprotection of tert-butoxycarbonyl (tBoc) groups is one of the more common chemical reactions used in "chemically amplified" photolithography, a technique used to create microcircuits.[17] Photolithography can be understood as the process of printing with light. Briefly, a thin polymer film—called a photoresist—covers the circuit forming material, e.g., silicon, and a mask that contains the circuit pattern is placed over the polymer film. The film is then irradiated through the mask and irradiated regions become acidic (due to photoacid generators present in the polymer film). The tBoc-protected polymer will then undergo acid-catalyzed deprotection in the irradiated areas and this leads to enhanced solubility of the

deprotected polymer. Irradiated (and deprotected) areas can then be washed away to expose the circuit forming material, which can be etched, and the remaining polymer film is baked off. The result of this multi-step process is a circuit that (ideally) matches the design of the original mask.

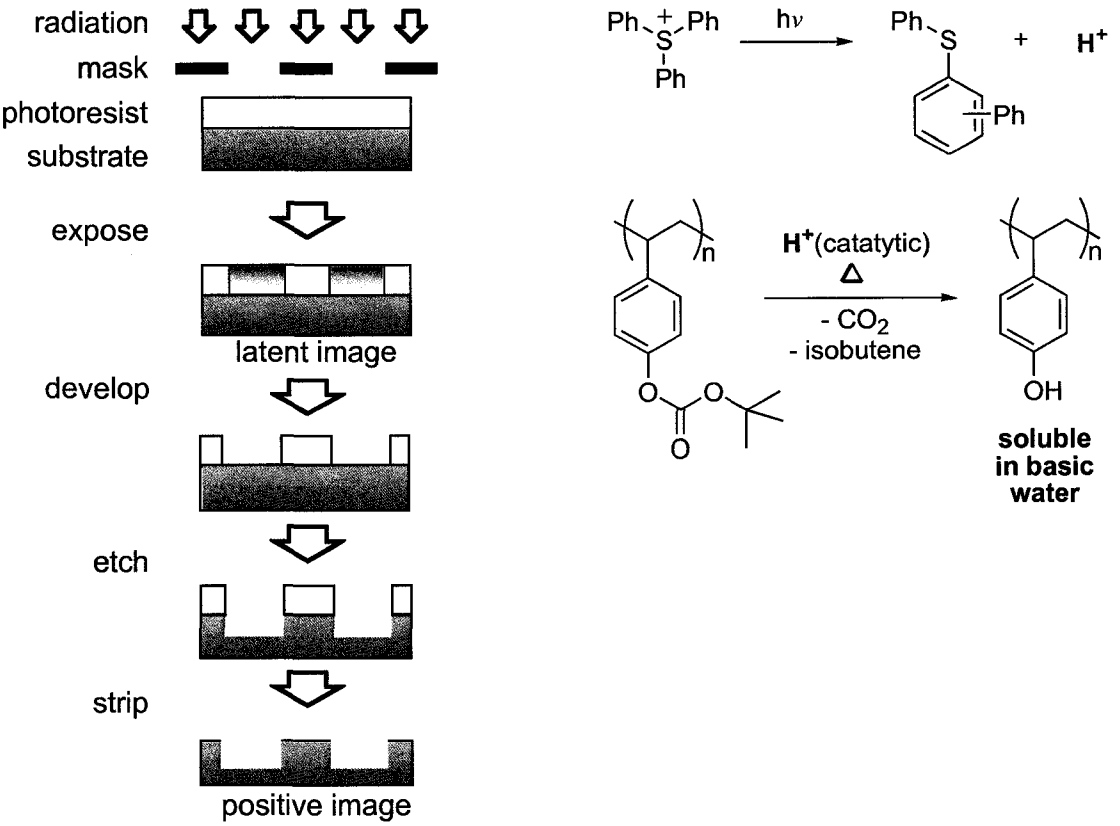

Figure 5-2. (Left) Schematic representation of the photolithographic process (see description in text, above) (Right) In the irradiated regions, the photoacid generator Ph_3S^+ photochemically rearranges to release acid. This acid catalyzes the decompostion of tBoc side chains to generate a polymer soluble in basic aqueous solutions.[17]

Optimizing this process without the ability to monitor each step of the process is a laborious task. For this reason, our group developed the prefluorescent C-OtBoc probe to monitor the deprotection chemistry occurring in polymer films. The

sensitivity of fluorescent probes was particularly useful in these systems since there is so little material available for analysis in thin polymer films.

Using C-OtBoc to quantify tBoc deprotection reactions and another coumarin fluorescent probe, coumarin 6, to quantify the amount of photogenerated acid, we could measure important parameters such as the catalytic chain length of the acid catalyzed tBoc-deprotection and the diffusion of acid necessary to complete the deprotection (this work was done with Marius Gabriel Ivan, PhD 2007). Dr. Ivan's work concentrated on acid detection, while my contribution centered on catalytic acid deprotection.

5.2.2 Fluorescent probes based on 7-mercaptocoumarin

While reports of fluorescence from 7-hydroxycoumarin derivatives are abundant, we found few scholarly publications that report fluorescent 7-mercaptocoumarin derivatives.[18,19] This is surprising considering that, in 1970, 7-alkylmercaptocoumarins were patented as optical whitening agents[20] (colourless fluorophores that absorb UV light and emit visible light). To the best of our knowledge, only one fluorescence quantum yield has been reported for a 7-mercaptocoumarin derivative (Scheme 5-3).[18]

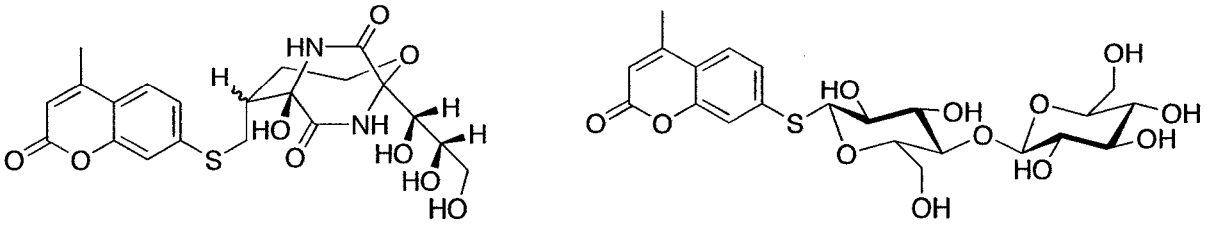

Scheme 5-3. (Left) Researchers covalently attached 7-mercapto-4-methylcoumarin to bicyclomycin to investigate its binding to the transcription termination factor Rho in *Escherichia coli* using Förster resonance energy transfer (FRET).[18] Spectroscopic data reported in aqueous buffer solution: λ_{MAX}(abs)=333nm, $\varepsilon_{MAX}=1.69\times10^{4}M^{-1}cm^{-1}$, λ_{MAX}(fluo)=426nm, and Φ_F=0.49. (Right) Fluorescent substrate for cellulase; 4-methyl-7-thioumbelliferyl-β-D-cellobioside λ_{MAX}(fluo)~400nm in aqueous buffer solution (pH=5.5).[19]

Another group reported fluorescence from 4-methyl-7-thioumbelliferyl-β-D-cellobioside (Scheme 5-3, right).[19] This molecule is a substrate for cellulase and its fluorescence was used to study the association between the two. In their paper the authors noted, "Interestingly, the fluorescence of [C-SH] is several orders of magnitude less intense than that of 4-methyl-7-thioumbelliferyl-β-D-cellobioside". This is effectively the opposite behavior to 7-hydroxycoumarin probes—free C-OH is usually more fluorescence than protected C-OR.

This chapter will explore the photophysical study of 7-mercapto-4-methylcoumarins that often behave opposite to 7-hydroxy-4-methylcoumarins.

5.3 Photophysics of C-SH and Derivatives in Non-Protic Solvents

In non-protic solvents, the photophysical properties of coumarins are largely dictated by the nature of the lowest singlet excited state, n,π* or π,π*.[5,21] In general, π→π* transitions (and π*→π transitions) are more allowed than n→π* transitions.[22] For this reason, π→π* transitions display higher absorption extinction coefficients and a faster rate of fluorescence than n,π* states. If the rate of fluorescence is faster than competing rates, the fluorescence quantum yield (Φ_F) will be high. The relationship between Φ_F and the radiative (fluorescent, k_{rad}) and non-radiative rate constants ($\Sigma k_{non\text{-}rad}$) is shown in eq [1]. Note that $(\Sigma k_{non\text{-}rad} + k_{rad})^{-1}$ is equal to the excited state lifetime (τ_F) and this value can be measured by time-resolved fluorescence spectroscopy. The sum of non-radiative rate constants can include thermal relaxation, inter-system crossing, electron ejection, isomerization and unimolecular or bimolecular chemical reactions. The presence of excited state quenchers can increase the rate of non-radiative decay, thus reducing the fluorescence quantum yield.

$$[1] \qquad \Phi_F = k_{rad} / (\sum k_{non-rad} + k_{rad}) = k_{rad} \tau_F$$

Many high quantum yield fluorophores, e.g., fluororescein, have short excited state lifetimes because k_{rad} is high.[23] Other fluorophores can have high Φ_F and long-lived excited states, as in the case of pyrene, because of slow non-radiative rates.[24]

In the following sections, we report the first extensive photophysical study of 7-mercapto-4-methylcoumarin (C-SH) and derivatives (C-SR), shown in Scheme 5-4. Before this, I would like to acknowledge the help of post-doctoral fellow María González Béjar and summer student Philip Campbell on this project.

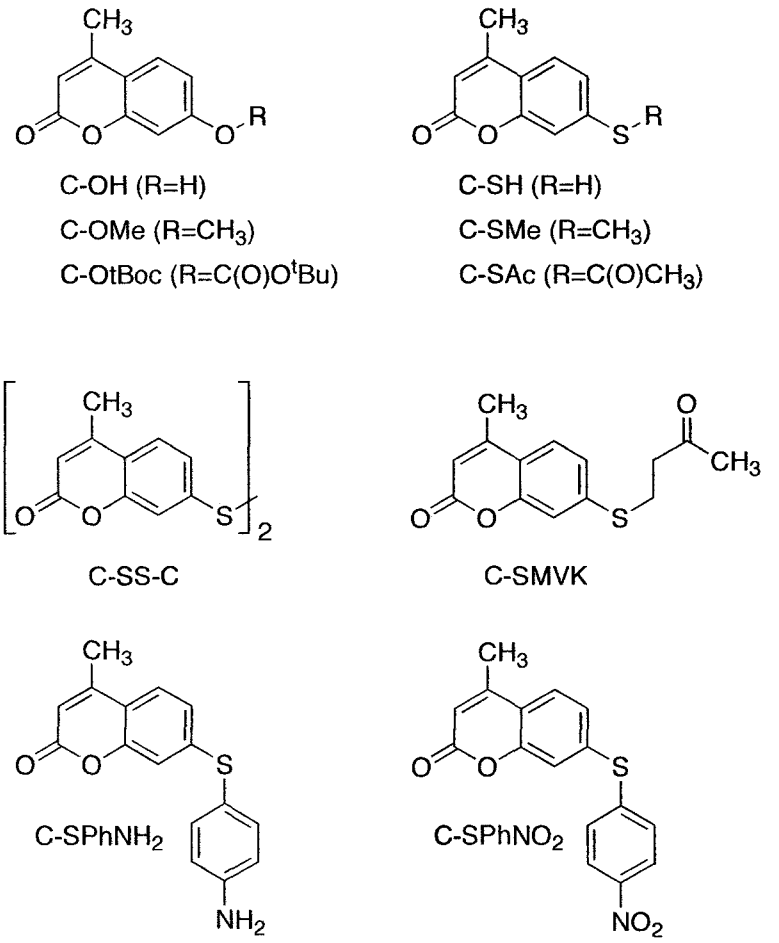

Scheme 5-4. Structure and abbreviation for the coumarins discussed in this chapter. The synthesis of compounds C-SMe, C-SAc, C-SS-C, C-SMVK, C-SPhNH$_2$ and C-SPhNO$_2$ are described in the Experimental Section.

5.3.1 *Absorbance and Fluorescence of C-SH and C-SR Derivatives*

To understand the photophysical properties of 7-mercapto-4-methylcoumarin (C-SH) and C-SR derivatives in non-protic solvents, we measured their UV-Visible absorption and fluorescence spectra in dichloromethane, chloroform and toluene. Note: Unless stated otherwise, in this chapter the excitation wavelength is 308 nm.

The absorbance and fluorescence of C-SH and C-SMe in dichloromethane (with C-SAc), chloroform and toluene are compared in Figure 5-3. These plots summarize quantitative absorbance and fluorescence data in a single figure. On the left side, the absorbance spectra are reported using the molar absorption coefficient (ε). And to the right, we show the normalized fluorescence spectra, scaled by the fluorescence quantum yield Φ_F. The fluorescence maximum thus corresponds to Φ_F on the right y-axis. This approach, we hope, allows for an easy comparison between fluorophores in a given environment. See Section 5.7.2 in the Experimental Section for a detailed description for the measurement of Φ_F.

The main concept of this chapter is well represented in the dichloromethane plot—that is, C-SR is fluorescent when R is an alkyl group, weakly fluorescent when R is hydrogen, and non-fluorescent when R is an electron-withdrawing group. In this solvent, C-SMe is 14x more fluorescent than C-SH. And C-SH is 15x more fluorescent than C-SAc (the fluorescence spectrum of C-SAc is buried in the baseline).

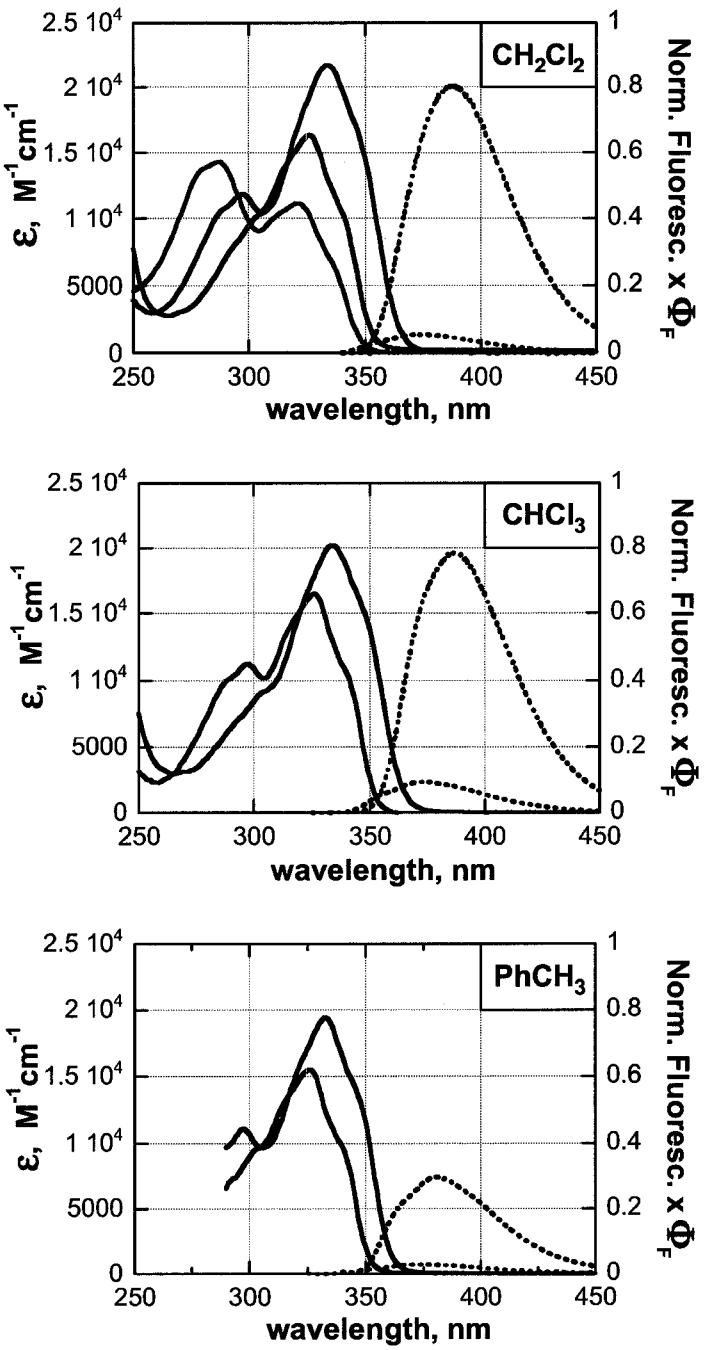

Figure 5-3. Molar absorption coefficient (ε, solid line) and fluorescence (λ_{EXC}=308nm, dashed line) for C-SH (red), C-SMe (blue) and C-SAc (grey) in dichloromethane (CH_2Cl_2), chloroform ($CHCl_3$) and toluene ($PhCH_3$). The fluorescence spectra were normalized and scaled by Φ_F, i.e., the fluorescence maximum corresponds to Φ_F on the right y-axis.

As discussed in Section 5.2.1, protected 7-hydroxycoumarins (C-OR) are generally less fluorescent than C-OH. For this reason, the deprotection of C-OR to yield the fluorescent C-OH is a successful prefluorescent probe strategy. Furthermore, it is well known that electron-withdrawing R-groups further lower the fluorescence intensity of C-OR, e.g. C-OtBoc is non-fluorescent.[15]

We also found that C-SR derivatives appear non-fluorescent when protected with electron-withdrawing R-groups; for example, I measured fluorescence quantum yields below 0.005 for C-SAc (see Table 5-1). Similarly, C-SPhNO$_2$ showed barely measurable fluorescence (Φ_F<0.005). The compound C-SPhNH$_2$ did not fluoresce either, but this is likely a result of excited-state quenching by the amine lone pair via intramolecular electron transfer.[25] While C-SAc is non-fluorescent, the application of C-SAc as a prefluorescent probe is not useful since deprotection will lead to C-SH, which is only weakly fluorescent.

On the other hand, alkylating C-SH to C-SMe showed a dramatic increase in fluorescence as seen in Figure 5-3. Similarly, alkylation of C-SH by methylvinylketone to make C-SMVK gave highly fluorescent compounds in these non-protic solvents. The results from our absorbance and fluorescence investigations are compiled in Table 5-1.

Table 5-1. Quantitative absorbance and fluorescence data for C-SH and derivatives (C-SR) in dichloromethane (CH_2Cl_2), chloroform ($CHCl_3$) and toluene ($PhCH_3$). The fluorescence standard used was 7-methoxycoumarin-4-carboxylic acid in methanol (Φ_F=0.18).[26]

		Absorbance		Fluorescence		
C-SR	Solvent	λ_{MAX} (nm)	ε (10^3 $M^{-1}cm^{-1}$)	λ_{MAX} (nm)	Φ_F	τ_F (ns)
C-SH	CH_2Cl_2	326	16.3	374	0.057	<0.1[a]
C-SH	$CHCl_3$	326	16.5	372	0.096	<0.1[a]
C-SH	$PhCH_3$	326	15.5	372	0.030	<0.1[a]
C-SMe	CH_2Cl_2	333	21.8	388	0.81	1.9
C-SMe	$CHCl_3$	334	20.1	387	0.79	1.6
C-SMe	$PhCH_3$	333	19.5	382	0.30	0.8
C-SAc	CH_2Cl_2	321	11.1	365	0.004	-
C-$SPhNO_2$	CH_2Cl_2	339	20.2	-	*n.f.*	-
C-$SPhNH_2$	CH_2Cl_2	337	18.8	-	*n.f.*	-
C-SS-C	CH_2Cl_2	329	30.6	-	*n.f.*	-
C-SMVK	CH_2Cl_2	333	20.1	389	0.64	1.09
C-SMVK	$CHCl_3$	333	-	387	0.74	1.50
C-SMVK	$PhCH_3$	333	-	383	0.28	~0.11

Note: $k_{rad} = \Phi_F/\tau_F$ and $\Sigma k_{non\text{-}rad} = k_{rad}(1\text{-}1/\Phi_F)$. [a] Faster than the time resolution of our system. *n.f.* = non-fluorescent (Φ_F<0.005).

Using time-resolved fluorescence, post-doctocal fellow María González Béjar measured longer fluorescence lifetimes for C-SMe than for C-SH in these solvents (see Table 5-1). C-SH displayed very short-lived excited states, $\tau_F < 0.1$ ns, while C-SMe gave fast, but measurable lifetimes; τ_F in dichloromethane, chloroform and toluene were 1.9 ns, 1.6 ns and 0.8 ns, respectively. Note: the measured fluorescence lifetime (τ_F) is equal to the singlet excited state lifetime—as long as singlet excited states exist, a fraction of them (Φ_F) will emit fluorescence.

From the excited state lifetime measurements and the fluorescence quantum yield, we can estimate $\Sigma k_{non\text{-}rad}$ and k_{rad} from eq [1]. The most remarkable result is that k_{rad} is *faster* for C-SH than it is for C-SMe. The low fluorescence of C-SH is therefore a result of fast non-radiative processes ($\Sigma k_{non\text{-}rad}$), rather than slow k_{rad}.

Another interesting point: k_{rad} is approximately constant for C-SMe in these solvents; from Φ_F and τ_F, we calculate k_{rad} to be $4.3 \times 10^8 s^{-1}$, $4.9 \times 10^8 s^{-1}$ and $3.3 \times 10^8 s^{-1}$ in dichloromethane, chloroform and toluene, respectively. The variations in Φ_F for these three solvents, therefore, are mostly due to variations in non-radiative rates, as is often the case. For example, this type of behavior is reported for 7-methoxy-3-chloro-4-methylcoumarin—the value for k_{rad} remained constant (±10% in 29 solvents) while $\Sigma k_{non\text{-}rad}$ changed almost two orders of magnitude to give Φ_F ranging from 0.08 to 0.88.[21]

Our results show that the majority of excited states from C-SH and C-SAc do not emit photons. To understand what these excited states do instead of fluoresce, we turned to laser-flash photolysis and singlet oxygen measurements described in the next two sections.

5.3.2 Laser-Flash Photolysis Study of C-SH and C-SR Derivatives

Laser-flash photolysis (LFP) allows us to monitor absorption changes occurring microseconds after the excited states of C-SH and C-SR are formed. For this, a short pulse (~6-8 ns) of 308 nm laser light excited the mercaptocoumarins and the difference in absorbance before and after laser excitation was monitored using time-resolved UV-visible spectroscopy. Typical intermediates such as delocalized radicals and triplets have large molar absorption coefficients and they can easily be observed using LFP.

The LFP generated signals for C-SH, C-SMe and C-SAc in dichloromethane could all be linked to their respective triplet states. The positive absorbance change (ΔA) above ~400 nm were assigned to the triplet states and these were rapidly quenched by oxygen; under air, no signals are observed on the time scale reported for these figures. Negative absorbance ~~(or emission)~~ change below ~360 nm are attributed to ground state bleaching. These signals were also rapidly quenched by oxygen indicating that the formation of triplets was the cause of the signals <360nm.

Triplet states are known to react with one another via triplet-triplet annihilation.[22] Due to spin statistics, 1/9 encounters will generate a singlet ground state and a singlet excited state. In the case of C-SMe, triplet-triplet annihilation generates the fluorescent singlet excited state as seen with the negative signal centered at 390 nm (a process called P type delayed fluorescence). As seen in Figure 5-5, the delayed fluorescence signal is 2x shorter than the triplet lifetime—the kinetic reason for this factor of '2' is derived in Section 5.8 at the end of this chapter. As it should, the spectrum of this emission corresponds to the steady-state fluorescence of C-SMe in dichloromethane. Since delayed fluorescence is generated by triplet-triplet reactions and triplets are efficiently quenched by oxygen, delayed fluorescence was not observed under air.

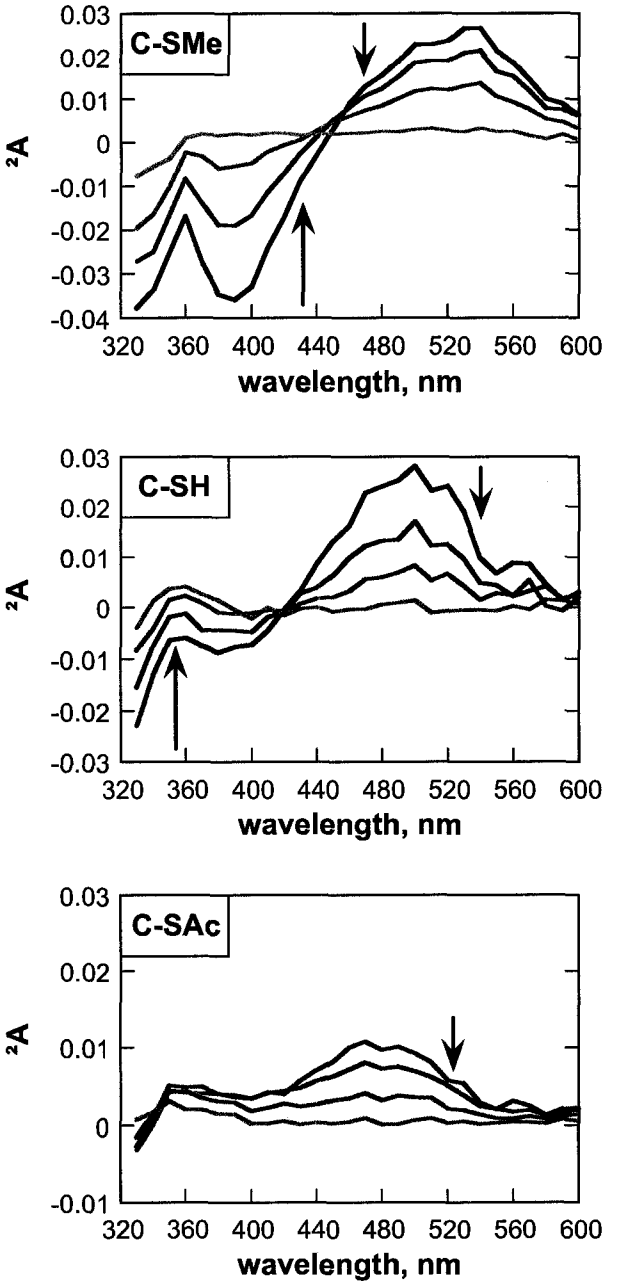

Figure 5-4. Transient absorbance observed after pulsed laser excitation at 308nm (~17mJ per pulse) for C-SMe (top), C-SH (middle) and C-SAc (bottom) in dichloromethane, under nitrogen. The transient absorbances were taken 2, 8, 20 and 86 μs after the laser pulse and ground state absorbance at 308 nm was 0.45 for all compounds. The arrows indicate the direction of the signal with time. All signals were rapidly quenched by oxygen indicating the involvement of triplet states (see text).

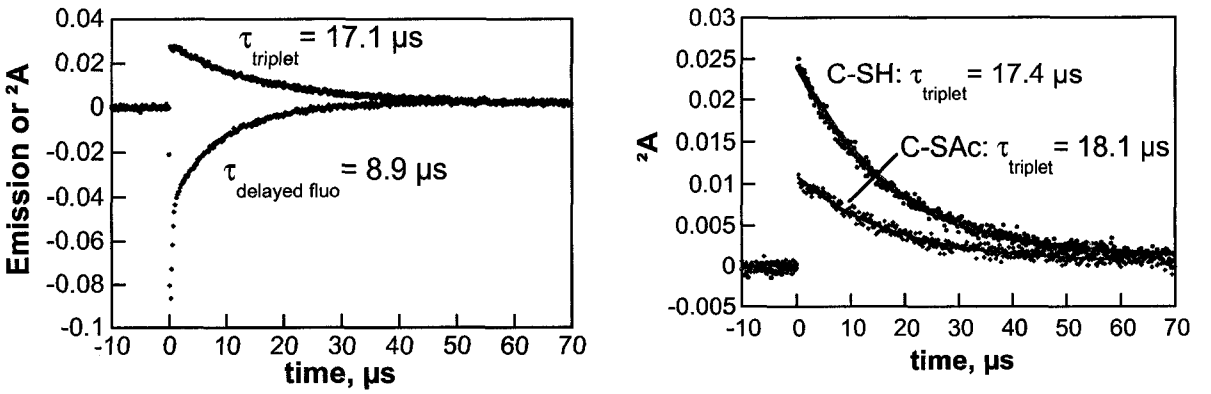

Figure 5-5. **(Left) Transient absorption generated by 308nm laser excitation for C-SMe in dichloromethane under nitrogen monitored at 520nm (green) and 390nm (purple). The triplet lifetime ($\tau_{triplet}$) and the delayed fluorescence lifetime are indicated on the graph. The fast dip near time 'zero' is fluorescence.**

(Right) Transient absorption from C-SH (red) and C-SAc (grey) in dichloromethane under nitrogen. The monitoring wavelengths were 490nm in both cases.

Like many aryl thiols, C-SH can oxidize to the disulfide (C-SS-C). This reaction occurs slowly in solution under air and is accelerated by the presence of base. The disulfide C-SS-C is non-fluorescent and no triplet state was detected during LFP investigations. Instead, excitation of C-SS-C at 308 nm gave ground state bleaching and a signal at ~360 nm. The signal at 360 nm decayed via second-order kinetics, i.e., the species decayed via self-reactions. These signals, which we attribute to the radicals formed by sulfur-sulfur bond cleavage (C-S•), eq [2], were not quenched by oxygen as seen in Figure 5-6.

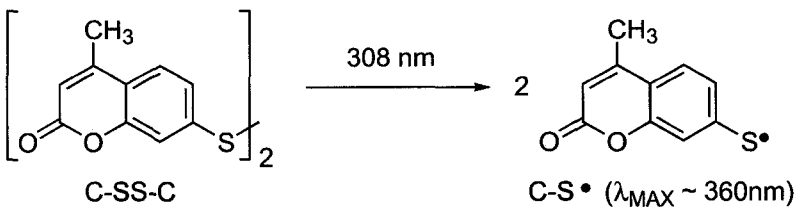

[2] C-SS-C C-S• (λ_{MAX} ~ 360nm)

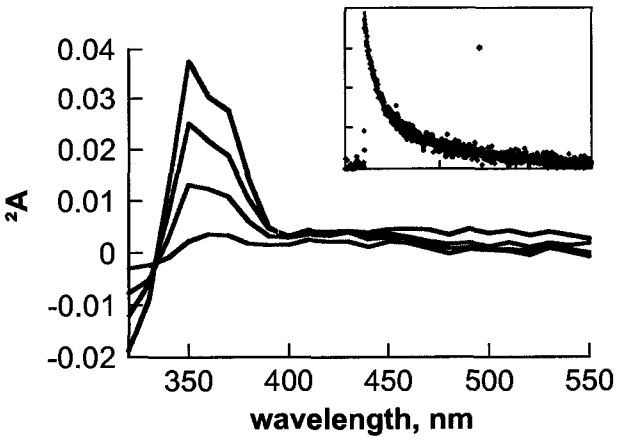

Figure 5-6. Transient absorption spectra for C-SS-C in dichloromethane taken 10.4 μs, 41.6 μs, 108.0 μs and 349.2 μs after 308nm laser excitation. Inset: The signal at 360 nm, attributed to the sulfur centered radical C-S•, decayed via 2ndorder kinetics and was not affected by O_2.

To confirm that the absorbance signal is indeed due to radicals, we measured the rate constant for the reaction between the transient C-S• and styrene (reaction [3]) using typical Stern-Volmer kinetics. The decay rate constant observed for C-S•, k_{obs}, at different concentrations of styrene is related to the bimolecular rate constant, k_{add}, according to eq [4].

[3] 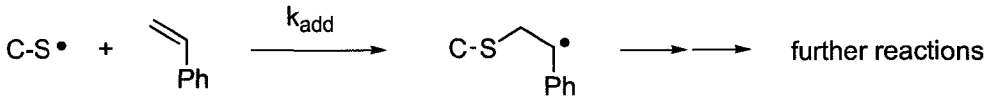

[4] $k_{obs} = k_o + k_{add}[PhCH=CH_2]$

Increasingly short pseudo-first order decays from the C-S• radical were observed with the increasing concentration of styrene (Figure 5-7). From this data, we obtained a bimolecular rate constant of (1.40±0.08) x 10^8 $M^{-1}s^{-1}$ for the addition of C-S• to styrene. This rate constant is the same order as the reaction of PhS• with

styrene (2.7×10^7 $M^{-1}s^{-1}$)[27] The larger value for C-S• may be due to its electron-poor nature; *p*-chlorophenylthiyl radicals, for instance, add to styrene with a $k_{add} = 5.2 \times 10^7$ $M^{-1}s^{-1}$.[27]

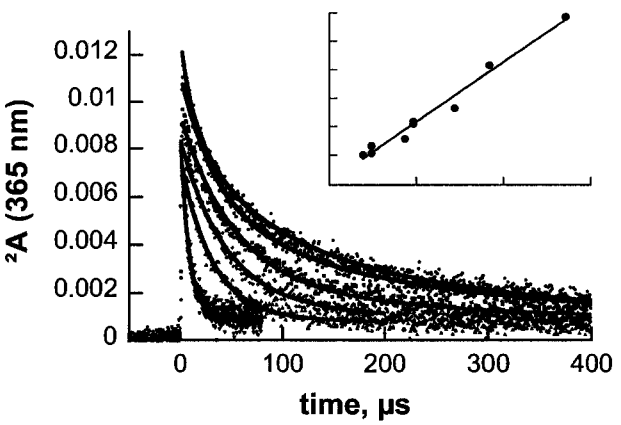

Figure 5-7. Decay curves of C-S• produced by 308 nm excitation of disulfide C-SS-C in dichloromethane (under air) in the presence of increasing styrene concentration, from 0 to 812 µM. Inset. Linear plot of the pseudo-first order rate constant observed for the decay of C-S• in function of styrene concentration according to eq [4].

5.3.3 Singlet Oxygen Generation from C-SH and C-SR Derivatives

Our LFP studies on C-SH, C-SMe and C-SAc in dichloromethane led to the observation of triplet states, reversible ground-state bleaching and some delayed fluorescence via triplet-triplet annihilation, but little was found in terms of photochemistry. For this reason, we assume that the fraction of excited state molecules that undergo chemical change is small.

fluorescence via triplet-triplet annihilation, but little was found in terms of photochemistry. For this reason, we assume that the fraction of excited state molecules that undergo chemical change is small.

From the work described so far, we come to the conclusion that C-SMe, C-SH and C-SAc will decay from the lowest singlet excited states via one of three paths as shown in Figure 5-8.

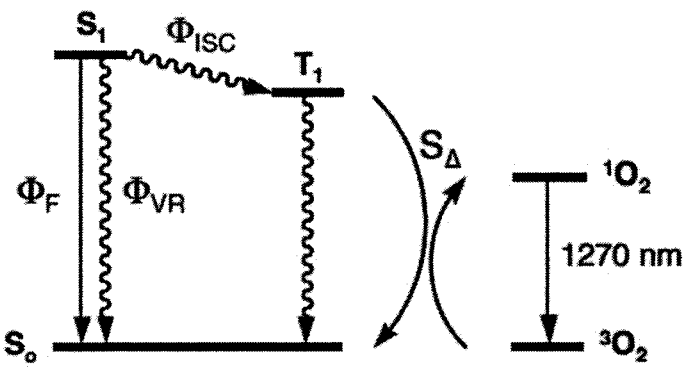

Figure 5-8. Mercaptocoumarins decay from the lowest singlet excited state (S_1) via three photophysical processes: fluorescence (Φ_F), vibrational relaxation (Φ_{VR}) and intersystem crossing (Φ_{ISC}). In the presence of oxygen, a fraction (S_Δ) of the longer-lived triplets (T_1) are quenched to form singlet oxygen that emits at 1270 nm. The product of Φ_{ISC} and S_Δ is the singlet oxygen quantum yield, $\Phi(^1O_2)$.

The fraction of excited states that emit fluorescence was measured (see Table 5-1). And in the previous section, we observed transient absorption signals associated to the formation of triplets, which were rapidly quenched by oxygen.

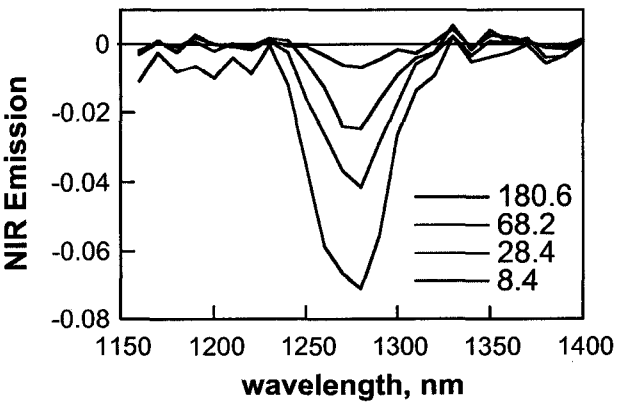

Figure 5-9. The quenching of triplet states generates singlet oxygen that can be observed and quantified by its characteristic near-infrared luminescence. These traces are from C-SH in chloroform excited at 308 nm under air; the time is indicated in μs.

Much like determining Φ_F, we measured the quantum yield of singlet oxygen, $\Phi(^1O_2)$, generated by mercaptocoumarins by comparison the luminescence intensity at 1270 nm with known singlet oxygen generators, see experimental section for more details. The top signal at 1270 nm after laser excitation can be plotted against the fraction of light absorbed, as shown in Figure 5-10. The ratio of two slopes from such plots is related to the ratio of $\Phi(^1O_2)$ for both compounds, as described in eq [5]. With the knowledge of $\Phi(^1O_2)_{STD}$, we could estimate $\Phi(^1O_2)$ for C-SR.

$$[5] \qquad \Phi(^1O_2) = \Phi(^1O_2)_{STD} \frac{slope_{C-SR}}{slope_{STD}}$$

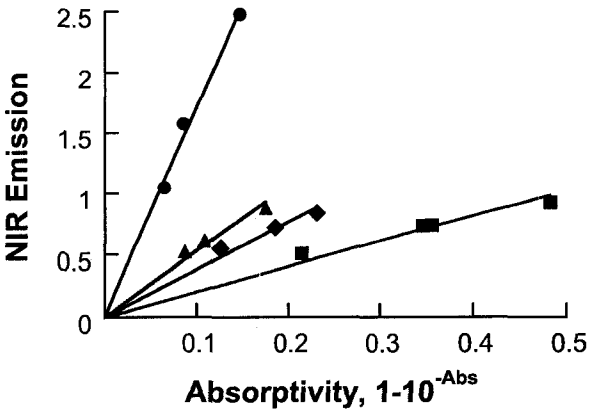

Figure 5-10. Example of $\Phi(^1O_2)$ determination by time-resolved NIR spectroscopy. NIR emission at 1270 nm is measured in function of the fraction of light absorbed ($1\text{-}10^{-Abs}$) for C-SH (■), C-SMe (◆) and C-SMVK (▲) in toluene. Phenalenone (●) has a known singlet oxygen quantum yield in toluene, $\Phi(^1O_2) = 1$. The ratio of the slopes is equal to the ratio of the singlet oxygen quantum yields.

C-SMe had slightly larger $\Phi(^1O_2)$ than C-SH in chloroform and toluene; dichloromethane values were similar for both compounds. Interestingly, the sum of $\Phi(^1O_2) + \Phi_F$ for C-SMe in dichloromethane is ~1.0. In this particular case, $\Phi(^1O_2) \approx \Phi_{ISC}$ appears valid since $\Phi(^1O_2)$ can only underestimate Φ_{ISC} and the result cannot amount to more than 1. Similarly, C-SMVK in $CHCl_3$ gives $\Phi(^1O_2) + \Phi_F = 1$. For C-SMe in dichloromethane and C-SMVK in chloroform, the excited-state photophysics is entirely explained by fluorescence and inter-system crossing to the triplet state.

Table 5-2. Compilation of singlet oxygen quantum yields, $\Phi(^1O_2)$, fluorescence quantum yield (Φ_F) and vibrational relaxation (Φ_{VR}) estimates for C-SAc, C-SH, C-SMVK and C-SMe in different solvents.

	Solvent	Φ_F	$\Phi(^1O_2)$	Φ_{VR} [a]	τ_F (ns)[b]
C-SAc	CH_2Cl_2	0.004	0.16	≤0.836	-
C-SH	$PhCH_3$	0.030	0.13	≤0.84	<0.1
C-SH	CH_2Cl_2	0.057	0.21	≤0.733	<0.1
C-SH	$CHCl_3$	0.096	0.096	≤0.808	<0.1
C-SMVK	$PhCH_3$	0.28	0.34	≤0.38	~0.11
C-SMVK	$CHCl_3$	0.74	0.26	~0	1.50
C-SMVK	CH_2Cl_2	0.64	0.30	≤0.06	1.09
C-SMe	$PhCH_3$	0.3	0.24	≤0.46	0.8
C-SMe	$CHCl_3$	0.79	0.15	≤0.06	1.6
C-SMe	CH_2Cl_2	0.81	0.19	~0	1.9

[a] Under the assumption that the fraction of excited states that do chemistry is small and the knowledge that $\Phi(^1O_2) \leq \Phi_{ISC}$; $\Phi_{VR} = 1 - \Phi_F + \Phi_{ISC} \leq 1 - \Phi_F + \Phi(^1O_2)$. [b] The rate constant for each process is equal to the quantum yield for that process divided by the excited state lifetime, e.g., k_{ISC}(C-SMe in $CHCl_3$) $\leq \Phi(^1O_2)/\tau_F = (0.15)/(1.6\times10^{-9}s) = 9.4\times10^7 s^{-1}$.

5.4 Photophysics of C-SH and Derivatives in Protic Solvents

5.4.1 C-SH Fluorescence in Water: Dramatic Contrast with C-OH

In protic solvents, 7-hydroxycoumarins display rich, complex photophysical and photochemical behavior that has been the subject of hundreds of publications.[28] On the other hand, we found only one statement published on the fluorescence properties of C-SH in protic solvents, basically saying that it doesn't fluoresce. Indeed, we observed very low fluorescence quantum yields for C-SH in water (Φ_F<0.005). This is contrary to C-OH that is most fluorescent in water. What's more, C-SH appears less fluorescent at high pH whereas C-OH is most fluorescent at high pH (see Figure 5-11). In basic water, C-SH emits at longer wavelengths—the weak emission centered at 448 nm is attributed to the C-SH anion. From the fluorescence intensity for C-SH in water at different pH, we can estimate a pK_a value of ~2.8 (the pH value corresponding to half of the sharp increase). This pK_a is quite low, c.f., benzenethiol[29] has a pK_a of 6.6 and the pK_a for C-OH is ~7.7.[30]

Essentially, the solvent dependence on the fluorescence from C-SH and C-OH are opposite from one another. C-OH is highly fluorescent in water and C-SH is more fluorescent in non-polar solvents (although C-SH displays low fluorescence quantum yields in all cases).

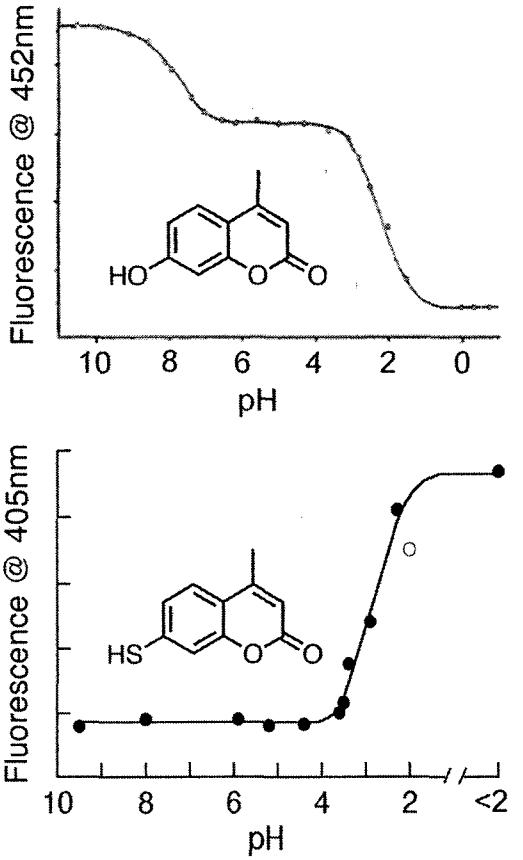

Figure 5-11. (Top) pH dependant fluorescence intensity (λ_{EXC}=335nm, λ_{MON}=452nm) for 7-hydroxy-4-methylcoumarin. The graph is adapted from ref [31]. (Bottom) pH dependant fluorescence intensity (λ_{EXC}=338nm, λ_{MON}=405nm) for 7-mercapto-4-methylcoumarin (this work).

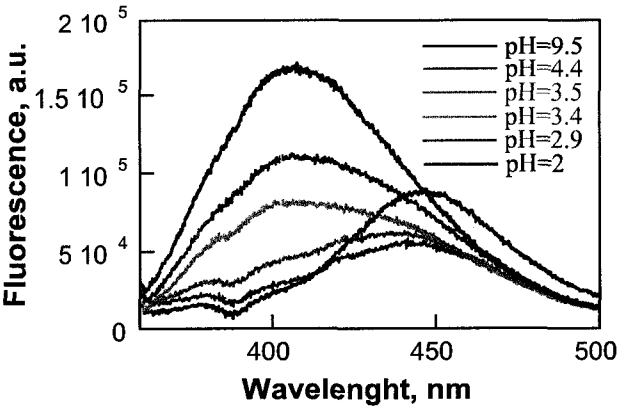

Figure 5-12. Weak fluorescence (arbitrary units) of C-SH in water at different pH (λ_{EXC}=335nm). The spectra were corrected for light scattering (see Experimental Section).

5.4.2 Photophysical Properties of C-SH and C-SR in Methanol

Quantitative absorbance and fluorescence data for C-SH and C-SMe in methanol are compiled in Figure 5-13 as before—molar absorption coefficients to the left and normalized fluorescence multiplied by the fluorescence quantum yield to the right. As we observed in water, C-SH in methanol is practically non-fluorescent (Φ_F<0.005), c.f., Φ_F = 0.057 in dichloromethane. The C-SH anion in methanol (formed using triethylamine) is slightly more fluorescent when excited at 377 nm; Φ_F = 0.009 with an emission centered at 443 nm. Again, C-SMe (Φ_F = 0.53) is more fluorescent than C-SH in methanol, but the contrast is much higher in this solvent. This will become important in the next chapter when I use C-SH as prefluorescent probe to detect alkylating electrophiles.

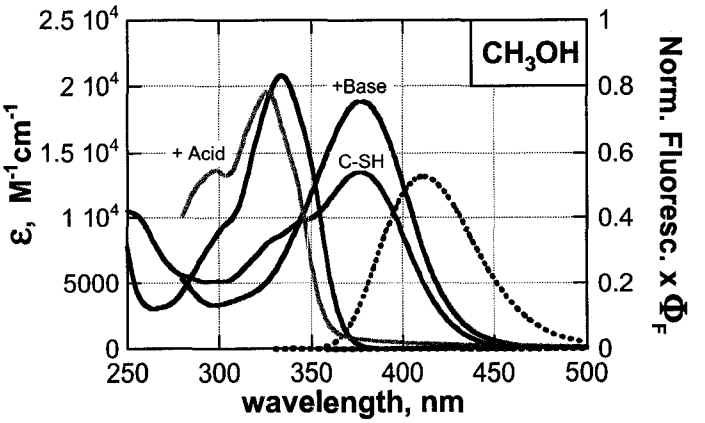

Figure 5-13. Molar absorption coefficient (ε, solid line) and fluorescence (λ_{EXC}=308nm, dashed line) for C-SH (red) and C-SMe (blue) in methanol. Fluorescence spectra are normalized and scaled by Φ_F; the fluorescence maximum therefore corresponds to Φ_F on the right axis. The absorbance of C-SH in methanol (labeled "C-SH") is a mixture of anionic form and neutral form due to the low pK_a of C-SH. The C-SH anion in methanol (green, labeled "+Base") was measured in 0.22M triethylamine; λ_{EXC}=377nm. The neutral C-SH (orange, labeled "+ Acid") was measured in 0.5M H_2SO_4.

5.5 Discussion

Our exploratory photophysical studies of 7-mercapto-4-methylcoumarin and derivatives generated many surprising results. Our group and others employed 7-hydroxy- and 7-amino-substituted coumarins in the past and their fluorescent nature makes them useful probes. We didn't expect such dramatically different photophysical properties by substitution of the oxygen or nitrogen for sulfur.

For one, the fluorescence from C-SH in polar, protic solvents is very low, while 7-hydroxycoumarins are most fluorescent in these solvents.[31] Both 7-hydroxy-4-methylcoumarin and 7-mercapto-4-methylcoumarin are non-fluorescent when protected with an electron withdrawing R-group. The lack of fluorescence from C-OR and C-SR with R=EWG can be explained by the nature of the lowest singlet excited state, i.e., n,π^*. Electron-withdrawing protecting groups on C-OR and C-SR basically cancel the effect of electron-donation by the alcohol and thiol moiety and the result is an excited state that resembles that of unsubstituted coumarin (non-fluroescent).[5]

The most interesting result is the complementarities between C-OH and C-SH upon alkylation to C-OR and C-SR. Many prefluorescent probes are based on the deprotection of a non-fluorescent C-OR to yield the fluorescent C-OH. Our results presented in this chapter indicate that alkylation of C-SH to C-SR can also be

a useful prefluorescent probe strategy. This latter approach will be discussed in the next chapter.

From the experimental results, we developed a working hypothesis to explain the fluorescence of C-SH and C-SR derivatives. In non-protic solvents and in the absence of excited state quenchers, we propose that Φ_F is largely dictated by the participation of a non-fluorescent n,π^* excited state. It is well known that n,π^* singlet excited states are usually short lived and non-fluorescent.[22] Unsubstituted coumarin, for example, is non-fluorescent because of the participation of a short-lived n,π^* excited state. Indeed, we measured faster k_{rad} for C-SH than for C-SMe. For this reason we cannot attribute higher Φ_F to faster k_{rad}.

Alkylation of C-SH to C-SR presumably raises the energy of the HOMO (π) orbital so that the π,π^* state is less affected by the non-fluorescent n,π^*. This interpretation is supported by the longer fluorescence lifetimes for C-SMe.

To verify these arguments, we calculated the orbital energies for C-SMe, C-SH and C-SAc. The calculations were performed at the B3LYP/6-311+G(2d,2p) level on the lowest energy conformer in the gas phase using Gaussian 03.[32] The energy of orbitals HOMO-1, HOMO, LUMO and LUMO+1 are shown in Figure 5-14.

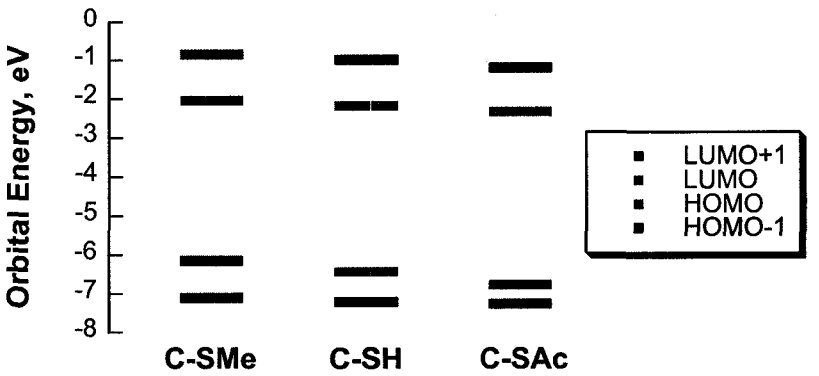

Figure 5-14. Calculated orbital energies using B3LYP/6-311+G(2d,2p) for C-SMe, C-SH and C-SAc in the gas phase. From left to right, the orbital energy for the HOMO (π) level decreases, while HOMO-1 (n) is unaffected. This increasing HOMO-LUMO gap is observed experimentally as a blue shift in the absorption maximum (see Figure 5-3).

The trend is clear. We see a decrease in energy for the HOMO (π) level in the order C-SMe, C-SH, C-SAc while the HOMO-1 (n) level is largely unaffected. These calculations indicate that a methyl protected mercaptocoumarin will have a lower π,π^* energy gap than C-SH and C-SAc. Furthermore, the excited state for C-SMe will be less affected by the presence of the n,π^* state due to a larger energy gap between the π,π^* and the n,π^* energy levels, *i.e.*, less excited-state mixing. These computational results are in agreement with the measured decrease in Φ_F from C-SMe to C-SH to C-SAc, which can be attributed to the increasing participation of a non-fluorescent n,π^* state. Of course, the orbital energies presented here are for ground state geometries and electronic configurations, but we expect the same trend in the excited state optimized structures of these largely rigid chromophores.

The calculated increase in HOMO-LUMO gap from C-SMe to C-SH to C-SAc is in agreement with the absorption spectra of these compounds. We observe a shift to higher energies in the absorption maximum from C-SMe to C-SH to C-SAc; in dichloromethane, for example, λ_{MAX} were 333, 326, and 321 nm, respectively. The absorbance peak due to the n,π^* transition (HOMO-1 to LUMO) is masked by the more allowed π,π^* transition. For this reason, theory was helpful in assigning the relative energy of the n,π^* state.

In protic solvents, C-SH is even less fluorescent. This is effectively the opposite from C-OH, which is most fluorescent in polar-solvents. Additionally, the low pK_a of C-SH (~2.8 in water) means that the anion will play a major role in the photophysical properties in polar, protic solvent. In methanol and water, both the neutral and anionic form of C-SH display low fluorescence quantum yields (Φ_F<0.01).

5.6 Conclusions

The work presented in this chapter is the first attempt to understand the photophysical properties of 7-mercaptocoumarins. We measured low fluorescence quantum yields ($\Phi_F < 0.1$) for C-SH in non-protic solvents, whereas alkylation of the thiol group (C-SMe and C-SMVK) made these coumarins very fluorescent ($\Phi_F = 0.30 - 0.81$). C-SR derivatives with electron withdrawing R-groups (C-SAc and C-$SPhNO_2$) were non-fluorescent ($\Phi_F < 0.005$). With this data and orbital energy calculations, we can put forth a working hypothesis to explain the fluorescence (or lack of fluorescence) of C-SR in non-protic solvents: Fast non-radiative processes induced by the participation of a low-lying n,π^* excited-states are responsible for lower fluorescence quantum yields.

In water, we measured very low fluorescence intensities from C-SH attributed to the neutral (405nm) and anionic (448nm) forms. Additionally, we observed triplet state formation for C-SH, C-SMe and C-SAc by laser-flash photolysis. These triplets behaved as photosensitizers for singlet oxygen, which was monitored by time-resolved near-infrared spectroscopy.

5.7 Experimental Section

7-mercapto-4-methylcoumarin (>97%) is commercially available from Fluka and was recrystallized from hexanes/dichloromethane before use. Methylvinylketone (Aldrich) was purified by filtration over silica gel before use. Styrene was distilled before use. All solvents were HPLC-grade or higher. Distilled, dionized (MilliQ purification systems) water was used. All other compounds were from Aldrich and used as received unless specified otherwise.

Steady-state absorbance and fluorescence measurements were recorded on a CARY-50 spectrophotometer and a Photon Technology International (PTI) fluorimeter. Laser Flash Photolysis experiments were performed on a Luzchem mini-LFP system or on a system described previously.[33] The excitation source was a Lumonics EX 530 XeCl excimer laser (λ = 308 nm, 6–8 ns, <20mJ per pulse). Time-resolved fluorescence was acquired on a Photon Technology International (PTI) EasyLife LS Fluorescence Lifetime System.

5.7.1 Molar Absorption Coefficient (ε) Determination

The compound of interest was dissolved in a concentrated stock solution of dichloromethane and aliquots of this stock solution were added to a 1cm x 1cm precision quartz cuvette containing the appropriate solvent. The added volume of dichloromethane stock solution was never more than 5% of the total volume.

Excellent linear correlation between absorbance and concentration were obtained with slopes equal to ε (Beer's law). The spectra shown in Figure 5-3 are simply the absorption spectrum divided by the concentration of mercaptocoumarin.

5.7.2 Fluorescence Quantum Yield Measurements (Φ_F)

The fluorescence standard used was 7-methoxycoumarin-4-acetic acid in methanol (Φ_{STD}=0.18, fluorescence λ_{MAX}=378nm).[26] When necessary, the fluorescence spectra were background-corrected by subtracting the signal obtained from the blank solvent. Each fluorescence quantum yield was determined using at least 4 fluorescence measurements.

To determine Φ_F, the fluorescence spectra at different concentrations are integrated and the results are plotted against the absorbance at the excitation wavelength (308 nm was employed). All plots gave excellent linear fits (the intercept was forced to go through the origin). Under identical measurement conditions, the slope of these graphs, (dF/dA), is related to the slope obtained from the standard, $(dF/dA)_{STD}$, by eq [6].[34] The values for the refractive index of each solvent, η, were also from reference[34].

$$[6] \qquad \Phi_F = \Phi_{STD} \frac{(dF/dA)}{(dF/dA)_{STD}} \left(\frac{\eta^2}{\eta_{STD}^2} \right)$$

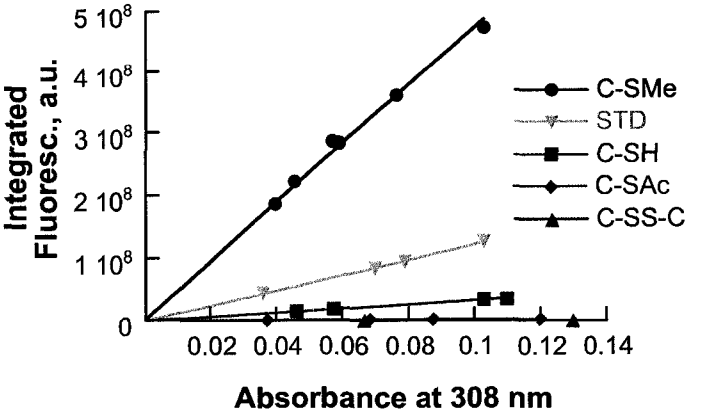

Figure 5-15. Integrated fluorescence vs absorbance at 308 for C-SMe (•), C-SH (▪), C-SAc (♦) and C-SS-C (▲) in dichloromethane and STD = 7-methoxycoumarin-4-acetic acid ( ) in methanol.

5.7.3 Fluorescence of C-SH vs pH

The supernatant part of a saturated aqueous solution of C-SH was filtered through 0.45 µm PTFE filters (Whatman, Inc.) and further diluted to achieve a maximum absorbance of ~0.2 above 320 nm. The solutions appeared clear, but the absorbance showed some light scattering (increasing baseline absorbance from long to short wavelengths) due to the very poor solubility of C-SH in water. The pH was adjusted with HCl and NaOH and the resulting pH was read with an electrode pH meter. The excitation wavelength was 338 nm (the approximate isosbestic point for the absorbance at all pH measured). Because the very low fluorescence signals were contaminated by scattering signals, we corrected all fluorescence spectra by subtracting the signal obtained from a dilute LUDOX® scattering solution in water.

5.7.4 *Time-Resolved Near Infrared Measurements*

The quantum yield of singlet oxygen photosensitization, $\Phi(^1O_2)$, is defined as the number of photosensitized $^1O_2$ molecules per photon absorbed. For this, samples of C-SR in the desired solvent were prepared in a 1cm x 1cm quartz cuvettes and their absorbance at 308nm was measured. In the same solvent we prepared samples of the standard. Laser excitation at 308nm generated singlet oxygen that was monitored using a time-resolved near-infrared photomultiplier tube detector (*vide infra*). The maximum signal intensity at 1270nm (near time 'zero') was then plotted in function of the sample's absorption factor ($1\text{-}10^{-A}$) at 308nm as shown in Figure 5-10. Absorbances (A) were kept below ~0.3. The slope of this graph for the sample ($slope_{C\text{-}SR}$) and the standard ($slope_{STD}$) are related by eq [7]. With the knowledge of $\Phi(^1O_2)_{STD}$, we can estimate $\Phi(^1O_2)$ for C-SR.

$$[7] \qquad \Phi(^1O_2) = \Phi(^1O_2)_{STD} \frac{slope_{C-SR}}{slope_{STD}}$$

The standards used were phenalenone in toluene or chloroform, $\Phi(^1O_2)$=1 from "Oliveros et al., New. J. Chem. 1999, 23, 85-93"; phenazine in dichloromethane ($\Phi(^1O_2)$=0.89) and chloroform ($\Phi(^1O_2)$=0.84) from "Redmond, R. W. and Braslavsky, S. E., NATO ASI Ser., Ser. H 15 (Photosensitisation), 1998, 93-95"; and methylene blue in dichloromethane, $\Phi(^1O_2)$=0.52 from "Chem. Lett. (Tokyo) 1973 (7) 743-744". Many values for $\Phi(^1O_2)$ are tabulated on the website: http://www.rcdc.nd.edu/

Singlet oxygen phosphorescence at 1270nm was monitored using a Hamamatsu NIR PMT Module (H10330-75) with detection capabilities from ~950 to 1700 nm. The excitation source was a Lumonics EX 530 XeCl excimer laser (λ = 308 nm, 6–8 ns, <20mJ per pulse) and the acquisition interface was based on a modified Luzchem laser flash photolysis system.

5.7.5 Synthetic Procedures

S-acetyl-7-mercapto-4-methylcoumarin (C-SAc)

In a 50mL round bottom flask equipped with a magnetic stir bar, 7-mercapto-4-methylcoumarin (201.2mg, 1.047mmol) was dissolved with 20mL dichloromethane. Triethylamine (0.16mL, 1.15mmol) and acetic anhydride (0.11mL, 1.15mmol) were added sequentially with stirring. The reaction was stirred for 40 minutes before the reaction (+50mL dichloromethane) was extracted with 10% HCl (50mL) and 2x50 distilled water in a separatory funnel. The organic layer was dried over $MgSO_4$. After the solids were removed by filtration and the liquid evaporated, the resulting solid was recrystallized from petroleum ether and dichloromethane to afford 113mg (46% yield) of off-white solid. ^{1}H NMR ($CDCl_3$, 400 MHz): δ 7.63 (*J*=8 Hz, d, 1H, *Ar*H), 7.42 (*J*=1.2Hz, d, 1H, *Ar*H), 7.35-7.33 (*J*=8Hz, q, 1H, *Ar*H), 6.34 (*J*=1.1Hz q, 1H, =*C*H), 2.47 (s, 3H, *C*H_3), 2.45 (*J*=1.2Hz, d, 3H, *C*H_3). ^{13}C NMR

($CDCl_3$, 400 MHz): δ 192.39, 160.11, 153.32, 151.68, 132.17, 129.75, 124.93, 122.44, 120.59 116.04, 30.44, 18.63. IR ν (cm^{-1}) 3058 (m), 1741 (s), 1692 (s), 1603 (m), 1400 (m), 1380 (m), 880 (m). m.p. 145-149°C. MS (EI) m/z 234.04 (9.0), 192.02 (100.0), 164.03 (18.5), 135.02 (4.3), 102.05 (3.4), 68.98 (4.3), 51.02 (4.9), 43.02 (81.0), 39.02 (4.9). HRMS Calcd. for $C_{12}H_{10}O_3S$: 234.00351. Found: 234.0353.

S-4-nitrophenyl-7-mercapto-4-methylcoumarin (C-SPhNO_2)

KOH pellets (777.0mg, 13.85mmol) were crushed in a mortar and pestel and then dissolved in DMSO (25mL) in a 50mL round bottom flask equipped with a stir bar. The reaction mixture was cooled over ice water and purged with argon. 7-mercapto-4-methylcoumarin (537.5mg, 2.796mmol) was added to the flask and purging was continued. 1-Fluoro-4-nitrobenzene (310µL, 2.922mmol) was added drop-wise to the stirring solution. The reaction was allowed to proceed for 15 min and then was brought to room temperature. After an additional 1.75 h of stirring, ether (100mL) was added to the reaction and then extracted with 3x100 mL distilled water in a separatory funnel. A yellow/green solid formed at the bottom of the ether layer and was filtered off using a Buchner funnel. The solid was then dissolved in dichloromethane, dried over $MgSO_4$, filtered off and brought to dryness under reduced pressure to afford 386.4mg (44% yield) of product. ^1H NMR ($CDCl_3$, 400 MHz): δ 8.172-8.149 (m, 2H, *Ar*H), 7.627 (*J*=8.4Hz, d, 1H, *Ar*H), 7.407-7.384 (m,

3H, *Ar*H), 7.33 (*J*=3.3Hz, q, 1H, *Ar*H), 6.335 (*J*=3.2Hz, d, 1H, =*C*H), 2.456 (*J*=1.2Hz, d, 3H, *C*H_3). ^{13}C NMR ($CDCl_3$, 400 MHz): δ 159.938, 153.947, 151.601, 144.621, 137.275, 129.592, 127.687, 125.688, 124.446, 120.325, 115.792, 18.670. IR ν (cm^{-1}) 3091 (w), 1718 (s), 1505 (s), 1394 (m), 1336 (s), 1316 (m), 848 (m). m.p. 191-196°C. MS (EI) *m/z* 313.04 (100.0), 285.04 (19.2), 161.99 (19.4), 142.99 (17.1), 111.99 (7.0), 72.04 (24.9), 30.99 (24.9). HRMS Calcd. for $C_{16}H_{11}NO_4S$: 313.0409. Found: 313.0402.

S-4-aminophenyl-7-mercapto-4-methylcoumarin (C-SPhNH$_2$)

Tin powder (657.8mg, 5.541mmol) and C-SPhNO$_2$ (134.0mg, 0.4729mmol) were added to a 50mL round bottom flask equipped with a stir bar. Four portions of concentration HCl (3mL each, 12mL total) were added sequentially. After the vigorous reaction subsided, the round bottom flask was equipped with a reflux condenser and the solution was refluxed in a water bath. During refluxing, ethanol (3mL) was added to help dissolved the nitro compound. After 1h of refluxing, the reaction flask was cooled and 20% w/v NaOH was added until the tin hydroxide was dissolved. Product was extracted from ethyl acetate (100mL) and washed with 20% w/v NaOH (100mL) and then twice with distilled water (100mL each, 200mL total). The organic layer was then dried over $MgSO_4$, filtered off and brought to dryness under reduced pressure to afford 47.9mg (40% yield) of product. ^{1}H NMR ($CDCl_3$,

400 MHz): δ 7.405 (*J*=8.4Hz, d, 1H, *Ar*H), 7.353-7.317 (m, 2H, *Ar*H), 7.021 (*J*=3.5Hz, q, 1H, ArH), 6.845 (*J*=2Hz, d, 1H, *Ar*H), 6.747-6.713 (m, 2H, NH_2), 6.164 (*J*=1.2Hz, d, 1H, =*C*H), 2.375 (*J*=1.2Hz, d, 3H, CH_3). ν (cm^{-1}) 3359 (m), 3451 (m), 1700 (s), 1595 (s), 1386 (m), 826 (m). m.p. 190-197°C. MS (EI) m/z 283.07 (100), 255.07 (5.2), 223.09 (5.0), 161.99 (13.2), 142.99 (11.0), 124.02 (13.08), 111.99 (5.6), 77.04 (7.2), 57.07 (7.6), 28.01 (37.1). HRMS Calcd. for $C_{16}H_{13}NO_2S$: 283.0667. Found: 283.0664.

S-3-oxobutyl-7-mercapto-4-methylcoumarin (C-SMVK)

7-mercapto-4-methylcoumarin (400mg, 2mmol) was dissolved with 25mL THF in a 50mL round bottom flask equipped with a stir bar. The reaction mixture was cooled over ice water and purged under argon. K_2CO_3 (289.0mg, 2.091mmol) and methylvinylketone (185.5μL, 2.226mmol) were added sequentially with stirring. After 30 min, the solvent was removed under reduced pressure. The resulting solid was dissolved in dichloromethane (100mL) and washed twice with distilled water (50mL each, 100mL total). The organic layer was then dried over $MgSO_4$, filtered off and brought to dryness under reduced pressure to afford 260mg (48% yield) of product. ^{1}H NMR ($CDCl_3$, 400 MHz): δ 7.484 (*J*=8Hz, *d*, 1H, *Ar*H), 7.184-7.154 (m, 2H, *Ar*H), 6.231 (*J*=1.2Hz, q, 1H, =*C*H), 3.224 (*J*=7.2Hz, t, 2H, CH_2), 2.844 (*J*=7.2Hz, t, 2H, CH_2), 2.413 (*J*=1.2Hz d, 3H, CH_3), 2.186 (s, 3H, CH_3). ^{13}C NMR

($CDCl_3$, 400 MHz): δ 205.797, 160.506, 153.883, 152.061, 142.340, 124.747, 123.177, 117.422, 114.453, 114.086, 42.406, 30.915, 30.089, 25.899, 18.564. IR ν (cm^{-1}) 3062 (w), 1712 (s), 1684 (m), 1605 (m), 1363 (m), 955 (m), 865 (m). m.p. 112-113°C. MS (EI) m/z 262.06 (100), 219.05 (16.6), 192.02 (63.7), 161.99 (67.9), 149.99 (24.7), 142.99 (62.9), 111.99 (28.9), 68.98 (25.3), 50.00 (28.8), 31.00 (62.5). HRMS Calcd. for $C_{14}H_{14}O_3S$: 262.0664. Found: 262.0662.

Di-4-methylumbelliferyl-disulfide (C-SS-C)

Using a mortar and pestle, 7-mercapto-4-methylcoumarin (151.3mg, 0.7871mmol), $KMnO_4$ (127.0mg, 0.8036mmol) and neutral Al_2O_3 (88.8mg, 0.871mmol) were grinded together for 10 min. The product was extracted using a generous amount of dichloromethane and the resulting mother liquor was evaporated to dryness using a rotatory evaporator. The residual solid was recrystallized from ethanol and dichloromethane to afford 41.4mg (28% yield) of pale yellow needles. ^1H NMR ($CDCl_3$, 400 MHz): δ 7.545 (*J*=1.2Hz, d, 1H, *Ar*H), 7.44 (d, 1H, *Ar*H), 7.385 (*J*=4Hz, q, 1H, *Ar*H), 6.25 (d, 1H, =*C*H), 2.415 (*J*=8Hz, d, 3H, CH_3). ^{13}C NMR ($CDCl_3$, 400 MHz): δ 160.143, 153.975, 151.800, 140.814, 125.255, 122.076, 119.052, 114.929, 114.363, 18.632. m.p. 234-245°C. MS (EI) m/z 382.03 (24.4), 318.10 (20.1), 290.05 (32.8), 191.01 (55.5), 163.02 (49.9), 91.1

(100.0), 77.04 (50.9), 68.98 (65.6). HRMS Calcd. for $C_{20}H_{14}O_4S_2$: 382.0334. Found: 382.0314.

S-methyl-7-mercapto-4-methylcoumarin (C-SMe)

In dry, distilled tetrahydrofuran, 7-mercapto-4-methylcoumarin (1g, 5.2mmol) and 1.2 eq. of imidazole (0.425g) were stirred at room temperature in a capped round bottom flask. Methyl Iodide (~1.2 eq., 0.4mL) was added dropwise to the solution via syringe. After the reaction appeared complete by TLC, the solution was rotovapped and the residue was purified by column silica gel chromatography to afford 0.9g (84% yield) of pale yellow powder. ^{1}H NMR ($CDCl_3$, 400 MHz): δ 7.467 (*J*=8.4Hz, d, 1H, *Ar*H), 7.148-7.115 (m, 2H, *Ar*H), 6.208 (*J*=0.4Hz, q, 1H, =*C*H), 2.533 (s, 3H, *C*H$_3$), 2.410-2.407 (*J*=1.2Hz, d, 3H, *C*H$_3$). ^{13}C NMR ($CDCl_3$, 400 MHz): δ 160.668, 154.000, 152.207, 144.740, 124.428, 121.752, 116.701, 113.640, 112.618, 18.569, 14.953. IR ν (cm^{-1}) 3055 (w), 1742 (s), 1601 (s), 1387 (m) 858 (s). m.p. 125-128°C. MS (EI) m/z 202.04 (100), 178.05 (52.3), 163.02 (53.2), 134.02 (67.9), 102.05 (5.1), 89.02 (6.8), 77.04 (8.6), 51.02 (9.7), 31.00 (7.1). HRMS Calcd. for $C_{11}H_{10}O_2S$: 206.0402. Found: 206.0390.

5.8 Appendix: Kinetic Treatment for P Type Delayed Fluorescence

After laser excitation and intersystem crossing, an initial amount of triplet is formed, $[T^*]_o$ and it decays with an apparent lifetime, τ_o. This is observed if the major quenching pathway of T* is not triplet-triplet annihilation. Therefore, the rate expression for T* decay will follow the traditional pseudo first-order decay, shown here in its integrated form,

$$[T^*]_t = [T^*]_o e^{-t/\tau_o},$$

where t is the time and $[T^*]_t$ is the concentration of T* at time t.

Two excited triplets can encounter and their reaction is called triplet-triplet annihilation. Due to spin statistics, one of nine excited triplet encounters yields two singlets and the sum of both triplet excited state energies are enough to generate one singlet excited state,

$$T^* + T^* \xrightarrow{1/9 k_{TT}} S^* + S_o.$$

Note that the actual yield of singlet excited-state may be different than 1/9 if the quenching is not diffusion limited for all triplet encounters.

This mechanism gives rise to an observable delayed fluorescence emission spectrally identical to the steady-state fluorescence spectrum. The lifetime for

delayed fluorescence from triplet-triplet annihilation (called P-type delayed fluorescence) is equal to $0.5\tau_o$. To explain the lifetime difference between the observed triplet decay and the delayed fluorescence signal, we derive the rate expression for the triplet-triplet annihilation relevant to the delayed-fluorescence,

$$\frac{d[S^*]}{dt} = 1/9\, k_{TT}[T^*]^2,$$

and substitute the expression for [T*] into this latter expression,

$$\frac{d[S^*]}{dt} = 1/9\, k_{TT}([T^*]_o e^{-t/\tau_o})^2$$

$$\frac{d[S^*]}{dt} = 1/9\, k_{TT}[T^*]_o^{\,2} e^{-t/(0.5\tau_o)}.$$

Integration on both sides with boundaries t=0 and t=t will give an expression reminiscent of a simple pseudo first-order decay with lifetime equal to $\frac{1}{2}\tau_o$ which is what we observe experimentally.

$$d[S^*] = 1/9\, k_{TT}[T^*]_o^{\,2} e^{-t/(0.5\tau_o)} dt$$

$$\int_{t=0}^{t=t} d[S^*] = \int_{t=0}^{t=t} 1/9 k_{TT}[T^*]_o^{\,2} e^{-t/(0.5\tau_o)} dt$$

$$\int_{t=0}^{t=t} d[S^*] = 1/9 k_{TT}[T^*]_o^{\,2} \int_{t=0}^{t=t} e^{-t/(0.5\tau_o)} dt$$

$$[S^*] = 1/9 k_{TT}[T^*]_o^{\,2} e^{-t/(0.5\tau_o)}$$

5.9 References

(1) Schade, B.; Hagen, V.; Schmidt, R.; Herbrich, R.; Krause, E.; Eckardt, T.; Bendig, J. "Deactivation behavior and excited-state properties of (coumarin-4-yl)methyl derivatives. 1. Photocleavage of (7-methoxycoumarin-4-yl) methyl-caged acids with fluorescence enhancement" *Journal of Organic Chemistry* **1999**, 64, 9109-9117.

(2) Eckardt, T.; Hagen, V.; Schade, B.; Schmidt, R.; Schweitzer, C.; Bendig, J. "Deactivation Behavior and Excited-State Properties of (Coumarin-4-yl)methyl Derivatives. 2. Photocleavage of Selected (Coumarin-4-yl) methyl-Caged Adenosine Cyclic 3', 5'-Monophosphates with Fluorescence Enhancement" *Journal of Organic Chemistry* **2002**, 67, 703-710.

(3) Trozzolo, A. M.; Dienes, A.; Shank, C. V. "Excited-state reactions of a laser dye. Evidence for a two-step phototautomerism in 7-hydroxy-4-methylcoumarin" *Journal of the American Chemical Society* **1974**, 96, 4699-4700.

(4) Dorlars, A.; Schellhammer, C. W.; Schroeder, J. "Heterocycles as Structural Units in New Optical Brighteners" *Angewandte Chemie International Edition* **1975**, 14, 665-679.

(5) Seixas de Melo, J. S.; Becker, R. S.; Macanita, A. L. "Photophysical Behavior of Coumarins as a Function of Substitution and Solvent: Experimental Evidence for the Existence of a Lowest Lying (n,pi*) State" *The Journal of Physical Chemistry* **1994**, 98, 6054-6058.

(6) Hammond, G. S.; Stout, C. A.; Lamola, A. A. "Mechanisms of Photochemical Reactions in Solution. XXV. The Photodimerization of Coumarin" *Journal of the American Chemical Society* **1964**, 86, 3103-3106.

(7) Gnanaguru, K.; Ramasubbu, N.; Venkatesan, K. "A study on the photochemical dimerization of coumarins in the solid state" *Journal of Organic Chemistry* **1985**, 50, 2337-2346.

(8) Wheelock, C. E. "The Fluorescence of Some Coumarins" *Journal of the American Chemical Society* **1959**, 81, 1348-1352.

(9) Wolfbeis, O. S.; Koller, E.; Hochmuth, P. "The Unusually Strong Effect of a 4-Cyano Group upon Electronic Spectra and Dissociation Constants of 3-Substituted 7-Hydroxycoumarins" *Bulleting of the Chemical Society of Japan* **1985**, 58, 731-734.

(10) Bloch, W.; Gorby, M. S. "Catalytic mechanism of Escherichia coli alkaline phosphatase: resolution of three variants of the acyl-enzyme mechanism" *Biochemistry* **1980**, 19, 5008-5018.

(11) Setsukinai, K.; Urano, Y.; Kikuchi, K.; Higuchi, T.; Nagano, T. "Fluorescence switching by O-dearylation of 7-aryloxycoumarins. Development of novel fluorescence probes to detect reactive oxygen species with high selectivity" *Journal of the Chemical Society, Perkin Trans. 2* **2000**, 2453-2457.

(12) Ivan, M. G.; Laferrière, M.; Sanrame, C. N.; Scaiano, J. C. "On the Question of Acid Generation upon 157-nm Laser Exposure of Fluorinated Polymers" *Chemistry of Materials* **2006**, 18, 2635-2641.

(13) de Monpezat, T. L.; de Jeso, B.; Butour, J. L.; Chavant, L.; Sancholie, M. "A fluorimetric method for measuring lipase activity based on umbelliferyl esters" *Lipids* **1990**, 25, 661.

(14) Goddard, J.; Reymond, J. "Recent advances in enzyme assays" *Trends in Biotechnology* **2004**, 22, 363-370.

(15) Frenette, M.; Coenjarts, C.; Scaiano, J. "Mapping Acid-Catalyzed Deprotection in Thin Polymer Films: Fluorescence Imaging Using Prefluorescent 7-

Hydroxycoumarin Probes" *Macromolecular Rapid Communications* **2004**, 25, 1628-1631.

(16) Frenette, M.; Ivan, M.; Scaiano, J. "Use of fluorescent probes to determine catalytic chain length in chemically amplified resists" *Canadian Journal of Chemistry* **2005**, 83, 869-874.

(17) Ito, H. "Chemical amplification resists: Inception, implementation in device manufacture, and new developments" *Journal of Polymer Science Part A Polymer Chemistry* **2003**, 41, 3863-3870.

(18) Brogan, A. P.; Widger, W. R.; Kohn, H. "Bicyclomycin Fluorescent Probes: Synthesis and Biochemical, Biophysical, and Biological Properties" *Journal of Organic Chemistry* **2003**, 68, 5575-5587.

(19) Barr, B. K.; Holewinski, R. J. "4-Methyl-7-thioumbelliferyl-beta-D-cellobioside: a fluorescent, nonhydrolyzable substrate analogue for Cellulases" *Biochemistry* **2002**, 41, 4447-4452.

(20) Sarkar, A. K. "7-Mercapto-Coumarins" 1970, US Patent 3,547,952.

(21) de Melo, J. S.; Becker, R. S.; Elisei, F.; Maçanita, A. L. "The photophysical behavior of 3-chloro-7-methoxy-4-methylcoumarin related to the energy separation of two lowest-lying singlet excited states" *Journal of Chemical Physics* **1997**, 107, 6062-6069.

(22) Turro, N. J.; Ramamurthy, V.; Scaiano, J. C., Principles of Molecular Photochemistry: An Introduction. University Science Publishers: New York, N.Y., 2008; pp 493.

(23) Magde, D.; Wong, R.; Seybold, P. G. "Fluorescence Quantum Yields and Their Relation to Lifetimes of Rhodamine 6G and Fluorescein in Nine Solvents: Improved Absolute Standards for Quantum Yields" *Photochemistry Photobiology* **2002**, 75, 327-334.

(24) Focsaneanu, K. S.; Scaiano, J. C. "Potential analytical applications of differential fluorescence quenching: pyrene monomer and excimer emissions as sensors for electron deficient molecules" *Photochemical and Photobiological Sciences* **2005**, 4, 817-821.

(25) Munkholm, C.; Parkinson, D. R.; Walt, D. R. "Intramolecular fluorescence self-quenching of fluoresceinamine" *Journal of the American Chemical Society* **1990**, 112, 2608-2612.

(26) Farinotti, R.; Siard, P.; Bourson, J.; Kirkiacharian, S. "4-bromomethyl-6, 7-dimethoxycoumarin as a fluorescent label for carboxylic acids in chromatographic detection" *Journal of Chromatography* **1983**, 269, 81-90.

(27) Ito, O.; Matsuda, M. "Polar Effects in Addition Reactions of Benzenethiyl Radicals to Substituted Styrenes and &-Methylstyrenes Determined by Flash Photolysis" *Journal of the American Chemical Society* **1982**, 104, 1701-1703.

(28) A SciFinder search for the 7-hydroxycoumarin core (without hydroxyl group protection) gave 754 publications reporting fluorescence.

(29) Lide, D. R.; Editor-in-Chief "CRC Handbook of Chemistry and Physics"; CRC Press, 2004-2005; Vol. 85.

(30) Moriya, T. "Excited-state Reactions of Coumarins in Aqueous Solutions. I. The Phototautomerization of 7-Hydroxycoumarin and Its Derivative" *Bulletin of the Chemical Society of Japan* **1983**, 56, 6-14.

(31) Schulman, S. G.; Rosenberg, L. S. "Tautomerization kinetics of 7-hydroxy-4-methylcoumarin in the lowest excited singlet state" *The Journal of Physical Chemistry* **1979**, 83, 447-451.

(32) Frisch, M. J. T., G. W.; Schlegel, H. B.; Scuseria, G. E.; Robb, M. A.; Cheeseman, J. R.; Montgomery, Jr., J. A.; Vreven, T.; Kudin, K. N.; Burant, J. C.; Millam, J. M.; Iyengar, S. S.; Tomasi, J.; Barone, V.; Mennucci, B.; Cossi, M.;

Scalmani, G.; Rega, N.; Petersson, G. A.; Nakatsuji, H.; Hada, M.; Ehara, M.; Toyota, K.; Fukuda, R.; Hasegawa, J.; Ishida, M.; Nakajima, T.; Honda, Y.; Kitao, O.; Nakai, H.; Klene, M.; Li, X.; Knox, J. E.; Hratchian, H. P.; Cross, J. B.; Bakken, V.; Adamo, C.; Jaramillo, J.; Gomperts, R.; Stratmann, R. E.; Yazyev, O.; Austin, A. J.; Cammi, R.; Pomelli, C.; Ochterski, J. W.; Ayala, P. Y.; Morokuma, K.; Voth, G. A.; Salvador, P.; Dannenberg, J. J.; Zakrzewski, V. G.; Dapprich, S.; Daniels, A. D.; Strain, M. C.; Farkas, O.; Malick, D. K.; Rabuck, A. D.; Raghavachari, K.; Foresman, J. B.; Ortiz, J. V.; Cui, Q.; Baboul, A. G.; Clifford, S.; Cioslowski, J.; Stefanov, B. B.; Liu, G.; Liashenko, A.; Piskorz, P.; Komaromi, I.; Martin, R. L.; Fox, D. J.; Keith, T.; Al-Laham, M. A.; Peng, C. Y.; Nanayakkara, A.; Challacombe, M.; Gill, P. M. W.; Johnson, B.; Chen, W.; Wong, M. W.; Gonzalez, C.; and Pople, J. A.; "Gaussian 03, revision D.01" Gaussian, Inc. 2003, Wallingford, CT.

(33) Chrétien, M.; Ph.D. thesis, "Photochemical, Photophysical, and Photobiological Studies of Zeolite Guest-Host Complexes." University of Ottawa, Ottawa, ON Canada, 2007.

(34) Scaiano, J. C.; Editor-in-Chief "CRC Handbook of Organic Photochemistry"; CRC Press: Boca Raton, FL, 1989; Vol. 1 and 2.

6. 7-Mercapto-4-methylcoumarin as a Prefluorescent Probe for Electrophilic Lipid Oxidation Products

6.1 Graphical Abstract

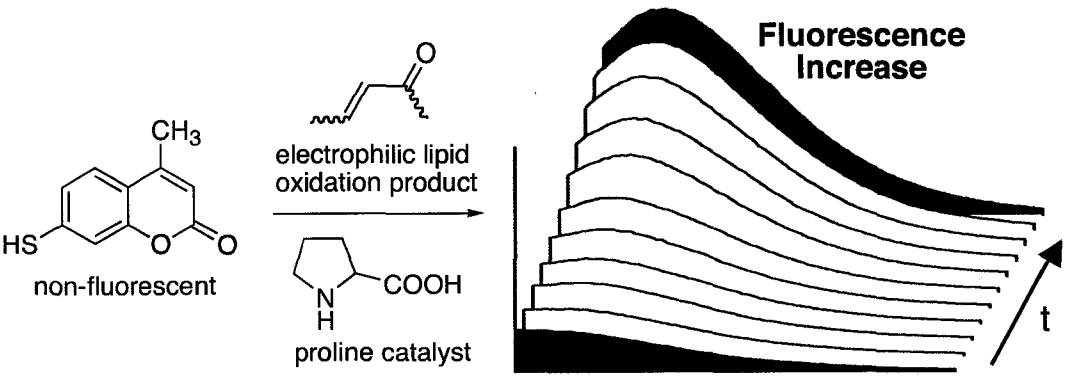

6.2 Electrophiiic Lipid Oxidation Products

There is growing evidence that electrophiles generated during lipid oxidation are disrupting normal biological behavior.[1,2] In fact, if one looks at the structure of warfare chemicals, the majority are also electrophiles (Scheme 6-1). VX gas and other organophosphate nerve agents are electrophilic molecules that covalently attach to acetylcholinesterase (AChE) and suppress nervous control of muscles—including the diafragm with deadly concequences.[3] Phosgene and mustard gas are other examples from a long list of electrophiles developed as warfare chemicals.[4] Some chemotherapy drugs[5] and insecticides[6] work on the same principles, albeit with increased selectivity and lower reactivity.

Hopefully every chemist knows of the toxicity of benzene. As C_6H_6 it is innocuous. In the liver, however, one of its double bonds is transformed into an epoxide (by cytochrome P450) to form benzene oxide[7] and this molecule causes electrophilic damage in bone marrow that leads to leukemia. Most people will go through life without suffering from deleterious effects of VX gas or benzene, but none of us can (yet) escape lipid oxidation and the electrophiles it generates.

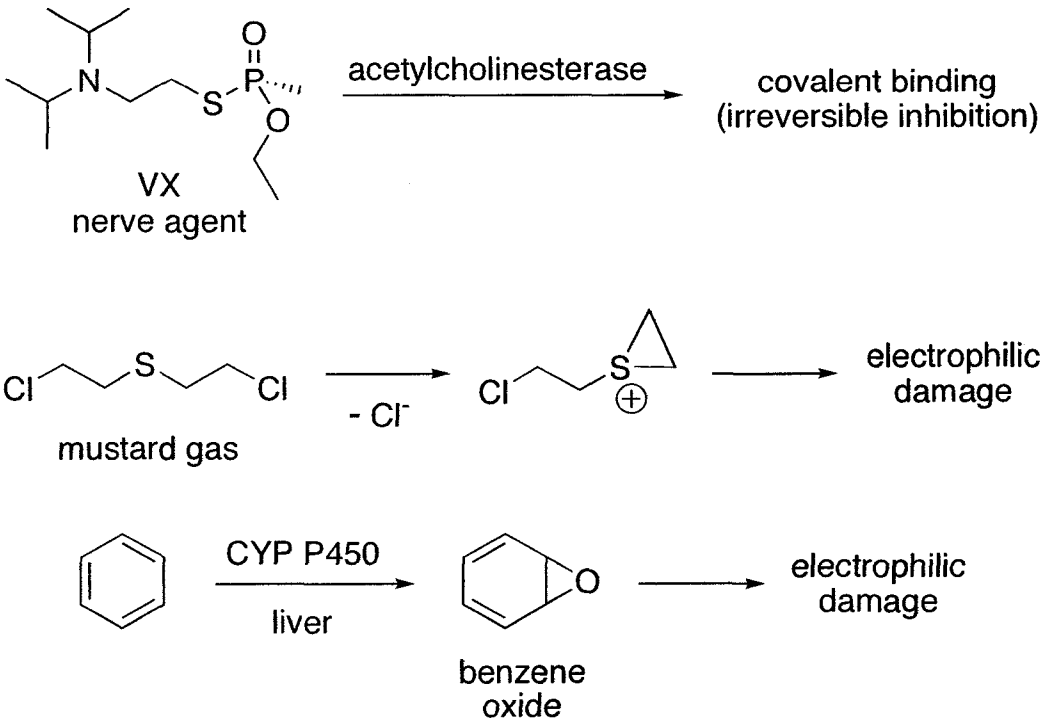

Scheme 6-1. Examples of electrophiles or electrophilic precursors with adverse biological effects: VX gas, mustard gas and benzene.

The autoxidation of polyunsaturated lipids (LH) was introduced in Chapter 1. The primary oxidation products are lipid hydroperoxides (LOOH) and these molecules can undergo further reactions. To say the least, these secondary reactions generate complex product mixtures. In Chapter 4 we proposed a mechanism that forms lipid oxodienes (L=O) as a secondary oxidation product of lipid autoxidation—this mechanism also introduces hydroxyl radicals as a reactive side-product. L=O derivatives, however, represent a small fraction of other known electrophiles generated during lipid peroxidation. Some major constituents and their common acronyms are shown in Scheme 6-2.

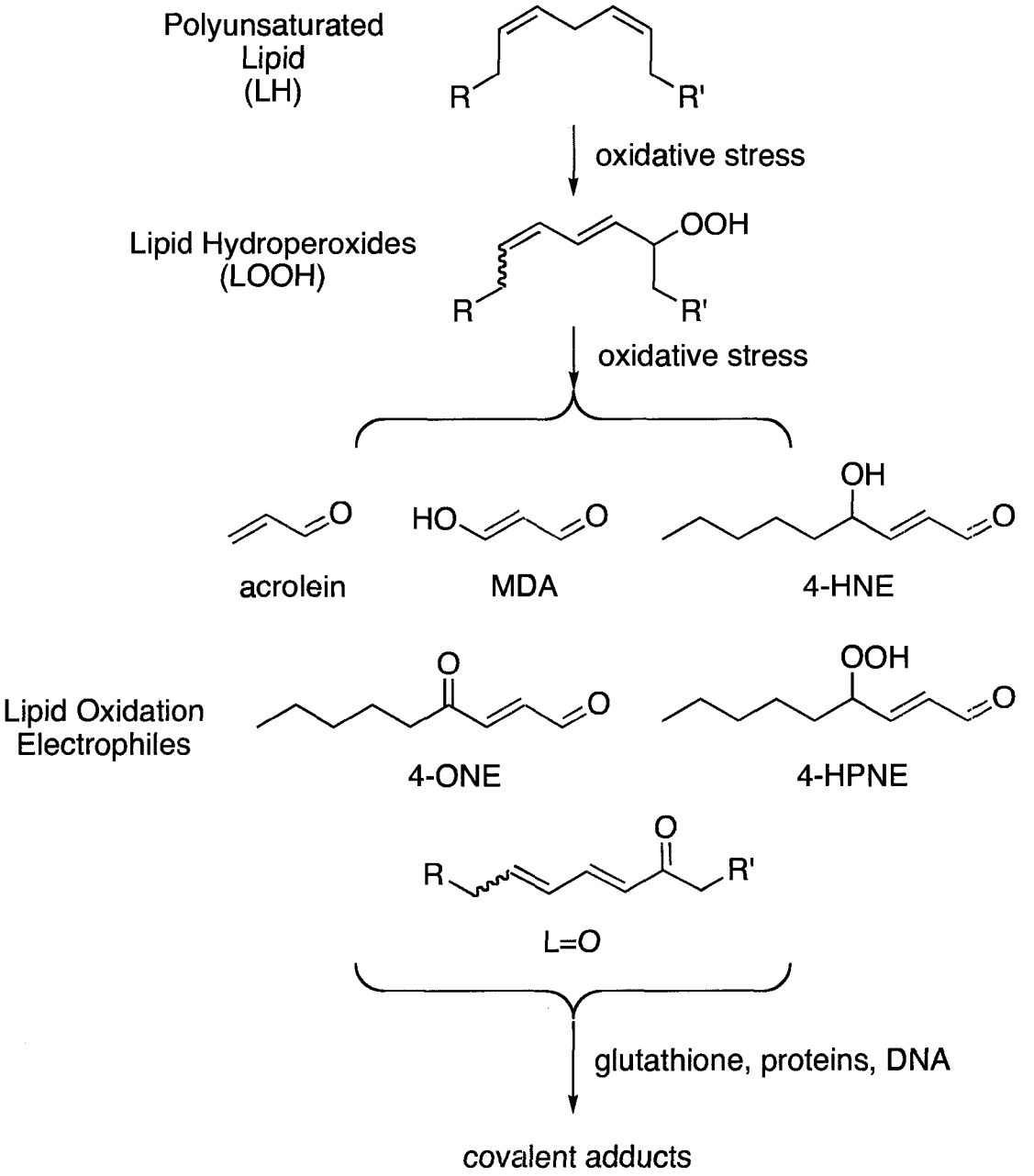

Scheme 6-2. The oxidation of polyunsaturated lipids (LH) generates electrophiles[1] with α,β-unsaturated aldehydes (or ketones) moieties (coloured in red); acrolein is the most reactive example. Malondialdehyde (MDA), 4-hydroxy-2-nonenal (4-HNE), 4-oxo-2-nonenal (4-ONE), 4-hydroperoxy-2-nonenal (4-HPNE) and oxodienes (L=O) are also found. These lipid oxidation electrophiles react with nucleophiles such as glutathione,[8] protein thiols and amines,[9] and DNA bases[10] to form covalent adducts.

These lipid electrophiles (and electrophilic warfare chemicals) are "bad" because they bind to biological nucleophiles: protein thiols and amines[9] or guanine bases in DNA.[10] Obviously, a guanine covalently bound to a lipid residue will behave differently than a regular guanine; DNA replication will be hindered and mutations could occur. Many research publications have linked these findings (and oxidative stress in general) to apoptosis,[11] neurodegenerative diseases,[12] and even aging in general.[13] In any case, the relationship between oxidative stress and disease needs more studies with better tools to monitor the extent of oxidative stress under various conditions.

One of the most popular tools to study lipid oxidation is the thiobarbituric acid (TBA) assay,[14,15] developed in the 1940s. This is a tedious technique that requires acid and heating during the analysis. Of course, the samples can undergo further oxidative damage during this treatment. It was observed that variations on the TBA assay, such as the inclusion of antioxidants or metal chelators, yield very different responses. Still, the TBA assay is increasingly used for the analysis of secondary lipid oxidation products.[16] At this point, the authoritative techniques to study lipid oxidation products are based on high-pressure liquid chromatography (HPLC).[17] The data obtained by HPLC, however, requires more expertise to interpret and the sequential acquisition of multiple samples can take several hours. As an alternative detection technique, fluorescent probes have emerged in recent years as useful analytical tools in biological systems.[18]

6.3 A Fluorescent Probe to Detect Lipid Oxidation Electrophiles

Fluorescent probes are successful since fluorescence detection is simple, sensitive, fast and can yield high-resolution images. Since fluorescence is more sensitive against a dark background, fluorescent probes are usually designed to increase in fluorescence after a desirable event occurs. The "desirable event" can be based on the following:

(i) **Location.** The simplest fluorescent probe design is location-based, i.e., wherever the fluorescent molecule goes, you can see it with great accuracy. For example, fluorescein—one of the few fluorophores allowed for medical injection in Canada—is used in ophthalmology to map blood flow in the eye. Another "location based" approach is the use of Förster (or Fluorescence) Resonance Energy Transfer (FRET), where excitation energy is transferred between two chromophores in a distance dependant manner.[9] Of course, every fluorescent probe is "location-based"; it needs to be there for you to see it.

(ii) **Environment.** We see many fluorescent molecules change their fluorescence (or excitation) spectra depending on their local environment. DNA-intercalator dyes such as Picogreen® are an

example where the environment changes the molecule's fluorescence intensity. Picogreen® is non-fluorescent in water because it releases excitation energy by internal rotations.[ref] Once intercalated in between DNA base pairs the imparted rigidity on the fluorophore causes it to be fluorescent. This technique is used to "stain" cell nuclei.

(iii) **Chemical change.** The terms prefluorescent, fluorogenic and "molecular beacon" have been used to describe fluorescent probes designed using this approach. Well-designed fluorescent probes can be very selective to monitor a particular chemical reaction.

Ideally, electrophilic lipid oxidation products could be detected in "real time" in "real samples". Fluorescence spectroscopy is one of the only techniques that can achieve these two requirements.

With the knowledge of mercaptocoumarin photochemistry described in the previous chapter, I decided to investigate the use of mercaptocoumarins to detect electrophilic lipid peroxidation products. The basic concept is shown in Scheme 6-3. Much like glutathione can protect the cell against lipid oxidation electrophiles, 7-mercapto-4-methylcoumarin (C-SH) becomes fluorescent after attacking the same compounds.

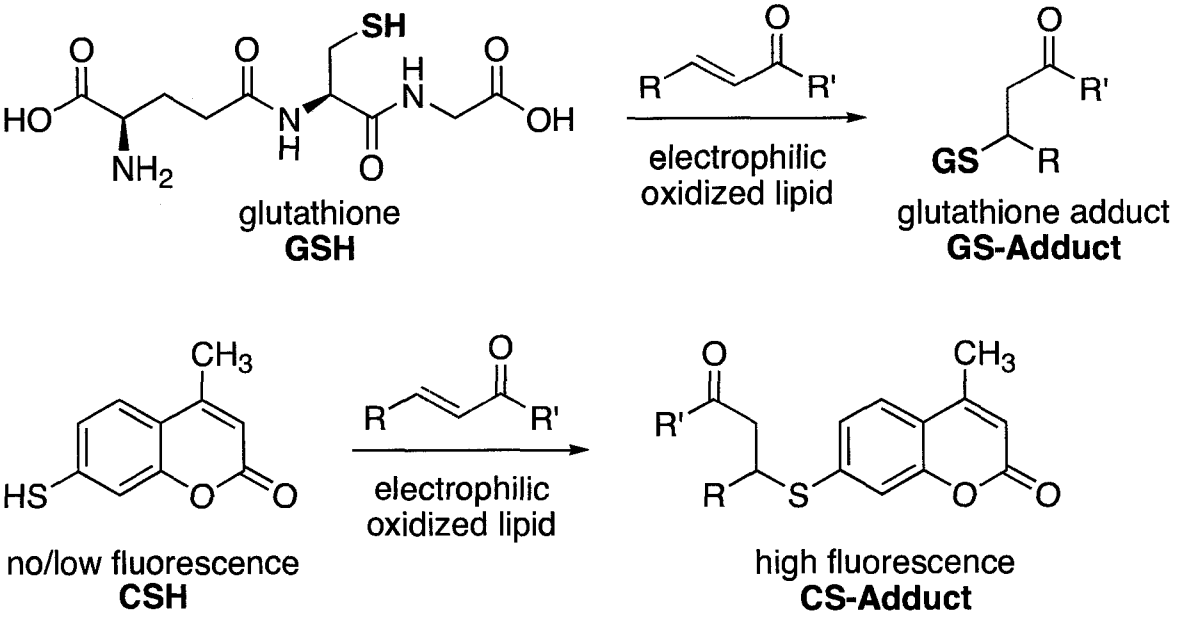

Scheme 6-3. We introduce the use of 7-mercapto-4-methylcoumarin as a prefluorescent probe to detect electrophilic oxidized lipids. The reaction that generates fluorescence is similar to the reaction of glutathione with these compounds *in vivo*.

Initial attempts to use C-SH in cells were thwarted because cell auto fluorescence was in the same region as the emission of C-SH (and C-SAdducts). The poor aqueous solubility of C-SH was also a limiting factor, so we decided to develop C-SH as a probe to detect electrophiles in extracted lipids using steady-state fluorescence. This approach has many practical advantages: any solvent can be chosen for the analysis (after evaporation of the extraction solvent), the analytes can be concentrated to facilitate detection and interfering cell material can be removed before the analysis. This chapter will describe the development of C-SH as a prefluorescent probe to quantify biologically relevant lipid oxidation electrophiles.

6.4 Detecting Reactive Lipid Oxidation Electrophiles

Methylvinylketone (CH_2=CHC(O)CH_3, MVK) was chosen as the electrophile to model the biologically relevant acrolein (CH_2=CHC(O)H); both compounds have non-hindered α,β-unsaturated carbonyls. This makes MVK and acrolein more reactive than other electrophiles with disubstituted alkenes such as MDA, 4-HNE or 4-HPNE.

In the previous chapter, we report the synthesis and photophysical properties of C-SMVK—the reaction product between C-SH and MVK. The fluorescence quantum yield (Φ_F) for C-SMVK was 5-10 times greater than C-SH. In chloroform, for example, C-SMVK and C-SH have fluorescence quantum yields of 0.74 and 0.096, respectively. Therefore it should be possible to detect MVK by monitoring the increase in fluorescence due to the formation of C-SMVK.

We immediately met challenges during the steady-state fluorescence experiments between 7-hydroxy-4-methylcoumarin (C-SH) and methylvinylketone (MVK). Because we were using typical 90° excitation, we required low concentrations of C-SH (~15 μM) for the excitation light beam to pass through the solution. Unfortunately, the low concentrations of C-SH reacted too slowly with the already dilute MVK. We then turned to front-faced fluorescence where higher concentrations of C-SH could be used (1mM was employed), but the reactions were

still slower than desired. To accelerate the reaction, acid-catalysis was investigated. Protic acids, however, caused an increase in fluorescence in the control experiment (with no MVK!). We speculate that acid accelerated the reaction between two C-SH to generated a fluorescent adduct (presumably via thiol attack at the 4-position). Lewis acid catalysis was not attempted due to their high sensitivity to water. Instead of acids, base (triethylamine) was used to accelerate nucleophilic attack of C-SH to MVK and this proved successful. A scan of several solvents pointed to chloroform as a good choice for these reactions; chloroform allowed for good contrast between C-SH and C-SMVK and it evaporated less quickly than dichloromethane (where good results were also obtained).

A typical fluorescence increase is shown in Figure 6-1(B). Working with a higher concentration of C-SH has the advantage that the initial rate of fluorescence increase is proportional to the concentration of MVK; the reaction gave pseudo-first order kinetics. We found excellent correlation between the initial rate of fluorescence increase and MVK concentration (Figure 6-1(C)).

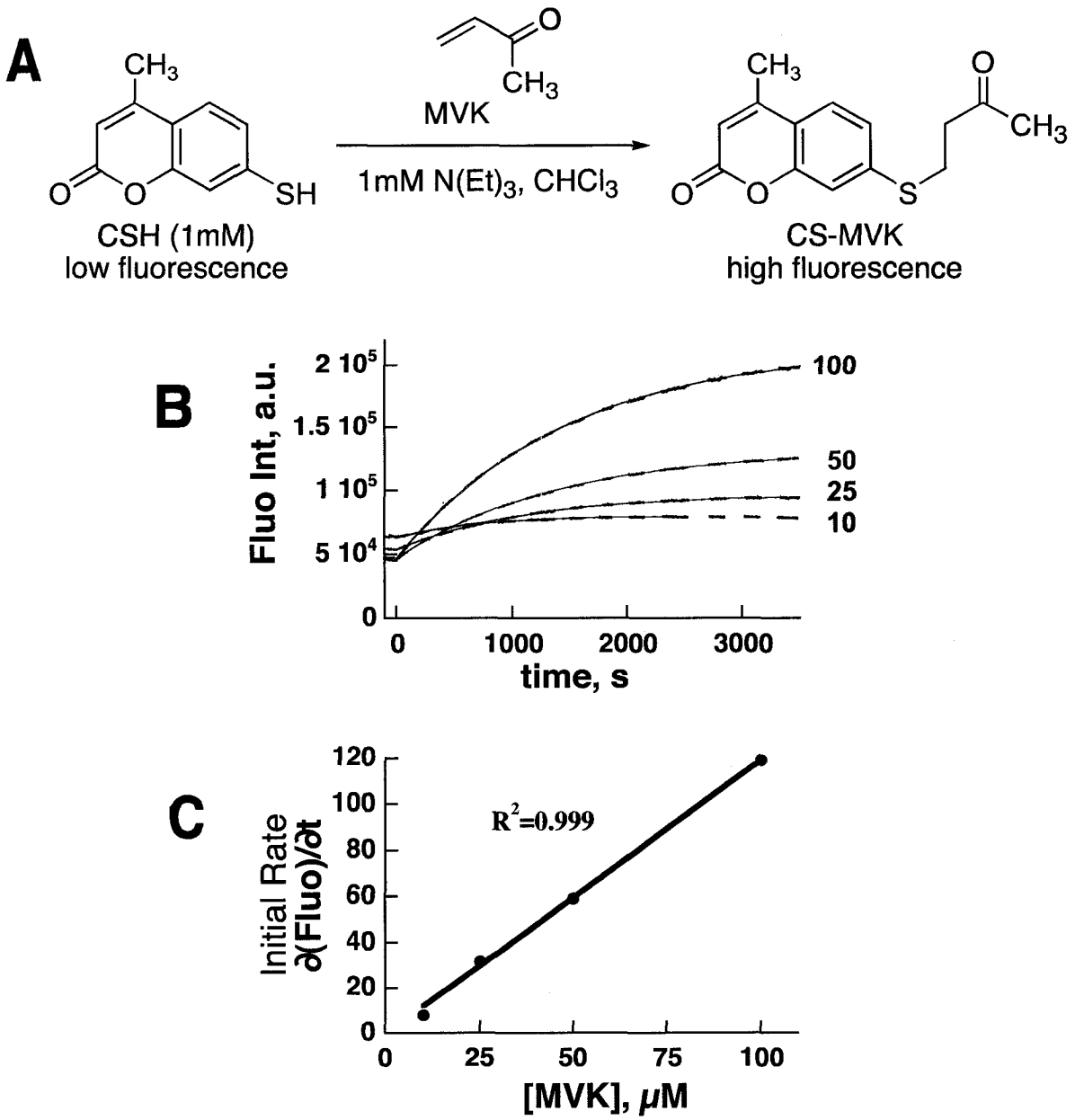

Figure 6-1. **(A) Conditions for the reaction between C-SH and MVK.**

(B) Steady-state, front-faced fluorescence (λ_{EXC} = 350 nm, λ_{MON} = 390 nm) of 1mM C4SH and 1mM triethylamine in chloroform with different concentrations of MVK—the concentrations (in μM) are indicated next to each trace. Note: the initial fluorescence intensity is not constant—the stock solution containing C-SH and triethylamine was oxidizing to the non-fluorescent disulfide (C-SS-C).

(C) Linear correlation between the initial rate of fluorescence increase from (B) and the concentration of MVK.

The addition of base to accelerate the reaction also lowered the background fluorescence; it was observed that deprotonated C-SH in $CHCl_3$ is less fluorescent. Unfortunately, C-SH is less stable in basic conditions—notice in Figure 6-1(B) how the baseline fluorescence measurement is not the same before each injection of MVK. This is because C-SH slowly (over hours) oxidizes to the disulfide C-SS-C in air, and this reaction is accelerated when C-SH is deprotonated. The formation of disulfide C-SS-C is not desired, but luckily, this product is non-fluorescent and does not interfere with the analysis.

The results shown here are largely a success; the electrophile MVK was detected using the prefluorescent probe C-SH by forming the fluorescent adduct C-SMVK.

6.5 Detecting Less Reactive Lipid Oxidation Electrophiles

Unfortunately, the reaction conditions used to detect MVK were not successful for less reactive Michael acceptors such as 4-hydroxynonenal (4-HNE) and 4-hydroperoxynonenal (4-HPNE) at sub-mM concentrations. For these less reactive electrophiles, proline was used to accelerate the reaction. Proline—a natural amino acid—catalyses the nucleophilic attack to Michael acceptors by forming an iminium cation at the aldehyde or ketone position[19] (Scheme 6-4). This activates the β-carbon as represented by the resonance structure shown below and so, nucleophilic attack by C-SH can occur faster.

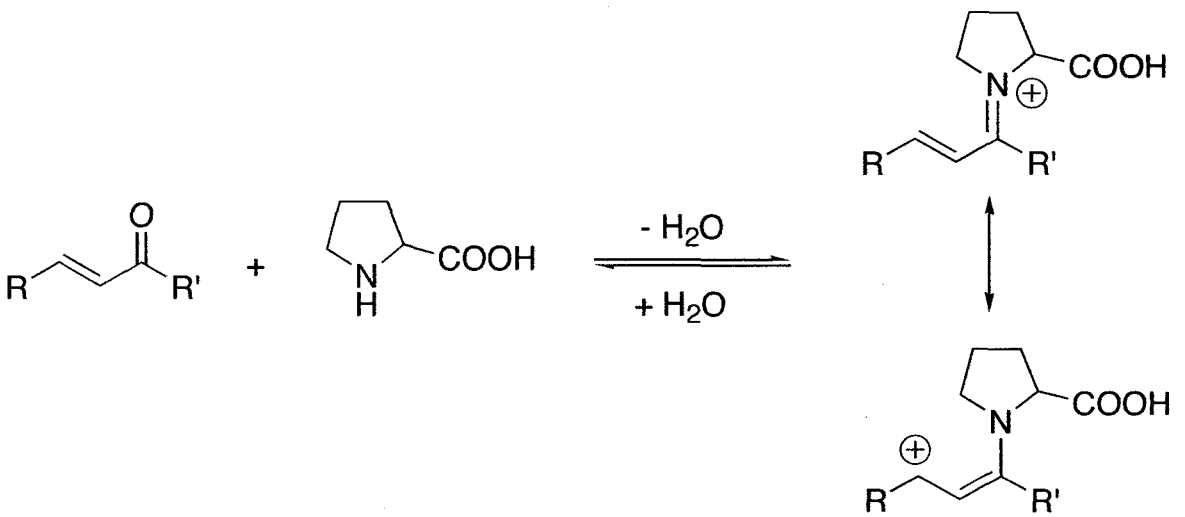

Scheme 6-4. Proline catalyzes nucleophilic addition to α,β-unsaturated ketones by the formation of an iminium that activates the β-position.

When using proline as a catalyst, we decided to carry out the experiments in methanol since the fluorescence intensity of C-SH is very low in this solvent (Φ_F <

0.005) compared to chloroform (Φ_F = 0.096). While it is a catalyst in this system, proline was used in a large excess (1mM) with respect to the analyte concentrations (sub-0.1mM). Using these concentrations—1mM proline and 1mM C-SH—we observed that the initial rate of fluorescence increase was proportional to the concentration of analyte (pseudo-first order kinetics). This greatly facilitates the analysis of the results.

Figure 6-2(B) shows the increase in fluorescence (λ_{EXC} = 360 nm, λ_{MON} = 410nm) of 1mM C-SH and 1mM proline solution in methanol with varying concentrations of 4-HPNE. The initial rate of fluorescence increase correlated well (R^2 = 0.994) with the concentration of 4-HPNE in the sample (Figure 6-2(C)).

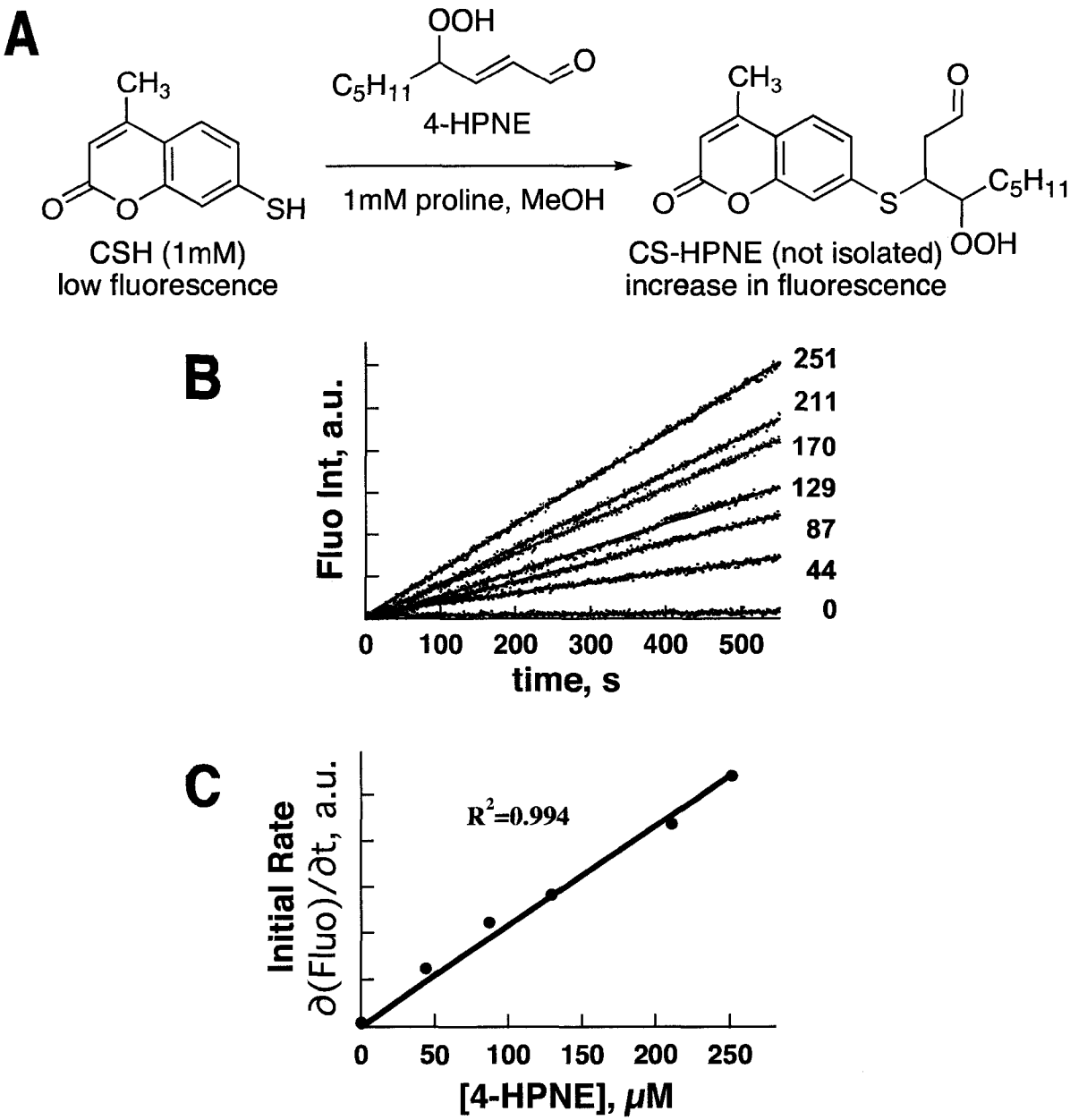

Figure 6-2. **(A) Conditions for the reaction between C-SH and 4-HPNE.**

(B) Steady-state, front-faced fluorescence (λ_{EXC} = 350 nm, λ_{MON} = 410 nm) of 1mM C-SH and 1mM proline in methanol with different concentrations of 4-HPNE—the concentrations in μM are indicated next to each trace. Note: the fluorescence intensity was set to zero at the initial time of measurement (after addition of 4-HPNE)

(C) Linear correlation between the initial rate of fluorescence increase and the concentration of 4-HPNE.

6.6 Discussion

When developing prefluorescent probes, the wish list is often repetitive: lower "off" fluorescence, higher "on" fluorescence, better selectivity, and longer emission wavelengths. Our experience with C-SH leaves us wanting in all four areas. The fluorescence of C-SR, for one, is mostly in the ultraviolet (λ_{max}~390nm); therefore naked eye detection and cell studies were not practical. For a red-shifted emission, the structure of the chromophore should be modified—for coumarins this is often done by substitutions at the 3 and/or 4 positions. I successfully applied this strategy for prefluorescent probes based on 7-hydroxycoumarin as described previously.[20] A similar approach could be used for 7-mercaptocoumarins, but we cannot be sure the desired photophysical properties will remain, i.e., non-fluorescent as the free thiol and fluorescent after attacking the oxidized lipid.

The reaction conditions proved crucial to the success of this technique and the concentration of C-SH played a large factor. Initially, we used low concentrations of C-SH (10-50 μM) to allow for 90° excitation. The reactions, if they were observed, were slow at this concentration. Since the reactions displayed 2nd order kinetics, we had to use the equilibrium fluorescence intensity (after many hours) as the indicator for analyte concentration. Apart from being long, these conditions were also plagued by the slow decomposition of C-SH to the disulfide C-SS-C. We finally decided to use higher concentrations of C-SH (1mM) and front-faced fluorescence. Because

the concentration of C-SH is much larger than the concentration of analyte, we could fit the fluorescence increase to pseudo-first order kinetics. The initial rate of fluorescence increase was found to be proportional to the concentration of analyte. Unlike most fluorescent probes based on "end point" fluorescence intensity, our approach is based on initial rates of fluorescence increase to quantify analyte concentrations. This approach has many advantages:

(i) The analysis can be much faster; only the initial portion of the reaction needs to be analyzed.

(ii) The reactions conditions can be changed to make the reaction faster or slower. Slower reactions may be desired for more accurate monitoring, i.e., the fluorescence increase could be measured over 20 minutes rather than 2 minutes.

(iii) Lipid oxidation samples often contain complex mixtures of electrophiles with different reactivities. In these cases, the initial rate of fluorescence increase could give a measure of the "total electrophilic activity" of the sample. In other words, more reactive electrophiles will react faster with C-SH to give a faster initial rate of fluorescence.

Point (iii) is particularly interesting. Many studies have tried to quantify oxidative stress using "markers" of oxidative stress; detecting 4-hydroxynonenal (HNE) by HPLC is one example.[21] This latter approach, however, has limited

applications as a tool for studying oxidative stress. For one, lipid peroxidation gives a complex mixture of products and this composition depends on many parameters. Therefore, quantifying one of many products leads to results that are difficult to compare between different studies. In our proposed approach, a "non-descriminant" detection of lipid oxidation electrophiles is measured. Such non-descriminant approaches, e.g., the FOX method,[22] are extensively used to detect lipid hydroperoxides.

6.6.1 Future Directions

As stated in point (iii), lipid oxidation electrophiles also display a range of reactivities. Acrolein is more reactive than 4-oxononenal (4-ONE) and 4-ONE is more reactive than 4-hydroxynonenal (4-HNE).[ref] On an ideal scale used to quantify "total electrophilic activity", acrolein would score higher than 4-HNE at the same concentration. Our approach based on initial rates naturally takes this into account. Reactive electrophiles will react faster with C-SH. This will result in a faster rate of fluorescence increase, which is the measure of "electrophilic activity" in the proposed technique.

Since fluorescence has arbitrary units, we cannot simply report a rate of fluorescence increase as a measure of electrophilic activity. A possible approach is to report the results in 4-HNE equivalents (or another electrophile). As such, a sample containing an unknown amount of electrophiles would be spiked with

different amounts of 4-HNE and all the samples would be measured by C-SH. From the rate of fluorescence increase vs. 4-HNE concentration, it will be possible to extrapolate the amount of "4-HNE equivalents" in the original sample. This approach would prevent solvent and environment effects from interfering since all the samples are the same (except for the added 4-HNE).

6.6.2 High-Throughput Fluorescence Analysis

Fluorescence spectroscopy as a tool for analysis becomes increasingly powerful when using a plate reader since a large number samples can be run at once. This is a major advantage for unstable biological samples containing oxidized lipids. I had the opportunity to use a plate reader to conduct experiments using the proline/methanol conditions and the preliminary results are promising. Very good correlation between the rate of fluorescence increase and 4-HNE were rapidly obtained with such an instrument (data not shown).

In the introduction of this chapter, we described the many preventive measures taken by cells against oxidative stress. Cooking oil, on the other hand, does *not* have many preventive measures against oxidative stress. Once antioxidants are consumed, lipid oxidation is prevalent in cooking oil. Is it harmful to eat these oxidized lipids? Does heart failure correlate with the amount of oxidized lipids we intake? Particularly, does it correlate with the amount of electrophilic oxidation products we intake? This chapter describes a fluorescent probe to quantify

the amount of electrophilic oxidation in such samples. Indeed, C-SH could also be used to detect the presence of any alkylating agent like mustard gas or iodomethane using the powerful combination of fluorescent probes and plate-readers.

6.7 Conclusion

A prefluorescent probe has been developed to detect and quantify electrophiles relevant to oxidative stress. We took advantage of the unusual property of 7-mercapto-4-methylcoumarin (C-SH)—it becomes fluorescent after the thiol is alkylated—to detect electrophiles such as methylvinylketone (MVK), 4-hydroxynonenal (4-HNE) and 4-hydroperoxynonenal (4-HPNE). The reaction between the electrophiles and C-SH was accelerated by the addition of base (triethylamine) or a catalyst (proline). Acid catalysis, unfortunately, led to an increase in fluorescence without electrophile, presumably due to the self-reaction of C-SH.

Optimized reaction conditions gave excellent correlations (R^2>0.99) between the initial rate of fluorescence increase and the electrophile concentrations. These promising results could prove useful as a tool to quantify lipid oxidation electrophiles, particularly in "real" sample where complex mixtures of electrophiles are present.

6.8 Experimental Details

7-mercapto-4-methylcoumarin (C-SH) is a commercial compound available from Fluka and it was recrystallized before use. 4-hydroperoxynonenal (4-HPNE), 4-oxononenal (4-ONE) and 4-hydroxynonenal (4-HNE) were obtained from Cayman Chemicals. These samples were kept in the freezer and used within a few days of receiving them. Solvents were HPLC grade or higher. Methylvinylketone and triethylamine were from Aldrich and both purified by filtration through a plug of silica gel (or neutral alumina). Proline (non-chiral) was from Aldrich.

UV-visible spectroscopy was performed on a CARY-50 spectrofluorometer and fluorescence was acquired on a Photon Technologies International instrument.

Optimizing the Sensitivity of C-SH as a Prefluorescent Probe.

Fluorescence can be very sensitive—single molecules are routinely observed using their fluorescence. But any technique is only as sensitive as the contrast between the signal and the background. The background in our case is the signal offered by the prefluorescent probe (C-SH) before any reaction. The signal is the fluorescent molecule generated after the desired event (C-SR). Prefluorescent probes enjoy a success because they offer a good contrast between signal and background. Advantages such as spatial resolution and temporal resolution and

chemical specificity would be less advantageous if the contrast with the background were poor. Short of changing the molecule, the contrast of a prefluorescent probe can be improved in two ways: modify the reaction conditions (see above) and modify the monitoring conditions. In fluorescence, "monitoring conditions" basically mean choosing λ_{EXC}, λ_{MON} and light intensities.

Before starting an experiment, we optimized λ_{EXC} and λ_{MON} to offer the maximum contrast between signal and background, i.e., between C-SR and unreacted C-SH, respectively. For this, two identical cuvettes containing C-SH in the desired reaction conditions are prepared. To one cuvette, the analyte (the oxidized lipid) is added; the other cuvette is labeled "control". After a few minutes (to allow for some C-SR to form) we measured the front-faced fluorescence spectra of both samples (λ_{EXC}~350 nm). The spectrum obtained from the sample containing the analyte is then divided by the "control" spectrum. The resulting graph should give a maximum; this corresponds to λ_{MON} that will offer the best contrast between signal and background.

At this monitoring wavelength (λ_{MON}), an excitation spectrum is run for both samples (keeping the monitoring wavelength constant while scanning shorter excitation wavelengths). Again these spectra are divided as "analyte" / "control". The maximum corresponds to the λ_{EXC} that will offer the best contrast for the detection of C-SR using this condition, on this particular fluorimeter. At this point, the light

intensities can be optimized and this approach can be cycled again to fine tune λ_{EXC} and λ_{MON}. Once optimized, the monitoring conditions should remain untouched to allow direct comparison between spectra.

Procedure for detecting methylvinylketone (MVK) in chloroform.

A stock solution containing 1 mM 7-mercapto-4-methylcoumarin (C-SH) and 1 mM triethylamine (previously filtered through a plug of silica gel) was made in chloroform. This stock solution (~1 mL) was added to a triangular quartz cell and front-faced fluorescence was measured as a function of time. The excitation and monitoring wavelengths were set to 350 nm and 390 nm, respectively. A baseline signal was measured for a few seconds before injecting methylvinylketone (MVK) to the desired final concentration (no more than 5% of the cuvette volume was added). The solutions were immediately mixed with the help of a clean pipette for a few seconds and the resulting increase in fluorescence was monitored for one hour with mild stirring afforded by a magnetic stirrer. Intermittently, we cut the excitation beam to prevent photo-degradation. The initial rate of the reaction is given in arbitrary units as the slope of the initial fluorescence increase; this value correlated very well with the concentration of MVK.

Procedure for detecting less reactive electrophiles in methanol.

A stock solution containing 1 mM 7-mercaptocoumarin (C-SH) and 1 mM proline was made in methanol. A 1.2 mL sample of the stock solution was added to a triangular quartz cell and front-faced fluorescence was measured in function of time. The excitation and monitoring wavelengths were set to 350 nm and 410 nm, respectively. (Note: The fluorescence maximum of C-SR in methanol is slightly red shifted from ~390nm to ~410nm) A baseline signal was measured before injecting 4-hydroperoxynonenal (4-HPNE) to the desired final concentration (no more than 5% of the cuvette volume was added). The solutions were immediately mixed with the help of a clean pipette for a few seconds and the resulting increase in fluorescence was monitored (without stirring) for ~ 20 min. The slope of the straight line obtained, i.e., the initial rate of the reaction, was measured at all concentrations for the same interval (400 – 1140 s). The initial rate of the reaction was then plotted against the concentration of 4-HPNE to give the calibration curve.

6.9 References

(1) Esterbauer, H.; Schaur, R. J.; Zollner, H. "Chemistry and biochemistry of 4-hydroxynonenal, malonaldehyde and related aldehydes" *Free Radical Biology & Medicine* **1991**, 11, 81-128.

(2) Sayre, L. M.; Zelasko, D. A.; Harris, P. L. R.; Perry, G.; Salomon, R. G.; Smith, M. A. "4-Hydroxynonenal-Derived Advanced Lipid Peroxidation End Products Are Increased in Alzheimer's Disease" *Journal of Neurochemistry* **1997**, 68, 2092-2097.

(3) Wiener, S. W.; Hoffman, R. S. "Nerve Agents: A Comprehensive Review" *Journal of Intensive Care Medicine* **2004**, 19, 22-37.

(4) Yang, Y. C.; Baker, J. A.; Ward, J. R. "Decontamination of chemical warfare agents" *Chemical Reviews* **1992**, 92, 1729-1743.

(5) Brock, N. "Oxazaphosphorine cytostatics: past-present-future." *Cancer Research* **1989**, 49, 1-7.

(6) Metcalf, R. L. "Insect Control " Ullmann's Encyclopedia of Industrial Chemistry; Wiley-VCH Verlag GmbH & Co. KGaA, 2002.

(7) Snyder, R.; Witz, G.; Goldstein, B. D. "The toxicology of benzene" *Environmental Health Perspectives* **1993**, 100, 293-306.

(8) Jian, W.; Lee, S. H.; Mesaros, C.; Oe, T.; Elipe, M. V. S.; Blair, I. "A Novel 4-Oxo-2(E)-nonenal-Derived Endogenous Thiadiazabicyclo Glutathione Adduct Formed during Cellular Oxidative Stress " *Chemical Research in Toxicology*, **2007**; 20; 1008-1018.

(9) Vila, A.; Tallman, K. A.; Jacobs, A. T.; Liebler, D. C.; Porter, N. A.; Marnett, L. J. "Identification of Protein Targets of 4-Hydroxynonenal Using Click

Chemistry for ex Vivo Biotinylation of Azido and Alkynyl Derivatives" *Chemical Research in Toxicology* **2008**, 21, 432-444.

(10) Falletti, O.; Douki, T. "Low Glutathione Level Favors Formation of DNA Adducts to 4-Hydroxy-2-(E)-nonenal, a Major Lipid Peroxidation Product" *Chemical Research in Toxicology* **2008**, ASAP, doi: 10.1021/tx800169a.

(11) Kruman, I.; Bruce-Keller, A. J.; Bredesen, D.; Waeg, G. "Evidence that 4-Hydroxynonenal Mediates Oxidative Stress-Induced Neuronal Apoptosis" *Journal of Neuroscience* **1997**, 17, 5089-5100.

(12) Simonian, N. A.; Coyle, J. T. "Oxidative Stress in Neurodegenerative Diseases" *Annual Reviews in Pharmacology and Toxicology* **1996**, 36, 83-106.

(13) Finkel, T.; Holbrook, N. J. "Oxidants, oxidative stress and the biology of ageing" *Nature* **2000**, 409, 239-247.

(14) Bernheim, F.; Bernheim, M. L. C.; Wilbur, K. M. "The reaction between thiobarbituric acid and the oxidation products of certain lipides" *Journal of Biological Chemistry* **1948**, 174, 257-264.

(15) Witz, G.; Lawrie, N. J.; Zaccaria, A.; Ferran Jr, H. E.; Goldstein, B. D. "The reaction of 2-thiobarbituric acid with biologically active alpha, beta-unsaturated aldehydes." *Journal of Free Radicals in Biology & Medicine* **1986**, 2, 33-39.

(16) A SciFinder analysis of 22000+ publications using "thiobarbiturate" shows the number is steadily increasing every year, with almost 1500 publications using "thiobarbiturate" in 2007.

(17) Yin, H.; Porter, N. A. "New Insights Regarding the Autoxidation of Polyunsaturated Fatty Acids" *Antioxidants & Redox Signaling* **2005**, 7, 170-184.

(18) Invitrogen's Molecular Probes offers the largest selection of fluorescent probes for biological applications: http://probes.invitrogen.com/handbook/

(19) List, B. "Proline-catalyzed asymmetric reactions" *Tetrahedron* **2002**, 58, 5573-5590.

(20) Frenette, M.; Coenjarts, C.; Scaiano, J. "Mapping Acid-Catalyzed Deprotection in Thin Polymer Films: Fluorescence Imaging Using Prefluorescent 7-Hydroxycoumarin Probes" *Macromolecular Rapid Communications* **2004**, 25, 1628-1631.

(21) Moore, K.; Roberts, L. J. "Measurement of Lipid Peroxidation" *Free Radical Research* **1998**, 28, 659-671.

(22) Jiang, Z. Y.; Hunt, J. V.; Wolff, S. P. "Ferrous ion oxidation in the presence of xylenol orange for detection of lipid hydroperoxide in low density lipoprotein" *Analytical Biochemistry* **1992**, 202, 384-389.

7. Conclusions and Future Directions

7.1 Conclusions

This work was inspired by three ideas that are summarized below.

In the first two chapters, I described persistent carbon-centered radicals (A•) and the dimers they form (A_2). As observed with triphenylmethyl radicals, the radical and dimer are in thermal equilibrium and we measured very low bond dissociation energies for these compounds (15-26 kcal/mol). The radicals studied here, however, were found to be relatively inert to air unlike triphenylmethyl and other non-hindered carbon-centered radicals. Furthermore, they form "head-to-head" dimers (dimerization via central carbon) and not "head-to-tail" dimers as do the majority of sterically hindered radicals.

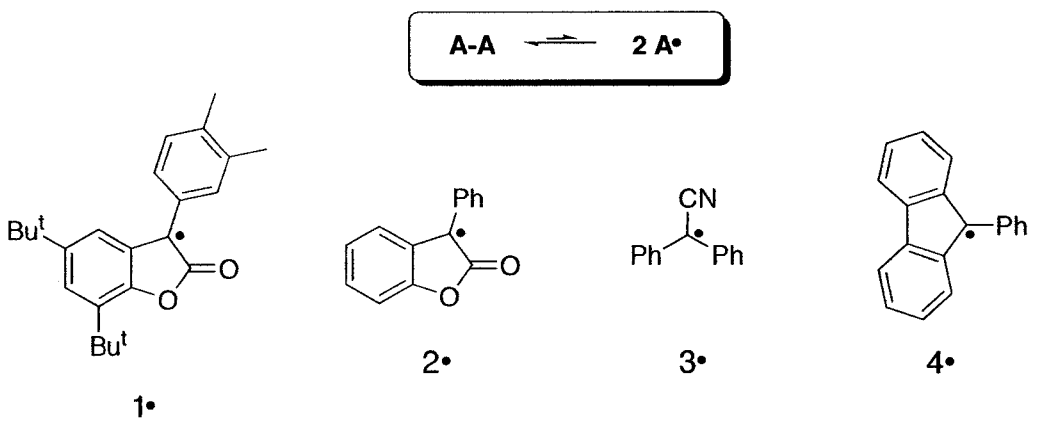

Scheme 7-1. Radicals 1• to 4• exist in thermal equilibrium with their dimer.

We had the idea of using these dimers as antioxidants, which turned out to be a successful approach to prevent free radical autoxidation reactions. This new

class of antioxidants takes advantage of the very fast nature of radical-radical reactions to trap peroxyl radicals. At higher temperatures, where more dimer is dissociated to the active radical form, the antioxidant activity of these compounds increases dramatically.

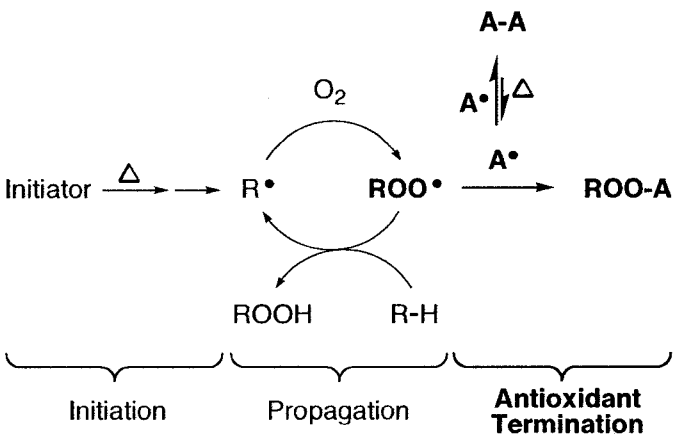

Scheme 7-2. Dimers 1_2, 2_2 and 3_2 can be used as thermally modulated antioxidants. The effect of heating dissociates more antioxidant radicals; therefore, the antioxidant activity increases dramatically with an increase in temperature.

The second idea deals with the mechanism for the autoxidation of lipids and cholesterol. These reactions are complex and the mechanism for the formation of many secondary oxidation products is not fully understood. In particular, the oxidation of hydroperoxides to ketones has not been explained. For this latter transformation, we proposed that αC-H abstraction by peroxyl radicals would generate the ketone product. Interestingly, the by-product of this reaction is the extremely reactive hydroxyl radical.

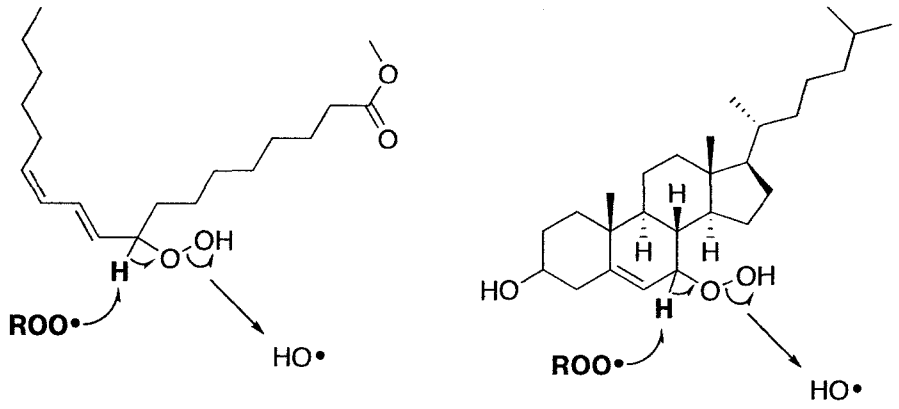

Scheme 7-3. The secondary oxidation of linoleate hydroperoxides and cholesterol hydroperoxides is proposed as a path to the generation of ketones and hydroxyl radicals. We studied the formation of hydroxyl radicals by their reaction with benzene.

And finally, we developed a fluorescent probe to detect some secondary oxidation products formed during lipid peroxidation. In particular, we observed that 7-mercapto-4-methylcoumarin (C-SH) is non-fluorescent in polar solvents and it becomes fluorescent upon alkylation. This observation was applied in the context of lipid oxidation. The non-fluorescent C-SH became fluorescent after nucleophilic attack of α,β-unsaturated ketones and aldehydes and the growth of the fluorescent signal allowed the detection of such compounds.

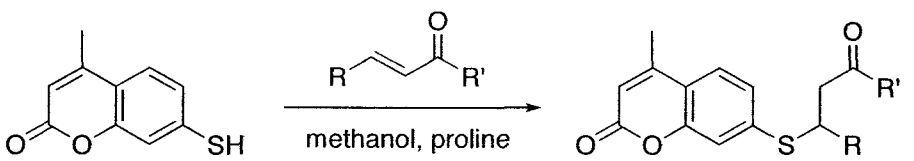

non-fluorescent fluorescent

Scheme 7-4. The alkylation of 7-mercapto-4-methylcoumarin, which is practically non-fluorescent in polar solvents, generates a fluorescent signal that can be related to the concentration of lipid oxidation products.

The work presented here are largely proofs of concepts with some fundamental studies of the chemistry at play. While the ideas may inspire novel chemistry in related or unrelated areas, the fundamental studies have also generated useful data. The thermodynamic properties measured for the dissociation of dimers, for example, may be useful as a benchmark for theoretical methods that treat highly delocalized radicals. We have worked extensively with C-SH during the past two years, and while the application to detect lipid oxidation products is exciting, the fundamental photophysical studies performed on this chromophore will enable others to rationally design fluorescent probes to detect other analytes.

This combination of idea–proof-of-concept–fundamental study is a particularly stimulating way to perform basic research. Novel ideas and their validation has led me on many dead-ends, but as shown here, the positive results that are sometimes obtained can yield remarkable results. Furthermore, the quest for a more thorough understanding of the chemistry involved is at the core of physical organic chemistry. The quantitative measurements obtained, e.g., rate constants and thermodynamic properties, create a clearer picture of organic chemistry that can lead to innovation.

7.2 Future Directions

7.2.1 Dimer Antioxidants

The novel class of antioxidants described in chapter 2 appears promising for protecting materials that suffer from heat-induced oxidation, e.g., the recycling of plastics (that are often melted), motor oil, tar, etc. Fellow graduate student Vasilisa Fillipenko has recently found that dimer antioxidants are not slowed down by hydrogen bonding solvents, as is often the case for phenolic antioxidants. This result indicates that water-soluble antioxidants based on carbon-centered radical dimers could be useful. The basic methods to study the chemistry involved in antioxidants of this class has been described and so, the developement of novel dimers as antioxidants is only limited by their synthesis. Computational chemistry may be useful to study the interaction of novel radicals with oxygen before the syntheses of new compounds are undertaken.

7.2.2 Hydroxyl Radicals Generation During Autoxidation Reactions

The chemistry described in this section explains the formation of hydroxyl radicals during the autoxidation of lipids in benzene. In this system, the hydroxyl radicals generated can be trapped by benzene to generate phenol, which is quantified by GC-MS. Oxidation reactions starting from the purified hydroperoxide

could allow for a better understanding of this chemistry. Preliminary results for the autoxidation of cholesterol appear to generate more hydroxyl radicals than lipid autoxidation. Again, studies using purified 7-hydroperoxycholesterol would help to understand this chemistry.

7.2.3 Fluorescent Probe to Detect Electrophiles

This project is particularly promising. The electrophiles generated during lipid peroxidation are known to disrupt normal cell behavior and a fluorescent probe that can detect these quantitatively is highly desirable. The preliminary results shown in Chapter 6 should be expanded using a recently acquired fluorescence plate reader. After the system is properly optimized, the determination of "total electrophilic content" in real samples could be pursued.

The design of a fluorescent probe that is less fluorescent before electrophilic attack and more fluorescent after would be advantageous to enhance the contrast. For studies *in vivo*, the fluorescence maximum of the fluorophore would need to be shifted to the visible. Also, one can imagine a fluorescent probe that combines the catalytic activity of proline and the nucleophilic attack of the thiol group (see below).

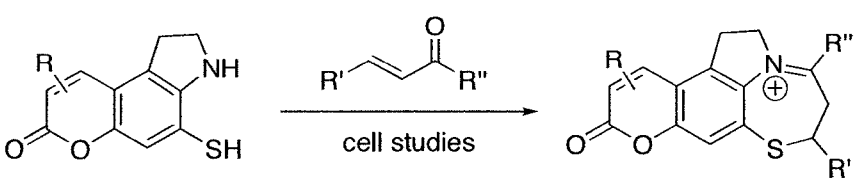

non-fluorescent? fluorescent?

7.3 Claims to Original Research

(i) Synthetic procedures to generate persistent carbon-centered radical dimers.

(ii) Measurement of thermodynamic properties for the radical-dimer equilibrium using Variable Temperature UV-visible and EPR spectroscopies.

(iii) Evaluation of the antioxidant activity by persistent carbon-centered radical dimers using the inhibited autoxidation of cumene and styrene.

(iv) Measurement of hydroxyl radicals generated during lipid and cholesterol peroxidation and theoretical evaluation of a proposed mechanism.

(v) First systematic study of 7-mercaptocoumarin photophysics.

(vi) Application of 7-mercapto-4-methylcoumarin as a prefluorescent probe used to detect secondary lipid oxidation products.

7.4 Publications

7.4.1 Publications resulting from work presented in this thesis

(i) Frenette, M., Aliaga, C., Font-Sanchis, E., Scaiano, J. C., "Bond Dissociation Energies for Radical Dimers Derived from Highly Stabilized Carbon-Centered Radicals", *Organic Letters*, **2004**, 6 (15), 2579-2582.

(ii) Frenette, M., MacLean, P. D., Barclay, L. R. C., Scaiano, J. C., "Radically Different Antioxidants: Thermally Generated Carbon-Centered Radicals as Chain-Breaking Antioxidants", *Journal of the American Chemical Society*, **2006**, 128 (51), 16432-16433.

(iii) Frenette, M., Scaiano, J. C., "Evidence for Hydroxyl Radical Generation During Lipid (Linoleate) Peroxidation", *Journal of the American Chemical Society*, **2008**, 130 (30), 9634-9635.

(iv) Frenette, M., González-Béjar, M., Campbell, P., Scaiano, J. C., "Photophysics of 7-Mercapto-4-methylcoumarin and Derivatives: Dramatic Contrast with 7-Hydroxy-4-Methylcoumarins", *Manuscript in preparation.*

(v) Frenette, M., Campbell, P., Scaiano, J. C., "7-Mercapto-4-methylcoumarin: A Prefluorescent Probe to Detect 4-Hydroxynonenal and Related Electrophiles Generated During Lipid Peroxidation", *Manuscript in preparation.*

7.4.2 Publications resulting from work not presented in this thesis

(i) Frenette, M., Coenjarts, C., Scaiano, J. C., "Mapping Acid-Catalyzed Deprotection in Thin Polymer Films: Fluorescence Imaging Using Prefluorescent 7-Hydroxycoumarin Probes", *Macromolecular Rapid Communications*, **2004**, 25 (18), 1628-1631.

(ii) Scaiano, J. C., Aliaga, C., Chrétien, M. N., Frenette, M., Focsaneanu, K. S., Mikelsons, L., "Fluorescence Sensor Applications as Detectors for DNA Damage, Free Radical Formation, and in Microlithography." *Pure and Applied Chemistry*, **2005**, 77, 1009-1018.

(iii) Frenette, M., Ivan, M. G., Scaiano, J. C., "Use of Fluorescent Probes to Determine Catalytic Chain Length in Chemically Amplified Resists", *Can. J. Chem.*, **2005**, 83, 869-874.